

PREDICTIVE SIMULATIONS OF GAIT AND THEIR APPLICATION IN
PROSTHESIS DESIGN

ANNE D. KOELEWIJN

Master of Science in Mechanical Engineering

Technische Universiteit Delft

July 2014

Bachelor of Science in Aerospace Engineering

Technische Universiteit Delft

September 2011

submitted in partial fulfillment of requirements for the degree

DOCTOR OF ENGINEERING IN MECHANICAL ENGINEERING

at the

CLEVELAND STATE UNIVERSITY

AUGUST 2018

We hereby approve this thesis for
ANNE D. KOELEWIJN
Candidate for the degree of Doctor of Engineering in Mechanical Engineering
Department of Mechanical Engineering
and the CLEVELAND STATE UNIVERSITY
College of Graduate Studies.

Dr. Antonie van den Bogert
Committee Chairperson
Department of Mechanical Engineering

Dr. Ann Reinalt
Committee Member
Department of Health Sciences

Dr. Hanz Richter
Committee Member
Department of Mechanical Engineering

Dr. Eric Schearer
Committee Member
Department of Mechanical Engineering

Dr. Dan Simon
Committee Member
Department of Electrical Engineering

Date of Defense: June 12, 2018

This student has fulfilled all requirements for the Doctor of Engineering degree.

Chandrasekhar Kothapalli
Doctoral Program Director

ACKNOWLEDGMENTS

First of all, I would like to thank my advisor, Dr. Van den Bogert, for all his help and support during my time at Cleveland State University. Over the last four years, I have really grown as a person, researcher, scientist and engineer and I would like to thank you for providing me with the right tools to do that.

I would like to thank my thesis committee: Dr. Hanz Richter, Dr. Eric Schearer, Dr. Dan Simon, and Dr. Ann Reinalth for their insightful comments and encouragement.

This dissertation was supported by the National Science Foundation under Grant No. 1344954 and by a Graduate Scholarship from the Parker-Hannifin Corporation. I would like to thank both for providing me with the neccesary funding to do research and make this dissertation.

Also, I would like to thank Dr. Dieter Heinrich, Eva Dorschky, Dr. Kenneth Sparks, Dr. Ross Miller and Chelsea Turowski for their help with the metabolic cost experiments and models. Chelsea was a great assistant during the experiments, and with her help I was able to run the experiments smoothly. Dr. Kenneth Sparks could solve any problem I had with our metabolic cart. Dr. Dieter Heinrich was very helpful during the data processing and pointed me to the right statistical tools. Dr. Ross Miller provided some great suggestions for adaptations to the metabolic energy models, and Eva Dorschky provided necessary data, helped generate the results and was a great co-author.

Of course, I should thank my awesome lab members for their support. Sandy, Huawei, Farbod, Milad, Sabrina, Ravi, Nicole, Farzad, Jason, Michael, and Dana, thanks for putting up with my awesome bad puns these last four years. I will miss you and wish you the best of luck in all your future endeavors! Do not forget to get Froyo on Thursday.

Next, I would like to thank Adidas AG and the members of the Machine Learning and Data Analytics lab at Friedrich-Alexander Universität Erlangen-Nürnberg, especially Heiko Schlarb, Dr. Björn Eskofier, Eva Dorschky, and Marlies Nitschke. Their collaboration on the musculoskeletal models was very important for my research. Also, I found the

visits to their sites very inspirational and useful.

My time at CSU would not have been as fun without all other graduate students I met here. Thanks to all that came to happy hours or lunches. I should also thank the Graduate and Professional Student Organization for providing opportunities to meet other graduate students, and especially our faculty advisor Patty Otcasek, who was always available for a chat whenever I needed it. Finally, thank you to everyone at Coffee House for welcoming international students, and hosting fun events.

My parents were a great help while finishing my degrees. Thank you especially for supporting me when I moved 3902 miles away to pursue my dream of getting a doctoral degree.

And lastly, I would like to thank Lebron James for following my example and coming to Cleveland to win a championship for this city.

PREDICTIVE SIMULATIONS OF GAIT AND THEIR APPLICATION IN
PROSTHESIS DESIGN
ANNE D. KOELEWIJN

ABSTRACT

Predictive simulations predict human gait by solving a trajectory optimization problem by minimizing energy expenditure. These simulations could predict the effect of a prosthesis on gait before its use. This dissertation has four aims, to show the application of predictive simulations in prosthesis design and to improve the quality of predictive simulations. Aim 1 was to explain joint moment asymmetry in the knee and hip in gait of persons with a transtibial amputation (TTA gait). Predictive simulations showed that an asymmetric gait required less effort. However, a small effort increase yielded a gait with increased joint moment symmetry and reduced joint reaction forces. This suggests that gait training could reduce the risk of developing osteoarthritis in persons with a transtibial amputation. Aim 2 was to compare the effect of different prosthesis alignments on TTA gait. Predictive simulations were solved using a three-dimensional musculoskeletal model with different prosthetic alignments. A flexion alignment of the prosthesis might be favored over a neutral alignment, since the metabolic cost and joint reaction forces were lower, though the differences were small. Also, predictions indicated that a lateral translation or an external rotation could alleviate skin problems by reducing skin-to-socket stresses. Aim 3 was to compare the gait objective of minimizing metabolic energy to minimizing muscular effort. Four metabolic energy expenditure models were selected after an experiment to compare metabolic cost calculated with seven metabolic energy models to metabolic cost from pulmonary gas exchange measurements. The minimum energy solution was more similar to normal gait in joint angles, while the minimum effort solution was more similar in joint moments, especially at the knee. However, neither solution could entirely explain human gait. Aim 4 was to propose an approach to optimize in a stochastic environment and implement it to explain antagonistic muscle co-contraction in human movement. In a stochastic

environment, muscle co-contraction was energy optimal for certain tasks and nonzero foot clearance was energy efficient. The approach was then applied to TTA gait to explain co-contraction of the upper-leg muscles on the prosthesis side. The results suggested that antagonistic co-contraction is energy optimal for human gait.

TABLE OF CONTENTS

	Page
ABSTRACT	v
LIST OF TABLES	xii
LIST OF FIGURES	xiii
CHAPTER	
I. INTRODUCTION	1
1.1 Research Goals	3
1.2 Organization of This Dissertation	5
1.3 References	6
II. BACKGROUND INFORMATION	9
2.1 Terms and Definitions of Human Motion	9
2.2 Human Gait	11
2.2.1 Adjustments in Gait of Persons With a Transtibial Amputation	15
2.2.2 Energy Expenditure in Gait of Persons with a Transtibial Amputation	17
2.2.3 Health Issues in Gait of Persons with a Transtibial Amputation	18
2.3 Lower-leg prostheses	19
2.3.1 Passive Prosthesis	20
2.3.2 Active Prosthesis	25
2.4 Human Modeling Studies	27
2.4.1 Studying Parameters that cannot be Measured	27
2.4.2 Analysis of Intervention	29
2.4.3 Explaining Human Movement	30
2.4.4 Predictive Simulations	32

2.5	Trajectory Optimization	33
2.5.1	Solution Methods	36
2.6	Human Model	40
2.6.1	Three Element Hill-Type Muscle Model	42
2.6.2	Ground Contact Model	49
2.7	References	50
III. JOINT CONTACT FORCES CAN BE REDUCED BY IMPROVING JOINT MOMENT SYMMETRY IN TRANSTIBIAL AMPUTEE GAIT SIMULATIONS		67
3.1	Introduction	69
3.2	Methods	70
3.2.1	Model	70
3.2.2	Optimal Control Problem	70
3.3	Results	72
3.4	Discussion	76
3.5	References	82
IV. THE EFFECT OF PROSTHESIS MISALIGNMENT ON GAIT - A PREDICTIVE SIMULATION STUDY		87
4.1	Introduction	89
4.2	Methods	91
4.2.1	Three-dimensional Musculoskeletal Model	91
4.2.2	Trajectory Optimization Problem	95
4.2.3	Predictive Simulations for Alignment Study	97
4.3	Results	99
4.3.1	Sagittal Rotational Alignment Change	103
4.3.2	Frontal Rotational Alignment Change	107
4.3.3	Frontal Translational Alignment Change	111

4.3.4	Transverse Rotational Alignment Change	114
4.3.5	Statistical Tests	117
4.4	Discussion	118
4.4.1	Comparison to Previous Studies	121
4.4.2	Limitations	124
4.5	Conclusion	125
4.6	References	126
V. COMPARING METABOLIC ENERGY MODELS USING		
EXPERIMENTAL DATA AND PREDICTIVE SIMULATIONS . . .		132
5.1	Introduction	134
5.2	Comparison of Metabolic Energy Expenditure Models	137
5.2.1	Methods	137
5.2.2	Analysis	141
5.2.3	Results	142
5.2.4	Discussion	149
5.2.5	Model Selection for Predictive Simulations	153
5.3	Predictive Simulation of Gait Minimizing Metabolic Cost Compared to Minimizing Effort	153
5.3.1	Adaptations to Models Necessary for Gradient-Based Optimization	154
5.3.2	Predictive Simulation of Gait	165
5.4	Conclusion	173
5.5	References	173
VI. PREDICTIVE SIMULATIONS IN A STOCHASTIC		
ENVIRONMENT		181
6.1	Introduction	183
6.1.1	Co-contraction of muscles	185

6.1.2	Trajectory Optimization in a Stochastic Environment	188
6.1.3	Goal of this Work	189
6.2	Proposed Method for Predictive Simulations in a Stochastic Environment	189
6.3	Pendulum Swing-Up	191
6.3.1	Methods	192
6.3.2	Results	195
6.3.3	Discussion	198
6.4	Pendulum with Muscular Control	199
6.4.1	Methods	200
6.4.2	Results	202
6.4.3	Discussion	205
6.5	Torque-driven Able-bodied Gait	206
6.5.1	Methods	206
6.5.2	Results	209
6.5.3	Discussion	211
6.6	Predictive Gait Simulation with a Lower Leg Prosthesis in a Stochastic Environment	213
6.6.1	Methods	213
6.6.2	Results	215
6.6.3	Discussion	216
6.7	Conclusion	220
6.8	References	221
VII.	CONCLUSION	227
7.1	Future Perspective	228
7.2	References	230

APPENDICES

A. Metabolic Models	231
B. Results of Single Joint Reaching Task with Other Models	240
C. Continuous Version of Model Umberger	244
D. Five Best Solutions of Optimization Problems in Chapter V	248
E. Marker Placement	255
F. Copyright Letters	257

LIST OF TABLES

Table	Page
I. Muscle Parameters	47
II. Muscle Moment Arms	47
III. Overview of the alignment conditions that will be studied.	98
IV. Means of variables used in statistical tests.	119
V. Repeated measured correlation results.	149
VI. Correlation coefficients for all models.	158
VII. Overview of muscle parameters used.	159
VIII. Overview of termination messages by IPOPT.	167
IX. Metabolic rate calculated by each model for predictive simulations.	167
X. Constants for slow twitch and fast twitch fibers.	237
XI. Marker placement.	256

LIST OF FIGURES

Figure	Page
1. Planes of the human body.	10
2. Human leg motions in sagittal plane.	11
3. Phases of the gait cycle.	12
4. Ground reaction forces, joint angles, and joint moments of normal gait. . . .	14
5. Human musculoskeletal model that is used in this dissertation.	41
6. Hierarchical structure of the multibody dynamics.	42
7. Hill-type muscle	44
8. Force-length and force-velocity relationship of the contractile element.	45
9. Pareto-front showing the trade-off between effort and symmetry.	73
10. Weight versus tracking error, effort, moment symmetry, and metabolic cost. .	74
11. Joint angles and moments of the predictive simulations.	75
12. Muscle forces of the predictive simulations.	77
13. Joint contact forces in the knee and hip for the predictive simulations. . . .	78
14. Updated Pareto-front.	81
15. Pennated Hill-type muscle.	93
16. Leg joint angles, joint moments and ground reaction forces for able-bodied and TTA gait.	101
17. Upper joint angles, joint moments and ground reaction forces for able-bodied and TTA gait.	102
18. Leg joint angles, joint moments and ground reaction forces for sagittal plane alignment change.	105
19. Upper joint angles, joint moments and ground reaction forces for sagittal plane alignment change.	106
20. Leg joint angles, joint moments and ground reaction forces for frontal plane rotational alignment change.	109

21.	Upper joint angles, joint moments and ground reaction forces for frontal plane rotational alignment change.	110
22.	Leg joint angles, joint moments and ground reaction forces for frontal plane translational alignment change.	112
23.	Upper joint angles, joint moments and ground reaction forces for frontal plane translational alignment change.	113
24.	Leg joint angles, joint moments and ground reaction forces for transverse plane alignment change.	115
25.	Upper joint angles, joint moments and ground reaction forces for transverse plane alignment change.	116
26.	Metabolic rate of soleus muscle at three speeds.	142
27.	Ground reaction forces, joint angles, joint moments, and muscle forces at nor- mal speed.	143
28.	Ground reaction forces, joint angles, joint moments, and muscle forces at slow speed.	145
29.	Calculated (separated by joint) and measured metabolic cost for all trials. . .	147
30.	Error between measured and calculated metabolic cost.	148
31.	Correlation between calculated and measured metabolic cost.	150
32.	Correlation between continuous and original metabolic energy model.	158
33.	Sketch of the arm, operated by muscles.	159
34.	Optimal trajectory of arm when minimizing metabolic energy.	162
35.	Optimal trajectory of arm when minimizing effort.	164
36.	Joint angles, joint moments, and muscle forces for predictive simulations. . .	170
37.	Pendulum used for the swing-up problem.	192
38.	Optimal trajectories and inputs in stochastic and deterministic environments. .	196
39.	Comparison of trajectories with and without feedback.	197
40.	Convergence analysis of the objective of the optimal solution.	198

41.	Pendulum with muscles.	201
42.	Optimal open-loop input for different weights and noise amplitudes.	203
43.	Comparison of optimal trajectory in deterministic and stochastic environment.	204
44.	Heel and toe clearance in deterministic and stochastic environments.	210
45.	Convergence analysis of the required number of gait cycles.	211
46.	Heel and toe clearance found with 50 gait cycles.	212
47.	Joint angles and moments for able bodied gait and TTA gait in a stochastic environment.	217
48.	Average muscle stimulation of the Vasti and Hamstrings for able-bodied gait and TTA gait in a stochastic environment.	218
49.	Average muscle stimulation of the Vasti and Hamstrings for TTA gait in a deterministic and a stochastic environment.	218
50.	Optimal trajectory for the single arm reaching task using model Bhargava. . .	241
51.	Optimal trajectory for the single arm reaching task using model Houdijk. . .	242
52.	Optimal trajectory for the single arm reaching task using model Lichtwark. .	243
53.	Results of five lowest objectives with model Lichtwark.	249
54.	Results of five lowest solution with model Bhargava.	250
55.	Results of five lowest solution with model Houdijk.	251
56.	Results of five lowest solution with model Umberger.	252
57.	Results of five lowest solution with effort minimization.	253
58.	Placement of markers on the body.	255

CHAPTER I

INTRODUCTION

The prevalence of limb amputation is expected to rise to one in every 95 Americans in 2050. Most of these amputations are transtibial [1]. Generally, patients rely on a prosthesis to regain some of the function of their lost limb. However, health issues, such as osteoarthritis in the joints of the intact leg and loss of bone mineral density in the intact leg, are prevalent among persons with a transtibial amputation who walk with a prosthetic leg for over five years [2–4]. These health issues are presumed to be caused by the change in gait kinetics and kinematics due to the prosthetic leg.

When an individual is prescribed a prosthetic leg, a socket is fitted to the residual part of the leg and a prosthetic ankle is connected to this socket. An appropriate prosthetic ankle is chosen from many different available options based on the patient’s lifestyle and physical needs [5, 6]. However, the effect of the ankle on the patient’s gait is not known before it is fitted to the patient, while the impact to gait mechanics and long term health could be significant.

A predictive simulation could address these issues and evaluate the prosthetic leg before the user wears the device. Such a simulation is created based on a computational model of the patient and the prosthesis and will give a prediction of the joint angles, moments, contact forces, and many other variables during the gait cycle [7, 8]. The advantage of a predictive simulation is its ability to predict possible health issues without requiring prototyping and experimentation on any patient, which could create a risk to the patient’s

health.

In a predictive simulation of a gait cycle, the muscular controls are found that minimize an objective, for example muscular effort [7, 8], metabolic cost [9], or joint contact forces [10]. This approach could potentially replicate a human gait cycle, because it is known that persons minimize some objective when walking [11]. To create a realistic prediction, it is necessary that the same objective is minimized as when a human is walking.

Accurate predictive simulations of normal gait have been found using a forward dynamics approach [9, 12]. In this approach, the gait cycle is simulated from the initial state, while the input is optimized. However, numerical difficulties exist because the control input at the beginning of the trajectory has a much larger influence on the objective than a control input near the end of the trajectory [13, 14]. This approach also makes it hard to create a periodic gait cycle [9], has limited control freedom [10, 12, 15] and requires many forward simulations, which is time-consuming [13]. Anderson and Pandy [9] required 10000 CPU hours to solve a predictive gait simulation [9]. A data driven initial guess could alleviate these issues [12], but this could bias the solution towards the initial guess.

However, a faster approach, without the use of a data-driven initial guess, is favored for evaluating a prosthesis. For such predictions, an approach known as *direct collocation* might be better suited. In this approach, the trajectory is split up into collocation points and the states and muscular inputs of the gait cycle are optimized simultaneously. Instead of a simulation, dynamics are enforced using constraints at each collocation point. Periodicity of the gait cycle can also be achieved with a constraint. This approach creates a large number of optimization variables and constraints, but an analytical gradient can be derived for the objective and all constraints, so the problem can be solved fairly quickly using a large-scale nonlinear optimization algorithm [13]. A more detailed review will be presented in chapter II.

However, current predictive simulations which use direct collocation are not yet accurate enough. Previous work showed that the main features of gait can be predicted by

minimizing muscle activation [16], and that predictions are improved when tracking of joint angles, ground reaction forces and duration of able-bodied gait is added to the objective [7]. However, this approach requires tracking of normal walking data, so the simulation is not strictly predictive.

This means that the use of strictly predictive simulations to evaluate prosthesis fitting is not yet possible. However, one could create simulations that track able-bodied gait to make predictions of gait of persons with a transtibial amputation (TTA gait). I aim to do both in this dissertation: apply predictive simulations that track able-bodied gait to increase understanding of TTA gait, and develop methods that can generate strictly predictive gait simulations that are sufficiently accurate.

1.1 Research Goals

The following research goals are proposed:

Aim 1: Application Explain joint moment asymmetry in the knee and hip in TTA gait using predictive simulations

This application of predictive simulations shows the effect of increased symmetry of joint moments in the knee and hip using a simple passive prosthesis. Subject studies show that patients have asymmetry in the joint moment distribution between the hips and the knees. However these joints are not affected by the amputation, so it should be possible to bear the same load in both legs. Predictive simulations can be used to find gaits with different levels of symmetry. This problem would be hard to study in an experiment, because it is difficult to change the level of symmetry in one's gait.

Aim 2: Application Compare the effect of different prosthesis alignments on TTA gait

The second application of predictive simulations is to study the effect of the prosthesis alignment on gait. Little information is available on the effect of a misaligned prosthesis on a person's gait. It is advantageous to investigate this using predictive simulations because

subjects do not have to walk with an alignment that is uncomfortable and possibly harmful. Predictive simulations are found using a three-dimensional musculoskeletal model, so that the alignment can be adjusted in different planes. Joint angles and moments, ground reaction forces, joint contact forces, and metabolic energy expenditure will be compared between the different alignments.

Aim 3: Improvement Compare the gait objective of metabolic energy minimization to muscular effort minimization

Many studies suggest that humans minimize their metabolic energy expenditure during locomotion. If so, predictions should be more accurate when they minimize metabolic energy expenditure instead of an objective related to effort, which is used for aim 1 and 2. Therefore, models of metabolic energy expenditure are compared to experimental data of metabolic cost to select a metabolic energy expenditure model that could be an objective in predictive gait simulations. These models are then used to find a predictive gait simulation that minimizes metabolic cost, which are compared to a predictive gait simulation that minimizes effort.

Aim 4: Improvement Propose an approach to solve predictive simulations in a stochastic environment and implement it to explain certain behaviors that are seen in human movement

A stochastic environment has some uncertainty in the dynamics. Humans always have some uncertainty in their control and in their environment. However, current predictive simulations assume a deterministic environment and deterministic control, without uncertainty. Humans take into account uncertainty when planning their movements, and so should predictive simulations. A solution method is proposed that can take into account uncertainty in a predictive simulations. This method is applied to several problems, with the ultimate goal to see if co-contraction of the upper leg muscles on the prosthesis side is

present due to uncertainty in the environment. This is computationally a hard problem to solve due to the complexity of the problem.

1.2 Organization of This Dissertation

First, chapter II introduces several concepts that are important for this thesis. This chapter will explain terms that are used throughout the dissertation, as well as concepts that were used in several chapters. This chapter first gives an overview of normal human gait, and discusses adjustments in TTA gait. Then, some background information is given on lower leg prostheses, both active and passive. This is followed by an overview of human modeling studies of gait. A general description of the trajectory optimization problem is presented, which is used to find the predictive gait simulations. Finally, the two dimensional musculoskeletal model is introduced that is used throughout this thesis. The multibody dynamics are described, as well as the model used to find the force in the muscle.

Chapter III presents how aim 1 was achieved. Joint moment symmetry was analyzed by adding an objective to the optimization problem. By changing the weights between this objective and the original one of effort and tracking, different levels of joint moment symmetry were created. It was found that adding a little symmetry reduced joint contact forces in the knee and hip on the intact side, while it increased the joint contact force in the knee on the prosthesis side. This might reduce the occurrence rate of osteoarthritis on the intact side and of loss of bone mineral density on the prosthesis side.

Chapter IV describes the study performed to meet aim 2. The alignment study was performed on a recently developed three-dimensional musculoskeletal model. The prosthesis alignment was changed by changing the multibody dynamics at the knee. Statistical tests showed that the alignment affected the hip angles, the knee and hip reaction force on the intact side, the knee abduction moment on the prosthesis side, and the metabolic cost. It was shown that a flexion alignment of the prosthesis might be advantageous because the reaction loads and the metabolic cost is lower. Also, it was found that stress on the skin could

be reduced by changing the alignment in the frontal or transverse plane, without affecting other parameters too much.

Chapter V details the study that was carried out for aim 3. Seven models of metabolic energy expenditure were compared using pulmonary gas exchange data of walking at two speeds, at different inclines. Three models were selected as objective in the predictive gait simulations due to their high correlation with the pulmonary gas exchange data, while a fourth model was chosen due to its widespread use in previous work. The predictive gait simulations found with metabolic energy minimization were characterized by the fact that not all lower leg muscles were used, while the joint angles were more realistic, and the joint moments were less realistic than a predictive gait simulation that minimized effort.

Chapter VI introduces a novel approach to take into account noise in predictive simulations, which was used to meet aim 4. The approach optimizes the trajectory over a number of noisy gait cycles, instead of a single deterministic one. The method was validated on a classic pendulum swing-up problem. Then, it was used to show that co-contraction was optimal in certain tasks in a stochastic environment, and that in gait nonzero foot clearance is optimal in a stochastic environment. Finally, it is attempted to analyze the effect of environmental uncertainty on TTA gait. The results indicate that co-contraction in the upper leg of a person with a transtibial amputation can be explained by the uncertainty, but this result should be verified with improved methods.

1.3 References

- [1] K Ziegler-Graham, EJ MacKenzie, PL Ephraim, TG Travison, and R Brookmeyer. Estimating the prevalence of limb loss in the United States: 2005 to 2050. *Archives of Physical Medicine and Rehabilitation*, 89(3):422–429, 2008.
- [2] ED Lemaire and FR Fisher. Osteoarthritis and elderly amputee gait. *Archives of Physical Medicine and Rehabilitation*, 75:1094–1099, 1994.

- [3] PA Struyf, CM van Heugten, MW Hitters, and RJ Smeets. The prevalence of osteoarthritis of the intact hip and knee among traumatic leg amputees. *Archives of Physical Medicine and Rehabilitation*, 90(3):440–446, 2009.
- [4] T Royer and M Koenig. Joint loading and bone mineral density in persons with unilateral, trans-tibial amputation. *Clinical Biomechanics*, 20(10):1119–1125, 2005.
- [5] VS Nelson, KM Flood, PR Bryant, ME Huang, PF Pasquina, and TL Roberts. Limb deficiency and prosthetic management. 1. decision making in prosthetic prescription and management. *Archives of Physical Medicine and Rehabilitation*, 87(3):3–9, 2006.
- [6] H Linde, ACH Geurts, CJ Hofstad, Klaas Postema, JH Geertzen, and J van Limbeek. A systematic literature review of the effect of different prosthetic components on human functioning with a lower limb prosthesis. *Journal of Rehabilitation Research and Development*, 41(3):555–570, 2004.
- [7] AJ van den Bogert, M Hupperets, H Schlarb, and B Krabbe. Predictive musculoskeletal simulation using optimal control: effects of added limb mass on energy cost and kinematics of walking and running. *Proceedings of the Institution of Mechanical Engineers, Part P: Journal of Sports Engineering and Technology*, pages 1–11, 2012.
- [8] AD Koelewijn and AJ van den Bogert. Joint contact forces can be reduced by improving joint moment symmetry in below-knee amputee gait simulations. *Gait & Posture*, 49:219–225, 2016.
- [9] FC Anderson and MG Pandy. Dynamic optimization of human walking. *Journal of Biomechanical Engineering*, 123(5):381–390, 2001.
- [10] RH Miller, SCE Brandon, and KJ Deluzio. Predicting sagittal plane biomechanics that minimize the axial knee joint contact force during walking. *Journal of Biomechanical Engineering*, 135(1):011007, 2013.

- [11] JEA Bertram and A Ruina. Multiple walking speed–frequency relations are predicted by constrained optimization. *Journal of Theoretical Biology*, 209(4):445–453, 2001.
- [12] RH Miller. A comparison of muscle energy models for simulating human walking in three dimensions. *Journal of Biomechanics*, 47(6):1373–1381, 2014.
- [13] JT Betts. Survey of numerical methods for trajectory optimization. *Journal of Guidance, Control, and Dynamics*, 21(2):193–207, 1998.
- [14] M Posa and R Tedrake. Direct trajectory optimization of rigid body dynamical systems through contact. In *Algorithmic Foundations of Robotics X*, pages 527–542. Springer, 2013.
- [15] AK Silverman and RR Neptune. Muscle and prosthesis contributions to amputee walking mechanics: a modeling study. *Journal of Biomechanics*, 45(13):2271–2278, 2012.
- [16] M Ackermann and AJ van den Bogert. Optimality principles for model-based prediction of human gait. *Journal of Biomechanics*, 43(6):1055–1060, 2010.

CHAPTER II

BACKGROUND INFORMATION

This chapter introduces and reviews several concepts that are used throughout this dissertation. The goal of this thesis is to apply predictive simulations towards design of lower-leg prosthesis and to improve the predictive simulations. Therefore, this chapter will introduce human gait in section 2.2. This section will introduce healthy human gait and the adaptations made by persons with a transtibial amputation. This is followed by an overview of lower-leg prosthesis research in section 2.3. Then, section 2.4 will introduce human modeling studies of gait and show different applications of such studies. The final two sections will be more specific for the current research. Section 2.5 introduces trajectory optimization problems. These problems are solved to obtain predictive simulations. This section will give an overview of solution methods of trajectory optimization methods and explain the method that will be used in this dissertation. Finally, section 2.6 introduces the sagittal plane musculoskeletal model that is used throughout this dissertation, except in chapter IV.

2.1 Terms and Definitions of Human Motion

Firstly, it is important that the reader understands the terms and definitions that describe human motion and that will be used in this thesis. Human motion is three-dimensional, but can be analyzed in two dimensional planes. Figure 1 shows the planes that are commonly used. The red and yellow plane show the sagittal plane, through the center of the body and

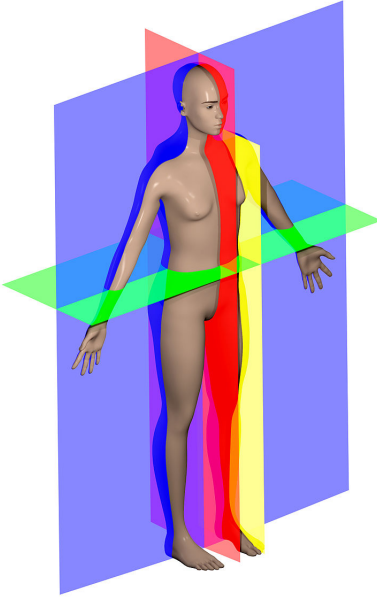


Figure 1: Sketch of human planes that are used to describe motion. The yellow and red planes show the sagittal plane, the blue plane is the frontal plane, and the green is the transverse plane. Copied from [1] with permission.

the center of the left leg, respectively. This plane is where most movement happens during gait. It is defined by an axis in the direction of the gait and another pointing from the toe to the head. The transverse plane is shown in green, and can be seen as the top view. The third plane, shown in blue, is the frontal plane.

To describe the location of part of the human body, anatomical terms of location are used. According to the Oxford English dictionary, a part of the human body that is distal is located further away from the center of mass, while a proximal part is located closer. Lateral defines a segment further away from the center of the body in the frontal plane, while medial describes a part closer to the center of the body [2].

Human motion is described by anatomical terms of motion. Flexion describes motion that decreases the angle between the segment and the connected, proximal segment. Extension is the opposite motion. These motions happen mostly in the sagittal plane. Abduction and adduction happen in the frontal plane. Abduction describes the motion that increases the distance between the segment and the center of the body, while adduction describes the

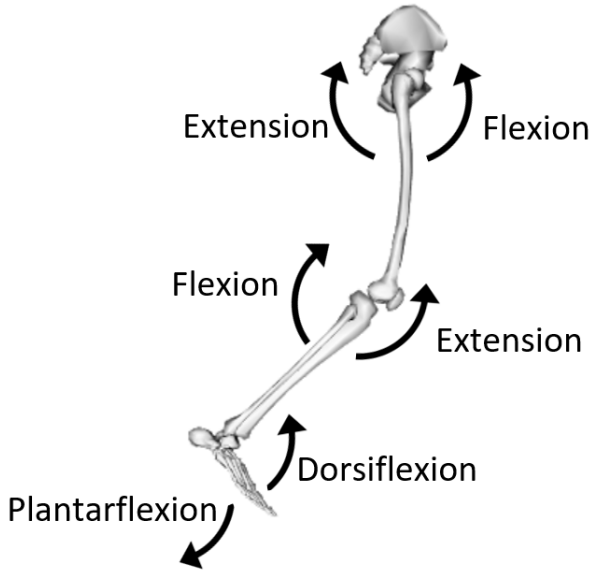


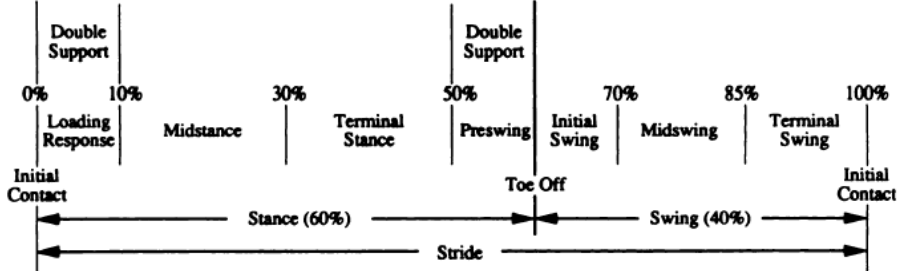
Figure 2: Illustration of the motion directions of the hip, knee and ankle in the sagittal plane.

opposite motion. Finally, internal and external rotation describe rotation of the frontal part of a segment towards or away from the axis of the body [2]. These rotations happen mostly in the transverse plane.

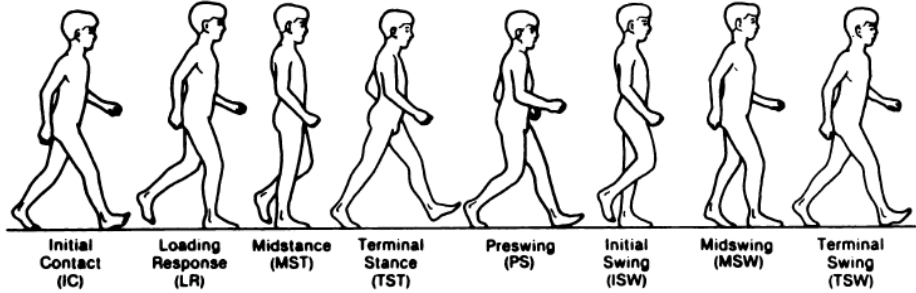
Figure 2 illustrates the motions of the leg in the sagittal plane. Flexion in the hip is described as the motion of the femur towards the belly, while extension is the motion of the femur towards the back. In the knee, flexion is the backwards motion of the lower leg, while extension straightens the leg. For the ankle, different definitions are used. Plantarflexion describes the motion where the forefoot move away from the tibia, while dorsiflexion describes the motion of the forefoot towards the tibia. Pronation describes the rotation of the foot such that the lateral part moves upwards, while supination describes the opposite motion [2].

2.2 Human Gait

Human gait can be described using many different parameters: spatiotemporal parameters describe the parameters that are a function of time or distance walked, such as stance time and swing time, gait kinematics describe the joint angles during a gait cycle, and gait



(a)



(b)

Figure 3: Overview of phases in the gait cycle. Copied from [3] with permission of Wolters Kluwer Health, Inc.

kinetics describe the joint moments, as well as joint work and power during a gait cycle. This dissertation mainly focuses on the motion in the sagittal plane (except in chapter IV). Therefore, this review of human gait focuses on the sagittal plane.

Figure 3 shows a schematic representation and a sketch of a person during a gait cycle. A gait cycle consists of one stride, in which there is a stance phase and a swing phase. The stance phase consist of approximately 60% of the gait cycle, while the swing phases is the other 40%. This means that in 20% of the gait cycle, both feet are on the ground, which is called double support [3].

A gait cycle starts at initial contact, or heel strike. After the heel makes contact with the ground, weight is shifted from the previous stance leg to the new stance leg in loading response, which will be called initial stance in this dissertation. After initial stance, the phase called midstance starts, where the weight shifts forward in the foot. Then, in late, or terminal stance the heel starts coming off the ground and the weight is shifted back to the other leg in preswing. This is followed by push-off, where the leg is pushed off the ground

and into swing. The swing phase consists of initial swing, where the swing is controlled by muscles, midswing and terminal swing, where the person prepares for contact. This phase ends at the next heel strike [3].

Figure 4 shows the mean and one standard deviation of the ground reaction forces (GRFs), joint angles, and joint moments of healthy gait from published measurements [4]. The horizontal GRF is characterized by a braking force in the first half of stance, and an accelerating force in the second half, which are almost equal but opposite. The vertical GRF has a characteristic shape with two peaks and a trough, one peak at about 20% of the gait cycle, where the weight is shifted to the new stance leg, and one during push-off, at 50% of the gait cycle.

The ankle angle (bottom left in figure 4) has a small dorsiflexion angle at heel strike. The ankle plantarflexes until the complete foot is on the ground. Then, the ankle dorsiflexes during stance, towards the peak dorsiflexion angle right before push-off. During push-off, the ankle plantarflexes again. During swing, it moves back to a small dorsiflexion angle. The knee is extended maximally just before heel strike. Then, a peak flexion angle of about 20 degrees is reached between 10-20% of the gait cycle. The knee extends again in late stance, before it is flexed during the swing phase, to an angle of over 60 degrees. In late swing, the knee extends again to prepare for heel strike. The hip achieves peak flexion during heel strike. Then, the hip extends during stance, while the upper body moves forward, to a peak extension angle at push-off. During swing, the hip flexes again to move the leg forward and prepare for the next heel strike.

The ankle has a small dorsiflexion moment during heelstrike (bottom right in figure 4). During stance, the moment increases, first sharply, then less sharp from about 25% of the gait cycle, until the peak plantarflexion moment is achieved at about 50% of the gait cycle, and reduces to 0 during push-off. The knee moment is flexion at heel strike, and reaches its peak extension at 20% of the gait cycle. Then, the moment decreases again and becomes flexion right before push-off. During push-off, the knee moment has a second, smaller

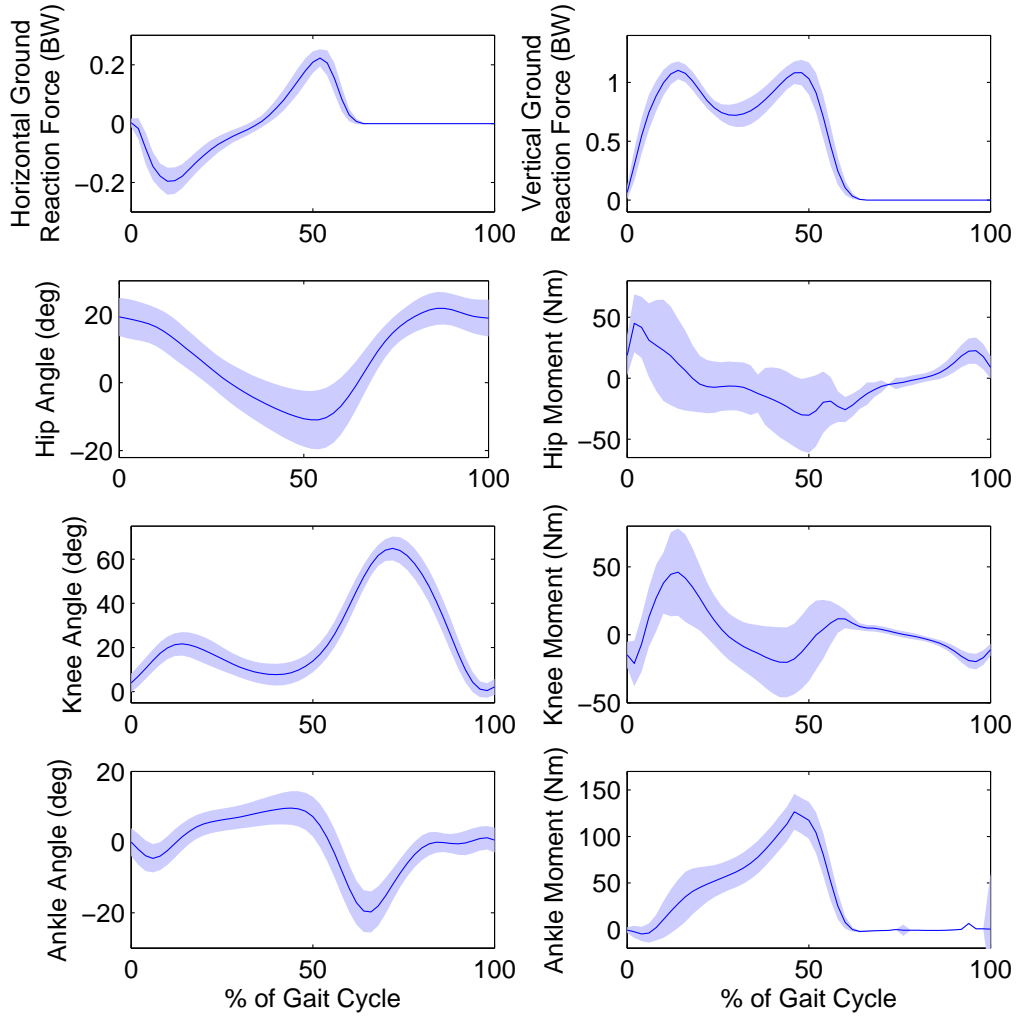


Figure 4: Normal ground reaction forces, normalized to body weight (BW) (top graphs), joint angles (left), and joint moments (right) of a gait cycle, starting at heel strike. Mean and ± 1 SD of data for a person of 75 kg, as recorded by Winter [5]. Following Winter's convention, for the knee and hip, flexion angles and extension moments are positive. For the ankle, a dorsiflexion angle and plantarflexion moment is positive.

extension moment peak to control knee flexion and stop the leg from swinging forward [5]. The hip moment has an extension moment in initial stance to absorb energy. Then, this moment decreases and becomes flexor to reverse the direction of movement for the hip. The peak hip flexion moment occurs during push-off and swings the leg forward, and late in the swing phase an extensor moment decelerates the swinging leg again [5].

2.2.1 Adjustments in Gait of Persons With a Transtibial Amputation

There are two main reasons for amputation: cardiovascular disease, due to diabetes, and trauma. A smaller group of patients receive an amputation due to other causes such as cancer. Patients with a traumatic amputation are generally younger, and are otherwise healthy, while patients with cardiovascular disease are older and will have other health issues related to their disease.

The muscles in the calf provide up to 80% of the mechanical power required for walking [6, 7]. A prosthesis cannot restore all lost function, and compensation is required in both legs to be able to walk. Lower-leg prostheses especially cannot take over the bilateral function of the Gastrocnemius. This muscle crosses both the knee and ankle and can transfer energy from one joint to the other. This function is lost with an amputation [7].

In gait of persons with a transtibial amputation (TTA gait), the legs are asymmetric, since there is a healthy ankle on the intact side and a prosthesis on the prosthesis side. Several adjustments are reported in the spatiotemporal parameters. The stance time is smaller in the prosthetic limb, and longer in the intact limb [8–14]. The walking speed decreases [9, 15, 16], the step length decreases [15] and the double limb support time increases [15]. These three adjustments are probably used to reduce the forces in the intact leg [15], since the loading is higher on the intact side than on the prosthesis side [11, 17–19]. Also, compared to the prosthetic limb, the intact step length is smaller, which is related to the longer support time and shorter swing time [14].

The kinematics are also adjusted in gait of persons with a transtibial amputation (TTA

gait). The joint angles are less symmetric than in normal gait [8]. The peak hip flexion angle is larger on the prosthesis side [9, 10]. Peak knee flexion is higher in the intact limb [9, 20]. Also, the range of motion in the knee on the prosthetic side and the prosthetic ankle is lower than in healthy controls or in the intact leg [10].

Similar to the loading in the leg, which is lower on the prosthesis side and higher on the intact side [11, 17–19], the ground reaction force is generally higher on the intact side than on the prosthesis side [11, 15, 17], though this depends on the prosthetic foot that the participants used [18]. Due to the larger forces in the intact side, more work is performed on this side than on the prosthesis side [9]. However, the loading in the intact side is not higher than in controls, since the walking speed is lower [8].

An important adaptation is made in the peak knee extensor moment on the intact side (see graph of knee moment in figure 4). In TTA gait, this moment can change into a flexor moment [14], while other studies report a smaller [9], or a normal extensor moment [9, 10]. On the intact side, the extensor moment is larger [9]. The increased loading on the intact side is also seen in the knee work, which was lower in the stance phase. [20]. Also, less power is generated in the knee [21]

Different adaptations have been reported for the hip moment, though there is a consensus that the peak moments increase. Some report that the extensor moment is higher on the intact side [22, 23]. However, Barr et al. report that the extensor moment on the prosthesis side is twice as high as the moment on the intact side [14]. Bateni and Olney report that the extensor moment on the prosthesis side is higher or normal, and that the extensor moment on the intact side is higher [9]. Furthermore, the flexor moments are higher on the intact side, which was shown using subject tests [24] and in simulation [25]. Work is higher in both legs during early stance [22, 23, 26].

The muscles on the prosthesis side also show several adaptations. Co-contraction is reported in the muscles of the upper leg compared to the intact side [12, 27, 28], and compared to a healthy control leg [21, 29, 30]. Due to the absence of the ankle muscles

on the prosthesis side, the hip muscles become more responsible for propulsion [24, 29]. Also, the Gluteus Maximus on the intact side is active longer [31, 32].

2.2.2 Energy Expenditure in Gait of Persons with a Transtibial Amputation

Different results have been reported about energy expenditure in TTA gait. Initially, most studies reported an increase in energy expenditure compared to able-bodied walking [13, 32–34]. For example, persons of over 40 years old walked 22% slower than normal, while on average the oxygen consumption increased 25% [35]. More recently, it was found that persons with a lower-leg amputation, who are otherwise fit and healthy, do not expend more energy than matched controls, despite often having secondary injuries [36, 37]. A recent simulation study suggested that this is related to the fact that these patients do not lose any muscle mass in the upper leg on the prosthesis side, and on the intact side [38].

The importance of fitness level was known already before this study. An earlier study showed that 40% of variation in energy expenditure between patients could be explained by fitness level [39]. Additionally, patients with an amputation due to a cardiovascular disease generally expend more energy [40–42] and have a slower walking velocity [41] than (often younger and fitter) patients who have lost their leg due to cancer or trauma. This can be due to decreased fitness levels, but also due to secondary health issues that cause higher than normal metabolic cost [33, 43].

Several parameters have been studied to analyze how a prosthesis could be made as energy-efficient as possible. It is known that energy expenditure correlates negatively with length of the residual limb [33, 35, 39], so it is desired to keep as much of the healthy leg as possible during surgery. Additionally, the weight and weight distribution of the prosthesis have been studied [13, 39]. It was found that especially the weight distribution is important, and that energy expenditure is lowest if most of the weight is located proximally [39]. The weight does not influence the energy expenditure up to a certain level [13, 44–46], but a weight as large as the original leg is undesired [13].

One possible reason for the increase in metabolic cost is the step-to-step work at push-off on the prosthetic side, which was found to be higher for persons with an amputation than for healthy control [47]. Donelan et al. [48] found that when the stance leg switches, the center of mass velocity should change direction. This velocity is changed most efficiently when the trailing leg generates a push-off force, and more work is required when the hip is used to generate the change in the velocity direction. However, after an amputation, the push-off of the ankle is lost, so this hip strategy cannot be avoided by persons with an amputation [47]

2.2.3 Health Issues in Gait of Persons with a Transtibial Amputation

Several health issues are more prevalent in persons with a transtibial amputation than in healthy persons, such as osteoarthritis in the knee and hip, especially on the intact side, osteopenia/porosis (loss of bone mineral density (BMD)) on the prosthesis side, and back pain [49]. These health issues do not increase with activity level [49].

These health issues are suspected to be related to an uneven force distribution between the two legs [15, 49]. When a prosthesis is fitted correctly, the forces in both legs are similar [8, 49]. However, small changes can already be degenerative in the long term. Therefore, a badly fitted prosthesis, which causes the forces to be uneven, is detrimental to gait and activity level of patients [17, 49].

Osteoarthritis is the degeneration of the cartilage in the joint, which leads to pain, decreased function, increased stiffness and a decreased ability to absorb shock [49]. The incidence of osteoarthritis is larger on the intact side compared to healthy individuals [49, 50], but patients with a lower-leg amputation are at higher risk of developing osteoarthritis in the hips of both legs [49, 50] and knee on the intact sides [49, 51]. In the intact knee, the risk of developing osteoarthritis does not increase with body weight, but it does with an increased force [49]. The increased force leads to a 45% greater BMD on the intact side than on the prosthesis side [49, 52]. The chances of developing osteoarthritis in the

hip is three times higher on the prosthesis side, and six times higher on the intact side than healthy persons [49].

Osteopenia refers to a BMD of one to 2.5 times the standard deviation below normal, while osteoporosis refers to an even larger loss of BMD [49, 53]. People with reduced BMD are at risk for bone fractures [49]. Several studies report an increased incidence of osteoporosis on the prosthesis side [49, 50, 54]. Causes for the loss of BMD could be disuse leading to decreased muscle mass, immobilization of the leg in the socket, lack of exercise, or the decreased vertical loading on the prosthesis side [49, 50]

Back pain can be caused by a poor prosthesis fit, or alignment, an uneven leg-length, an abnormal posture, the length of the stump, and due to the lack of fitness. However, since many persons, healthy and disabled, report back pain at some time during their lives, it is unclear exactly how much higher the risk of developing back pain is, since it is possible that patients who report back pain would have also developed back pain if they had not lost their leg [49].

2.3 Lower-leg prostheses

After a transtibial amputation, a person relies on a prosthesis to regain the ability to walk. A prosthesis consists of several parts, the socket, the foot and ankle joint, and a connector part. Patients with a transtibial amputation are mostly prescribed a patellar-tendon-bearing (PTB) socket, which was designed in 1959 at the University of California [31]. This type of socket is created by casting the shape of the stump in plaster and molding a plastic shell that fits around the stump exactly. Before the PTB socket was developed, the socket was excavated from wood, or shaped from metal, which were skills that were difficult to learn, or mold with leather, which would deform under load [55]

Prosthetic legs have three functions: they have to replace the functions of the leg for several activities, they have to be comfortable to the wearer, and they have to look as much as possible like a healthy leg [56]. Ideally, a prosthesis is designed that can restore all

the function that is lost with the lower leg, but the main aim of the prosthesis is to regain the ability to walk. For that, prosthetic legs have to provide stability and compensate for the lost movement and muscle action to reduce the additional demands on especially the proximal joints [31]. Depending on the cause of amputation, patients can have different additional requirements for their prosthesis, and respond differently to different feet [57].

Current prostheses can be split up into two main categories: those that do not have an external source of power, passive prostheses, and those that have some external source of power, active prostheses. For slower speeds, the ankle dissipates energy, so passive prostheses should be able to restore walking function. However, at higher speeds, larger than 0.9-1.3 m/s, the ankle provides energy, and an active element would be required to restore function [58, 59].

2.3.1 Passive Prostheses

Passive prostheses can be split up into two types: ones that have a rigid ankle, or conventional feet, and so-called energy storage and return (ESAR) prostheses. These use a spring in the ankle to absorb energy during stance and subsequently release this energy to aid push-off. This restores about half of the energy and peak power that is provided by the muscles in a healthy ankle [9, 10, 25].

Conventional feet were designed to restore basic walking function. It is still recommended to prescribe these feet to patients that walk slowly, often elderly patients with a cardiovascular disease [60]. Two types are commonly prescribed to patients, the solid ankle cushioned heel (SACH) foot and the single axis foot [57]. Multiple axis feet, which allow motion in the sagittal and transverse plane, are available as well [61].

A SACH foot has long been the industry standard foot with a rigid ankle [32, 57]. It consists of a rigid keel, a cushioning heel, and a covering of rubber that is shaped to look like a healthy foot [61]. The cushioned heel allows for plantarflexion during heel strike, while its flexibility is adjusted to best fit the patients' need [61]. The rigid keel

provides stability during mid-stance, but there is little dorsiflexion, or aid in push-off [57]. It is possible to manufacture a foot for several types of shoes, ranging from flat heeled to high-heeled shoes [61]. This type of foot does not have a rotational axis, but it is able to withstand transverse and frontal plane stress, which allows the patient to use it on uneven terrain [61]. However, due to the lack of ankle axis, a large force is required to put the foot flat on the ground during stance [61].

The single axis foot has been around for longest [61]. The single axis foot is a wooden foot with a rotational joint at the ankle in the sagittal plane, that allows for a smaller than normal range of motion. The movement is constrained using rubber bumpers, which can be stiffer or more flexible depending on the walking patterns of the subject [57, 61]. It is also possible to adjust the resting angle to allow the user to wear heels [61]. The rubber bumpers allow the foot to touch the ground faster than the SACH foot, but the foot is heavier [57]. Also, the gap between the upper and lower part allows dirt to enter the prosthesis, which limits its durability, the prosthesis can become noisy over time, and the range of motion is not large enough to enable walking on slopes [61].

A comparison of electromyography (EMG) signals in patients wearing a SACH and a single-axis foot did not show any differences on the intact side, but the hamstrings and vasti were active longer on the prosthesis side, especially when wearing the SACH foot, likely due to the lack of dorsiflexion [31].

Examples of multiple axis foot are the Greissinger multi-axis assembly and the Mauch hydraulic ankle [61]. The advantage of these feet are that their range of motion is larger, which allows for walking on more difficult surfaces. The Mauch foot is lightweight and has an oil-filled chamber that can adapt automatically to different slopes, while the Greissinger foot is heavy. However, patients will still prefer this type of foot over single-axis feet or SACH feet on slopes or uneven terrains [61].

However, persons with an amputation desire to participate in sports, which increases the demands on the prosthesis. The SACH foot is unable to return energy due to fatiguing

of the materials [62]. Therefore, ESAR feet were developed. These prosthetic feet store energy during stance and release this energy during push-off [32, 57]. The first ESAR foot, the Seattle foot, was developed in 1981 [57]. ESAR feet are made of some flexible material in a shell of polyurethane [57]. The flexible material compresses during the stance phase, when the ankle dorsiflexes. Then, the stored energy is released during push-off, when the ankle dorsiflexes. See Versluys et al. [57] for an overview of existing ESAR feet.

ESAR feet have been developed further in recent years to improve their performance. One problem with ESAR feet is that the spring stiffness at heel strike is high. This high stiffness creates difficulty bending, which is different from the behavior of a normal ankle joint. Therefore, a prosthesis was designed to have a similar loading response to a biological ankle, which reduced metabolic cost of walking 4%-12% compared to regular ESAR feet [63]. Another design used an active microprocessor controller to control the energy storage and timing of the return. It was possible to store more energy, especially in 0%-20% of the stance, which allowed the push-off power and work to be similar to the intact leg. However, despite requiring less work on the center of mass, the metabolic cost did not decrease, possibly to some unknown gait compensation [64].

Differences between conventional and ESAR feet

ESAR feet can reduce the impact on the intact side and thus the first peak in the GRF, while the knee flexion moment on the intact side increases [49]. The SACH foot tends to put more force on the intact leg and increases knee flexion [65]. Rollover is more stable as well for ESAR feet [49, 65]. It was found that compared to a conventional foot, an ESAR foot will provide more power and work [14, 22] and yield a larger range of moment in the prosthetic ankle [42, 65, 66] as well as a larger peak plantarflexion moment [42], a larger peak ankle dorsiflexion moment [14, 32, 65] due to the increased range of motion [67], a knee extension torque during stance instead of a flexion torque (though still smaller than normal) [67], a smaller GRF peak on the intact side [15, 18, 42, 67], and a larger propulsive

force on the prosthesis side [67].

However, there was no change in power output of the knee and hip on the prosthesis side [22], the gait symmetry in peak GRFs [63] or stance and swing time [32], the self-selected walking speed [14, 42, 65], EMG recordings with surface or needle electrodes [67], and the metabolic cost [15, 32, 41, 42, 65, 68]. Snyder et al. [18] did find a different walking speed between the SACH and Flex-foot, but not for four other feet that were tested. Torburn et al. suggest that the lack of improvement of walking with an ESAR foot is because the energy that is added by the foot is absorbed by the shank [32].

Several studies did find improvements of ESAR feet for these parameters in certain cases. Casillas et al. [60] found that metabolic cost of walking did decrease, especially at higher velocities, for traumatic amputees who used the Proteor foot in level, uphill and downhill walking. Nielsen et al. [34] found a decrease in energy expenditure at greater velocities. Colborne et al. [69] found that children (mean age 13 year old) expended less energy with an ESAR foot than with a conventional foot. Hsu et al. [70] found lower energy expenditure, but this prosthesis had a shock absorbing pylon in addition to the energy storage and return capability. Therefore, despite no overall advantage, an ESAR foot might be advantageous for a subgroup of patients [67]

Several parameters have also been studied without a consistent result. For example, several studies found a larger second peak in the vertical GRF with an ESAR foot, due to the larger energy release by the prosthesis, while other studies were not able to confirm this result [71]. Also, the increased ankle range of motion, and peak dorsiflexion angle that is reported in many studies could be due to the design of the SACH foot, which is usually used as the conventional foot. The SACH foot does not have an axis at the ankle, which limits movement but increases stability [41, 71]. A conventional foot with an axis at the ankle does allow for a larger range of motion [71]. However, the increased stability might be beneficial for patients who suffer from neuropathy due to diabetes [60, 71].

Despite the small objective benefit of ESAR feet over conventional feet, patients, clin-

icians, and prosthetist all prefer ESAR feet [32, 67, 71]. Many subjective studies found that patients prefer a ESAR foot, especially at higher velocities [34], because of a perceived higher walking velocity [32], while the cosmetics are important as well [32]. Patients report similar or higher gait quality, stability, as well as similar or less pain and skin problems [72, 73], and larger ankle motion [73]. Additionally, activities other than level walking, such as walking up and down the stairs, up and down a slope, on uneven ground, and jogging and dancing are easier with an ESAR prosthesis [67, 72, 74, 75]. One study did find a potential problem walking downstairs [72].

However, in a literature review, Hafner et al. [67] found little objective support for the perceived improvements. There is overall no significant increase in self-selected walking speed, though there is a trend of a higher velocity when walking with an ESAR foot. However, the difference is not clinically significant, meaning that the normal day-to-day variation in walking speed is larger than the reported increase. Similarly, despite a small difference in cadence, this was not clinically significant. However, a trend of increased stride length was clinically significant. This increase is caused by the increased flexibility of the prosthesis, which increased the step length on the sound side, and reduced gait asymmetry [67].

Hafner et al. [67] summarized that the changes between the conventional feet and ESAR feet are due to the flexible keel in the ESAR foot. This allows for more ankle motion, which increases the peak plantarflexion moment and decreases the vertical motion of the center of mass. This could explain the lower vertical GRF and the increased step length, which also increases the gait symmetry.

It should be noted that ESAR feet were designed to increase performance in different situations, such as walking on sloped or uneven terrain, or with varying speeds [36], while gait studies often focus on level walking on even terrain. As said before, subjective studies have shown that users report that other activities than walking are easier with an ESAR feet, but little evidence collaborates these findings [67]. For example, Perry and Shanfield

[42] did not find an advantage in using an ESAR for stair climbing.

Different prostheses are advised to different subgroups of patients. For example, Barth et al. advise that the SACH foot is used by patients who require stability in late stance, that the S.A.F.E. II foot is prescribed to patients who are more active, the Seattle Lightfoot to patients with average activity level, and the Quantum or Carbon Copy II feet should be prescribed to patients who require protection of the sound limb [41]. Casillas et al. [60] advice a conventional, or SACH foot, for elderly patients with a slow walk, while an ESAR foot is more appropriate for patients who are active and walk fast.

2.3.2 Active Prosthesis

Active power is required to restore the function of the healthy ankle to provide 80% of the power in a gait cycle, while allowing for a similar to normal range of motion and joint moment [10]. An active ankle prosthesis with a motor that can give the same power as a healthy ankle would be too heavy and require a large battery [76–79]. Elastic elements can help reduce the power and energy requirements of the motor, and thus reduce the weight of the prosthesis [76, 79]. It also allows for energy regeneration by storing energy in springs [79].

Two active prosthetic ankles were developed based on pneumatic actuation. Klute et al. [80] built a prosthesis that was designed as an artificial muscle with a contractile element, damping element and tendon. The contractile element was powered by two parallel pneumatic actuators to generate close to the desired force. This was the first prosthesis that generated positive work, but it was not developed further or tested on a subject. Versluyts et al. [81, 82] also developed an active prosthesis based on pneumatic artificial muscles. This prosthesis requires a separate actuator for plantarflexion and dorsiflexion of the ankle [82]. The pneumatic actuators that were used have a favorable power-to-weight ratio for prosthesis applications [81]. The required push-off ankle torque was generated for two different speeds, using a tethered power source and a time-based feedforward controller [82].

Several prostheses have been developed using motors for actuation. The BiOM foot was the first commercially available foot that was active during stance [78]. It could power level walking and stair walking. Activating the Tibialis Anterior or Gastrocnemius enabled the user to switch between different controllers [78]. Hitt et al. [79] designed a prosthesis that could achieve a power amplification of 3.7, allowing for a smaller motor, while still providing power and movement similar to a healthy ankle. LaPre et al. proposed an active prosthesis that aligns the GRF with the tibia. This approach significantly reduced the sagittal plane moment that is present at the socket and stresses the skin of the residual limb, which could be painful and damage tissue [83]. Grimmer et al. developed another active prosthesis for both walking and running, and was able to match torque and movement of a healthy ankle up to 2.6 m/s, but was only tested on healthy individuals [76].

Several studies have compared active feet to passive feet, mostly using the BiOM foot. Gardinier et al. [84] found no significant difference in energy expenditure between the BiOM and a passive prosthesis. A prosthetist fitted the BiOM foot to each participant, but they had little time to adapt to the new foot. Participants who had more experience with the BiOM, or who were more active, benefitted more from the foot [84]. Herr and Grabowski compared the BiOM foot to a passive foot on five different walking speeds. The metabolic cost was lower with the BiOM foot for all but the lowest speed. Also, the preferred velocity was higher when participants wore the BiOM foot. The decrease in metabolic cost corresponded to the decrease in human work [7]. Mancinelli et al. also found a decrease in energy expenditure and an increase in power provided by the ankle when using the BiOM instead of a traditional passive-elastic prosthesis [85]. Quesada et al. [86] compared seven work conditions using a tethered active prosthesis. They found that despite a decrease in human work with an increase in prosthesis work, the metabolic rate was not affected.

2.4 Human Modeling Studies

The previous sections have mentioned many variables that are used in gait analysis. Some, such as energy expenditure or GRFs, can be measured, while many others, such as joint angles, moments, and muscle forces, cannot be measured. These can be calculated using a musculoskeletal model of the human. A musculoskeletal model describes the muscles, the skeletal geometry, and connections between bones (the joints) and between bones and muscles.

Several software packages can be used to develop a musculoskeletal model. Packages like OpenSim [87], SIMM/Dynamics Pipeline (Motion Analysis, Santa Rosa, CA, USA), or Anybody (AnyBody Technology A/S, Aalborg, Denmark) provide a complete rigid body model for the skeletal structure, and have muscle dynamics built in. One could also use a multibody dynamics package, such as MSC ADAMS (MSC Software, Santa Ana, CA, USA), or Autolev (OnLine Dynamics, Inc., Sunnyvale, CA, USA) to construct the multi-body dynamics model and create the muscle models separately. Finally, one could derive both the multibody and muscle model in any coding language by hand.

Human modeling studies are performed for multiple reasons. Models can be used to calculate parameters that cannot be measured at all, or only using invasive techniques. Other than that, models can be used to create simulations of human movements. The main goals for these simulations are to analyze the effect of an intervention such as a prosthesis or an ankle-foot orthosis, or to explain human movement. An overview is given on studies of these types, limited to studies about walking or running.

2.4.1 Studying Parameters that cannot be Measured

Some gait variables cannot be measured, or can only be measured by surgically implanting a measurement device, which is undesired. Several muscles, for example the Iliacus and the Psoas muscle, are located deeper in the body and therefore their activity cannot be measured using a surface EMG sensor. Also, knee reaction forces can be very

helpful to understand osteoarthritis and find methods of prevent this from occurring. Invasive methods can be used to record both: deep muscles can be measured with needle EMG sensors, and knee reaction forces can be measured after a full knee replacement with a sensing device. However, it is desired to develop methods to find these variables without requiring an invasive technique.

In non-invasive gait analysis, the measured variables are marker trajectories, GRFs, and possibly surface EMG and pulmonary gas exchange data. All other variables are estimated using these measurements. Joint angles can be determined with inverse kinematics (e.g., [87]) and joint moments can be determined using inverse dynamics (e.g. Winter's method [5]). The muscle forces can then be determined by solving a static optimization problem, forward dynamics to match the experimental data, using an EMG-driven approach [88], using computed muscle control (CMC) [87], or by solving a dynamic optimization problem that takes into account muscle dynamics [89], after which other variables, such as the knee reaction forces, can be determined. It is also possible to do these last two steps simultaneously using a more complex model of the knee [90, 91].

Studies in this field are mostly for clinical applications. For example, a good estimate of the reaction forces in the knee can help clinicians diagnose musculoskeletal and nervous system disorders and prescribe effective treatments [90]. Currently, the treatment decision is made on a subjective basis, and a patient could get a different treatment depending on what doctor they visit [92]. Musculoskeletal models will enable clinicians to explore treatment options before subscription and help them make a more informed decision [92]. Other applications are analysis of crouch gait in children with cerebral palsy [93, 94].

However, models are currently not accurate enough for clinical purposes. Therefore, many studies aim to improve predictions of knee reaction forces of musculoskeletal models. A grand challenge was created to predict a data set in-vivo knee reaction force measurements as accurately as possible [92]. Research for this challenge focuses on personalization of models [95, 96], since currently models are general, and locations of muscle

attachments to the bone, joint centers, and other anatomical landmarks are usually based on specimens [97], and on improvement of the methods, for example to find muscle forces and knee forces simultaneously [90, 91].

2.4.2 Analysis of Intervention

A second application of human models is to predict the effect of an intervention, such as a prosthesis or an orthosis, on gait. Then, the goal is to find a simulation of the desired movement with and without the intervention. These simulations are compared to find the effect of the intervention.

An example of an intervention is an ankle-foot orthosis (AFO). These are prescribed to persons who have lost muscle strength in their lower legs, for example after a stroke. However, it is unknown what stiffness, or range of stiffnesses, is optimal. Therefore, this study found gaits for a simple planar walking model with propulsion at the hip, with a varying stiffness at the ankle to simulate the AFO. It was found that there was a stiffness with optimal push-off timing [98].

Analysis of interventions are important for sports science, for example to study the effect of a newly developed piece of training equipment. Van den Bogert et al. [99] studied the effect of an added mass to the thigh, knee, shank, and foot. For every 100 g that was added to the foot, the energy cost of the running simulation increased 0.73%. The added mass mostly effected the peak force in the Hamstrings and Rectus Femoris, meaning that these muscles are trained when mass is added to the limbs while running [99].

Another intervention study analyzed if gait training could help reduce the risk of developing osteoarthritis by reducing the peak knee contact force. This study used a sagittal plane model with 11 degrees of freedom and nine muscles in each leg. Predictive simulations were solved for several objectives, such as minimal cost of transport, or minimal peak knee contact force. It was shown that with an increase in cost of transport of 11-14%, the peak knee contact force could be reduced 12-25% [100].

Millard et al. [101] analyzed if an exoskeleton could reduce the risk of lower back injury in a bend-grip-lift motion. The human, a box that was lifted, and the exoskeleton were modeled separately. Simulations were generated by solving an optimal control problem that minimized effort, the squared muscle activation. These simulations showed that the exoskeleton was able to decrease the peak lumbar joint moments, while the motion was performed faster. It was also found that different objectives yielded solutions where the exoskeleton was used in different ways, to support the wearer or to increase the strength [101].

2.4.3 Explaining Human Movement

Finally, human models can be used to explain human movement. People move in a way that is optimal towards a certain objective [102], however the exact objective is still unknown. Therefore, the goal of many studies is to find this objective, and explain healthy or impaired human gait by proposing a specific objective or comparing some. These simulations are created without using any data, but the result will be compared to behaviors that are seen in practice.

The earliest studies towards this goal handled the accuracy of the musculoskeletal model. Due to small computer power, much work was done to develop accurate models that were simple enough for the available computers. For example, it was shown that a model of a muscle should include the tendon to provide accurate predictions of muscle force [103].

A major milestone was reached by Anderson and Pandy [104], who created the first walking simulation that only minimized an objective related to energy expenditure, meaning that no data was used. After 10000 CPU hours of optimization a solution was found that resembled human walking reasonably well, since the joint angles were within one standard deviation of experimental data for most of the gait cycle, while the largest discrepancy was seen in the pelvis. Also, the pattern of the GRFs was normal, and so were the muscle excitation patterns. However, the solution was not periodic, and the metabolic energy

consumption was a lot higher than in normal human walking [104]. This paper does not mention the initial guess that was used in the optimization algorithm, while the choice of initial guess could influence the final solution significantly.

Later work also aimed to find a realistic walking or running motion by trying different objectives. For example, Ackermann and Van den Bogert found that a fatigue-like objective, related to a higher power of the muscle activation, predicts walking more accurately than an energy-like objective, which is related to activation linearly, as well as to the muscle volume [105]. Miller et al. applied different objectives, minimizing cost of transport, muscle activations, or muscle stress to find a running simulation. It was found that the cost of transport was lowest when cost of transport was minimized, but that the value of cost of transport was more realistic when the muscle activations were minimized. This objective also yielded a more realistic gait [106].

Mombaur and Clever aimed to find the true objective of human walking. They used a two-level optimization approach. In the high level optimization, the weights of several objectives, like minimal torque, head stability, step length, and step frequency, were optimized to minimize a tracking error between the simulation and recorded data, whereas on the lower level a simulation was found that minimized the weighted sum of those objectives. This was applied to data of six subjects. Different optimal weights were found for each, but there was a large correlation between them. The multi-objective functions that were found could then be applied to trajectory optimization in robots [107].

This type of research can also be useful to understand how humans might move in different environments. For example, Ackermann and Van den Bogert found that in an environment with low gravity, such as the moon, a skipping gait is optimal with respect to effort and fatigue objectives [108]. Song and Geyer showed that energy cost of walking increases for elderly persons mainly due loss of muscle strength and mass. Using simulations, they could individually simulate different adaptations that are seen in elderly persons and investigate the effect of specific adaptations [109].

2.4.4 Predictive Simulations

The last two applications use so-called predictive gait simulations, which are simulations that predict a gait cycle. Since humans minimize some energy-related objective in gait, a trajectory optimization problem can be solved to find a prediction of human gait. This requires a model of the human and a representation for energy expenditure.

Predictive simulations should not use any data when the aim is to explain human motion. However, when an application is analyzed, walking data is sometimes tracked to ensure that a realistic gait cycle is found. If data is tracked of a different condition (for example normal data in case of an impaired gait), the simulation is still called a predictive simulation. If data is tracked of the same motion that is performed in the simulation, the simulation is called a tracking simulation. The relative weight that is placed on effort versus tracking of data also defines the predictive quality of the simulation. Walking data that is tracked could include joint angles, joint moments, GRFs, and gait cycle duration, among others.

Model dimensioning is an important aspect of the study. If a tracking simulation is created, the model can be scaled to the height and weight of the person for which the data was taken. However, in case the study is predictive, there is no model for scaling purposes. The state-of-the-art approach for predictive simulations is to solve the predictive simulation for one person [99, 110–112]. However, recently predictive studies have used a number of so-called ‘virtual subjects’ [38], where the height and weight of the model are drawn from a distribution and simulations are solved for each ‘virtual subject’. Then, it is possible to perform statistical analysis and generalize the results to a broader population.

Simulation Studies of Gait of Persons with a Transtibial Amputation

Simulation studies have also been used to study TTA gait. This has been done both to analyze the intervention, or the prosthesis [113, 114], or to explain the movement [38]. These studies have all used a two-dimensional sagittal plane musculoskeletal model.

Fey et al. [113] studied the effect of different prostheses' stiffness. They recorded data for a nominal stiffness variables, and used simulated annealing to find simulations of TTA gait with different stiffness parameters. Their objectives were to minimize metabolic cost, knee force or an equally weighted sum of both. They found that when the toe and midfoot were stiffened, and the ankle and heel were made less stiff, it was possible to offload the Vasti muscle on the intact side, which would reduce the force in the knee, and thus the chance of developing osteoarthritis.

Handford and Srinivasan [114] solved predictive simulations using an objective of minimizing a combination of human metabolic cost and prosthesis power. They created a Pareto front (a set of optimal solutions) by varying the weighting between the objectives of human and prosthesis power. They found that it should be possible to walk with less metabolic cost than healthy individuals when sufficient power is provided by the prosthesis. Also, they found that an asymmetric TTA gait was more energy efficient than a symmetric gait.

Esposito and Miller [38] used predictive simulations to study why young and fit persons with a transtibial amputation do not expend more energy than healthy individuals. They solved predictive simulations of normal gait and TTA gait, with 0%, 10%, 20%, and 30% loss of muscle strength. The objective was to minimize a tracking error with normal data and metabolic cost for 25 virtual subjects. With a passive prosthesis, the metabolic cost was similar in normal gait and TTA gait in case of 0% loss of muscle strength. For an active prosthesis, it was possible to have similar metabolic cost up to 20% loss of muscle strength.

2.5 Trajectory Optimization

Predictive gait simulations are found by solving a trajectory optimization problem. Trajectory optimization is used in aerospace, robotics and other fields to find the control inputs that perform a task optimally with respect to some performance criteria. For example,

the procedure to change lanes on a highway could be optimized. A trajectory optimization problem could be defined to find the steering wheel angles that minimize the fuel consumption, or to finish the maneuver as fast as possible, for example. Using the steering wheel angles, the car follows a path of positions and velocities to switch lanes.

Dynamics and boundary conditions are important in trajectory optimization. The dynamics define how the system moves as a function of the state, and the boundary conditions define the start and end of the trajectory. Control inputs operate the system. Many acceptable control inputs exist that will move the system from the start to the end of the trajectory. A specific trajectory is preferred based on the performance criterion. The objective function defines this criterion [115].

An optimization problem is solved to find the preferred trajectory. An optimization problem can be described using optimization variables, an objective, bounds and constraints. The objective defines the performance criteria that decides which trajectory is best. The optimization variables are the variables that are altered to optimize the performance criteria. Bounds define the search space of the optimization variables. Constraints are similar to bounds, but placed on a function of the optimization variables, instead of the optimization variables themselves [116].

The objective can consist of two parts, the Lagrange term, which is integrated over the full trajectory, and the Mayer term, which is only present at the boundary conditions (the start and/or end point) [115]. The optimization variables are the control inputs, $u(t)$, and possibly the initial state, $x(0)$ and some other parameters p . Bounds can be used to limit the control input, and also to place limits on the start and end position. The constraints are the dynamics, since the system has to move according to the laws of physics, and optionally boundary constraints to define the start and end of the trajectory and path constraints, if for example a certain location should be visited somewhere in the trajectory [115, 116].

An optimization problem is described mathematically as follows:

$$\underset{x(t), u(t), p}{\text{minimize}} \quad J(x(t), u(t), p) \quad (2.1)$$

$$\text{Subject to:} \quad \dot{x}(t) = f(x(t), u(t), p) \quad 0 \leq t \leq T \quad (2.2)$$

$$g(x(t_k), u(t_k), p) = 0 \quad \forall k \in 1, \dots, N_g \quad (2.3)$$

$$c_{low(x)}(t) \leq x(t) \leq c_{upp(x)}(t) \quad 0 \leq t \leq T \quad (2.4)$$

$$c_{low(u)}(t) \leq u(t) \leq c_{upp(u)}(t) \quad 0 \leq t \leq T \quad (2.5)$$

$$c_{low(p)} \leq p \leq c_{upp(p)} \quad (2.6)$$

$$(2.7)$$

where N_g denotes the number of boundary and path constraints. Equation 2.1 denotes the objective, equation 2.2 denote the dynamics constraints at all time points, equation 2.3 denote the boundary constraints, and equations 2.4, 2.5 and 2.6 denote the bounds c on the state, input and parameters p , respectively. $x(t)$ and $u(t)$ denote the state and input at time t , respectively [116].

When a predictive gait simulation is solved in this dissertation, the system is a model of the human, and the dynamics describe how the different parts of the human interact with each other and the environment. The control inputs are torques if the model does not have muscles, or muscle stimulations if a musculoskeletal model is used. The objective is usually related to energy expenditure or muscular effort, and consists only of a Lagrange term. The optimization parameters are the human control inputs, and possibly some other parameters. These can be related to a prosthesis, for example. Dynamics constraints are derived from the model dynamics, and boundary constraints are used to ensure periodicity. Path constraints are not used.

The objective can be described as follows when only a Lagrange term is used:

$$J(x(t), u(t), p) = \frac{1}{T} \int_{t=0}^{t=T} c(x(t), u(t), p) dt \quad (2.8)$$

where $c(x(t), u(t), p)$ is a function that is evaluated at each time point.

2.5.1 Solution Methods

Three methods exist to solve trajectory optimization problems: dynamic programming, indirect methods, and direct methods. In dynamic programming, the Hamilton-Jacobi-Bellman equations are solved for the complete state space, which requires significant computational effort. A direct method analyzes the objective function itself to find the optimum, while an indirect method aims to find the optimum by looking at the derivative of the objective, and finds the optimum by setting the derivative equal to zero [116].

Indirect methods require the user to derive the Hamiltonian and its derivatives with respect to the states and inputs. This is time-consuming and would have to be redone for every problem that is solved. Also, it requires the user to estimate certain variables that are present in the optimization problem. However, these are not related to physical quantities, so this is very difficult. Some of these variables can also be ill-conditioned and very sensitive, which makes it very hard to solve the problem [116].

Therefore, a direct approach is used in this dissertation. Direct methods can be solved in three ways, using shooting, multiple shooting, and direct collocation. Shooting means that the trajectory is simulated from an initial point using the controls that are being optimized. In multiple shooting, a simulation is made separately for several parts of the trajectory, with constraints between the parts. Direct collocation does not use a forward simulation, but splits the trajectory into a number of collocation points, or time nodes, and replaces the differential equation that represents the dynamics with dynamics constraints [116]. All these methods are solved iteratively, where each iteration the optimization variables are updated until the objective cannot be improved any further.

In shooting, the optimization variables are the initial state, $x(0)$ and the control trajectories, $u(t), 0 \leq t \leq T$. During every iteration, the complete trajectory is simulated from the initial state, using the controls. This approach can be solved using gradient-based and

gradient-free algorithms. Gradient-based algorithms can handle constraints, but require the gradient of the objective, and the constraints. These can be found using finite difference method, but this requires an additional simulation of the full trajectory for each unknown. Gradient-free algorithms require constraints to be converted to a penalty in the objective. This method also requires many forward simulations, which is time-consuming [117]. For human gait, 10000 CPU hours were required to solve the predictive simulation [104]. A data driven initial guess could alleviate these issues [111]. However, this can affect the final solution. For example, Lin and Pandy found a predictive simulation that differed only very slightly from their initial guess [118], meaning that the optimization likely ended in a local optimum.

Another disadvantage of shooting is that the control input at the beginning of the trajectory has a much larger influence on the objective than a control input near the end of the trajectory. This creates numerical difficulties [117, 119]. This problem also makes it hard to find a periodic gait cycle [104]

Additionally, when constraints are converted to a penalty function, it is possible that an optimal solution is found without meeting the constraints, for example if the derivative of the objective is zero while the penalty function is nonzero. Also, the penalty functions will often conflict with the objective. Then, several optimal solution exists depending on the weighting of the different objectives. Therefore, a balance should be found manually between minimizing the objective and ensuring that penalty function is sufficiently close to zero.

Finally, by reducing the number of optimization variables, the problem becomes easier to solve and fewer simulations will have to be solved. Therefore, usually a small number of variables is used to find the muscle input. For example, Miller and his coworkers use only four [100, 111] or six [112] parameters per muscle to define the muscle excitations. Silverman and Neptune also use six [120], while Anderson and Pandy used 15 [104].

Multiple shooting is similar to shooting, except the simulations are performed over

parts of the trajectory. Constraints ensure that the final state of one part matches the initial state of the next part. This decreases the nonlinearity of the relationship between the optimization variables and the constraints and objective, and reduces the influence of the beginning of the trajectory on the objective. It also increases the number of optimization variables, since the unknowns are now the initial state of each part, as well as the controls, and the number of constraints. However, the Jacobian of the constraints will be sparse, meaning that most elements of the matrix are equal to zero, which increases efficiency of solving. Still, a numerical method (finite differences) is required to determine the derivatives of the objective and the constraints [116].

Direct collocation does not use forward simulation. Instead, the trajectory is split up into collocation points and constraints are defined between each two consecutive collocation points. These constraints ensure that the state and input at a collocation point yield the state at the next collocation point. The optimization variables are the states and inputs of each collocation point. The constraint Jacobian of the dynamics constraints can be derived analytically. A larger number of collocation points is required to get an accurate result, which creates a problem with a large number of variables and constraints. However, also in this case the constraint Jacobian will be sparse, and solvers can take advantage of that.

In this dissertation, direct collocation is used to solve trajectory optimization problems. The trajectory is discretized into N collocation points and the optimization is performed over the states and inputs of all the collocation points, $X = [x(1), u(1), \dots, x(N), u(N), p]$. The integral of the objective in equation 2.8 is replaced by a sum over the collocation points, and divided by N instead of T . The dynamics constraints are applied to each collocation point i , which ensures that the state and input of one collocation point yield the state of the next collocation point. The task constraints remain the same, but will be applied to the

collocation point j at the time t_h [116]. This yields the following optimization problem:

$$\underset{x}{\text{minimize}} \quad J([x(1), u(1), \dots, x(N), u(N), p]) = \frac{1}{N} \sum_{i=1}^N c(x(i), u(i), p) \quad (2.9)$$

$$\text{Subject to:} \quad \dot{x}(i) = f(x(i), u(i), p) \quad \forall i \in 1, \dots, N \quad (2.10)$$

$$g(x(j), u(j), p) = 0 \quad \forall j \in 1, \dots, N_g \quad (2.11)$$

$$c_{low(x)}(i) \leq x(i) \leq c_{upp(x)}(i) \quad \forall i \in 1, \dots, N \quad (2.12)$$

$$c_{low(u)}(i) \leq u(i) \leq c_{upp(u)}(i) \quad \forall i \in 1, \dots, N \quad (2.13)$$

$$c_{low(p)} \leq p \leq c_{upp(p)} \quad (2.14)$$

$$(2.15)$$

Many discretization methods can be used to approximate the dynamics, such as mid-point Euler, a trapezoidal method, or a Runge-Kutta method (see Betts [116]). In this dissertation, backward Euler (BE) is used. This is an implicit method that uses the state of the next time point to determine the state derivative \dot{x} of the current time point [116]:

$$\dot{x}(i) = \frac{x(i+1) - x(i)}{h} = f(x(i+1), u(i+1)) \quad (2.16)$$

where h denotes the time step. Note that an extra collocation point $N + 1$ was added to calculate the dynamics at the last collocation point. This discretization method improves the stability of the system because it adds numerical damping, which removes some energy from the system.

This problem yields a large-scale nonlinear optimization problem with a finite (but large) number of optimization variables, the objective (equation 2.9), and a finite number of constraints (equation 2.10 and equation 2.11). Such a problem can be solved with a gradient-based algorithm. Many solvers exist, such as SNOPT [121], IPOPT [122], GPOPS [123], WORHP [124] and several options within the MATLAB function `fmincon` (Mathworks, Natick, MA, USA).

IPOPT is used throughout this dissertation, since it is freely available, and a compiled version is available for use in MATLAB. Version 3.11.0 is used, since this version produces reproduceable results. Newer and faster versions exist, which take advantage of parallel computing. However, due to numerical differences resulting from parallel computing, the results were not always reproduceable.

Regularization

In chapter IV and chapter V regularization is used to aid the algorithm. This objective will favor solutions with smaller first derivatives, which are usually smoother. Smoother trajectories are more realistic for human gait. Then, an objective is added to minimize the integral of the squared first derivative of the trajectory:

$$J_{reg}(x, u) = \frac{W_{reg} N}{N_{st} + N_{con}} \sum_{i=1}^N \left(\sum_{s=1}^{N_{st}} (x_s(i+1) - x_s(i))^2 + \sum_{c=1}^{N_{con}} (u_c(i+1) - u_c(i))^2 \right) \quad (2.17)$$

where W_{reg} is the weight of the regularization term, N_{st} the number of states, N_{con} the number of controls. The regularization weight is chosen such that the objective J_{reg} is much smaller than the other objectives.

2.6 Human Model

Figure 5 shows the human model that is used throughout this dissertation. It was developed by Van den Bogert et al. [99]. It has seven segments: the trunk, which includes the head and the arms, and for each leg a thigh, shank and foot. All segments are connected using frictionless hinge joints, so there are nine degrees of freedom. Dimensions and inertial properties are taken from Winter [5]. The following generalized coordinates, q , are used to define the orientation of the model: the position and orientation of the trunk, and the hip angle, knee angle, and ankle angle in both legs. The ground is defined to have zero height.

Figure 6 shows the hierarchical structure of the model, which is used to find the dynam-

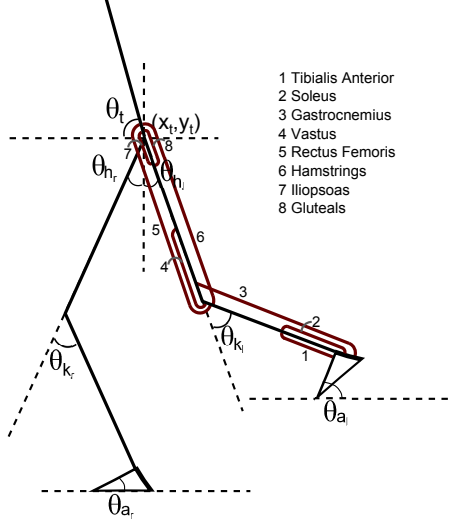


Figure 5: Human musculoskeletal model that is used in this dissertation.

ics equations. The orientation of each segment is described relative to its parent segment, which is shown higher in the tree, using the degree of freedom between the two segments. For example, the location of the left shank will be described relative to the left thigh using the knee angle. Using the hierarchy, the locations and velocities, v , of all segments can then be described as a function of the generalized coordinates only. Van den Bogert et al. [99] derived the dynamics equations with Autolev in the following form:

$$M(q(t))\ddot{q}(t) + C(q(t), \dot{q}(t))\dot{q}(t) + G(q(t)) = \tau(t) + J_c(t)^T F_c(t) + T_{pas}(t) \quad (2.18)$$

where $M(q)$ was the mass matrix, $C(q, \dot{q})$ contained the Coriolis forces, $G(q)$ the gravity forces, $J_c^T F_c$ the ground reaction forces, T_{pas} the passive joint torques, and τ was a vector of generalized forces. This system is second order, meaning that the acceleration is required to find the behavior of the system. This system is converted to a first order system with state $x(t) = [q(t) \quad \dot{q}(t)]^T$, where $q = [x_t \ y_t \ \theta_t \ \theta_{hr} \ \theta_{kr} \ \theta_{ar} \ \theta_{hl} \ \theta_{kl} \ \theta_{al}]^T$, and with state derivative $\dot{x}(t) = [\dot{q}(t) \quad \ddot{q}(t)]^T$. The first three elements of the generalized force vector, τ , are zero since these degrees of freedom were unactuated. The other six are provided by a torque controller or by the muscles shown in figure 5.

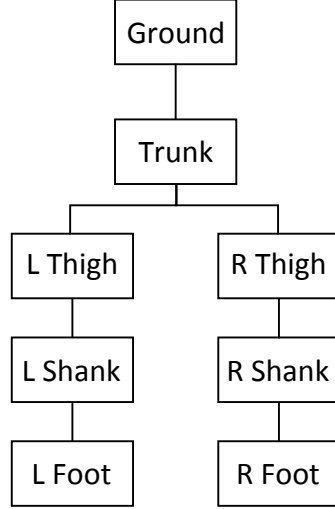


Figure 6: Hierarchical structure of the human model that is used to find the dynamics equations.

Eight muscles were modeled in each leg: the Rectus Femoris and Hamstrings were biarticular muscles between the hip and knee, and the Gastrocnemius between the knee and ankle (see figure 5). The Iliopsoas and Gluteals operated the hip, while the Vasti operated the knee. The Soleus and Tibialis Anterior operated the ankle. These muscles were modeled as three element Hill-type muscles with quadratic springs for the parallel and series elastic element. The contractile element had activation dynamics, a force-length relationship, and a force-velocity relationship [99]. The following section will introduce how these are modeled.

2.6.1 Three Element Hill-Type Muscle Model

Skeletal muscles create motion in humans and animals. A muscle consists of bundles of muscle fibers. Each fiber contains sarcoplasm, which contains sarcomeres, the basic contractile unit. Sarcomeres consist of actin and myosin filaments. Crossbridges can be created between these two filaments, which creates movement when shortening the muscle or a force when the movement is restricted. The creation of crossbridges is normally prevented by unbound troponin. An electrical neural stimulation creates a series of biochemical processes that allow calcium ions to enter the sarcoplasm and bind to troponin to

allow the creation of crossbridges [125].

This process is complex and therefore requires an elaborate description. A less complex model can be created by observing input and output data, without describing the processes inside the muscle exactly. Such a model is called a phenomenological model. The Hill-type muscle model is a phenomenological model that describes most features of muscle mechanics [126]. There are three possible inputs to a Hill-type muscle, the activation state, the muscle length and the muscle force. The model was created by using two of these three as input. Activation usually was one of those. One of the inputs would be held constant, while the other was varied. Then, the third, either length or force, was measured during an experiment [126].

Early experiments led to the belief that the muscle could be modeled as a damped spring, or spring-like element, in series with an undamped spring [126]. In these experiments, a maximal force was applied at constant length. Then, the activation state was changed suddenly, such that the force changes. The presence of the undamped spring was shown by an instantaneous change in length following the release of the force in the muscle. The damped element was shown by a change in muscle length with a constant speed after the instantaneous response. Further work determined that the damping component was nonlinear. Katz [127] found that a spring should also be modeled in parallel with the spring-like, damped element [125].

Figure 7 shows a three element Hill-type muscle. It consists of a parallel elastic element (PEE), a series elastic element (SEE) and the contractile element (CE). The SEE is a nonlinear spring that represents the tendon and aponeurosis that connects the muscle to the bone. The PEE is a nonlinear spring and represents the connective tissue that is inside the muscle and surrounds it. The CE is the element that represents the actual muscle fibers [126]. It determines the force in these fibers as a function of the activation state, *a*

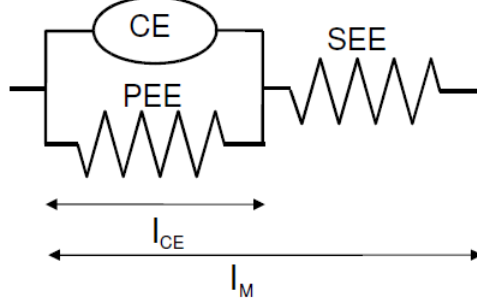


Figure 7: Schematic of a Hill-type muscle consisting of a parallel elastic element (PEE), series elastic element (SEE) and contractile element (CE).

and the muscle fiber length, l_{CE} and velocity, v_{CE} :

$$F_{CE} = af(l_{CE})g(v_{CE})F_{ISO} \quad (2.19)$$

where F_{ISO} is the maximum force that can be generated by the muscle at zero velocity and optimal muscle fiber length, also called the maximum isometric force.

Figure 8a shows a typical force-length relationship of a muscle. There is an optimal length, at which the maximum isometric force is generated, which is very close to the resting length. Force is generated between around 0.5 and 1.5 times this optimal length. The following equation will be used to model this relationship:

$$f(l_{CE}) = \exp \left(- \left(\frac{l_{CE} - l_{CE(OPT)}}{Wl_{CE(OPT)}} \right)^2 \right) \quad (2.20)$$

where $l_{CE(OPT)}$ denotes the optimal fiber length. W is a width parameter that is different for each muscle, as given in [128].

Figure 8b shows a typical force-velocity relationship of a muscle. A larger force can be generated during lengthening, up to 1.5 times the isometric maximum force. The force decreases to zero when the muscle is shortened. This relationship is constructed using two

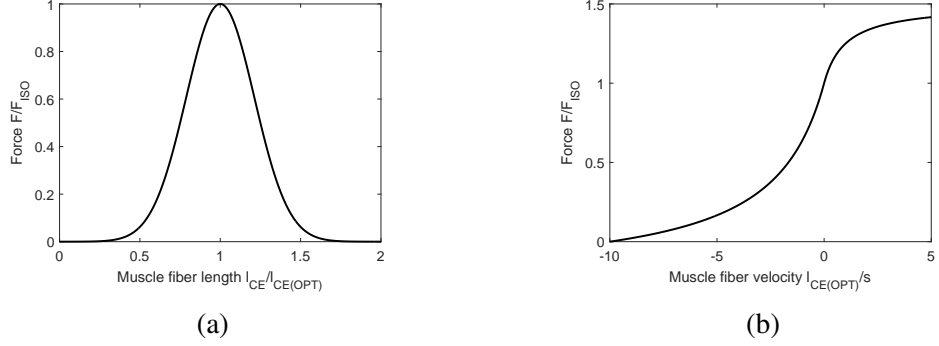


Figure 8: Typical force-length (a) and force-velocity (b) relationships of the CE. The force is normalized to maximum isometric force.

curves, one for lengthening velocities and one for shortening velocities:

$$g(v_{CE}) = \begin{cases} \frac{v_{CE(max)}+v_{CE}}{v_{CE(max)}-v_{CE}/A} + \beta v_{CE} & \text{if } v_{CE} \leq 0 \\ \frac{g_{max}v_{CE}+c_3}{v_{CE}+c_3} + \beta v_{CE} & \text{if } v_{CE} > 0 \end{cases} \quad (2.21)$$

where $v_{CE(max)}$ denotes the maximum shortening velocity, equal to 10 times the optimal fiber length and $g_{max} = 1.5$ denotes the maximum force that can be generated. A is the Hill curve parameter, equal to 0.25. βv_{CE} is a small damping term to ensure that the derivative of the force with respect to the fiber velocity is never zero, where $\beta = 0.001 F_{ISOS}/l_{CE(OPT)}$. c_3 is a constant that is chosen such that the derivative of $g(v_{CE})$ is continuous:

$$c_3 = \frac{v_{CE(max)} A (g_{max} - 1)}{A + 1} \quad (2.22)$$

Finally, the muscle force in the CE is also dependent on the activation state. This state is related to the amount of calcium that is bound to troponin. This changes when the muscle is stimulated and thereby regulates the attachment of crossbridges between the actin and myosin filaments and thus the muscle force [126]. Bahler [129] found that the dynamics of the activation state could be modeled as a first order process, with a time constant for activation and for deactivation. In this work, the equation presented by He et al. [130] is

used:

$$\dot{a} = (u - a)(c_1 u + c_2) \quad (2.23)$$

where u denotes the neural stimulation, and $c_1 = 3.3 \text{ s}^{-1}$ and $c_2 = 16.7 \text{ s}^{-1}$ are rate constants, corresponding with time constants of 50 ms for activation and 60 ms for deactivation [131].

The force in the PEE and SEE is found based on the model presented by McLean et al. [132]. The following equation is used:

$$F(l) = \begin{cases} k_1(l - l_{slack}) & \text{if } l \leq l_{slack} \\ k_1(l - l_{slack}) + k_2(l - l_{slack})^2 & \text{if } l > l_{slack} \end{cases} \quad (2.24)$$

where l denotes the length of the element and l_{slack} the slack length. k_1 and k_2 are stiffness constants. k_1 represents a small linear stiffness, which was added in this version to ensure that the force is never zero, which aids the optimization. It is equal to 0.01 F_{ISO}/m . k_2 is equal to the following:

$$k_2(PEE) = \frac{F_{ISO}k_{PEE}}{l_{CE(OPT)}^2} \quad (2.25)$$

$$k_2(SEE) = \frac{F_{ISO}}{(u_{max}l_{CE(OPT)})^2} \quad (2.26)$$

where $k_{PEE} = 1$ and $u_{max} = 0.04$ are dimensionless constants.

Table I shows the maximum isometric force F_{max} , optimal fiber length, $l_{CE(OPT)}$, width of the force-length curve, the slack length of the parallel elastic element (PEE) and the series elastic element (SEE), the nominal muscle length, l_0 , and the percentage of fast twitch fibers for each muscle. Table II shows the moment arms of each muscle for the hip, knee and ankle joints. Several parameters were the same for each muscle: the maximum shortening velocity, $v_{CE(max)} = 12 l_{CE(OPT)}/\text{s}$, the maximum force during lengthening, $g_{max} = 1.5 F_{max}$, and the normalized Hill constant, $A_{hill} = 0.25$.

Table I: Maximum isometric force, optimal fiber length, width of the force-length curve, slack length of the parallel and series elastic element, muscle length, and percentage of fast twitch fibers for all muscles in the model.

Muscle	F_{max} [N]	$l_{CE(OPT)}$ [m]	Width	PEE slack [$l_{CE(OPT)}$]	SEE slack [m]	L_0 [m]	% FT fibers
Iliopsoas	1500	0.102	1.298	1.2	0.142	0.248	0.5
Gluteals	3000	0.2	0.625	1.2	0.157	0.271	0.45
Hamstrings	3000	0.104	1.197	1.2	0.334	0.383	0.35
Rectus Femoris	1200	0.081	1.443	1.4	0.398	0.474	0.65
Vastus	7000	0.093	0.627	1.4	0.223	0.271	0.5
Gastrocnemius	3000	0.055	1.039	1.2	0.42	0.487	0.5
Soleus	4000	0.055	1.039	1.2	0.245	0.284	0.2
Tibialis Anterior	2500	0.082	0.442	1.2	0.317	0.381	0.25

Table II: Muscle moment arms. Positive moment arms indicate flexion for the hip, extension for the knee, and dorsiflexion for the ankle.

Muscle	Hip moment arm [cm]	Knee moment arm [cm]	Ankle moment arm [cm]
Iliopsoas	5	0	0
Gluteals	-6.2	0	0
Hamstrings	-7.2	-3.4	0
Rectus Femoris	3.4	5	0
Vastus	0	4.2	0
Gastrocnemius	0	-2	-5.3
Soleus	0	0	-5.3
Tibialis Anterior	0	0	3.7

The muscle dynamics are coupled with the multibody dynamics using the principle of virtual work. The length of the muscle, l_m , is dependent on the pose of the skeleton, which affects the force that is produced. Using the principle of virtual work, the torque at joint j due to the muscle force in muscle i is equal to [133]:

$$\tau_{ij} = -\frac{\partial l_{m,i}}{\partial \theta_j} F_{SEE,i}(l_{m,i}(\theta) - l_{CE,i}) \quad (2.27)$$

where the derivative $\partial L_{m,i}/\partial \theta_j$ denotes the moment arm of the muscle i at joint j . These partial derivatives are approximated by fitting a first order polynomial function to existing data of muscle length versus skeletal pose, resulting in constant moment arms. This is sufficiently accurate in a two-dimensional model [134].

The activation dynamics and force-length and force-velocity relationships are sufficient to find the force in the muscles and the moments they generate around the joints. Both the dynamics of the contractile element due to the force-length and force-velocity relationships and the activation dynamics are first order systems. This means that for each muscle i two states are added to the state of the human model, the activation state and the muscle fiber length, which is normalized to the optimal fiber length. Therefore, for the musculoskeletal system, the state is $x(t) = [q(t) \quad v(t) \quad l_{CE_i}(t) \quad a_i(t)]^T$.

However, if the dynamics are described with the state derivative on the left-hand side, $\dot{x}(t) = f(x(t), u(t))$, equation 2.19 would have to be inverted to obtain a relationship with respect to the muscle fiber velocity. This would yield a division by zero when there is no activation [134]. Typically, this problem is avoided by having a small, non-zero, lower bound on the neural stimulation and activation state. This will make it impossible to fully relax the muscle, and also make the dynamics equations very stiff and difficult to solve. Therefore, an implicit description of the dynamics, $f(x(t), \dot{x}(t), u(t)) = 0$, will be used in the dynamics constraints of the optimization problem (equation 2.2). Then, instead of creating a function with respect to the fiber velocity, one can balance the force in the CE

and PEE with the force in the SEE, since these should be equal according to Newton's first law (see figure 7):

$$f(x(t), \dot{x}(t), u(t)) = F_{SEE}(x(t), \dot{x}(t), u(t)) - F_{CE}(x(t)) - F_{PEE}(x(t)) = 0 \quad (2.28)$$

2.6.2 Ground Contact Model

Contact between the foot and the ground was modeled using four contact points, one at the heel and one at the toe of each foot. The ground reaction forces are added to the multibody dynamics using the Jacobian of the locations of these contact points (see equation 2.18). The vertical ground reaction force, F_y depends on the vertical position y of the contact point, as follows:

$$F_y(d) = kd(1 - b\dot{y}) - k_g y \quad (2.29)$$

The first term represents a visco-elastic force due to a deformation, d , of the contact point. The second term is a weak linear spring to aid the optimization. To ensure differentiability, d was calculated as

$$d = \frac{1}{2} \left(\sqrt{y^2 + y_0^2} - y \right) \quad (2.30)$$

where y_0 is the size of the transition region between contact and no contact. The following parameter values were used: $k = 2 \cdot 10^4$ N/m, $b = 1$ s/m, $k_g = 1$ N/m, $y_0 = 1 \cdot 10^{-3}$ m.

The horizontal ground reaction force was modeled as a continuous approximation of Coulomb friction:

$$F_x(f_y, \dot{x}) = -\mu F_y \frac{\dot{x}}{\sqrt{\dot{x}^2 + v_0^2}} \quad (2.31)$$

where \dot{x} is the sliding velocity of the contact point, $\mu = 1$ is the friction coefficient and $v_0 = 0.1$ m/s is a small velocity parameter that determines how much change in velocity is needed to produce a sign change in the friction when there is a change in the sliding

direction.

2.7 References

- [1] D Richfield. Medical gallery of David Richfield. *WikiJournal of Medicine*, 1(2), 2014. doi: 10.15347/wjm/2014.009.
- [2] Oxford English Dictionary. Oxford English dictionary. *The Library*, 2002.
- [3] JR Gage, PA DeLuca, and TS Renshaw. Gait analysis: principle and applications with emphasis on its use in cerebral palsy. *Instructional Course Lectures, The American Academy of Orthopaedic Surgeons*, 77(10):1607–1623, 1995.
- [4] DA Winter. *Biomechanics and motor control of human gait: normal, elderly and pathological*. University of Waterloo Press, 2 edition, 1991.
- [5] DA Winter. *Biomechanics and motor control of human movement*. John Wiley & Sons, 2005.
- [6] DA Winter. Energy generation and absorption at the ankle and knee during fast, natural, and slow cadences. *Clinical Orthopaedics and Related Research*, (175): 147–154, 1983.
- [7] HM Herr and AM Grabowski. Bionic ankle–foot prosthesis normalizes walking gait for persons with leg amputation. *Proceedings of the Royal Society of London B: Biological Sciences*, 279(1728):457–464, 2012.
- [8] GRB Hurley, R McKenney, M Robinson, M Zadravec, and MR Pierrynowski. The role of the contralateral limb in below-knee amputee gait. *Prosthetics and Orthotics International*, 14(1):33–42, 1990.
- [9] H Bateni and SJ Olney. Kinematic and kinetic variations of below-knee amputee gait. *JPO: Journal of Prosthetics and Orthotics*, 14(1):2–10, 2002.

- [10] AE Ferris, JM Aldridge, CA Rábago, and JM Wilken. Evaluation of a powered ankle-foot prosthetic system during walking. *Archives of Physical Medicine and Rehabilitation*, 93(11):1911–1918, 2012.
- [11] DJ Sanderson and PE Martin. Lower extremity kinematic and kinetic adaptations in unilateral below-knee amputees during walking. *Gait & Posture*, 6(2):126–136, 1997.
- [12] E Isakov, O Keren, and N Benjuya. Trans-tibial amputee gait: Time-distance parameters and EMG activity. *Prosthetics and Orthotics International*, 24(3):216–220, 2000.
- [13] SJ Mattes, PE Martin, and TD Royer. Walking symmetry and energy cost in persons with unilateral transtibial amputations: matching prosthetic and intact limb inertial properties. *Archives of Physical Medicine and Rehabilitation*, 81(5):561–568, 2000.
- [14] AE Barr, K Lohmann Siegel, JV Danoff, CL McGarvey III, A Tomasko, I Sable, and SJ Stanhope. Biomechanical comparison of the energy-storing capabilities of SACH and Carbon Copy II prosthetic feet during the stance phase of gait in a person with below-knee amputation. *Physical Therapy*, 72(5):344–354, 1992.
- [15] CM Powers, L Torburn, J Perry, and E Ayyappa. Influence of prosthetic foot design on sound limb loading in adults with unilateral below-knee amputations. *Archives of Physical Medicine and Rehabilitation*, 75(7):825–829, 1994.
- [16] ED Lemaire, FR Fisher, and DGE Robertson. Gait patterns of elderly men with trans-tibial-amputations. *Prosthetics and Orthotics International*, 17(1):27–37, 1993.
- [17] L Nolan, A Wit, K Dudziński, A Lees, M Lake, and M Wychowański. Adjustments in gait symmetry with walking speed in trans-femoral and trans-tibial amputees. *Gait & Posture*, 17(2):142–151, 2003.

- [18] RD Snyder, CM Powers, C Fontaine, and J Perry. The effect of five prosthetic feet on the gait and loading of the sound limb in dysvascular below-knee amputees. *Journal of Rehabilitation Research and Development*, 32(4):309, 1995.
- [19] MS Pinzur, W Cox, J Kaiser, T Morris, A Patwardhan, and L Vrbos. The effect of prosthetic alignment on relative limb loading in persons with trans-tibial amputation: a preliminary report. *Journal of Rehabilitation Research and Development*, 32(4):373, 1995.
- [20] C Beyaert, C Grumillier, N Martinet, J Paysant, and J-M André. Compensatory mechanism involving the knee joint of the intact limb during gait in unilateral below-knee amputees. *Gait & Posture*, 28(2):278–284, 2008.
- [21] CM Powers, S Rao, and J Perry. Knee kinetics in trans-tibial amputee gait. *Gait & Posture*, 8(1):1–7, 1998.
- [22] A Gitter, JM Czerniecki, and DM DeGroot. Biomechanical analysis of the influence of prosthetic feet on below-knee amputee walking. *American Journal of Physical Medicine & Rehabilitation*, 70(3):142–148, 1991.
- [23] AK Silverman, NP Fey, A Portillo, JG Walden, G Bosker, and RR Neptune. Compensatory mechanisms in below-knee amputee gait in response to increasing steady-state walking speeds. *Gait & Posture*, 28(4):602–609, 2008.
- [24] H Sadeghi, P Allard, and M Duhaime. Muscle power compensatory mechanisms in below-knee amputee gait. *American Journal of Physical Medicine & Rehabilitation*, 80(1):25–32, 2001.
- [25] RJ Zmitrewicz, RR Neptune, and K Sasaki. Mechanical energetic contributions from individual muscles and elastic prosthetic feet during symmetric unilateral transtibial amputee walking: a theoretical study. *Journal of Biomechanics*, 40(8):1824–1831, 2007.

- [26] C Grumillier, N Martinet, J Paysant, J-M André, and C Beyaert. Compensatory mechanism involving the hip joint of the intact limb during gait in unilateral trans-tibial amputees. *Journal of Biomechanics*, 41(14):2926–2931, 2008.
- [27] NP Fey, AK Silverman, and RR Neptune. The influence of increasing steady-state walking speed on muscle activity in below-knee amputees. *Journal of Electromyography and Kinesiology*, 20(1):155–161, 2010.
- [28] MS Pinzur, M Asselmeier, and D Smith. Dynamic electromyography in active and limited walking below-knee amputees. *Orthopedics*, 14(5):535–538, 1991.
- [29] DA Winter and SE Sienko. Biomechanics of below-knee amputee gait. *Journal of Biomechanics*, 21(5):361–367, 1988.
- [30] M Seyedali, JM Czerniecki, DC Morgenroth, and ME Hahn. Co-contraction patterns of trans-tibial amputee ankle and knee musculature during gait. *Journal of Neuroengineering and Rehabilitation*, 9(1):29, 2012.
- [31] EG Culham, M Peat, and E Newell. Below-knee amputation: a comparison of the effect of the SACH foot and single axis foot on electromyographic patterns during locomotion. *Prosthetics and Orthotics International*, 10(1):15–22, 1986.
- [32] L Torburn, J Perry, E Ayyappa, and SL Shanfield. Below-knee amputee gait with dynamic elastic response prosthetic feet: a pilot study. *Journal of Rehabilitation Research and Development*, 27(4):369, 1990.
- [33] RL Waters, J Perry, D Antonelli, and H Hislop. Energy cost of walking of amputees: the influence of level of amputation. *The Journal of Bone and Joint Surgery. American Volume*, 58(1):42–46, 1976.
- [34] DH Nielsen, DG Shurr, JC Golden, and K Meier. Comparison of energy cost and gait efficiency during ambulation in below-knee amputees using different prosthetic

- feeta preliminary report. *JPO: Journal of Prosthetics and Orthotics*, 1(1):24–31, 1988.
- [35] EG Gonzalez. Energy expenditure in below-knee amputees: correlation with stump length. *Archives of Physical Medicine and Rehabilitation*, 55:111–119, 1974.
- [36] HL Jarvis, AN Bennett, M Twiste, RD Phillip, J Etherington, and R Baker. Temporal spatial and metabolic measures of walking in highly functional individuals with lower limb amputations. *Archives of Physical Medicine and Rehabilitation*, 98(7):1389–1399, 2017.
- [37] ER Esposito, KM Rodriguez, CA Ràbago, and JM Wilken. Does unilateral transtibial amputation lead to greater metabolic demand during walking? *Journal of Rehabilitation Research and Development*, 51(8):1287, 2014.
- [38] ER Esposito and RH Miller. Maintenance of muscle strength retains a normal metabolic cost in simulated walking after transtibial limb loss. *PloS one*, 13(1):e0191310, 2018.
- [39] RS Gailey, MA Wenger, M Raya, N Kirk, K Erbs, P Spyropoulos, and MS Nash. Energy expenditure of trans-tibial amputees during ambulation at self-selected pace. *Prosthetics and Orthotics International*, 18(2):84–91, 1994.
- [40] L Torburn, CM Powers, R Guitierrez, and J Perry. Energy expenditure during ambulation in dysvascular and traumatic below-knee amputees: a comparison of five prosthetic feet. *Journal of Rehabilitation Research and Development*, 32(2):111, 1995.
- [41] DG Barth, L Schumacher, and SS Thomas. Gait analysis and energy cost of below-knee amputees wearing six different prosthetic feet. *JPO: Journal of Prosthetics and Orthotics*, 4(2):63–75, 1992.

- [42] J Perry and S Shanfield. Efficiency of dynamic elastic response prosthetic feet. *Journal of Rehabilitation Research*, 30(1):137–143, 1993.
- [43] RL Waters and S Mulroy. The energy expenditure of normal and pathologic gait. *Gait & posture*, 9(3):207–231, 1999.
- [44] RS Gailey, MS Nash, TA Atchley, RM Zilmer, GR Moline-Little, N Morris-Cresswell, and LI Siebert. The effects of prosthesis mass on metabolic cost of ambulation in non-vascular trans-tibial amputees. *Prosthetics and Orthotics International*, 21(1):9–16, 1997.
- [45] CM Godfrey, R Brett, and AT Jousse. Foot mass effect on gait in the prosthetic limb. *Archives of Physical Medicine and Rehabilitation*, 58(6):268–269, 1977.
- [46] JF Lehmann, R Price, R Okumura, K Questad, BJ De Lateur, and A Négretot. Mass and mass distribution of below-knee prostheses: effect on gait efficacy and self-selected walking speed. *Archives of Physical Medicine and Rehabilitation*, 79(2):162–168, 1998.
- [47] H Houdijk, E Pollmann, M Groenewold, H Wiggerts, and W Polomski. The energy cost for the step-to-step transition in amputee walking. *Gait & Posture*, 30(1):35–40, 2009.
- [48] JM Donelan, R Kram, and AD Kuo. Simultaneous positive and negative external mechanical work in human walking. *Journal of Biomechanics*, 35(1):117–124, 2002.
- [49] R Gailey. Review of secondary physical conditions associated with lower-limb amputation and long-term prosthesis use. *Journal of Rehabilitation Research and Development*, 45(1):15, 2008.

- [50] J Kulkarni, J Adams, E Thomas, and A Silman. Association between amputation, arthritis and osteopenia in british male war veterans with major lower limb amputations. *Clinical Rehabilitation*, 12(3):274–279, 1998.
- [51] ED Lemaire and FR Fisher. Osteoarthritis and elderly amputee gait. *Archives of Physical Medicine and Rehabilitation*, 75:1094–1099, 1994.
- [52] T Royer and M Koenig. Joint loading and bone mineral density in persons with unilateral, trans-tibial amputation. *Clinical Biomechanics*, 20(10):1119–1125, 2005.
- [53] JA Kanis, O Johnell, A Oden, B Jonsson, C De Laet, and A Dawson. Risk of hip fracture according to the World Health Organization criteria for osteopenia and osteoporosis. *Bone*, 27(5):585–590, 2000.
- [54] MJ Burke, V Roman, and V Wright. Bone and joint changes in lower limb amputees. *Annals of the Rheumatic Diseases*, 37(3):252, 1978.
- [55] B Fleer and AB Wilson Jr. Construction of the patellar-tendon-bearing below-knee prosthesis. *Artificial Limbs*, 6(2):25–73, 1962.
- [56] R Leskovar, A Körner, and F Breitenecker. System based modelling approach for biomechanical models in the field of prosthetics. *Proceedings of the UKSim-AMSS 19th International Conference on Modelling and Simulation*, pages 13–18, 2017.
- [57] R Versluys, P Beyl, M Van Damme, A Desomer, R Van Ham, and D Lefeber. Prosthetic feet: State-of-the-art review and the importance of mimicking human ankle-foot biomechanics. *Disability and Rehabilitation: Assistive Technology*, 4(2):65–75, 2009.
- [58] ML Palmer. *Sagittal plane characterization of normal human ankle function across a range of walking gait speeds*. PhD thesis, Massachusetts Institute of Technology, 2002.

- [59] AH Hansen, DS Childress, SC Miff, SA Gard, and KP Mesplay. The human ankle during walking: implications for design of biomimetic ankle prostheses. *Journal of Biomechanics*, 37(10):1467–1474, 2004.
- [60] J-M Casillas, V Dulieu, M Cohen, I Marcer, and J-P Didier. Bioenergetic comparison of a new energy-storing foot and SACH foot in traumatic below-knee vascular amputations. *Archives of Physical Medicine and Rehabilitation*, 76(1):39–44, 1995.
- [61] JE Edelstein. Prosthetic feet: state of the art. *Physical Therapy*, 68(12):1874–1881, 1988.
- [62] R Arbogast and CJ Arbogast. The Carbon Copy II – from concept to application. *JPO: Journal of Prosthetics and Orthotics*, 1(1):32–36, 1988.
- [63] AM Grabowski, J Rifkin, and R Kram. K3 PromoterTM prosthetic foot reduces the metabolic cost of walking for unilateral transtibial amputees. *JPO: Journal of Prosthetics and Orthotics*, 22(2):113–120, 2010.
- [64] AD Segal, KE Zelik, GK Klute, DC Morgenroth, ME Hahn, MS Orendurff, PG Adamczyk, SH Collins, AD Kuo, and JM Czerniecki. The effects of a controlled energy storage and return prototype prosthetic foot on transtibial amputee ambulation. *Human Movement Science*, 31(4):918–931, 2012.
- [65] JF Lehmann, R Price, S Boswell-Bessette, A Dralle, K Questad, et al. Comprehensive analysis of energy storing prosthetic feet: Flex Foot and Seattle foot versus standard SACH foot. *Archives of Physical Medicine and Rehabilitation*, 74(11):1225–1231, 1993.
- [66] J Wagner, S Sienko, T Supan, and D Barth. Motion analysis of SACH vs. Flex-Foot in moderately active below-knee amputees. *Clinical Prosthetics & Orthotics*, 11(1):55–62, 1987.

- [67] BJ Hafner, JE Sanders, J Czerniecki, and J Fergason. Energy storage and return prostheses: does patient perception correlate with biomechanical analysis? *Clinical Biomechanics*, 17(5):325–344, 2002.
- [68] M-J Hsu, DH Nielsen, S-J Lin-Chan, and D Shurr. The effects of prosthetic foot design on physiologic measurements, self-selected walking velocity, and physical activity in people with transtibial amputation. *Archives of Physical Medicine and Rehabilitation*, 87(1):123–129, 2006.
- [69] GR Colborne, S Naumann, PE Longmuir, and D Berbrayer. Analysis of mechanical and metabolic factors in the gait of congenital below knee amputees. a comparison of the SACH and Seattle feet. *American Journal of Physical Medicine & Rehabilitation*, 71(5):272–278, 1992.
- [70] M-J Hsu, DH Nielsen, HJ Yack, and DG Shurr. Physiological measurements of walking and running in people with transtibial amputations with 3 different prostheses. *Journal of Orthopaedic & Sports Physical Therapy*, 29(9):526–533, 1999.
- [71] K Postema, HJ Hermens, J De Vries, HFJM Koopman, and WH Eisma. Energy storage and release of prosthetic feet part 1: Biomechanical analysis related to user benefits. *Prosthetics and Orthotics International*, 21(1):17–27, 1997.
- [72] MR Menard and DD Murray. Subjective and objective analysis of an energy-storing prosthetic foot. *JPO: Journal of Prosthetics and Orthotics*, 1(4):220–230, 1989.
- [73] DD Murray, WJ Hartvikson, H Anton, E Hommonay, and N Russell. With a spring in one's step. *Clinical Prosthetics & Orthotics*, 12:28 – 135, 1988.
- [74] H Alaranta, A Kinnunen, M Karkkainen, T Pohjolainen, and M Heliovaara. Practical benefits of Flex-Foot in below-knee amputees. *JPO: Journal of Prosthetics and Orthotics*, 3(4):179–81, 1991.

- [75] PA Macfarlane, DH Nielsen, DG Shurr, and K Meier. Perception of walking difficulty by below-knee amputees using a conventional foot versus the Flex-Foot. *JPO: Journal of Prosthetics and Orthotics*, 3(3):114–119, 1991.
- [76] M Grimmer, M Holgate, R Holgate, A Boehler, J Ward, K Hollander, T Sugar, and A Seyfarth. A powered prosthetic ankle joint for walking and running. *Biomedical Engineering Online*, 15(3):141, 2016.
- [77] S Sahoo, DK Pratihar, and S Mukhopadhyay. A novel energy efficient powered ankle prosthesis using four-bar controlled compliant actuator. *Proceedings of the Institution of Mechanical Engineers, Part C: Journal of Mechanical Engineering Science*, page 0954406217753461, 2018.
- [78] S Au, M Berniker, and H Herr. Powered ankle-foot prosthesis to assist level-ground and stair-descent gaits. *Neural Networks*, 21(4):654–666, 2008.
- [79] JK Hitt, TG Sugar, M Holgate, and R Bellman. An active foot-ankle prosthesis with biomechanical energy regeneration. *Journal of Medical Devices*, 4(1):011003, 2010.
- [80] GK Klute, JM Czerniecki, and B Hannaford. Artificial muscles: Actuators for biorobotic systems. *The International Journal of Robotics Research*, 21(4):295–309, 2002.
- [81] R Versluys, A Desomer, G Lenaerts, O Pareit, B Vanderborght, G Perre, L Peeraer, and D Lefeber. A biomechatronical transtibial prosthesis powered by pleated pneumatic artificial muscles. *International Journal of Modelling, Identification and Control*, 4(4):394–405, 2008.
- [82] R Versluys, G Lenaerts, M Van Damme, I Jonkers, A Desomer, B Vanderborght, L Peeraer, G Van der Perre, and D Lefeber. Successful preliminary walking experiments on a transtibial amputee fitted with a powered prosthesis. *Prosthetics and Orthotics International*, 33(4):368–377, 2009.

- [83] AK LaPre, BR Umberger, and FC Sup. A robotic ankle–foot prosthesis with active alignment. *Journal of Medical Devices*, 10(2):025001, 2016.
- [84] ES Gardinier, BM Kelly, J Wensman, and DH Gates. A controlled clinical trial of a clinically-tuned powered ankle prosthesis in people with transtibial amputation. *Clinical Rehabilitation*, page 0269215517723054, 2017.
- [85] C Mancinelli, BL Patritti, P Tropea, RM Greenwald, R Casler, HM Herr, and P Bonato. Comparing a passive-elastic and a powered prosthesis in transtibial amputees. In *Engineering in Medicine and Biology Society, EMBC, 2011 Annual International Conference of the IEEE*, pages 8255–8258. IEEE, 2011.
- [86] RE Quesada, JM Caputo, and SH Collins. Increasing ankle push-off work with a powered prosthesis does not necessarily reduce metabolic rate for transtibial amputees. *Journal of Biomechanics*, 49(14):3452–3459, 2016.
- [87] SL Delp, FC Anderson, AS Arnold, P Loan, A Habib, CT John, E Guendelman, and DG Thelen. OpenSim: open-source software to create and analyze dynamic simulations of movement. *IEEE Transactions on Biomedical Engineering*, 54(11):1940–1950, 2007.
- [88] U Trinler, K Hollands, R Jones, and R Baker. A systematic review of approaches to modelling lower limb muscle forces during gait: applicability to clinical gait analyses. *Gait & Posture*, 61:353–361, 2018.
- [89] F de Groote, AL Kinney, AV Rao, and BJ Fregly. Evaluation of direct collocation optimal control problem formulations for solving the muscle redundancy problem. *Annals of Biomedical Engineering*, 44(10):2922–2936, 2016.
- [90] Y-C Lin, JP Walter, SA Banks, MG Pandy, and BJ Fregly. Simultaneous prediction of muscle and contact forces in the knee during gait. *Journal of Biomechanics*, 43(5):945–952, 2010.

- [91] DG Thelen, KW Choi, and AM Schmitz. Co-simulation of neuromuscular dynamics and knee mechanics during human walking. *Journal of Biomechanical Engineering*, 136(2):021033, 2014.
- [92] BJ Fregly, TF Besier, DG Lloyd, SL Delp, SA Banks, MG Pandy, and DD D’lima. Grand challenge competition to predict in vivo knee loads. *Journal of Orthopaedic Research*, 30(4):503–513, 2012.
- [93] TA Correa, R Baker, HK Graham, and MG Pandy. Accuracy of generic musculoskeletal models in predicting the functional roles of muscles in human gait. *Journal of Biomechanics*, 44(11):2096–2105, 2011.
- [94] KM Steele, MS DeMers, MH Schwartz, and SL Delp. Compressive tibiofemoral force during crouch gait. *Gait & posture*, 35(4):556–560, 2012.
- [95] MA Marra, V Vanheule, R Fluit, BHFJM Koopman, J Rasmussen, N Verdonschot, and MS Andersen. A subject-specific musculoskeletal modeling framework to predict in vivo mechanics of total knee arthroplasty. *Journal of Biomechanical Engineering*, 137(2):020904, 2015.
- [96] A Muller, C Pontonnier, and G Dumont. Uncertainty propagation in multibody human model dynamics. *Multibody System Dynamics*, 40(2):177–192, 2017.
- [97] SC White, HJ Yack, and DA Winter. A three-dimensional musculoskeletal model for gait analysis. anatomical variability estimates. *Journal of Biomechanics*, 22(8-9): 885–893, 1989.
- [98] DJJ Bregman, MM Van der Krog, V De Groot, J Harlaar, M Wisse, and SH Collins. The effect of ankle foot orthosis stiffness on the energy cost of walking: a simulation study. *Clinical Biomechanics*, 26(9):955–961, 2011.

- [99] AJ van den Bogert, M Hupperets, H Schlarb, and B Krabbe. Predictive musculoskeletal simulation using optimal control: effects of added limb mass on energy cost and kinematics of walking and running. *Proceedings of the Institution of Mechanical Engineers, Part P: Journal of Sports Engineering and Technology*, pages 1–11, 2012.
- [100] RH Miller, SCE Brandon, and KJ Deluzio. Predicting sagittal plane biomechanics that minimize the axial knee joint contact force during walking. *Journal of Biomechanical Engineering*, 135(1):011007, 2013.
- [101] M Millard, M Sreenivasa, and K Mombaur. Predicting the motions and forces of wearable robotic systems using optimal control. *Frontiers in Robotics and Artificial Intelligence*, 4:41, 2017.
- [102] JEA Bertram and A Ruina. Multiple walking speed–frequency relations are predicted by constrained optimization. *Journal of Theoretical Biology*, 209(4):445–453, 2001.
- [103] MG Hoy, FE Zajac, and ME Gordon. A musculoskeletal model of the human lower extremity: the effect of muscle, tendon, and moment arm on the moment-angle relationship of musculotendon actuators at the hip, knee, and ankle. *Journal of Biomechanics*, 23(2):157–169, 1990.
- [104] FC Anderson and MG Pandy. Dynamic optimization of human walking. *Journal of Biomechanical Engineering*, 123(5):381–390, 2001.
- [105] M Ackermann and AJ van den Bogert. Optimality principles for model-based prediction of human gait. *Journal of Biomechanics*, 43(6):1055–1060, 2010.
- [106] RH Miller, BR Umberger, J Hamill, and GE Caldwell. Evaluation of the minimum energy hypothesis and other potential optimality criteria for human running. *Pro-*

ceedings of the Royal Society of London B: Biological Sciences, pages 1498–1505, 2011.

- [107] K Mombaur and D Clever. Inverse optimal control as a tool to understand human movement. In *Geometric and Numerical Foundations of Movements*, pages 163–186. Springer, 2017.
- [108] M Ackermann and AJ van den Bogert. Predictive simulation of gait at low gravity reveals skipping as the preferred locomotion strategy. *Journal of Biomechanics*, 45(7):1293–1298, 2012.
- [109] S Song and H Geyer. Predictive neuromechanical simulations indicate why walking performance declines with aging. *The Journal of Physiology*, 2018.
- [110] TW Dorn, JM Wang, JL Hicks, and SL Delp. Predictive simulation generates human adaptations during loaded and inclined walking. *PloS one*, 10(4):e0121407, 2015.
- [111] RH Miller. A comparison of muscle energy models for simulating human walking in three dimensions. *Journal of Biomechanics*, 47(6):1373–1381, 2014.
- [112] RH Miller, AY Esterson, and JK Shim. Joint contact forces when minimizing the external knee adduction moment by gait modification: a computer simulation study. *The Knee*, 22(6):481–489, 2015.
- [113] NP Fey, GK Klute, and RR Neptune. Altering prosthetic foot stiffness influences foot and muscle function during below-knee amputee walking: a modeling and simulation analysis. *Journal of Biomechanics*, 46(4):637–644, 2013.
- [114] ML Handford and M Srinivasan. Robotic lower limb prosthesis design through simultaneous computer optimizations of human and prosthesis costs. *Scientific Reports*, 6, 2016.

- [115] M Kelly. An introduction to trajectory optimization: How to do your own direct collocation. *SIAM Review*, 59(4):849–904, 2017.
- [116] JT Betts. *Practical methods for optimal control and estimation using nonlinear programming*, volume 19. SIAM, 2010.
- [117] JT Betts. Survey of numerical methods for trajectory optimization. *Journal of Guidance, Control, and Dynamics*, 21(2):193–207, 1998.
- [118] Y-C Lin and MG Pandy. Three-dimensional data-tracking dynamic optimization simulations of human locomotion generated by direct collocation. *Journal of Biomechanics*, 59:1–8, 2017.
- [119] M Posa and R Tedrake. Direct trajectory optimization of rigid body dynamical systems through contact. In *Algorithmic Foundations of Robotics X*, pages 527–542. Springer, 2013.
- [120] AK Silverman and RR Neptune. Muscle and prosthesis contributions to amputee walking mechanics: a modeling study. *Journal of Biomechanics*, 45(13):2271–2278, 2012.
- [121] PE Gill, W Murray, and MA Saunders. SNOPT: An SQP algorithm for large-scale constrained optimization. *SIAM Review*, 47(1):99–131, 2005.
- [122] A Wächter and LT Biegler. On the implementation of an interior-point filter line-search algorithm for large-scale nonlinear programming. *Mathematical Programming*, 106(1):25–57, 2006.
- [123] MA Patterson and AV Rao. GPOPS-II: A MATLAB software for solving multiple-phase optimal control problems using hp-adaptive gaussian quadrature collocation methods and sparse nonlinear programming. *ACM Transactions on Mathematical Software (TOMS)*, 41(1):1, 2014.

- [124] C Büskens and D Wassel. The ESA NLP solver WORHP. In *Modeling and Optimization in Space Engineering*, pages 85–110. Springer, 2012.
- [125] GI Zahalak. Modeling muscle mechanics (and energetics). In *Multiple Muscle Systems*, pages 1–23. Springer, 1990.
- [126] JM Winters. Hill-based muscle models: a systems engineering perspective. In *Multiple Muscle Systems*, pages 69–93. Springer, 1990.
- [127] B Katz. The relation between force and speed in muscular contraction. *The Journal of Physiology*, 96(1):45, 1939.
- [128] KGM Gerritsen, W Nachbauer, and AJ van den Bogert. Computer simulation of landing movement in downhill skiing: anterior cruciate ligament injuries. *Journal of Biomechanics*, 29(7):845–854, 1996.
- [129] AS Bahler. Series elastic component of mammalian skeletal muscle. *American Journal of Physiology—Legacy Content*, 213(6):1560–1564, 1967.
- [130] J He, WS Levine, and GE Loeb. Feedback gains for correcting small perturbations to standing posture. *IEEE Transactions on Automatic Control*, 36(3):322–332, 1991.
- [131] JM Winters and L Stark. Muscle models: what is gained and what is lost by varying model complexity. *Biological Cybernetics*, 55(6):403–420, 1987.
- [132] SG McLean, A Su, and AJ van den Bogert. Development and validation of a 3-D model to predict knee joint loading during dynamic movement. *Journal of Biomechanical Engineering*, 125(6):864–874, 2003.
- [133] KN An, K Takahashi, TP Harrigan, and EY Chao. Determination of muscle orientations and moment arms. *Journal of Biomechanical Engineering*, 106(3):280–282, 1984.

- [134] AJ van den Bogert, D Blana, and D Heinrich. Implicit methods for efficient musculoskeletal simulation and optimal control. *Procedia IUTAM*, 2:297–316, 2011.

CHAPTER III

JOINT CONTACT FORCES CAN BE REDUCED BY IMPROVING JOINT MOMENT SYMMETRY IN TRANSTIBIAL AMPUTEE GAIT SIMULATIONS

Despite having a fully functional knee and hip in both legs, asymmetries in joint moments of the knee and hip are often seen in gait of persons with a unilateral transtibial amputation (TTA), possibly resulting in excessive joint loading. We hypothesize that persons with a TTA can walk with more symmetric joint moments at the cost of increased effort or abnormal kinematics. The hypothesis was tested using predictive simulations of gait. Open loop controls of one gait cycle were found by solving an optimization problem that minimizes a combination of walking effort and tracking error in joint angles, ground reaction force and gait cycle duration. A second objective was added to penalize joint moment asymmetry, creating a multi-objective optimization problem. A Pareto front was constructed by changing the weights of the objectives and three solutions were analyzed to study the effect of increasing joint moment symmetry. When the optimization placed more weight on moment symmetry, walking effort increased and kinematics became less normal, confirming the hypothesis. TTA gait improved with a moderate increase in joint moment symmetry. At a small cost of effort and abnormal kinematics, the peak hip extension moment in the intact leg was decreased significantly, and so was the joint contact force in the knee and hip. Additional symmetry required a significant increase in walking effort and the joint contact forces in both hips became significantly higher than in able-bodied gait.

Statement of Contribution

This chapter contributes to the understanding of gait of persons with a transtibial amputation. It shows that an asymmetric gait is chosen because this is optimal in terms of energy expenditure. It also suggests a possible rehabilitation strategy to reduce the knee reaction force in the intact leg, which could be beneficial to the patient's health.

Publications:

Koelewijn, A. D., and Van den Bogert, A. J. (2016). Joint contact forces can be reduced by improving joint moment symmetry in below-knee amputee gait simulations. *Gait & Posture*, 49, 219–225.

Conference Presentations:

- Koelewijn, A., and Van den Bogert, A. J. (2015). Improving Below-knee Amputee Gait – a Simulation Study of Pareto-optimal Movement Trajectories. Dynamic Walking, Columbus (OH).
- Koelewijn, A., and Van den Bogert, A.J. (2015). Is Kinetic Asymmetry in Below-knee Amputee Gait Inevitable? – a Predictive Simulation Study. XXV Congress of the International Society of Biomechanics, Glasgow (UK).

3.1 Introduction

Most amputations are transtibial amputations due to complications of diabetes [1]. However, amputations due to trauma are more common in young and physically active individuals [1]. Persons with a transtibial amputation (TTA) who have worn a prosthesis for over five years have a higher occurrence rate of osteoarthritis in the knee and hip of the intact leg [2, 3]. Also, other health issues exist among persons with an amputation, such as residual limb pain, back pain and phantom pain [4].

Studies analyzing gait of persons with a TTA have reported asymmetries between the residual and intact leg in the joint moments, the stance and swing time, the ground reaction force (GRF) [5] and EMG data [6]. These asymmetries, especially in the joint loading, may cause higher forces in the intact leg compared to the residual leg and to able-bodied gait, which is suspected to be related to the aforementioned higher occurrence rate of osteoarthritis [2]. Therefore, it is desirable to reduce the level of asymmetry in the joint moments of the knee and hip in TTA gait and distribute the load more equally between both legs.

The asymmetries are presumably caused by compensations required after amputation and the resulting loss of the biological ankle function [7, 8]. Elastic storage and return (ESAR) feet were developed to improve TTA gait [9, 10]. However, the joint moments remain distinctly asymmetric when using the ESAR feet [8, 11, 12].

Asymmetry is inevitable because the prosthetic limb does not replicate the mechanics and control of the intact limb. However, the knee and hip, and the entire intact limb, still have a sufficient set of muscles under voluntary neural control for flexion and extension. Therefore, we hypothesize that persons with a TTA can walk with symmetric joint moments using a passive prosthesis, but prefer not to do so because it would require additional effort or abnormal kinematics.

If humans choose their gait to minimize energy [13], this question can be investigated by predictive simulations of gait. In such simulations, an optimal control problem is for-

mulated to find open loop controls that produce walking with minimal cost. Previous work showed that the main features of gait can be predicted by minimizing muscle activation [14, 15], and that predictions are improved when tracking of joint angles, GRFs and duration of normal gait is added to the objective [16]. This objective has been used to predict the effect of sports equipment on performance [16] which is conceptually similar to predicting TTA gait, because both cases predict how an altered mechanical environment affects gait.

In the present study, a second objective is added to penalize asymmetry in joint moments. The second objective creates a multi-objective optimization problem, which is used to study the effect of different levels of joint moment symmetry on TTA gait.

3.2 Methods

3.2.1 Model

Section 2.6 describes the human model that is used in this study. To simulate TTA gait, the Gastrocnemius, Soleus and Tibialis Anterior were removed in one of the legs and replaced by a passive spring with a stiffness of 600 Nm/rad and damping of 15 Nm/s/rad, as used by Zmitrewicz et al. [17]. The mass and inertial properties were not altered.

3.2.2 Optimal Control Problem

Predictive simulations were performed by solving an optimal control problem: find periodic state trajectories $x(t)$ and control trajectories $u(t)$ that satisfy the system dynamics and minimize a cost function. The formulation and solution method were identical to [16], but no left-right symmetry was assumed and a full gait cycle was simulated. A two-part cost function was used, using a weight w to determine the relative importance of each objective:

$$\min_{x,u} J_1(x, u) + w \cdot J_2(x, u) \quad (3.1)$$

The first objective, J_1 , was used by Van den Bogert et al. [16] to perform predictive simulations of walking and running. This objective penalizes muscular effort and deviation from normal joint angles, GRFs and gait duration:

$$\begin{aligned} J_1(x, u) = & \frac{1}{11} \left(\frac{1}{T} \sum_{k=1}^{10} \int_0^T \left(\frac{s_k(x(t)) - x_{m_k}(t)}{\sigma_k} \right)^2 dt \right. \\ & \left. + \left(\frac{T - T_m}{\sigma_T} \right)^2 \right) + \frac{W_{\text{effort}}}{16T} \sum_{j=1}^{16} \int_0^T u_j(t)^2 dt \end{aligned} \quad (3.2)$$

The eleven tracked variables $s_k(x(t))$ were six joint angles, the horizontal and vertical GRFs of both legs, and the duration of the gait cycle, T . Tracking data, $x_{m_k}(t)$ and T_m , and standard deviations, σ_k , were provided by Winter [18]. Based on [16], $W_{\text{effort}} = 10$ was used to scale the effort term.

The second objective function, J_2 , was added to study the effect of encouraging symmetric joint moments in knee and hip. Joint moment symmetry is encouraged indirectly by the tracking term in J_1 , but the amputation makes the model asymmetrical. Asymmetrical movement will therefore occur if this reduces the effort term in J_1 . Furthermore, even if joint angles and GRFs are symmetric, there may be asymmetry in the center of pressure, which affects joint moments but is not included in the tracking term. Joint moment asymmetry was defined as the root mean square difference between the left and right joint moment of joint i , accounting for a phase shift of a half-cycle:

$$J_2(x, u) = \frac{1}{2} \sum_{i=1}^2 \int_0^T \left(M_{i_r}(t) - M_{i_l} \left(t + \frac{T}{2} \right) \right)^2 dt \quad (3.3)$$

The optimal control problem was solved through direct collocation, with 60 collocation points per gait cycle and a backward Euler formulation. One collocation point was added to ensure periodicity of the gait cycle, so the final state matches the initial state with a forward translation. Details can be found in [15] and [16]. The resulting constrained optimization problem was solved using IPOPT 3.11.0 [19].

First, the optimal control problem was solved for the able-bodied model (ABLE). To obtain this solution, standing was solved first, followed by a series of able-bodied gait solutions with increasing speed. Then, using the able-bodied solution as an initial guess, TTA gait was solved using only objective J_1 , thus without considering asymmetry in joint moments (TTA1).

Then, objective J_2 was added, creating a multi-objective optimization problem for TTA gait due to the asymmetry between the left and right leg. A Pareto-front was obtained by solving the optimization problem using different weights for objective J_2 .

Two solutions (TTA2 and TTA3) on the Pareto-front were analyzed and compared against the baseline and the able-bodied solution to analyze the effect of J_2 . Joint angles, joint moments, muscle forces, GRFs and joint contact forces were examined to find kinetic and kinematic changes. The energy required for each of the predicted gaits is compared using the effort term in equation 3.2 and a metabolic cost model [20]. GRFs, joint angles and muscle forces were used to find the joint contact force (JCF) magnitudes, the Euclidean norm of the components in the x- and y-direction.

3.3 Results

First, able-bodied gait was solved. A gait cycle of 1.14 seconds with a speed of 1.325 m/s required 3.12 W/kg metabolic energy. Joint angles and ground reaction forces of this solution were all within one standard deviation of the tracking data [18]. Only the peak hip flexion angle was slightly higher. The able-bodied solution was found in 7 minutes and 52 seconds on a computer with an Intel Core i5-3210M CPU at 2.5 GHz clock speed.

The Pareto-front (Figure 9) shows the trade-off between symmetry in the joint moment and the objective of low effort and normal gait. Initially, the increase in joint moment symmetry had a small effect on the tracking and effort term. However, as joint moment symmetry improved, the cost of more joint moment symmetry increased considerably. All gaits are theoretically feasible for a person with a TTA, the choice between them depending

on the relative weight of the optimization objectives, which are reported in figure 10.

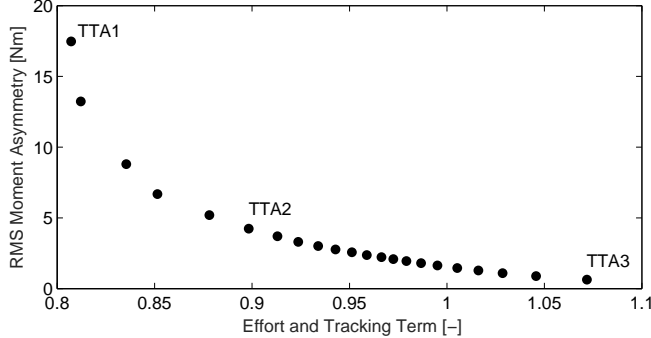


Figure 9: Pareto-front showing the trade-off between effort and symmetry in the joint moments. Solutions TTA1, TTA2 and TTA3 will be analysed further.

Three points are of interest in the Pareto-front. Solution TTA1 is the baseline solution, where the weight of objective J_2 was zero. Solution TTA2, which used $w = 0.3$, is a solution where the symmetry of the joint moments greatly improved with little extra effort and deviation from normal kinematics (11% increase in J_1). Solution TTA3 , where $w = 10$, required an increase in effort and tracking error of almost 33%.

Figure 10 shows the tracking error, effort, RMS moment asymmetry and metabolic cost as a function of the weight w in equation 3.1. Tracking error increased almost linearly from 0.55 at $w = 0$ to 0.79 at $w = 10$. Effort stayed approximately constant at 0.0257 until $w = 0.2$, after which it increased to 0.0282 at TTA3. Joint moment asymmetry decreased from 17.5 Nm to 5.19 Nm at $w = 0.2$ and then to 0.635 Nm at solution TTA3. The metabolic cost first decreased from 3.09 W/kg to 3.05 W/kg at $w = 0.05$, after which it increases to 3.21 W/kg at TTA3.

Joint angles (Figure 11) were within one standard deviation of the tracking data, except the peak hip flexion angle at heel strike, which deviated more than two standard deviations, and the intact knee angle in TTA3 between 20% and 40% of the gait cycle, which deviated more than one standard deviation. Furthermore, the knee and hip joint kinematics were similar and nearly symmetric in all solutions. However, the joint kinetics distinctly differed between the solutions.

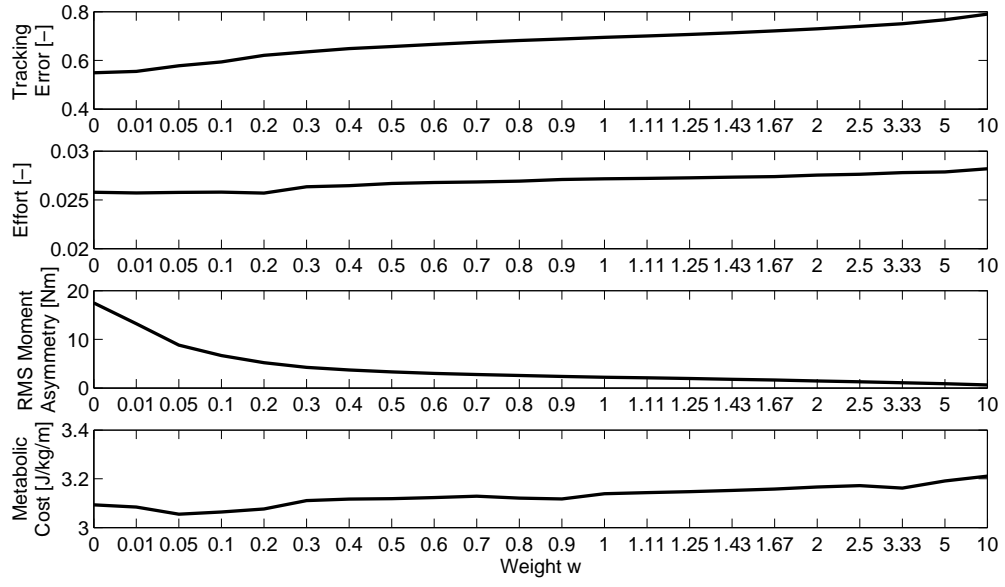


Figure 10: Relationship between the weight w of equation 3.1 and the different objectives of tracking error, effort and moment symmetry, as well as the metabolic cost as a function of the weight w . Tracking increases linearly, while effort stays approximately constant until $w = 2$ and increases for larger weights. The moment asymmetry decreases with increased weight. The metabolic energy expenditure is lowest at $w = 0.05$ and increases beyond the initial value for weights larger than 0.2.

In TTA 1, which did not consider joint moment asymmetry, joint moments were distinctly asymmetric and differed from ABLE (Figure 11). The peak extension moment in the hip of the prosthesis side was 38 Nm, compared to 100 Nm on the intact side and 44 Nm in ABLE. The peak extension moment in the knee was 28 Nm on the prosthesis side and 51 Nm in the intact side, compared to 42 Nm in ABLE.

In solution TTA2, tracking error increased by 16%, effort increased by 2% and joint moment asymmetry was reduced by 76%. Peak extension moment in the hip was 67 Nm on the prosthesis side and 76 Nm on the intact side, more symmetrical than in TTA1 but higher than in ABLE. The peak knee extension moment was also more symmetrical, 26 Nm on the prosthesis side and 34 Nm on the intact side. Both values were lower than in ABLE.

Solution TTA3 reduced joint moment asymmetry by 88%, but required an increase in effort of 10% and in tracking error of 43%. In this solution, the peak hip extension moment

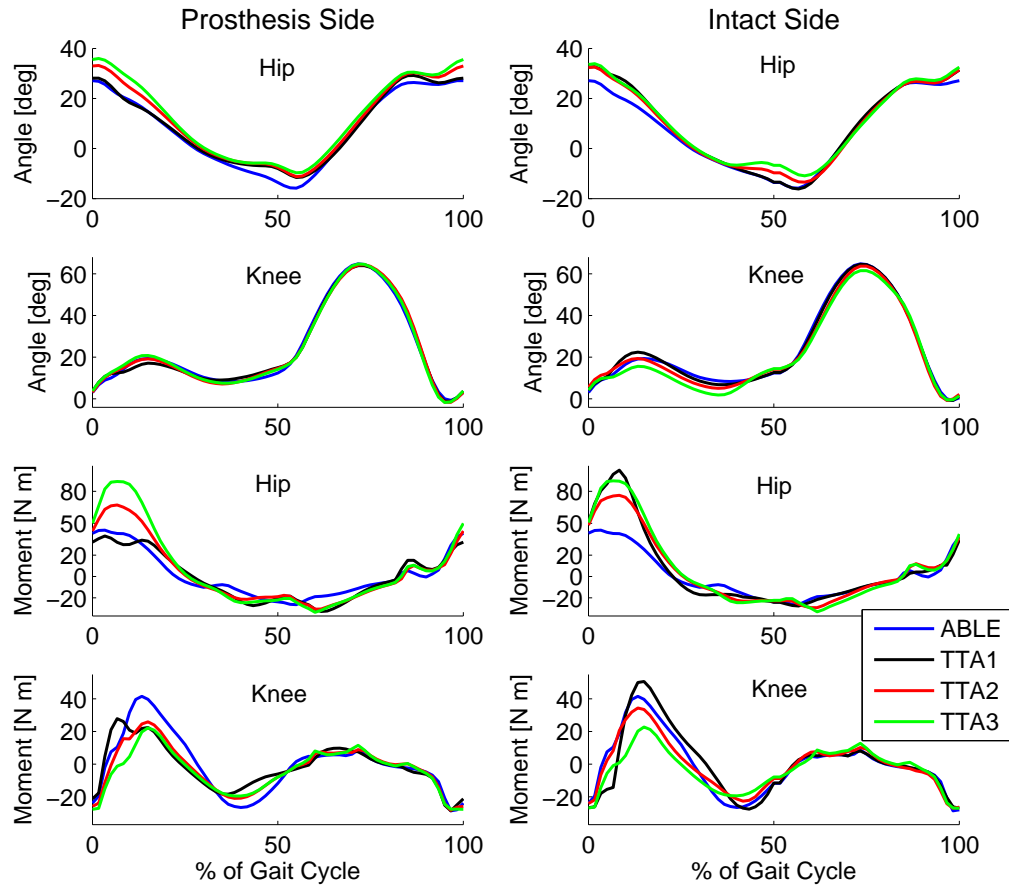


Figure 11: Joint angles, moments for the prosthesis side (left) and the intact side (right) for solutions ABLE, TTA1, TTA2 and TTA3. The gait cycle starts at heel strike on both sides. The angles show flexion positive, while in the moment graphs, extension is positive. Joint angles were within one standard deviation of the tracking data, except for the peak hip flexion angle at heel strike and the intact knee angle in TTA3. Joint moments are distinctly asymmetric and different from ABLE in TTA1, while the symmetry increases in solution TTA2 and TTA3, but at the cost of a larger peak hip extension moment.

was equal to 89 Nm on the prosthesis side and 90 Nm on the intact side, more than twice as high as in ABLE. The peak knee moment is equal to 22 Nm on the prosthesis side and 23 Nm on the intact side, which is about half that of ABLE.

Figure 12 shows the muscle forces in the musculoskeletal model. Hip muscle forces were lowest in ABLE. In TTA1, the Hamstrings force was high in early stance on the intact side, 603 N, compared to 356 N on the prosthesis side. The peak force in the Gluteals was 986 N on the intact side, compared to 307 N on the prosthesis side. Also, the peak force in

the Iliopsoas was high on the prosthesis side during late stance, 883 N, compared to 280 N on the intact side. In TTA2 and TTA3, peak forces in the hip muscles on the prosthesis side increased compared to TTA1. The peak force in the Gluteals on the intact side decreased, and so did the peak force in the Hamstrings in TTA2. The other peak forces remained similar to TTA1.

The vertical ground reaction force on the prosthesis side was similar for all solutions and within one standard deviation of the tracking data (Figure 13). Large differences were seen in the joint contact forces (Figure 13). Hip joint contact forces were higher than in ABLE for both legs in all conditions. In the intact side, the peak joint contact force was lowest in TTA2, but higher than in ABLE. The joint contact force in the knee of the prosthesis side was lower than ABLE for all solutions.

3.4 Discussion

An able-bodied solution was found using the approach presented by Van den Bogert et al. [16]. Joint moments are symmetric between the two legs. Their values correspond to results found in studies with human subjects. Also, the metabolic energy was similar to metabolic energy found in studies with human subjects [21].

Any of the solutions on the Pareto-front can theoretically be chosen as a gait by persons with a TTA. Therefore, the hypothesis that persons with a TTA can walk with more symmetry in the joint moments at the cost of increased effort and abnormal kinematics is confirmed. Figure 10 shows that joint moment asymmetry can be reduced by 70% with little increase in effort or metabolic cost.

If persons with a TTA select a gait with normal kinematics and minimal effort, we would expect them to select solution TTA1. The largely symmetric joint angles in the knee and hip in TTA1 are also seen in studies of persons with a TTA [11, 22]. The predicted reduction of the knee joint moment on the prosthesis side in TTA1 is also seen in subjects with a TTA [8, 11, 12].

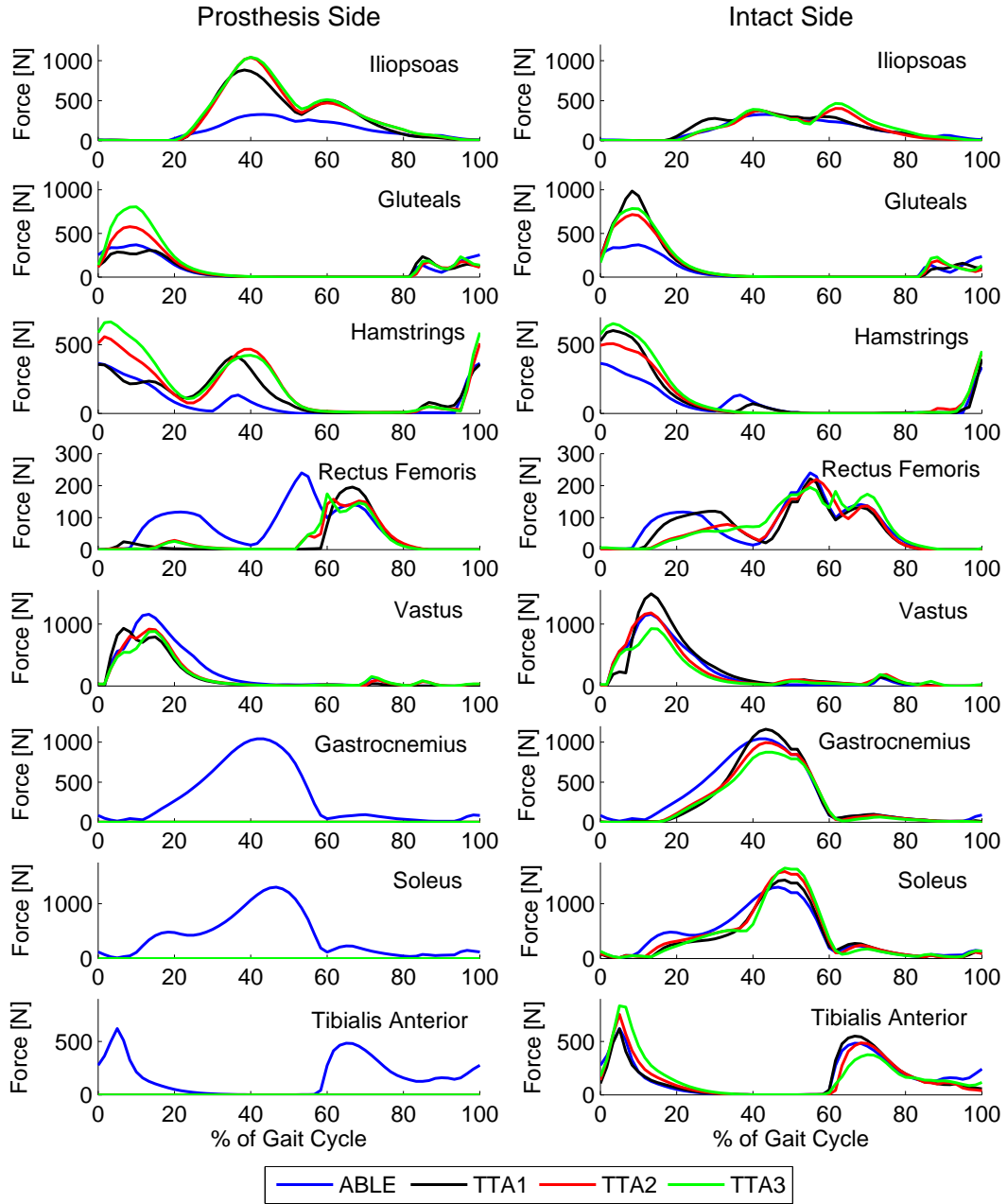


Figure 12: Muscle forces of all muscles in the musculoskeletal model for solutions ABLE, TTA1, TTA2 and TTA3. The gait cycle starts at heel strike on both the prosthesis side (left) and the intact side (right). Muscle forces were lowest in ABLE. Peak forces in the hip muscles on the prosthesis side increased in solution TTA2 and TTA3, compared to TTA1, while the peak force in the Gluteals and Hamstrings on the intact side decreased.

Nolan and Lees [23] and Ferris et al. [8] report a higher peak extension hip moment in the intact leg compared to able bodied walking, which agrees with our predictions in TTA1.

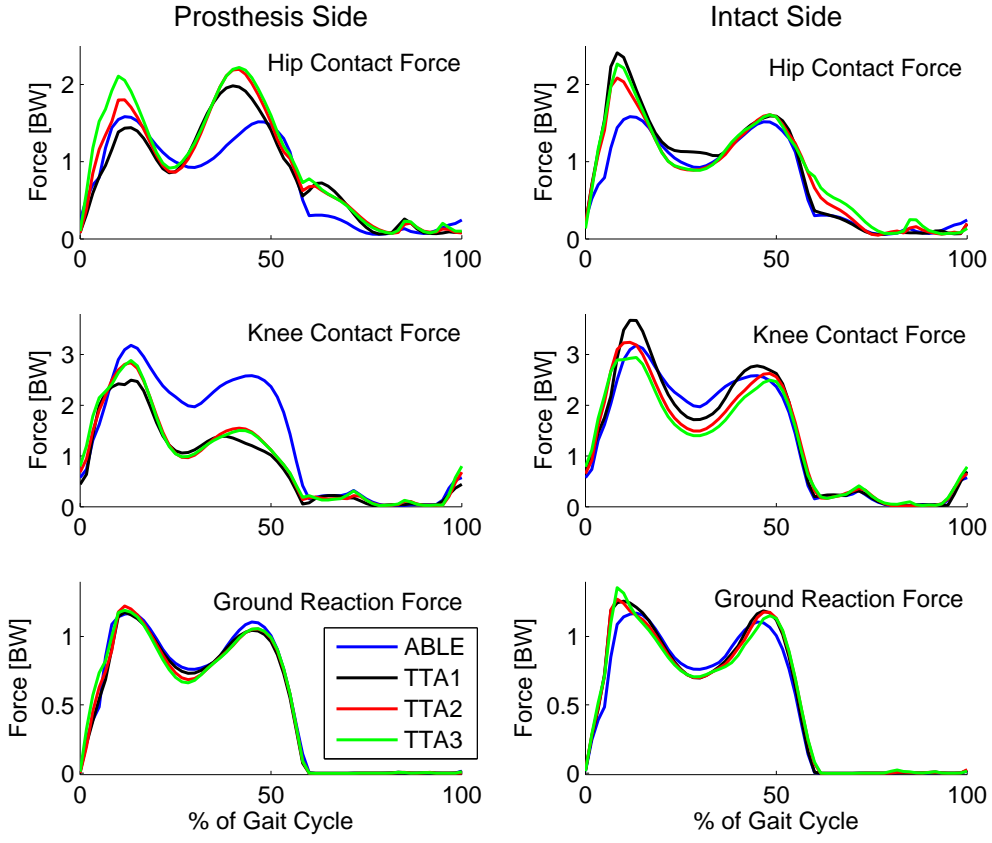


Figure 13: Joint contact force in the knee and hip for solutions ABLE, TTA1, TTA2 and TTA3. Hip joint contact forces are higher than in ABLE for all TTA conditions. On the intact side, the peak hip contact force was lowest in TTA2. The peak knee contact force on the prosthesis side was lower than ABLE for all conditions and it was higher than ABLE on the intact side for TTA1.

However, some literature reports more symmetry in the peak hip extension moment of the intact and residual leg [24, 25], which is more similar to TTA2. TTA1 and TTA2 require a similar amount of effort or metabolic work, which suggests persons with a TTA operate around TTA1 and TTA2 in the Pareto-front.

Solution TTA2 has several advantages over TTA1 and TTA3. A lower peak extension moment in the hip and knee reduced joint moment asymmetry and yielded a lower joint contact force in both joints. A high joint contact force is suspected to be related to a higher incidence rate of osteoarthritis in persons with a TTA [2], so the lower joint contact forces could decrease this higher incidence rate. Another potential benefit in TTA2 is the higher knee joint contact force in the residual leg compared to TTA1 and to ABLE, which might

reduce the loss of bone mineral density in the proximal tibia and femur neck, which is reported for persons with a TTA [26]. Therefore, teaching persons with a TTA to walk using TTA2 may be useful in rehabilitation.

TTA3 emphasized joint moment symmetry too much, which is disadvantageous for TTA gait. Apart from a 10% increase in effort compared to TTA1, the peak hip extension moment increased in both legs, which also yielded a higher joint contact force in the hip. Currently, prevalence of osteoarthritis in the intact hip is already higher in persons with a TTA [3] and TTA3 could increase the risk of developing osteoarthritis in the hips of both legs.

On the prosthesis side, there is no active push-off and the biarticular Gastrocnemius is removed completely. This might cause the Iliopsoas force to increase on the prosthesis side during late stance, because this muscle now initiates the swing phase and compensates for the activation of the biarticular Hamstrings, which flexes the knee instead of the Gastrocnemius. Some persons with a TTA can still use the Gastrocnemius to control the knee, which might reduce this effect. Additionally, the lack of push-off increases the impact force on the intact side (Figure 13) [27]. A passive foot that stores and releases energy using microprocessor control, such as the artificial foot by Collins and Kuo [27] or a prosthesis with a motor can better restore the push-off function of the biological ankle and reduce these effects.

The metabolic model produced a lower metabolic cost for TTA gait than for able-bodied gait, which contradicts subject studies [21]. The predicted metabolic cost for TTA gait is lower because three muscles are removed that would otherwise contribute significantly. While our predictions are theoretically possible, actual TTA gait may require more energy due to antagonistic co-contraction to stabilize the prosthetic side [6], for example due to an unstable connection between the prosthesis and residual leg. Such co-contraction will not be predicted by a simulation where effort is optimized and no stability is required. Therefore, we conclude that other objectives might also influence TTA gait, like stability,

joint pain or comfort. The underestimation of metabolic energy suggest that we may also have underestimated the muscle forces and joint contact forces.

The modeled prosthesis had the same mass and moment of inertia as the intact leg. This ensured that this study only predicted effects due of control and not of a change in prosthesis parameters. Prosthetic legs have different mass and inertial properties than a normal leg, but this will mostly affect the swing phase, where forces and moments are low. Therefore, we expect that there is little effect of mass properties on the peak loading variables.

Additionally, the prosthesis was modeled as a linear spring with a stiffness of 600 Nm/rad, a nominal stiffness based on measurements by Lehmann et al. [28]. However, stiffness of prostheses vary between feet, and affects kinetic and kinematic variables during the gait cycle [29], but less so than the difference between the intact and the prosthesis side and individual variability [30]. Early work showed that the asymmetry in the knee joint moment was not affected by the choice of stiffness for weight $w = 0$ for stiffnesses equal to or larger than the stiffness of a human ankle [31]. Therefore, it is not expected that a different conclusion would have been reached with a different stiffness value, but this remains an open question.

The Pareto-front in figure 9 was created by varying the weights between the effort and data tracking term and the joint moment asymmetry term. With this approach, it is possible that a non-convex optimization problem finds a local optimum instead of the global optimum given a certain weight [32]. Therefore, the optimizations were repeated using the approach described by Hays et al. [33], where only the objective of effort and data tracking is optimized, while the objective of joint moment asymmetry is added to the problem as a constraint with an upper bound. The added constraint created numerical difficulties for IPOPT. By varying the value of the constraint, a Pareto-front was developed with the lowest possible effort and data tracking given a certain level of asymmetry. Figure 14 shows the original Pareto-front, and the data points that were found with this constraint approach.

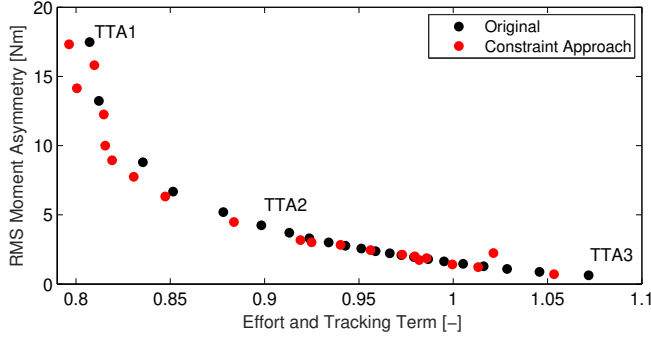


Figure 14: Original Pareto-front in black with new data points that were found with the constraint approach described by Hays et al. [33].

The shape of the curve was not as smooth as for the original Pareto-front. This could reflect the actual shape of the pareto curve, but it also possible that some of the solutions found with the new approach are local minima. Data points on the new Pareto-front closest to TTA1, TTA2, and TTA3 were analyzed and the same conclusions were reached with these solutions.

This study used a two-dimensional musculoskeletal model. Hip joint forces may have been underestimated by neglecting the abductor moments. However, we expect the main conclusions to be valid. This should be verified with a three-dimensional musculoskeletal model or with subject tests. Further tests with a three dimensional model could also analyze the effects of having joint moment symmetry in the frontal and transverse plane, while a subject study could verify if subjects can maintain the suggested gait modifications.

The model was created for a specific height and weight and walking data was tracked from Winter [18]. It is expected that the conclusions are valid for a more general population. However, in future studies, it is advised that the predictive simulations are found for models with a range of heights and weights, such that a more general population is taken into account.

We conclude from this study that:

1. Asymmetric knee and hip joint moments in persons with a TTA with a passive foot can be explained by a predictive simulation model that minimizes effort and deviation

from normal kinematics.

2. Considerable improvement in moment symmetry is theoretically possible with a small increase in effort and almost no change in kinematics. The hip joint moment will, however, remain elevated above able-bodied values, which is currently also reported for persons with a TTA [24, 25].

3.5 References

- [1] K Ziegler-Graham, EJ MacKenzie, PL Ephraim, TG Travison, and R Brookmeyer. Estimating the prevalence of limb loss in the United States: 2005 to 2050. *Archives of Physical Medicine and Rehabilitation*, 89(3):422–429, 2008.
- [2] ED Lemaire and FR Fisher. Osteoarthritis and elderly amputee gait. *Archives of Physical Medicine and Rehabilitation*, 75:1094–1099, 1994.
- [3] PA Struyf, CM van Heugten, MW Hitters, and RJ Smeets. The prevalence of osteoarthritis of the intact hip and knee among traumatic leg amputees. *Archives of Physical Medicine and Rehabilitation*, 90(3):440–446, 2009.
- [4] PL Ephraim, ST Wegener, EJ MacKenzie, TR Dillingham, and LE Pezzin. Phantom pain, residual limb pain, and back pain in amputees: results of a national survey. *Archives of Physical Medicine and Rehabilitation*, 86(10):1910–1919, 2005.
- [5] MR Menard, ME McBride, DJ Sanderson, and DD Murray. Comparative biomechanical analysis of energy-storing prosthetic feet. *Archives of Physical Medicine and Rehabilitation*, 73(5):451–458, 1992.
- [6] E Isakov, O Keren, and N Benjuya. Trans-tibial amputee gait: Time-distance parameters and EMG activity. *Prosthetics and Orthotics International*, 24(3):216–220, 2000.

- [7] GRB Hurley, R McKenney, M Robinson, M Zadravec, and MR Pierrynowski. The role of the contralateral limb in below-knee amputee gait. *Prosthetics and Orthotics International*, 14(1):33–42, 1990.
- [8] AE Ferris, JM Aldridge, CA Rábago, and JM Wilken. Evaluation of a powered ankle-foot prosthetic system during walking. *Archives of Physical Medicine and Rehabilitation*, 93(11):1911–1918, 2012.
- [9] NP Fey, GK Klute, and RR Neptune. The influence of energy storage and return foot stiffness on walking mechanics and muscle activity in below-knee amputees. *Clinical Biomechanics*, 26(10):1025–1032, 2011.
- [10] J Wagner, S Sienko, T Supan, and D Barth. Motion analysis of SACH vs. Flex-Foot in moderately active below-knee amputees. *Clinical Prosthetics & Orthotics*, 11(1):55–62, 1987.
- [11] DJ Sanderson and PE Martin. Lower extremity kinematic and kinetic adaptations in unilateral below-knee amputees during walking. *Gait & Posture*, 6(2):126–136, 1997.
- [12] H Bateni and SJ Olney. Kinematic and kinetic variations of below-knee amputee gait. *JPO: Journal of Prosthetics and Orthotics*, 14(1):2–10, 2002.
- [13] JEA Bertram and A Ruina. Multiple walking speed–frequency relations are predicted by constrained optimization. *Journal of Theoretical Biology*, 209(4):445–453, 2001.
- [14] FC Anderson and MG Pandy. Dynamic optimization of human walking. *Journal of Biomechanical Engineering*, 123(5):381–390, 2001.
- [15] M Ackermann and AJ van den Bogert. Optimality principles for model-based prediction of human gait. *Journal of Biomechanics*, 43(6):1055–1060, 2010.
- [16] AJ van den Bogert, M Hupperets, H Schlarb, and B Krabbe. Predictive musculoskeletal simulation using optimal control: effects of added limb mass on energy cost and

- kinematics of walking and running. *Proceedings of the Institution of Mechanical Engineers, Part P: Journal of Sports Engineering and Technology*, pages 1–11, 2012.
- [17] RJ Zmitrewicz, RR Neptune, and K Sasaki. Mechanical energetic contributions from individual muscles and elastic prosthetic feet during symmetric unilateral transtibial amputee walking: a theoretical study. *Journal of Biomechanics*, 40(8):1824–1831, 2007.
 - [18] DA Winter. *Biomechanics and motor control of human gait: normal, elderly and pathological*. University of Waterloo Press, 2 edition, 1991.
 - [19] A Wächter and LT Biegler. On the implementation of an interior-point filter line-search algorithm for large-scale nonlinear programming. *Mathematical Programming*, 106(1):25–57, 2006.
 - [20] BR Umberger, KGM Gerritsen, and PE Martin. A model of human muscle energy expenditure. *Computer Methods in Biomechanics and Biomedical Engineering*, 6(2):99–111, 2003.
 - [21] D Hunter, ES Cole, JM Murray, and TD Murray. Energy expenditure of below-knee amputees during harness-supported treadmill ambulation. *Journal of Orthopaedic & Sports Physical Therapy*, 21(5):268–276, 1995.
 - [22] E Isakov, H Burger, J Krajnik, M Gregoric, and C Marincek. Influence of speed on gait parameters and on symmetry in transtibial amputees. *Prosthetics and Orthotics International*, 20(3):153–158, 1996.
 - [23] L Nolan and A Lees. The functional demands on the intact limb during walking for active trans-femoral and trans-tibial amputees. *Prosthetics and Orthotics International*, 24(2):117–125, 2000.

- [24] N Vanicek, S Strike, L McNaughton, and R Polman. Gait patterns in transtibial amputee fallers vs. non-fallers: Biomechanical differences during level walking. *Gait & Posture*, 29(3):415–420, 2009.
- [25] JD Ventura, GK Klute, and RR Neptune. The effects of prosthetic ankle dorsiflexion and energy return on below-knee amputee leg loading. *Clinical Biomechanics*, 26(3):298–303, 2011.
- [26] T Royer and M Koenig. Joint loading and bone mineral density in persons with unilateral, trans-tibial amputation. *Clinical Biomechanics*, 20(10):1119–1125, 2005.
- [27] SH Collins and AD Kuo. Recycling energy to restore impaired ankle function during human walking. *PLoS One*, 5(2):e9307, 2010.
- [28] JF Lehmann, R Price, S Boswell-Bessette, A Dralle, K Questad, et al. Comprehensive analysis of energy storing prosthetic feet: Flex Foot and Seattle foot versus standard SACH foot. *Archives of Physical Medicine and Rehabilitation*, 74(11):1225–1231, 1993.
- [29] Glenn K Klute, Carol F Kallfelz, and Joseph M Czerniecki. Mechanical properties of prosthetic limbs: adapting to the patient. *Journal of rehabilitation research and development*, 38(3):299, 2001.
- [30] A Cortes, E Viosca, JV Hoyos, J Prat, and J Sanchez-Lacuesta. Optimisation of the prescription for trans-tibial (tt) amputees. *Prosthetics and orthotics international*, 21(3):168–174, 1997.
- [31] AH Hansen, DS Childress, SC Miff, SA Gard, and KP Mesplay. The human ankle during walking: implications for design of biomimetic ankle prostheses. *Journal of Biomechanics*, 37(10):1467–1474, 2004.

- [32] V Sevastyanov. Gradient-based multi-objective optimization technology. In *13th AIAA/ISSMO Multidisciplinary Analysis Optimization Conference*, pages 9092–10011, 2010.
- [33] J Hays, A Sandu, C Sandu, and D Hong. Parametric design optimization of uncertain ordinary differential equation systems. *Journal of Mechanical Design*, 134(8):081003, 2012.

CHAPTER IV

THE EFFECT OF PROSTHESIS MISALIGNMENT ON GAIT - A PREDICTIVE SIMULATION STUDY

The effect of prosthesis alignment on gait of persons with a transtibial amputation is largely unknown. A predictive simulation study with 20 virtual subjects was performed to verify four hypotheses: (1) the hip angles on the prosthesis side are adjusted to compensate for the alignment change, (2) the hip and knee reaction force on the intact side are the lowest in the reference alignments, (3) the change in alignment will increase the knee reaction moment on the prosthesis side, (4) metabolic energy expenditure is lowest in the reference alignment. Predictive simulations were found with a flexion, extension, abduction, adduction, internal rotation, external rotation, medial translation, and lateral translation alignment change. All hypotheses were confirmed for one or more of the alignment changes. The predictive simulations with a flexion alignment change seemed beneficial, since the metabolic cost was lower than the reference, and so were the reaction forces in the knee and hip on the intact side, and the peak knee abduction moment on the prosthesis side. Also, by rotating a prosthesis externally, or by using a lateral translation, the knee abduction moment on the prosthesis side could be reduced without affecting other gait parameters. This could reduce skin stress and related health issues. These results should be verified using experimental studies.

Statement of Contribution

This chapter contributes in several aspects. Its main contribution is a comprehensive study on prosthesis alignment. Previously, experimental studies have been performed of a smaller number of different alignments, while a smaller set of parameters was analyzed. With an experiment, it is not possible to study many different alignments at once, since this would be very cumbersome for participants. This was the first simulation based study into prosthesis alignment, which allowed us to compare many alignments at once. Since little data (such as metabolic cost, joint moments) on the effect of alignment changes is available in literature, this study can be used as a starting point for further experimental studies on prosthesis alignment. These experiments should be used to verify if the alignments that yielded a good performance in simulation, will also be good in practice.

A secondary contribution of this work is related to the methods. The three-dimensional model that is used was developed recently. This study was the first application of this model and highlights its potential to provide insight in different gait interventions. Additionally, this work is the first three dimensional predictive simulation that was solved using direct collocation, and was found to be much faster than previous three-dimensional predictive simulations.

4.1 Introduction

Currently, when a patient requires a prosthesis, the prosthetist and the patient use a subjective process to fit the prosthesis [1, 2]. The prosthetist relies on visual gait analysis and feedback of the patient to find an appropriate alignment [3, 4]. This method is time-consuming, and can require multiple sessions, and the success will depend on the experience of the prosthetist [5, 6]. However, comfort and function of the prosthesis are directly related to the prosthesis alignment.

Studies on prosthesis' alignment have found a range of alignments to be acceptable to the patient [4, 6, 7]. Also, prosthetists have difficulty reproducing what they think is the optimal alignment [4]. Different optimality criteria exist, such as symmetry of the gait, step-to-step variability and roll-over shape of the foot [2]. Another criterion defines that the center of pressure in the sagittal plane when standing on just the prosthetic foot should be within 1 cm of the center of pressure when standing on both feet [6].

Gait symmetry can exist in many parameters. Six parameters were suggested to have a high symmetry index when the alignment is good: the first and second peak of the vertical ground reaction force and its trough, the stance duration, step length, and the time to full knee flexion during the swing phase [1]. Additionally, Hannah et al. found that the joint angles are most symmetric in an optimal alignment [8]. However, it should be noted that due to the asymmetric dynamics of a person with a below-knee prosthesis, an asymmetric gait might be optimal [2, 9].

A misalignment can be introduced by a translation or a rotation at the connection between the socket and leg, or at the prosthetic ankle. When a prosthesis is misaligned, the loading of the legs changes [4, 5, 10, 11]. This effect is larger when a misalignment is introduced in the frontal plane than in the sagittal plane [3, 11]. Also, a misalignment could lead to walking and standing instability [3, 10, 12], an increased peak vertical ground reaction force and impact on the prosthetic leg [10], increased muscle forces [5], discomfort [10], pain [13] and skin trauma [3, 10]. Gait adaptations due to a misalignment can lead to

long-term orthopedic health issues [4, 11] and reduced mobility [11].

Several compensation mechanisms have been reported. An external rotation of the prosthesis is compensated by internally rotating the hip [13]. A misalignment in the sagittal plane is compensated such that the weight remains above the center of pressure [6]. This changes the loading of the knee on the prosthesis side [2, 6, 14]. When the prosthetic leg was internally rotated, the loading in the knee remained the same on the prosthesis side, while a compensatory effect was reported in the knee on the intact side [15].

It is important that the prosthetist understand the force transmission between the prosthesis and the leg [11]. The current practice of analyzing symmetry, stability and ground reaction forces might not be accurate enough [3]. The joint moments might be more sensitive to alignment changes than ground reaction forces [16, 17].

This information can be obtained using a full gait analysis [3, 11], but it would not be possible to do a comprehensive assessment of different alignments in an experimental study, since this is time consuming and cumbersome to participants. The participants would have to walk many trials to test all different alignments, and the alignments might be uncomfortable and possibly lead to injuries. Another option is to add a device to the prosthesis to measure the joint moments in the socket [11], but this will only provide information on the loading at the socket.

However, a predictive simulation study could provide insight to joint loading of both legs without being intrusive to a person, because it does not require anyone to walk with a misaligned prosthesis. Also, many different alignments can be studied and compared easily. A three-dimensional model is required to change the alignment of the prosthesis in the frontal and transverse plane and study the effects of the alignment in these planes as well.

This predictive simulation study aims to compare gait of persons with a transtibial amputation (TTA gait) with different prosthesis alignments to gain insight into the effect of an alignment change on joint loads and metabolic cost. These simulations will be found by

solving trajectory optimization problems similar to Van den Bogert et al. [18] and chapter III using a three-dimensional model. Four hypotheses were tested: it was hypothesized that (1) the subject will adjust the hip angles on the prosthesis side to compensate for the alignment change, (2) the hip and knee reaction force on the intact side are the lowest in the reference alignments, (3) the change in alignment will increase the knee reaction moment on the prosthesis side, (4) metabolic energy expenditure is lowest in the reference alignment.

4.2 Methods

4.2.1 Three-dimensional Musculoskeletal Model

The three-dimensional musculoskeletal model was adapted from the model created by Hamner et al. [19]. This model is available in OpenSim [20]. The model has 33 degrees of freedom and is operated by 92 muscles in the trunk and legs and 10 torques in the arms. Mass and inertial properties were taken from the unscaled model [19].

The talus bone and the MTP joint were changed. The talus bone was given a mass of 0 kg instead of 0.1 kg. The MTP joint was not fixed, but given a range of motion. Passive joint moments were added to all joints outside the range of motion using a quadratic spring with stiffness 5000 Nm/rad². For numerical reasons, a linear spring with a very small stiffness of 1 Nm/rad was added to each joint. This spring is active for the full range of motion.

The multibody dynamics equations were derived using Autolev (Online Dynamics, Sunnyvale, CA, USA) with respect to the generalized coordinates q , following the procedure described in chapter II:

$$M(q)\dot{v} + C(q, v)v + G(q) = \tau + J_c^T F_c + T_{pas} \quad (4.1)$$

where $M(q)$ was the mass matrix, $C(q, v)$ contained the Coriolis forces, and $G(q)$ the

gravity forces, J_c was the Jacobian of the contact forces, F_c , and T_{pas} were the passive joint torques. $\tau = \tau_{mus} + \tau_{ext}$ were the joint moments, which are the sum of the torque due to the muscle forces, τ_{mus} and the actuation torques of the arm and other external torques, such as from a prosthesis, τ_{ext} .

Ground contact was modeled using a penetration based model, similar to section 2.6.2. Eight contact points were added to each foot, four were connected to the talus segment, and four to the toe segment.

The vertical ground reaction force, F_y depends on the vertical position y of the contact point, as follows:

$$F_y(d) = kd(1 - by) \quad (4.2)$$

where the vertical force is determined from the visco-elastic effects due to a deformation, d , of the contact point. To ensure differentiability, d was calculated as

$$d = \frac{1}{2} \left(\sqrt{y^2 + y_0^2} - y \right) \quad (4.3)$$

where y_0 is the size of the transition region between contact and no contact. The following parameter values were used: $k = 100$ BW/m, $b = 0.75$ s/m, $y_0 = 1 \cdot 10^{-3}$ m, where BW denotes body weight.

The fore/aft and sideways ground reaction forces were modeled as a continuous approximation of Coulomb friction:

$$F_x(F_y, \dot{x}) = -\mu F_y \frac{\dot{x}}{\sqrt{\dot{x}^2 + v_0^2}} \quad (4.4)$$

$$F_z(F_y, \dot{z}) = -\mu F_y \frac{\dot{z}}{\sqrt{\dot{z}^2 + v_0^2}} \quad (4.5)$$

where \dot{x} is the fore/aft sliding velocity, and \dot{z} the sideways sliding velocity of the contact point, $\mu = 1$ is the friction coefficient and $v_0 = 10^{-4}$ m/s is a small velocity parameter that

ensures a sign change in the friction when there is a change in the sliding direction.

All muscles were modeled as Hill-type muscles with a parallel elastic element (PEE), a series elastic element (SEE), a contractile element (CE) with contraction and activation dynamics, and a pennation angle. Figure 15 shows this muscle model. The pennation angle created a rotation between the SEE and the CE and the PEE. The pennation angle increased when the muscle contracted and decreased when the muscle lengthened. With the pennation angle, a larger force was produced with a smaller range of motion.

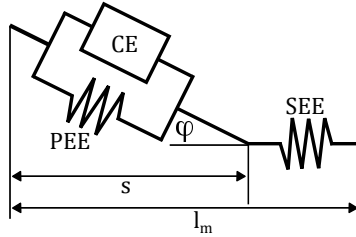


Figure 15: Schematic of a pennated Hill-type muscle with length l_m used in the three-dimensional musculoskeletal model. It consists of a contractile element (CE), a parallel elastic element (PEE), and a series elastic element (SEE). A pennation angle ϕ is present between the SEE and the CE and PEE. To avoid singularities, the length s will be used as a state instead of the length of the CE.

To avoid singularities with the pennation angle ϕ , the state $s = l_{CE} \cos(\phi(s))$ was used instead of the length of the contractile element l_{CE} [21]. Muscle dynamics were formulated implicitly as a function of the contraction state s and activation state a as follows:

$$F_{SEE}(l_m(q) - s) - (F_{CE}(a, s, \dot{s}) + F_{PEE}(s))\cos(\phi(s)) = 0 \quad (4.6)$$

$$\dot{a} - r(u)(u - a) = 0 \quad (4.7)$$

where F_{SEE} was the force in the series elastic element, $l_m(\theta)$ was the muscle length, F_{CE} was the force in the contractile element, F_{PEE} was the force in the passive elastic element, u was the muscle stimulation, a the activation, and $r(u)$ described the activation dynamics. The force-length and force-velocity relationships that were used in this model are described in section 2.6.1.

The force in the PEE and SEE was found based on the model presented by McLean

et al. [22], as follows:

$$F(l) = \begin{cases} k_1(l - l_{slack}) & \text{if } l \leq l_{slack} \\ k_1(l - l_{slack}) + k_2(l - l_{slack})^2 & \text{if } l > l_{slack} \end{cases} \quad (4.8)$$

where l denoted the length of the element and l_{slack} the slack length. k_1 and k_2 were stiffness constants. k_1 represented a small linear stiffness, which was added in this version to ensure that the force was never zero to aid the optimization. It was equal to $0.0022 F_{ISO}/m$. k_2 is equal to the following in F_{ISO}/m :

$$k_2(PEE) = \frac{k_{PEE}}{W^2} \quad (4.9)$$

$$k_2(SEE) = \frac{1}{(u_{max}l_{SEE(slack)})^2} \quad (4.10)$$

where W is the width of the force-length curve, $k_{PEE} = 1$ and $u_{max} = 0.04$ are dimensionless constants.

The muscle dynamics were coupled with the skeletal dynamics using the muscle moment arms as follows:

$$\tau_{m(ij)} = -\frac{\partial l_{m,i}}{\partial \theta_j} F_{SEE,i}(l_{m,i}(\theta) - l_{CE,i}) \quad (4.11)$$

where $\frac{\partial l_{m,i}}{\partial \theta_j}$ is the partial derivative of the muscle length to the joint angle θ_j . This derivative was constant in the two-dimensional model (see chapter II), but this approximation was not accurate enough in the three-dimensional model. Therefore, a higher order polynomial was fitted to the data of muscle length versus joint angle that was available in OpenSim, since a polynomial has a well defined derivative [23]. The smallest order polynomial was used that yielded less than 5% RMS error. In OpenSim, at large joint angles, the muscles would sometimes wrap around the bones incorrectly, and the moment arm would become unrealistic. If this happened, the range of motion was decreased to where the wrapping was

correct. The decreased range of motion was used throughout.

The prosthetic leg was modeled as a passive prosthesis with one degree of freedom in the sagittal plane. Size, mass and inertia properties were the same as the original leg. Twelve muscles in the right lower leg were removed by changing the bounds on activation and stimulation such that these cannot exceed zero, and setting the maximum isometric force to 10^{-4} . A passive rotational spring was added to the ankle with a stiffness of 600 Nm/rad and a damping ratio of 15 Nms/rad, which is the same as used in chapter III and by Zmitrewicz et al. [24]. To do so, the quadratic spring was disabled by setting its spring constant to 1 Nm/rad², while the linear spring was changed to have the stiffness and damping parameters of the prosthesis. Also, the MTP and subtalar joint were fixed using a very high linear stiffness (5000 Nm/rad) while the quadratic spring was disabled.

The alignment of the prosthesis was changed at the knee by changing the alignment of the tibia with respect to the femur. It was chosen to change the alignment at the knee for simplicity and because the effect on the dynamics is equivalent to a change in alignment of the socket between the residual limb and the prosthesis. This also eliminates the choice of the length of the residual leg.

The multibody dynamics (equation 4.1), the muscle dynamics (equations 4.6 and 4.7) and the ground contact model (equations 4.2 to 4.5) were combined into a set of differential equations $f(x, \dot{x}, u) = 0$ with $x = [q, v, a, s]^T$. They were coded in C and compiled as a MEX-function for MATLAB (Mathworks, Natick, MA). The partial derivatives with respect to the states and inputs were also included in this MEX-function.

4.2.2 Trajectory Optimization Problem

A trajectory optimization problem was defined to find the muscle stimulations $u(t)$, $0 \leq t \leq T$ and initial state $x(0)$ that yield a periodic gait trajectory minimizing muscular effort

and tracking of normal gait cycle data:

$$\underset{X}{\text{minimize}} \quad J(x(t), u(t)) = \int_{t=0}^T c(x(t), u(t)) dt \quad (4.12)$$

$$\text{subject to} \quad f(x(t), \dot{x}(t), u(t)) = 0 \quad 0 \leq t \leq T \quad (4.13)$$

where $X = [x(0) \ u(t), 0 \leq t \leq T]$ denote the optimization variables, the states and inputs of the trajectory.

Similar to chapter III, an objective of minimizing muscular effort and tracking of normal data was used [18]. Despite using tracking, the simulation remains predictive because data of able-bodied gait was used to predict TTA gait, and the weighting of the effort is chosen high to place more emphasis on effort.

In this work, 17 joint angles and 6 ground reaction forces were tracked from Lin and Pandy [25]. However, no data was available for the arms. To generate a realistic walking motion, two objectives were added to the existing function: minimization of the trunk velocity, to keep the head stable, and minimization of the shoulder adduction angle, to prevent the arm from moving through the body. The trunk velocity was minimized by summing the global and lumbar velocity around the two axes except the rotation axis, such that the head remained in the same position. This yields the following objective:

$$J(x(t), u(t)) = J_{tra}(x(t)) + W_{eff}J_{eff}(x(t), u(t)) + \quad (4.14a)$$

$$W_{tru}J_{tru}(x(t)) + W_{sho}J_{sho}(x(t))$$

$$\text{Where: } J_{tra}(x(t)) = \frac{1}{N_{\text{track}} + 1} \quad (4.14b)$$

$$\left(\frac{1}{T} \sum_{k=1}^{N_{\text{track}}} \int_0^T \left(\frac{x_k(t) - x_{k(\text{meas})}(t)}{\sigma(t)_k} \right)^2 dt + \left(\frac{T - T_{\text{meas}}}{\sigma_T} \right)^2 \right)$$

$$J_{eff}(x(t), u(t)) = \frac{1}{92T} \sum_{j=1}^{92} \frac{V_j}{\sum_{k=1}^{92} V_k} \int_0^T u_j(t)^2 dt + \frac{1}{100T} \sum_{n=1}^{10} W_{tor} \tau_{ext(n)}(t)^2 dt \quad (4.14c)$$

$$J_{tru}(x(t)) = \int_0^T ((x_{34}(t) + x_{54}(t))^2 + (x_{35}(t) + x_{55}(t))^2) dt \quad (4.14d)$$

$$J_{sho}(x(t)) = \int_0^T (x_{25}(t)^2 + x_{30}(t)^2) dt \quad (4.14e)$$

where N_{track} was the number of variables that are tracked next to the duration, $x_{k(\text{meas})}$ was the measured joint angles and ground reaction forces, T the duration, and T_{meas} the measured duration. W_{eff} denotes the effort weighting of the individual muscle, and W_{tor} denotes the weight of the arm torques. The effort term was also weighted using the muscle volume V_j , normalized to the total muscle volume to account for muscle decompositions [26]. x_i denotes the i th location in the state vector. Index 34 was the global tilt velocity, index 54 the lumbar extension velocity, and index 35 and 55 were the global list velocity and the lumbar bending velocity, respectively. Indices 25 and 30 referred to the shoulder adduction angles on the right and left side. The following weights were used: $W_{eff} = 150$, $W_{tor} = 150$, $W_{tru} = 0.5$, and $W_{sho} = 10$.

4.2.3 Predictive Simulations for Alignment Study

Predictive simulations were solved for 20 virtual subjects. The virtual subjects had a random mass and BMI. The mass was drawn from a distribution with mean \pm SD: 75 ± 10 kg, and the BMI was drawn from 23 ± 2.7 kg/m², which was taken from the BMI distribution of 20 year old American males [27]. Muscle parameters (isometric muscle force, optimal fiber length, maximum shortening velocity, activation time, deactivation time, and

the square of the width parameter of the force-length relationship (see equation 2.20)) were varied with a standard deviation of 5% of the nominal value.

Table III describes the simulations that were solved. A maximum alignment change of 10° was chosen since up to this angle a change in sagittal and frontal plane alignment does not affect the ground reaction force [10], which is tracked in the objective (equation 4.14c). Also, when the alignment was changed to 15° in a previous study, it was not possible to have sufficient balance to walk [10]. A speed of 1 m/s will be used for all simulations, since it has been shown that gait speed is not affected by an alignment change [13].

The able-bodied solution will be found from a standing initial guess for each virtual subject. The simulation of TTA gait in the reference alignment is found using the able-bodied solution as initial guess. The simulations with a misalignment are found using the reference alignment as an initial guess. The optimal control problems were solved through direct collocation, with 60 collocation points per gait cycle and a backward Euler formulation (see section 2.5). Regularization was added, $W_{reg} = 1$ to aid the optimization (see section 2.5.1). All simulations were solved in MATLAB (Mathworks, Natick, MA, USA) using IPOPT 3.11.0 [28]

Table III: Overview of the alignment conditions that will be studied.

Intervention	First alignment change	Name	Second alignment change	Name
Able-Bodied	-	ABLE	-	
Reference Alignment	-	REF	-	
Internal Rotation	5 deg	INR1	10 deg	INR2
External Rotation	5 deg	EXR1	10 deg	EXR2
Abduction	5 deg	ABD1	10 deg	ABD2
Adduction	5 deg	ADD1	10 deg	ADD2
Flexion	5 deg	FLE1	10 deg	FLE2
Extension	5 deg	EXT1	10 deg	EXT2
Lateral Translation	5 mm	LTR1	2 cm	LTR2
Medial Translation	5 mm	MTR1	2 cm	MTR2

Joint angles, joint moments, muscle forces, ground reaction forces and joint contact forces were studied to find kinetic and kinematic changes following a change in alignment.

Joint contact forces and moments were calculated using the Analysis tool in OpenSim [20]. The femur was used as a reference frame. All forces were normalized to weight in kg, and the joint moments were normalized to height (m) and weight (kg) of the subjects [29]. The metabolic cost for each predicted gait cycle was compared using a metabolic energy expenditure model [30].

Ten variables were analyzed to test our hypotheses: the peak hip angle, negative and positive, in three planes, the resultant knee and hip reaction force in the intact leg, the peak knee abduction moment, and the metabolic cost of walking. A repeated measures model was constructed in MATLAB for each of the variables. A repeated measures ANOVA test was performed to test for statistically significant difference. Using Bonferroni correction, $p = 0.005$ was used for statistical significance. In case of a significant difference, post-hoc paired two-tailed t-tests were performed to find which alignments were significantly different from the reference alignment, again using $p = 0.005$.

4.3 Results

Figure 16 shows the joint angles, joint moments and ground reaction forces of the legs for the predictive simulations of able-bodied gait and TTA gait. The joint moments were normalized to the height and weight of the subjects. The ground reaction forces were normalized to weight.

In the sagittal plane, the hip angle was similar between the two solutions. The knee angle on the prosthesis side was different, since there was no knee extension in late stance. The range of motion of the prosthetic ankle was smaller than the healthy ankle, due to a smaller peak plantarflexion and dorsiflexion angle. The peak hip adduction angle on the intact side was lower during late stance (80-100% of the gait cycle) in TTA gait compared to able bodied gait. The external rotation angle on the prosthesis side was lower in late stance as well (30-50% of the gait cycle). The inversion and toe flexion angle on the prosthesis side were zero, these angles were very similar between TTA gait and able-bodied gait on

the intact side.

The hip moment was similar between the solutions in the sagittal plane. On the prosthesis side, the peak knee extension moment was lower. It was also lower on the intact side, but not as much. The ankle moment on the prosthesis side was higher and also present longer than in the able-bodied solution, where the ankle moment was zero until late stance. The peak hip abduction moment was lower on the prosthesis side, and so was the peak hip internal rotation moment. The inversion and flexion moment on the prosthesis side were quite large, due to the large stiffness of these joints in the prosthesis.

On the prosthesis side, the center of pressure moved forward slower than in able-bodied gait, which required a larger peak push-off force. The vertical ground reaction force was similar to able-bodied on the prosthesis side, while the first peak was slightly larger in TTA gait on the intact side. The sideways force was larger in TTA gait during early stance on the intact side (60-80% of the gait cycle), while on the prosthesis side it was larger during mid and late stance. The final peak at push-off on the prosthesis side was smaller and almost absent.

Figure 17 shows the knee and hip reaction loads, as well as the joint angles and joint moments of the lumbar joint and the arms for the predictive simulations of able-bodied gait and TTA gait. The joint and reaction moments were normalized to height and weight of the virtual subjects, the reaction forces were normalized to weight.

The peak abduction moment in the prosthesis side knee was lower than in able-bodied gait and similar on the intact side, while the peak reaction force in the knee was lower on the prosthesis side and similar on the intact side, and the peak reaction force in the hip is similar on the prosthesis side and higher on the intact side. On the prosthesis side the reaction force is higher for TTA gait in midstance in both the hip and knee.

The lumbar joint remained extended longer in TTA gait than in able bodied gait, while the peak bending angle to the right, or the prosthesis side, was larger. The rotation was very similar, though the peak rotation to the right was slightly larger in able-bodied gait

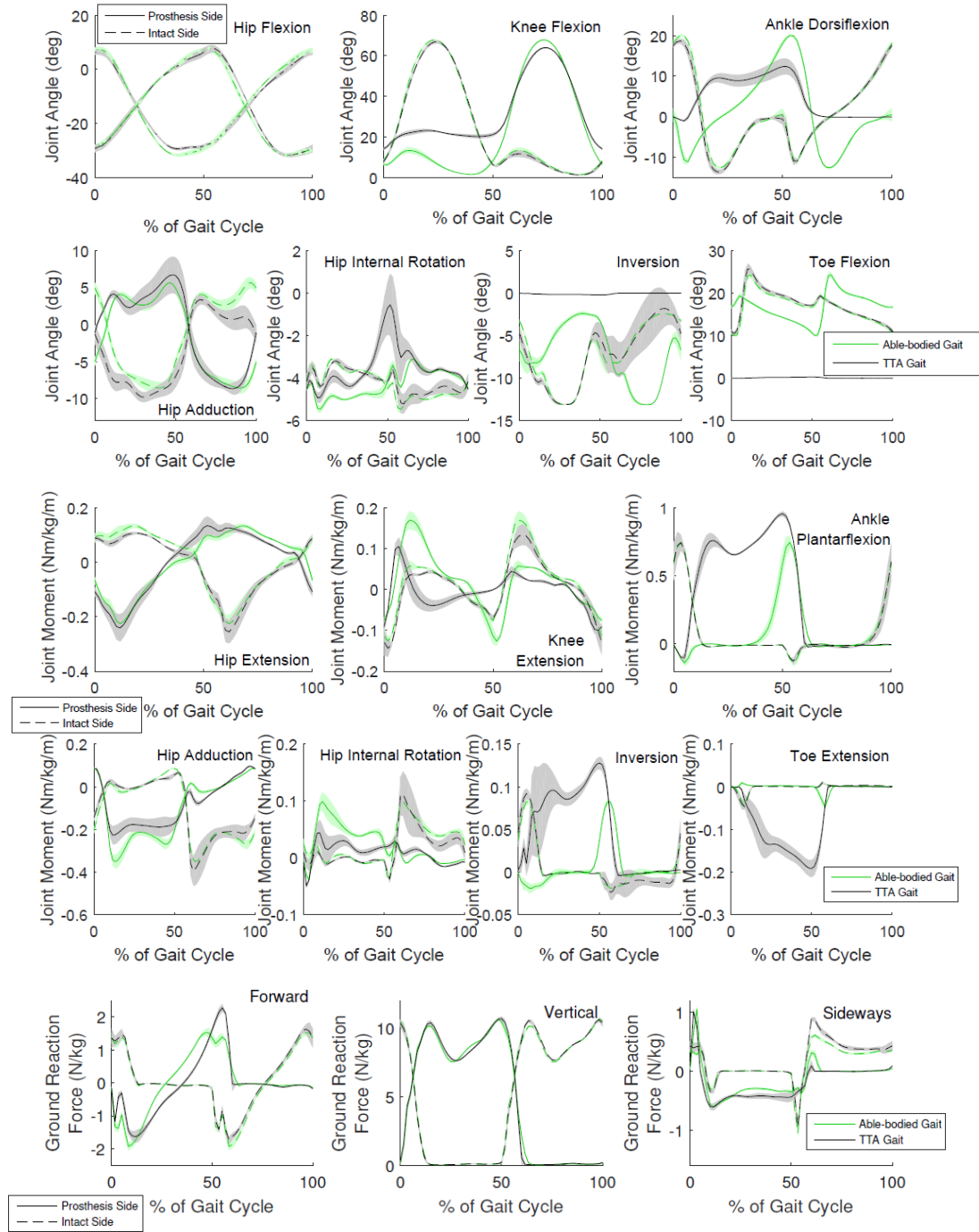


Figure 16: Joint angles, joint moments, and ground reaction forces of the legs for the predictive simulations of able-bodied gait and TTA gait, starting at heel strike of the prosthesis side. The title inside each graph denotes the positive direction.

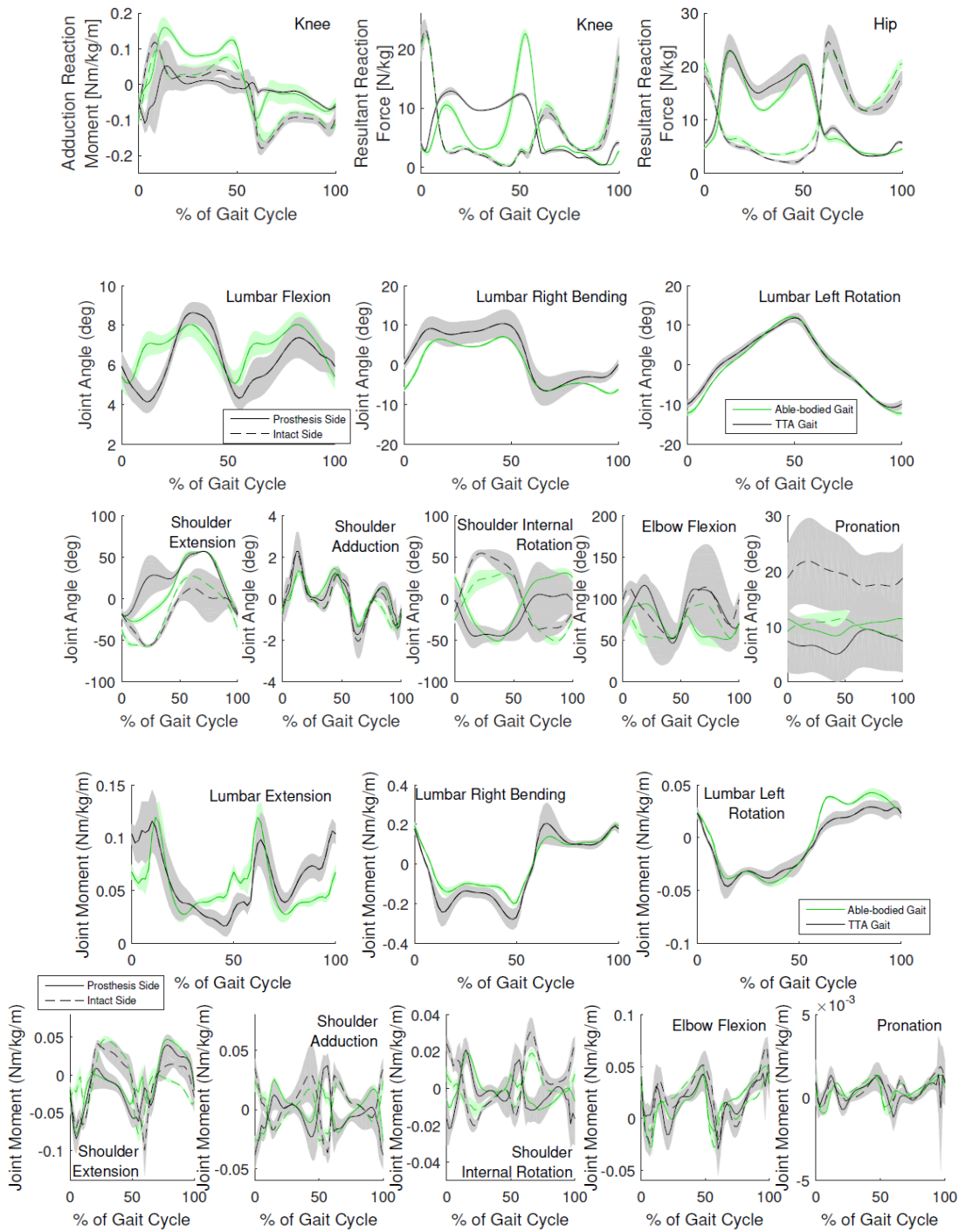


Figure 17: Knee and hip reaction loads, and joint angles and joint moments of the lumbar joint and arms of the legs for the predictive simulations of able-bodied gait and TTA gait, starting at heel strike of the prosthesis side. The title inside each graph denotes the positive direction.

than in TTA gait. The arm motion was largely similar between the two solutions, except the shoulder extension on the prosthesis side during stance and internal rotation on the intact side, which are larger in TTA gait, while internal rotation on the prosthesis side was smaller.

The lumbar extension moment in TTA gait was larger than able-bodied gait during early stance, and smaller in late stance. The bending moment was larger towards the intact side during prosthetic side stance in TTA gait, and similar to able-bodied gait during swing. The rotation was similar during prosthesis side stance, but the peak moment during prosthesis side swing was smaller. The moments in the arms were largely similar, except in TTA gait there was an extra peak elbow extension moment at about 20% stance on the prosthesis side.

4.3.1 Sagittal Rotational Alignment Change

Figure 18 shows the joint angles and joint moments of the legs, as well as the ground reaction forces for the predictive simulations FLE1, FLE2, EXT1, and EXT2. The upper two graphs show the joint angles, the middle two the joint moments, and the bottom graph the ground reaction forces. The joint moments were normalized to height and weight of the virtual subjects, while the ground reaction force was normalized to weight.

On the prosthesis side, the peak hip extension angle in late stance was smaller for the flexion alignments and larger for the extension alignments. The prosthesis side knee angle during stance was more extended for the flexion alignments and vice versa. Also, prosthesis side dorsiflexion was earlier for the extension alignments and later for the flexion alignments. Hip adduction on the intact side was smaller during stance for the flexion alignments and larger for the extension alignments.

The peak hip extension moment was slightly larger for the flexion alignments and smaller for the extension alignments on the prosthesis side, while the peak knee flexion and extension moment were also larger for the flexion alignments and smaller for the flex-

ion alignments. The onset of the plantarflexion moment at the ankle was later for the flexion alignments and earlier for the extension alignments, while the peak dorsiflexion moment (10% of gait cycle) was larger for the flexion alignments. The hip abduction moment and internal rotation moment were smaller for the flexion alignments and larger for the extension alignments during stance. The moments in the prosthetic foot were smaller for the flexion alignments and larger for the extension alignments, meaning there was less movement in the prosthesis. The joint moments on the intact side did not change with the sagittal plane alignment changes.

The ground reaction forces are largely similar between the solutions, though center of pressure progressed forward slightly later for the flexion alignments, and the sideways ground reaction force was larger for the flexion alignments and smaller for the extension alignments on the prosthesis side.

Figure 19 shows the knee and hip reaction loads, as well as the joint angles and joint moments of the lumbar joint and the arms for the predictive simulations FLE1, FLE2, EXT1, and EXT2. The top graph shows the reaction loads, followed by the joint angles of the lumbar joint, and the arms, respectively. The bottom two graphs show the joint moments of the lumbar joint and the arms. The joint and reaction moments were normalized to height and weight of the subjects, while the reaction forces were normalized to weight.

The peak abduction moment did not change with the alignment. The first peak of the knee reaction force on the prosthesis side occurred later and was smaller for the flexion alignments, and occurred earlier and was larger for the extension alignments. The peak hip reaction force on the prosthesis side was larger for the extension alignments and smaller for the flexion alignments. The reaction loads were similar for all alignments on the intact side.

The lumbar flexion angle was smaller during 60-100% of the gait cycle for the flexion alignments and larger for the extension alignments. Also, the lumbar joint was bended more towards the right (prosthesis side) throughout the whole gait cycle for the flexion

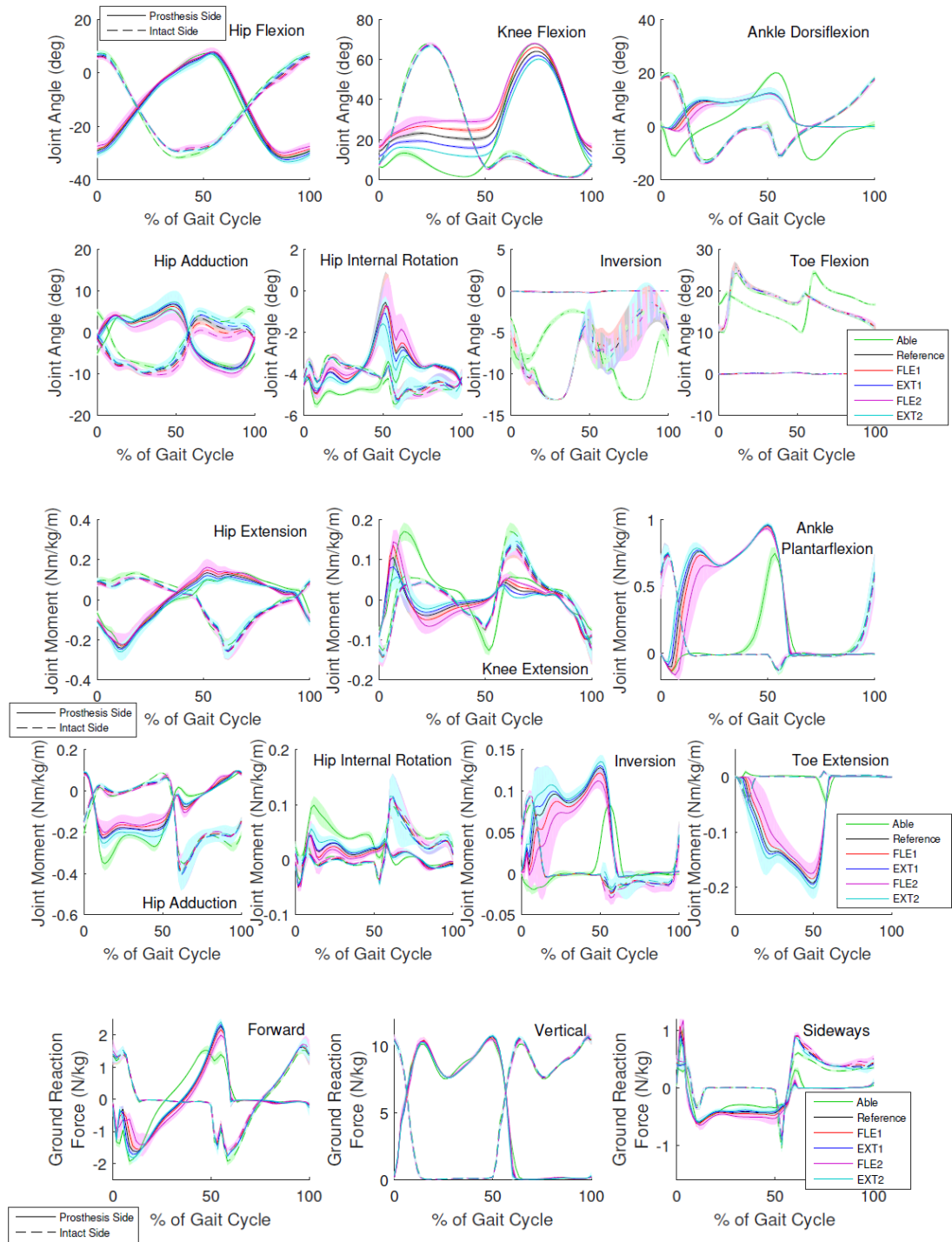


Figure 18: Joint angles, joint moments, and ground reaction forces of the legs for the predictive simulations with a sagittal plane alignment change, starting at heel strike of the prosthesis side. The title inside each graph denotes the positive direction.

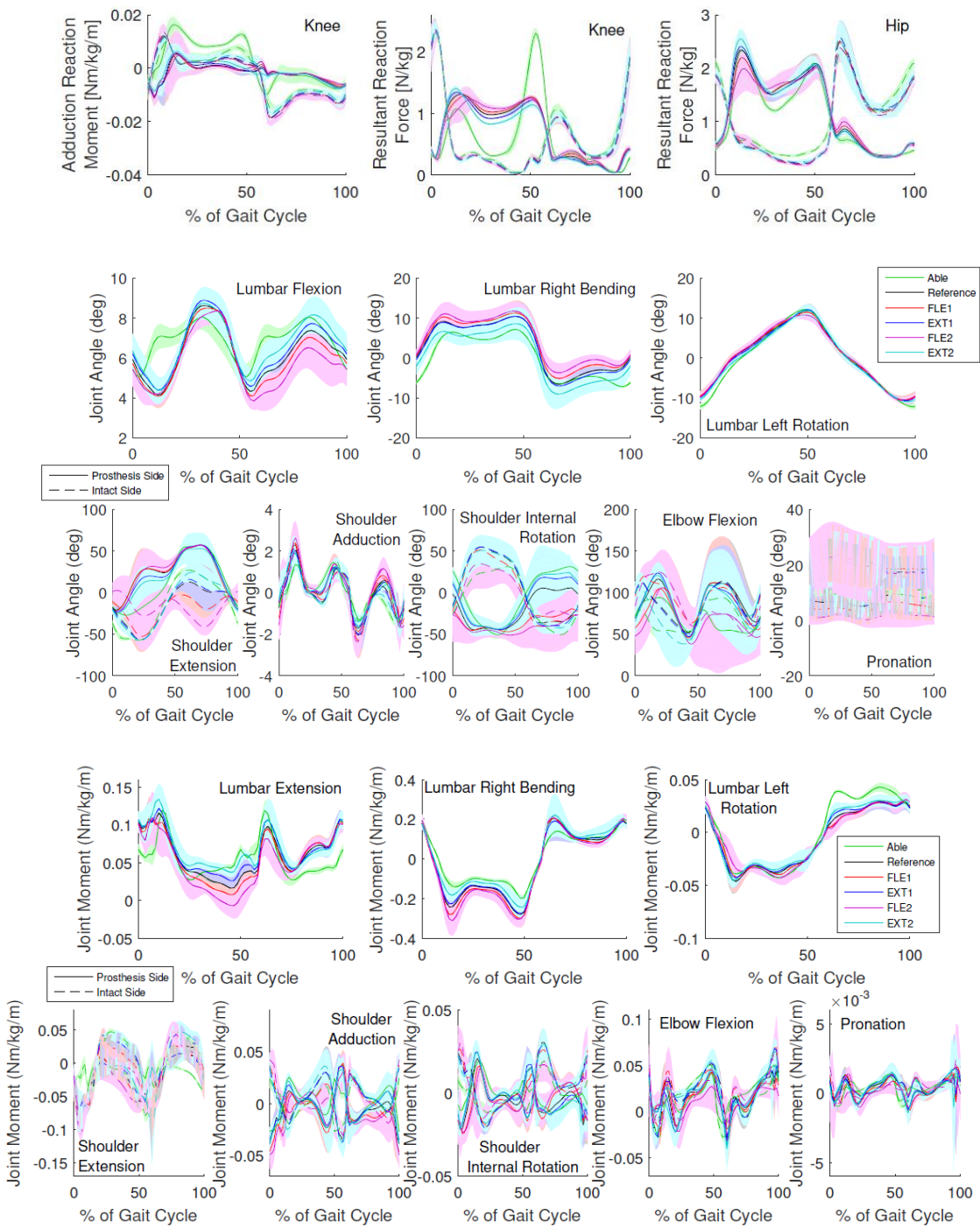


Figure 19: Knee and hip reaction loads, and joint angles and joint moments of the lumbar joint and arms of the legs for the predictive simulations with a sagittal plane alignment change, starting at heel strike of the prosthesis side. The title inside each graph denotes the positive direction.

alignments and more towards the left for the extension alignments. The rotation did not change with alignment. The arm angles were mostly similar between the simulations, though their variability was large, and the shoulder angle on the intact side was flexed instead of extended during stance with a flexion alignment. Also, elbow flexion was larger with for the flexion alignments and smaller for the extension alignments on the intact side during stance. The peak lumbar flexion and left bending moment were larger for the flexion alignments, and smaller for the extension alignments, while the rotation moment did not change with the alignment. The moments in the arm remained similar.

4.3.2 Frontal Rotational Alignment Change

Figure 20 shows the joint angles and joint moments of the legs, as well as the ground reaction forces for the predictive simulations ADD1, ADD2, ABD1, and ABD2. The upper two graphs show the joint angles, the middle two the joint moments, and the bottom graph the ground reaction forces. The joint moments were normalized to height and weight of the virtual subjects, while the ground reaction force was normalized to weight.

This alignment change did not affect the angles in the sagittal plane. The hip adduction angle on the prosthesis side was larger at 10% of the gait cycle for an adduction alignment, while the peak internal rotation angle on the prosthesis side increased for the abduction alignment, and decreased for the adduction alignment. On the intact side, the peak internal rotation angle was largest for alignment ADD2, and the peak eversion angle during stance on the intact side increased with an adduction alignment, and decreased with an abduction alignment.

The peak knee extension moment was the only joint moment in the sagittal plane that was affected by the alignment changes. It was slightly lower for alignment ADD2. The peak hip abduction moment on the prosthesis side was larger for the abduction alignments than the other alignments. The eversion moment on the intact side was larger for the adduction alignments, and smaller for the abduction alignments, while in the prosthesis, both the

inversion moment and the toe extension moment were larger for the abduction alignments, and smaller for the adduction alignments.

From the ground reaction forces, only the sideways force was affected. The sideways ground reaction force was larger in both legs for the solutions with an adduction alignment, and smaller for the simulations with an abduction alignment.

Figure 21 shows the knee and hip reaction loads, as well as the joint angles and joint moments of the lumbar joint and the arms for the predictive simulations ADD1, ADD2, ABD1, and ABD2. The top graph shows the reaction loads, followed by the joint angles of the lumbar joint, and the arms, respectively. The bottom two graphs show the joint moments of the lumbar joint and the arms. The joint and reaction moments were normalized to height and weight of the subjects, while the reaction forces were normalized to weight.

The knee adduction reaction moment became abduction during stance with an abduction alignment, and increased to values above normal for the adduction alignments. The knee reaction force was the same between the solutions, while the peak hip reaction force was lower for ADD2 on the intact side, and was higher for ABD2 on the prosthesis side.

The alignment change did not affect the lumbar joint angles, except for the bending angle, which was more towards the left for alignments ABD2 and ADD2. The arm angles were not affected by the alignment change, except the shoulder extension angle on the intact side, which was smaller for the solution with an adduction alignment, and the shoulder rotation angle, which was rotated externally instead of internally during 60%-100% of the gait cycle for the abduction alignments.

The lumbar moments were affected slightly by the changes in alignment. The peak flexion moment and right rotation moment were larger for the simulation with 10 degree adduction alignment, while the right rotation moment at 40% stance was lower both for the 10 degree adduction and abduction alignment.

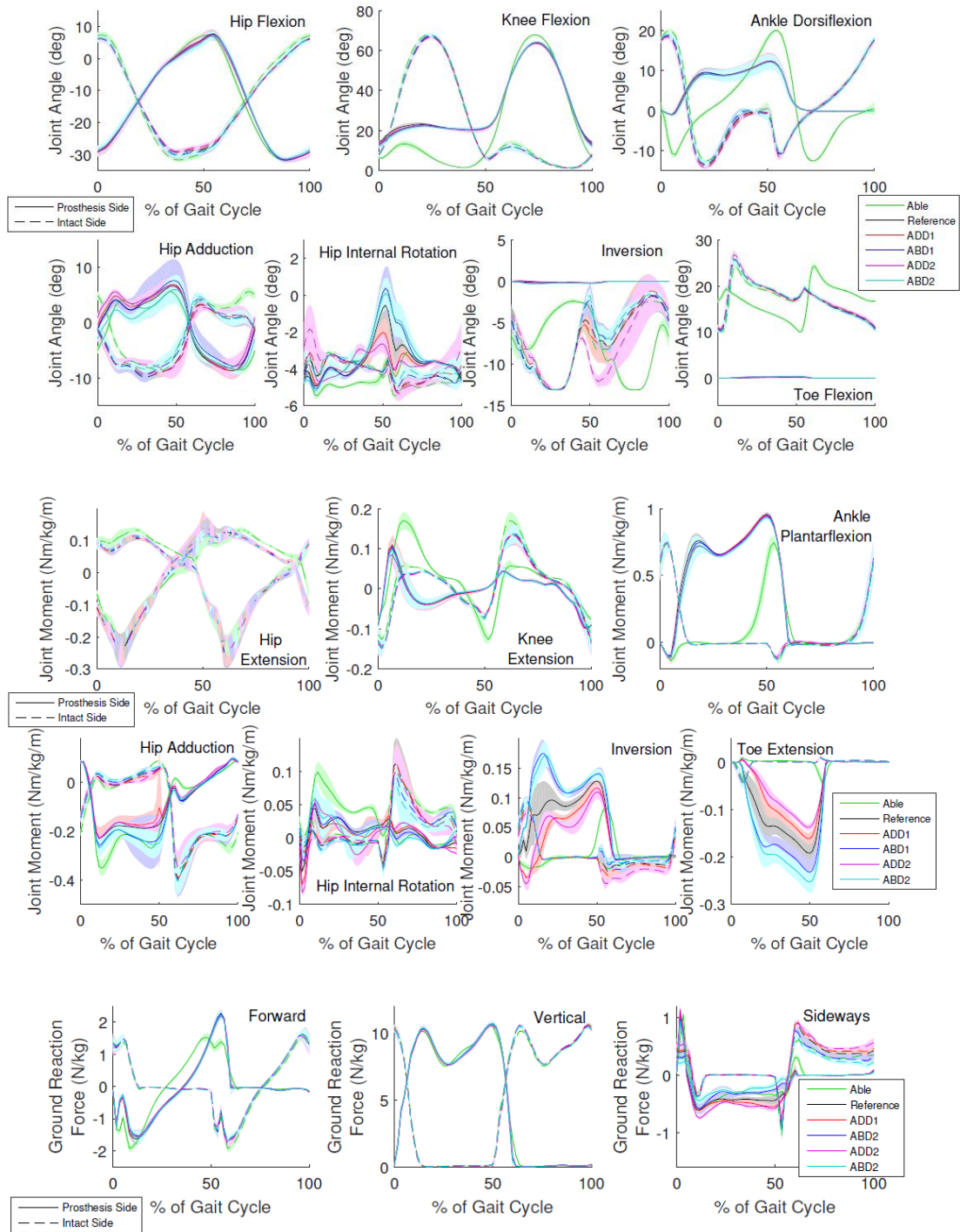


Figure 20: Joint angles, joint moments, and ground reaction forces of the legs for the predictive simulations with a frontal plane rotational alignment change, starting at heel strike of the prosthesis side. The title inside each graph denotes the positive direction.

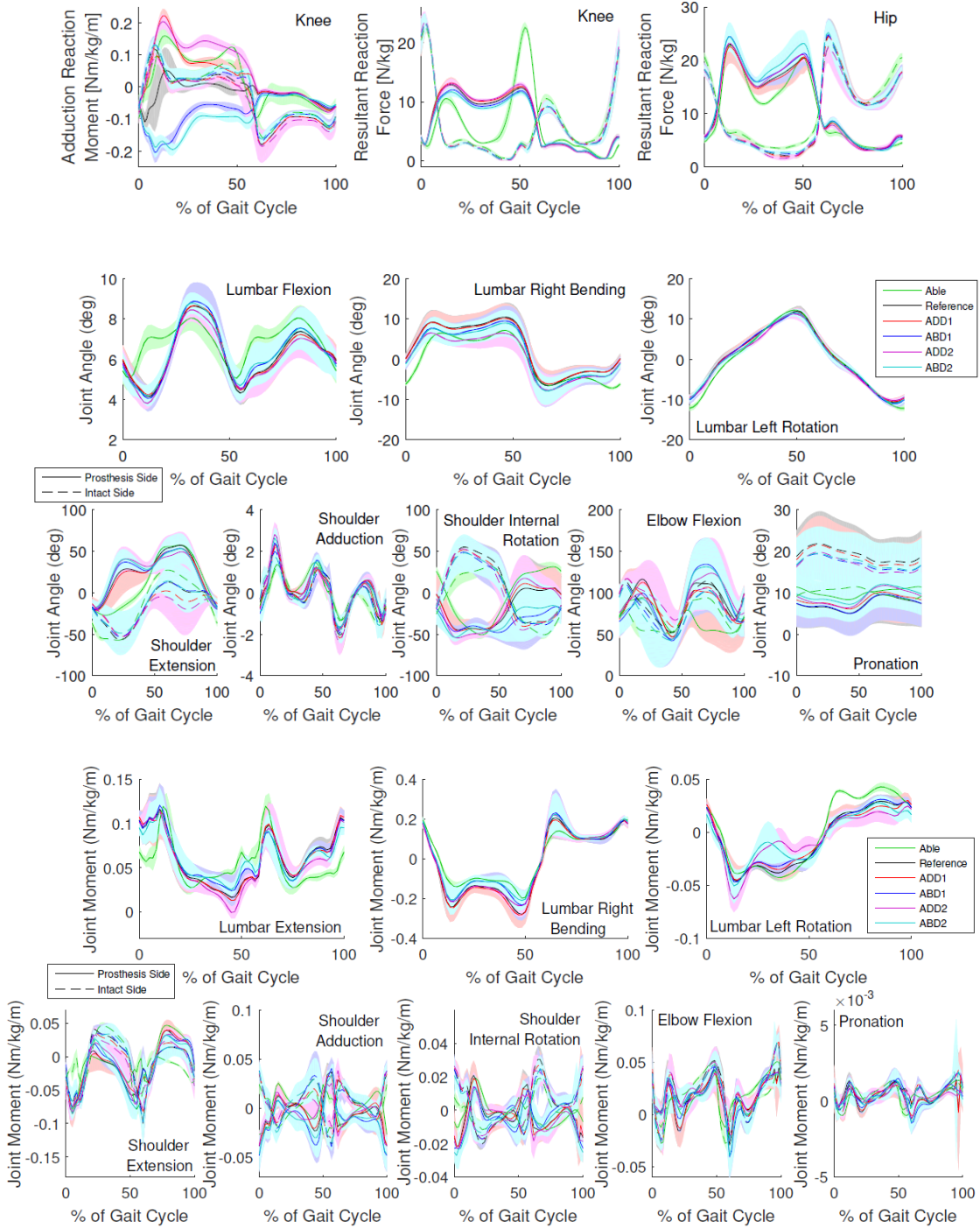


Figure 21: Knee and hip reaction loads, and joint angles and joint moments of the lumbar joint and arms of the legs for the predictive simulations with a frontal plane rotational alignment change, starting at heel strike of the prosthesis side. The title inside each graph denotes the positive direction.

4.3.3 Frontal Translational Alignment Change

Figure 22 shows the joint angles and joint moments of the legs, as well as the ground reaction forces for the predictive simulations MTR1, MTR2, LTR1, and LTR2. The upper two graphs show the joint angles, the middle two the joint moments, and the bottom graph the ground reaction forces. The joint moments were normalized to height and weight of the virtual subjects, while the ground reaction force was normalized to weight.

With a lateral alignment, the knee flexion angle on the prosthesis side during stance was slightly larger, while the hip flexion angle was slightly smaller. On the intact side, the hip adduction angle during stance (60-90% of gait cycle) was smaller for a lateral translation and larger for a medial translation. The hip moment was more extended for the medial translations, and more flexed for the lateral translations. The hip internal rotation moment during stance on the prosthesis side was lower for MTR2. The inversion moment on the prosthesis side was slightly larger for the simulations with a medial translation at 10% stance. The ground reaction forces in all directions were not affected by the alignment change.

Figure 23 shows the knee and hip reaction loads, as well as the joint angles and joint moments of the lumbar joint and the arms for the predictive simulations MTR1, MTR2, LTR1, and LTR2. The top graph shows the reaction loads, followed by the joint angles of the lumbar joint, and the arms, respectively. The bottom two graphs show the joint moments of the lumbar joint and the arms. The joint and reaction moments were normalized to height and weight of the subjects, while the reaction forces were normalized to weight.

The knee adduction reaction moment became abduction for LTR2, while LTR1 had a very small peak adduction moment during stance. For the medial translations, the peak adduction moment increased, almost to normal value for MTR2. The knee and hip reaction force are not influenced by a translational alignment change.

The lumbar joint was more flexed for a lateral alignment change, and more extended for a medial alignment change, while for a lateral alignment change, there was also more bend-

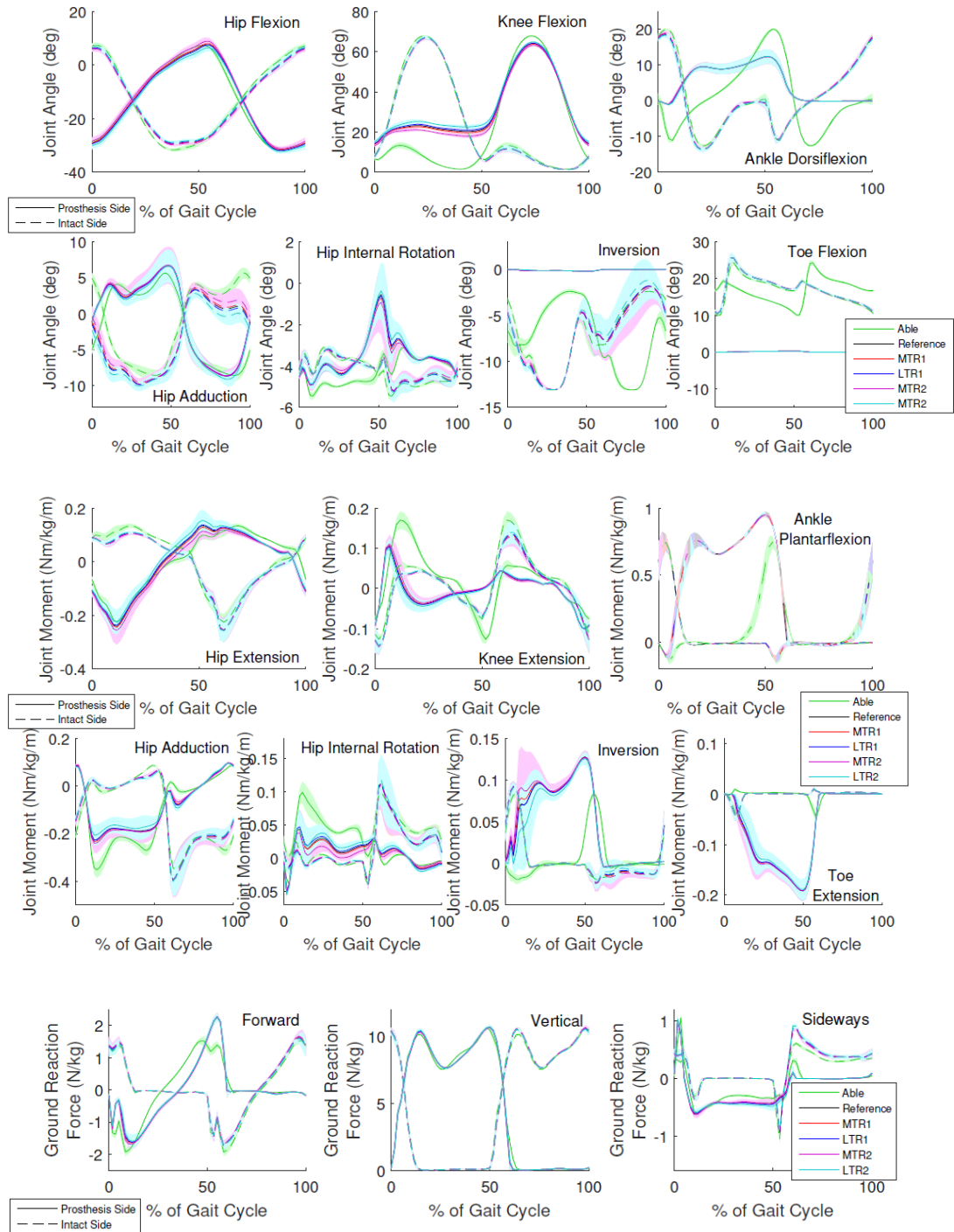


Figure 22: Joint angles, joint moments, and ground reaction forces of the legs for the predictive simulations with a frontal plane translational alignment change, starting at heel strike of the prosthesis side. The title inside each graph denotes the positive direction.

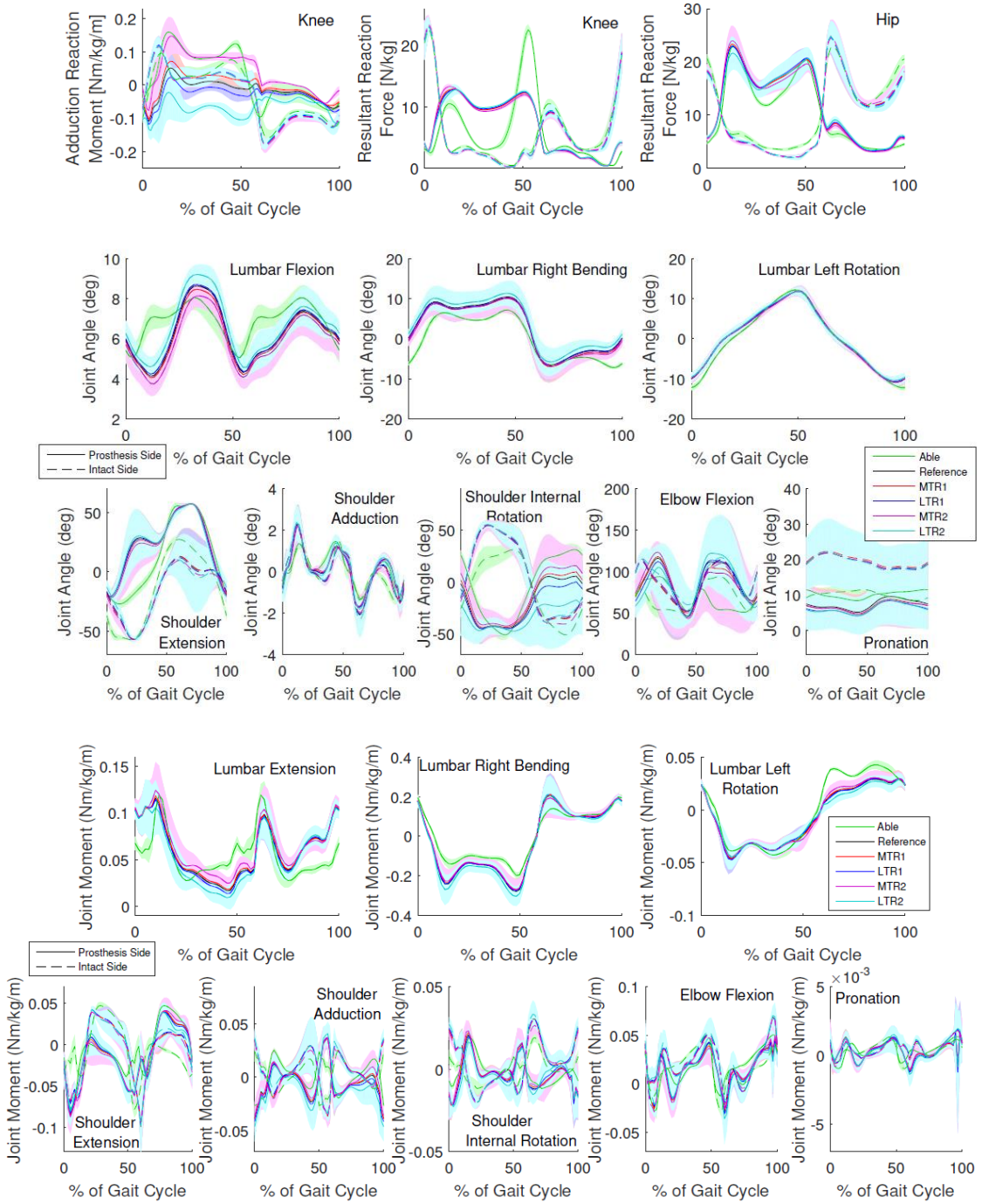


Figure 23: Knee and hip reaction loads, and joint angles and joint moments of the lumbar joint and arms of the legs for the predictive simulations with a frontal plane translational alignment change, starting at heel strike of the prosthesis side. The title inside each graph denotes the positive direction.

ing towards the right. The shoulder rotation angle on the prosthesis side during 60%-100% of the gait cycle was externally rotated for a lateral alignment change, and moved towards an internal rotation angle with a more medial alignment. The moment in the lumbar joint was more extended for a medial translation, and more flexed for a lateral translation. The peak left bending moment was larger for the lateral alignment. The peak shoulder external rotation moment was larger for a medial translation, and smaller for a lateral translation.

4.3.4 Transverse Rotational Alignment Change

Figure 22 shows the joint angles and joint moments of the legs, as well as the ground reaction forces for the predictive simulations INR1, INR2, EXR1, and EXR2. The upper two graphs show the joint angles, the middle two the joint moments, and the bottom graph the ground reaction forces. The joint moments were normalized to height and weight of the virtual subjects, while the ground reaction force was normalized to weight.

The sagittal plane angles were not affected by the alignment change. The hip adduction angle at 15% of the gait cycle was lower for an externally rotated alignment, and higher for an internally rotated alignment. The peak internal rotation angle on the prosthesis side was larger for an externally rotated alignment, and smaller for an internally rotated alignment. The eversion angle on the intact side during 70%-90% of the gait cycle was smaller for an internally rotated alignment.

The moments in the sagittal plane were not affected, except for the peak knee extension moment on the prosthesis side, which was lower for alignment EXR2. The hip adduction moment on the prosthesis side during 20%-50% of the gait cycle was larger for an externally rotated alignment and smaller for an internally rotated alignment. Also, the inversion and toe flexion moment in the prosthesis were larger for an externally rotated alignment and smaller for an internally rotated alignment. The sideways ground reaction force was larger for an internally rotated alignment on the prosthesis side and smaller for an externally rotated alignment. A similar effect, but to a lesser extent, was seen on the intact side.

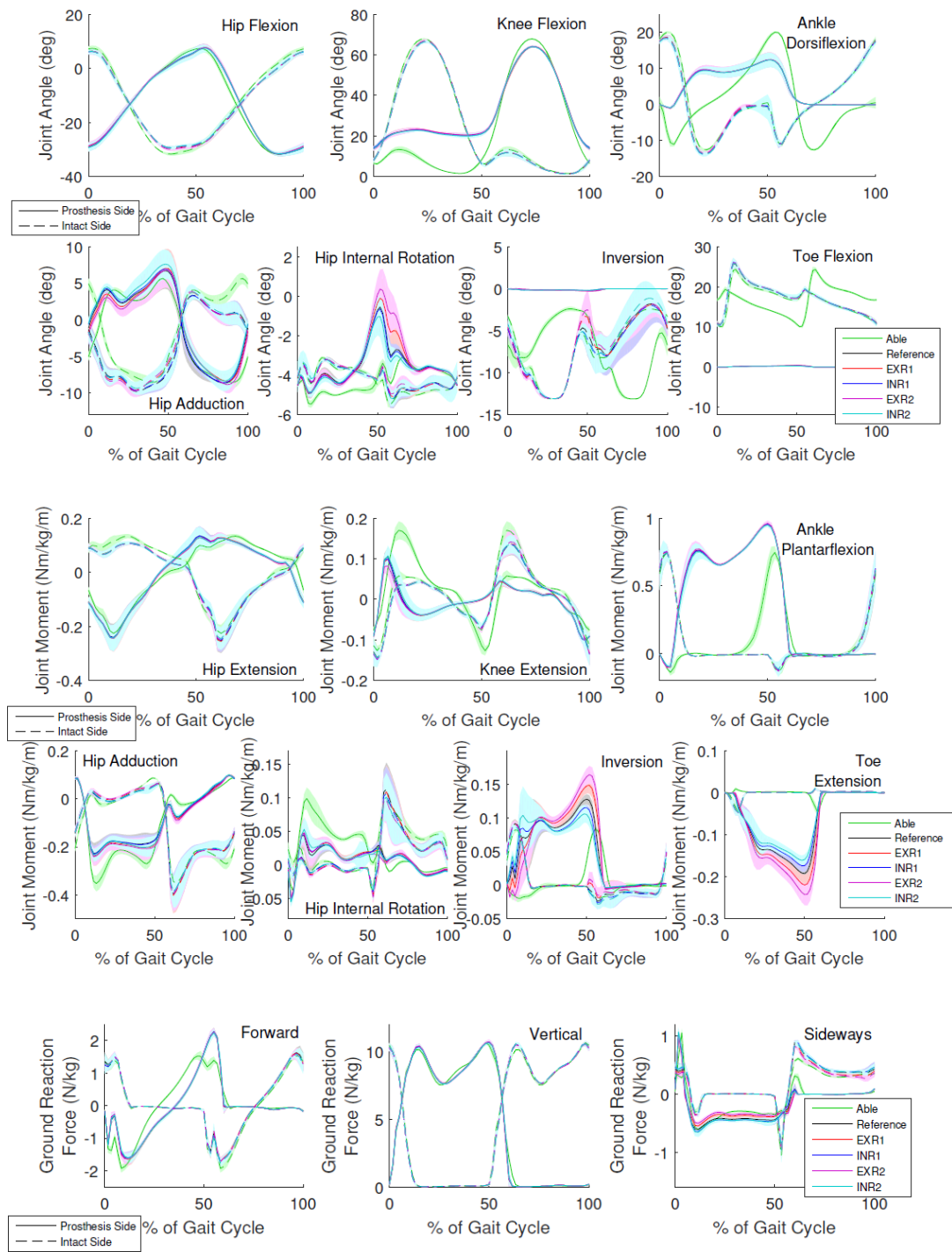


Figure 24: Joint angles, joint moments, and ground reaction forces of the legs for the predictive simulations with a transverse plane alignment change, starting at heel strike of the prosthesis side. The title inside each graph denotes the positive direction.

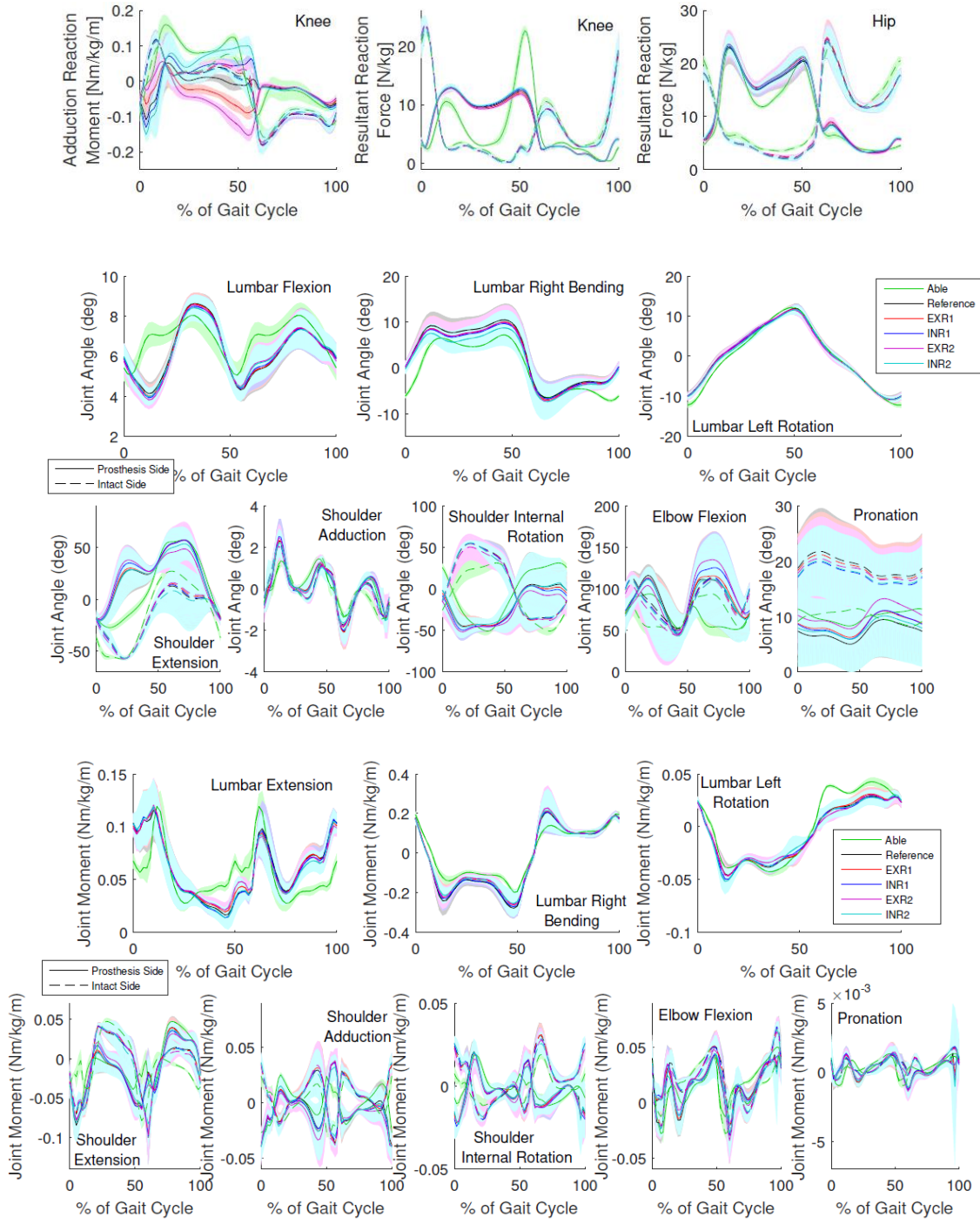


Figure 25: Knee and hip reaction loads, and joint angles and joint moments of the lumbar joint and arms of the legs for the predictive simulations with a transverse plane alignment change, starting at heel strike of the prosthesis side. The title inside each graph denotes the positive direction.

Figure 25 shows the knee and hip reaction loads, as well as the joint angles and joint moments of the lumbar joint and the arms for the predictive simulations INR1, INR2, EXR1, and EXR2. The top graph shows the reaction loads, followed by the joint angles of the lumbar joint, and the arms, respectively. The bottom two graphs show the joint moments of the lumbar joint and the arms. The joint and reaction moments were normalized to height and weight of the subjects, while the reaction forces were normalized to weight.

The rotational alignments affected the knee adduction reaction moment in late stance, which became abduction for the externally rotated alignments, and larger for the internally rotated alignments. The reaction forces were unaffected. The lumbar joint angles were not affected by the alignment changes. The lumbar flexion moment was less at about 50% of the gait cycle for the externally rotated alignments. The shoulder extension angle at 30% of the gait cycle, and the peak elbow flexion angle on the prosthesis side were largest for the alignment changes of 10 degrees, while the shoulder internal rotation angle at 70%-100% gait cycle was lower. The arm moments were not affected by the alignment changes,

4.3.5 Statistical Tests

Table IV shows the results of the repeated measures ANOVA test, as well as means and standard deviations of the parameters that were statistically tested. Bolded text indicates that a significant difference was found in the post-hoc t-tests. All ANOVA tests indicated a significant difference. The peak hip flexion angle was significantly different for 11 simulations (FLE1, FLE2, EXT1, EXT2, EXR2, ABD2, ADD2, MTR1, MTR2, LTR1, and LTR2), and so was the peak hip extension angle (FLE1, EXT1, EXT2, INR2, ABD1, ABD2, ADD2, MTR1, MTR2, LTR1, and LTR2). The peak hip adduction angle was significantly different for 3 simulations (FLE1, FLE2, and ABD2), and so was the peak abduction angle (FLE2, ABD1, and LTR1). The peak hip external rotation angle was significantly different for four simulations (EXT1, ABD1, ABD2, and ADD2). The peak hip internal rotation angle was significantly different for six simulations (EXT1, EXT2, EXR1, ABD1, ADD1,

ADD2). The peak hip reaction force was significantly higher in two simulations (EXT2 and INR2) and lower for the simulation ADD2. The peak knee reaction force was significantly lower in LTR1. The peak knee abduction moment was significantly lower in four simulations (ABD1, ABD2, LTR1, and LTR2) and higher in five simulations (INR1, INR2, ADD1, ADD2, MTR2). The metabolic cost was significantly lower for FLE1, and higher for EXT2 and EXR1.

4.4 Discussion

Four hypotheses were tested and confirmed by the statistical tests. Table IV showed that the hip angles were significantly different with a change in alignment, that the joint reaction forces were significantly higher in several changed alignments, that the knee adduction moment was significantly different, and that the metabolic cost was significantly different in three alignments.

However, when simulations with an alignment change were compared to the reference alignment individually, most parameters were significantly different for less than half the alignment changes, and no alignment change yielded statistical significance for all tested parameters. The alignment with the most significantly different parameters was ADD2 with six, followed by EXT2 and LTR2 with five. Alignments EXR1 and INR1 had only one significant difference.

The metabolic cost was significantly higher only for two alignment changes, EXT2 and EXR1 and lower in alignments FLE1, FLE2, INR2, ADD1, and LTR1 though the difference was 1% or less and statistically significant only for FLE1. A 1% difference is quite small, for example in running a 2.4% increase is required for athletes to detect a difference [31]. Also, the reaction forces and moments are lower in several alignments, compared to the reference alignment. In FLE2, the reaction forces on the intact side are lower than the reference alignment, while the knee abduction reaction moment is lower than able on the prosthesis side. The difference is quite small and hardly visible (e.g. see figure 18) despite

Table IV: Means \pm standard deviations of the variables that were tested for significance. Bolded font indicates a significant difference in the post-hoc test. After Bonferroni correction, p=0.005 was used for the ANOVA and post-hoc test.

Variable		ANOVA result	ABLE	REF	FLE1	FLE2	EXT1	EXT2
Hip angles (deg)	Flexion	p<< 0.005	31.7 \pm 0.54	31.7 \pm 0.72	30.9 \pm 0.76	29.9 \pm 0.79	32.5 \pm 0.68	33.3 \pm 0.78
	Extension	p<< 0.005	-7.35 \pm 1.1	-7.75 \pm 1.3	-8.01 \pm 1.4	-7.88 \pm 1.6	-7.41 \pm 1.3	-7.07 \pm 1.3
	Adduction	p<< 0.005	5.69 \pm 0.75	6.91 \pm 2.2	6.48 \pm 2.0	5.93 \pm 1.9	7.16 \pm 2.4	7.43 \pm 2.53
	Abduction	p<< 0.005	-8.55 \pm 0.77	-8.91 \pm 0.56	-9.18 \pm 0.75	-10.0 \pm 0.94	-8.98 \pm 0.48	-9.08 \pm 0.46
	External Rotation	p<< 0.005	-5.47 \pm 0.17	-4.94 \pm 0.23	-4.99 \pm 0.25	-4.93 \pm 0.23	-4.87 \pm 0.25	-4.84 \pm 0.24
	Internal Rotation	p<< 0.005	-3.06 \pm 0.051	-0.505 \pm 1.4	-0.672 \pm 1.5	-0.635 \pm 1.3	-0.971 \pm 1.4	-1.47 \pm 1.2
Reaction forces (N/BW)	Hip	p<< 0.005	22.9 \pm 0.99	24.7 \pm 3.0	24.5 \pm 2.7	23.4 \pm 2.4	25.4 \pm 2.9	25.2 \pm 3.1
	Knee	p= 0.0028	22.7 \pm 0.72	23.5 \pm 1.3	23.4 \pm 1.5	23.2 \pm 1.4	23.3 \pm 1.3	23.5 \pm 1.1
Reaction Moment (x100 Nm/BW/m)	Knee Abduction	p<< 0.005	16.4 \pm 2.1	6.74 \pm 5.0	7.43 \pm 5.2	8.18 \pm 4.5	6.53 \pm 4.2	6.26 \pm 2.7
Metabolic Cost	(J/kg/m)	p<< 0.005	2.66 \pm 0.13	2.35 \pm 0.14	2.33 \pm 0.15	2.33 \pm 0.15	2.35 \pm 0.13	2.38 \pm 0.12
			INR1	INR2	EXR1	EXR2	ABD1	ABD2
Hip angles (deg)	Flexion		31.7 \pm 0.75	31.6 \pm 0.80	31.6 \pm 0.62	31.5 \pm 0.64	31.7 \pm 0.65	31.3 \pm 0.62
	Extension		-7.66 \pm 1.4	-7.46 \pm 1.3	-7.68 \pm 1.3	-7.69 \pm 1.3	-7.44 \pm 1.3	-7.17 \pm 1.2
	Adduction		7.01 \pm 2.11	7.66 \pm 2.0	7.11 \pm 2.6	6.84 \pm 2.4	7.83 \pm 3.7	6.22 \pm 3.4
	Abduction		-8.78 \pm 0.77	-8.44 \pm 1.3	-8.60 \pm 0.81	-8.97 \pm 1.0	-8.05 \pm 0.98	-8.62 \pm 0.69
	External Rotation		-4.89 \pm 0.22	-4.86 \pm 0.23	-4.90 \pm 0.24	-4.86 \pm 0.19	-5.09 \pm 0.21	-5.23 \pm 0.15
	Internal Rotation		-0.618 \pm 0.97	-0.886 \pm 1.1	-0.0454 \pm 0.93	0.404 \pm 0.99	0.426 \pm 1.1	0.118 \pm 0.85
Reaction forces (N/BW)	Hip		24.3 \pm 3.2	24.2 \pm 2.8	25.1 \pm 3.1	24.7 \pm 2.9	24.9 \pm 3.0	25.2 \pm 2.4
	Knee		23.8 \pm 0.84	23.6 \pm 1.5	23.7 \pm 1.0	23.8 \pm 1.1	23.5 \pm 1.1	23.5 \pm 1.3
Reaction moment (x100 Nm/BW/m)	Knee Abduction		10.2 \pm 3.6	12.5 \pm 2.6	5.52 \pm 5.2	5.86 \pm 3.4	-1.68 \pm 0.54	-2.00 \pm 0.36
Metabolic Cost	(J/kg/m)		2.35 \pm 0.12	2.34 \pm 0.13	2.36 \pm 0.13	2.36 \pm 0.13	2.36 \pm 0.12	2.37 \pm 0.14
			ADD1	ADD2	MTR1	MTR2	LTR1	LTR2
Hip angles (deg)	Flexion		31.7 \pm 0.58	31.4 \pm 0.60	31.6 \pm 0.74	31.1 \pm 0.71	31.9 \pm 0.74	32.3 \pm 0.70
	Extension		-7.57 \pm 1.4	-7.08 \pm 1.4	-8.10 \pm 1.3	-9.00 \pm 1.3	-7.47 \pm 1.3	-6.51 \pm 1.3
	Adduction		7.16 \pm 1.4	7.00 \pm 1.2	6.82 \pm 2.1	6.86 \pm 2.4	6.82 \pm 2.2	6.79 \pm 2.1
	Abduction		-8.78 \pm 1.4	-8.30 \pm 1.6	-8.87 \pm 0.52	-8.81 \pm 0.45	-8.88 \pm 0.60	-9.31 \pm 0.67
	External Rotation		-4.88 \pm 0.27	-4.73 \pm 0.19	-4.94 \pm 0.24	-4.94 \pm 0.24	-4.95 \pm 0.23	-4.89 \pm 0.23
	Internal Rotation		-1.80 \pm 0.72	-2.50 \pm 0.37	-0.664 \pm 1.5	-0.866 \pm 1.5	-0.564 \pm 1.4	-0.341 \pm 1.3
Reaction forces (N/BW)	Hip		24.5 \pm 2.5	22.5 \pm 2.7	24.7 \pm 3.0	24.9 \pm 2.9	24.7 \pm 3.0	24.9 \pm 2.7
	Knee		23.5 \pm 1.4	23.8 \pm 1.3	23.5 \pm 1.3	23.7 \pm 1.2	23.4 \pm 1.3	23.3 \pm 1.2
Reaction moment (x100 Nm/BW/m)	Knee Abduction		22.4 \pm 2.1	20.5 \pm 2.3	8.68 \pm 4.8	15.4 \pm 5.0	4.43 \pm 4.7	0.995 \pm 3.4
Metabolic Cost	(J/kg/m)		2.32 \pm 0.14	2.35 \pm 0.11	2.35 \pm 0.13	2.35 \pm 0.13	2.35 \pm 0.14	2.33 \pm 0.14

being significant, but the peak force becomes more similar to able-bodied gait, so it might still be beneficial.

The hip flexion and extension angles were statistically different in 11 alignments. However, normally people have a standard deviation of approximately 6° in their hip angle [32]. None of the peak angles in the hip were outside this range, when compared to the reference solution. This means that despite a theoretical significant difference between the alignments, it will not be noticeable in practice.

The flexion alignments should be studied further. In this work, the metabolic cost was less than the reference for solutions FLE1 and FLE2. It was found that less power was absorbed in the ankle in the flexion alignments than in the reference alignment. Less work was performed in both hips, the lumbar joint, and the healthy ankle in FLE1 and FLE2 compared to the reference solution. Also, the reaction forces at the knee and the hip on the intact side were lower than the reference, albeit not significant, and the knee abduction moment on the prosthesis side was lower as well. Therefore, a flexion alignment might be more optimal than the reference alignment. This is possible due to the fact that the foot points downwards compared to the reference alignment, which is similar to having the neutral angle at a small plantarflexion angle, meaning that more energy can be stored during stance.

When the alignment was changed in the frontal or the transverse plane, the knee adduction reaction moment on the prosthesis side was affected, and for some solutions reduced to zero. A reaction adduction moment in the socket could yield stresses in the skin. This results shows that the alignment influenced this reaction moment. Especially an external rotation or a lateral translation reduced the knee adduction reaction moment without affecting other gait parameters. Therefore, skin problems might be reduced in some patients by changing the alignment in one of those directions.

4.4.1 Comparison to Previous Studies

Able-bodied Solution

The solution was compared to gait analysis studies of human gait. Hip and knee flexion angles were similar to Gage et al. [33]. Ankle dorsiflexion was different, since during stance the ankle dorsiflexed later in the gait cycle. The delayed dorsiflexion was also seen in the data that was used in the tracking objective [25]. Hip adduction angle was very similar, though there was a second peak adduction angle at about 50% stance that was absent in Gage et al. [33]. Hip rotation, and ankle inversion were similar to Gage et al. [33]. Hip abduction moment was similar to Royer and Wasilewski [34].

The peak knee reaction forces were similar to Fregly et al. [35], and smaller than Miller et al. [36]. The knee abduction moment was slightly lower than Miller et al. [36], but within normal variation. However, the first peak in the knee joint reaction force was lower than normal in all simulations. This is probably due to the ankle moment which is absent in early stance (see figure 16), which is different from normal (see chapter II).

It was observed that the ankle only becomes active in late stance. We suspect that this happens since stability is not taken into account. Note that in the two-dimensional model, the ankle moment was as expected (see chapter III), while stability was not taken into account either. However, the three-dimensional model has much more muscles, which increases the control flexibility. Possibly, the abnormal joint ankle angle data that was tracked could also have influenced the joint moment.

Usually, the plantarflexor muscles are active in early stance (see chapter II) to control the forward velocity of the leg [37]. We suspect that in the predictive simulations energy is saved by activating these muscles only in late stance, during push-off. This is possible if the leg has exactly the desired speed at heel strike, but this will be hard to control in practice. The effort weight was decreased to see if this would create a more realistic ankle moment. This was true for $W_{eff} = 1$, but in this solution the knee extension moment was

absent during stance. It appeared that in this solution the strategy was changed from using the knee extensors during early stance to using the ankle plantarflexors, which created an unrealistically high knee reaction force.

The metabolic cost of 2.66 J/kg/m was as expected for normal walking. The resting metabolic rate of about 1.13 W/kg [38] was not taken into account, and a metabolic cost of about 3.3 J/kg/m to 3.6 J/kg/m is considered normal [38].

Reference Solution

In the reference simulation with TTA gait, it was observed that the knee on the prosthesis side does not extend during late stance. This is probably due to the high stiffness that was chosen for the MTP joint in the prosthesis. This stiffness was chosen to be high to fix the joint, and create a prosthesis similar to the one used in the two-dimensional study (see chapter III). However, this makes it impossible to extend the knee during late stance, because the knee buckles (and flexes) once the center of pressure has moved forward in the foot.

The knee reaction force in the TTA simulations was lower than previous work [39]. The ground reaction force was similar between the two legs. In subject studies, it was found that the intact vertical ground reaction force is higher, but this depends on the prosthetic foot (e.g. [40, 41]). Similar to Royer and Wasilewski [34], the knee adduction moment was lower than able-bodied on the prosthesis side and higher than able-bodied on the intact side. The numbers were also of similar order of magnitude.

The metabolic cost in the simulations of TTA gait was 2.35 J/kg/m when taking into account the mass of the prosthesis. However, if this mass was disregarded, the metabolic cost was 2.52 J/kg/m, which is still lower than the metabolic cost of the able-bodied solution, while subject studies usually report a higher than normal or similar metabolic cost [42–45]. When looking at the joints, the lumbar muscles expend 34% more energy, the prosthesis side hip muscles expend 19% more energy, and the knee muscles 2% more, or 19% if

the Gastrocnemius is not taken into account in either simulation. On the intact side, less energy is expended by the muscles: 19% less in the hip muscles, 27% less in the knee muscles, and 29% less in the ankle muscles.

However, when mechanical work at the joints was studied, it was found that more work was performed in the hip, knee and ankle joint on the intact side, which is similar to previous work [15, 46, 47]. It is surprising that less work is performed in the muscles, while more work is performed in the joints on the intact side. This could be due to passive moments that were not taken into account. However, the motion was inside the range of motion, so very little passive moments should be added. Another reason is that due to the elasticity of the SEE, the maximum muscle force (in the CE) and shortening velocity do not necessarily coincide with the maximum joint moment and angular velocity. No data is available to compare the result of the muscle work.

Effect of Alignment Changes

The effect of the sagittal plane alignment change on the peak knee extension moment (higher for the flexion alignment and lower for the extension alignment) was similar to Boone et al. [3], and Schmalz et al. [14], who changed the angle of the foot with respect to the shank. Fang et al. found that the hip and knee moment in the sagittal plane increased compared to the reference for a flexion and an extension alignment change [5], which was not seen in this work. Similar to Kobayashi et al. [11], we predicted a smaller knee extension moment with the extension alignment. However, they did not predict a higher peak moment with flexion, and it was also found that in this work the peak occurs earlier in the stance phase than reported by Kobayashi et al.

Similar to Pinzur et al. [10], the vertical ground reaction force was larger on the intact side than on the prosthesis side, but it was not affected by an alignment change in the frontal or the sagittal plane. This was expected, because the ground reaction forces were tracked as well.

Fridman et al. [13] suggest that external or internal rotation of the hip compensates for a rotational alignment change in the foot, such that the foot has the same direction during stance phase. The hip compensation was not seen in this work. It is possible that the subjects care about the foot alignment for other reason than energy efficiency, which is why this is not seen in this work.

Due to the limited and sometimes conflicting previous results that are available, the quality of the predictive simulations cannot be assessed easily. The adjustment in the knee moment and vertical ground reaction force seem to agree with some previous studies, but the knee moment conflicts with others, and much data of this study cannot be compared to subject studies since they have not been measured, like the knee reaction force, joint angles and moments, especially on the intact side, and the metabolic cost. Future subject studies could help verify the results of this work. It is recommended to test metabolic cost and joint reaction forces of alignment changes in the sagittal plane especially.

4.4.2 Limitations

It should be noted that all simulations were found with tracking data from one subject [25]. Since no information was available on the standard deviation, it was assumed to be 0.1 rad for all degrees of freedom. This number was compared to the standard deviation between subjects of the data presented in chapter V. It was found that the chosen standard deviation was similar, but slightly lower than the average standard deviation. Therefore, it is expected that the variation of the results is similar to the expected variation.

Tracking data of the arm swing was not available. Instead, two objectives were added to the optimization to create a realistic solution. The objective of trunk stability was added since it is required to keep the head in a somewhat stable location to avoid blurry vision. The objective of minimizing shoulder adduction movement was added because otherwise the arms would move through the body. Ideally, path constraints would be added to avoid this, but this would have been cumbersome. Experimentation with the objective found that

this simple objective created a sufficiently realistic motion of the trunk and legs and that similar objectives did not yield a significantly different solution.

More work should be done to improve the quality of the predictive simulations and make them more realistic, for example the ankle joint moment and the arm swing were not sufficiently realistic. A different dataset for tracking could improve the results, because the dataset used in this work did not include arm motion, and the ankle motion seemed somewhat unrealistic. Also, including uncertainty of the environment could improve the results, especially the ankle joint moment. This could be especially important for an alignment study as well, because certain alignments might be more or less stable than others, and therefore require more energy expenditure. This study could not assess this.

4.5 Conclusion

It was concluded that all hypotheses were accepted. We showed that the hip angles were significantly changed with a change in alignment, that the joint reaction forces were significantly higher in several changed alignments, that the knee adduction moment was significantly different, and that the metabolic cost was significantly higher than the reference in several alignments. However, it could not be concluded that the reference alignment was the single most optimal alignment. It was shown that the flexion alignment could be more advantageous, since the reaction forces on the intact side were lower, as well as the abduction moment on the prosthesis side and the metabolic cost. It was also shown that when the alignment was changed by a lateral translation or an external rotation, the knee adduction moment would reduce without changing other parameters too much. Such an alignment change could potentially alleviate skin stress and related health issues. Future work into prosthesis alignment is necessary, and this work can be used as a reference for future subject studies, since it provides information that has not been measured or calculated previously.

4.6 References

- [1] DHK Chow, AD Holmes, CKL Lee, and SW Sin. The effect of prosthesis alignment on the symmetry of gait in subjects with unilateral transtibial amputation. *Prosthetics and Orthotics International*, 30(2):114–128, 2006.
- [2] X Jia, R Wang, M Zhang, and X Li. Influence of prosthetic sagittal alignment on trans-tibial amputee gait and compensating pattern: a case study. *Tsinghua Science & Technology*, 13(5):581–586, 2008.
- [3] DA Boone, T Kobayashi, TG Chou, AK Arabian, KL Coleman, MS Orendurff, and M Zhang. Influence of malalignment on socket reaction moments during gait in amputees with transtibial prostheses. *Gait & Posture*, 37(4):620–626, 2013.
- [4] M Zahedi, W Spence, S Solomonidis, and J Paul. Alignment of lower-limb prostheses. *Journal of Rehabilitation Research & Development*, 23:2–19, 1986.
- [5] L Fang, X Jia, and R Wang. Modeling and simulation of muscle forces of trans-tibial amputee to study effect of prosthetic alignment. *Clinical Biomechanics*, 22(10):1125–1131, 2007.
- [6] S Blumentritt, T Schmalz, R Jarasch, and M Schneider. Effects of sagittal plane prosthetic alignment on standing trans-tibial amputee knee loads. *Prosthetics and Orthotics International*, 23(3):231–238, 1999.
- [7] SW Sin, DHK Chow, and JCY Cheng. Significance of non-level walking on transtibial prosthesis fitting with particular reference to the effects of anterior-posterior alignment. *Journal of Rehabilitation Research and Development*, 38(1):1, 2001.
- [8] RE Hannah, JB Morrison, and AE Chapman. Prostheses alignment: effect on gait of persons with below-knee amputations. *Archives of Physical Medicine and Rehabilitation*, 65(4):159–162, 1984.

- [9] DA Winter and SE Sienko. Biomechanics of below-knee amputee gait. *Journal of Biomechanics*, 21(5):361–367, 1988.
- [10] MS Pinzur, W Cox, J Kaiser, T Morris, A Patwardhan, and L Vrbos. The effect of prosthetic alignment on relative limb loading in persons with trans-tibial amputation: a preliminary report. *Journal of Rehabilitation Research and Development*, 32(4):373, 1995.
- [11] T Kobayashi, MS Orendurff, M Zhang, and DA Boone. Effect of transtibial prosthesis alignment changes on out-of-plane socket reaction moments during walking in amputees. *Journal of Biomechanics*, 45(15):2603–2609, 2012.
- [12] E Isakov, J Mizrahi, Z Susak, I Ona, and N Hakim. Influence of prosthesis alignment on the standing balance of below-knee amputees. *Clinical Biomechanics*, 9(4):258–262, 1994.
- [13] A Fridman, I Ona, and E Isakov. The influence of prosthetic foot alignment on transtibial amputee gait. *Prosthetics and Orthotics International*, 27(1):17–22, 2003.
- [14] T Schmalz, S Blumentritt, and R Jarasch. Energy expenditure and biomechanical characteristics of lower limb amputee gait: The influence of prosthetic alignment and different prosthetic components. *Gait & Posture*, 16(3):255–263, 2002.
- [15] C Beyaert, C Grumillier, N Martinet, J Paysant, and J-M André. Compensatory mechanism involving the knee joint of the intact limb during gait in unilateral below-knee amputees. *Gait & Posture*, 28(2):278–284, 2008.
- [16] ES Neumann, K Yalamanchili, J Brink, and JS Lee. Transducer-based comparisons of the prosthetic feet used by transtibial amputees for different walking activities: a pilot study. *Prosthetics and Orthotics International*, 36(2):203–216, 2012.

- [17] GF Fernie. Biomechanics of gait and prosthetic alignment. *Amputation Surgery and Rehabilitation*. Kostuik JP, Gillespie R, editors. New York: Churchill Livingstone, pages 259–265, 1981.
- [18] AJ van den Bogert, M Hupperets, H Schlarb, and B Krabbe. Predictive musculoskeletal simulation using optimal control: effects of added limb mass on energy cost and kinematics of walking and running. *Proceedings of the Institution of Mechanical Engineers, Part P: Journal of Sports Engineering and Technology*, pages 1–11, 2012.
- [19] SR Hamner, A Seth, and SL Delp. Muscle contributions to propulsion and support during running. *Journal of Biomechanics*, 43(14):2709–2716, 2010.
- [20] SL Delp, FC Anderson, AS Arnold, P Loan, A Habib, CT John, E Guendelman, and DG Thelen. OpenSim: open-source software to create and analyze dynamic simulations of movement. *IEEE Transactions on Biomedical Engineering*, 54(11):1940–1950, 2007.
- [21] AJ van den Bogert, D Blana, and D Heinrich. Implicit methods for efficient musculoskeletal simulation and optimal control. *Procedia IUTAM*, 2:297–316, 2011.
- [22] SG McLean, A Su, and AJ van den Bogert. Development and validation of a 3-D model to predict knee joint loading during dynamic movement. *Journal of Biomechanical Engineering*, 125(6):864–874, 2003.
- [23] SG McLean, X Huang, A Su, and AJ van den Bogert. Sagittal plane biomechanics cannot injure the ACL during sidestep cutting. *Clinical Biomechanics*, 19(8):828–838, 2004.
- [24] RJ Zmitrewicz, RR Neptune, and K Sasaki. Mechanical energetic contributions from individual muscles and elastic prosthetic feet during symmetric unilateral transtibial amputee walking: a theoretical study. *Journal of Biomechanics*, 40(8):1824–1831, 2007.

- [25] Y-C Lin and MG Pandy. Three-dimensional data-tracking dynamic optimization simulations of human locomotion generated by direct collocation. *Journal of Biomechanics*, 59:1–8, 2017.
- [26] LJ Holmberg and A Klarbring. Muscle decomposition and recruitment criteria influence muscle force estimates. *Multibody System Dynamics*, 28(3):283–289, 2012.
- [27] Data table of BMI-for-age charts, 2001. URL https://www.cdc.gov/growthcharts/html_charts/bmiagerev.htm. Accessed: 08-2017.
- [28] A Wächter and LT Biegler. On the implementation of an interior-point filter line-search algorithm for large-scale nonlinear programming. *Mathematical Programming*, 106(1):25–57, 2006.
- [29] KC Moisio, DR Sumner, S Shott, and DE Hurwitz. Normalization of joint moments during gait: a comparison of two techniques. *Journal of Biomechanics*, 36(4):599–603, 2003.
- [30] LJ Bhargava, MG Pandy, and FC Anderson. A phenomenological model for estimating metabolic energy consumption in muscle contraction. *Journal of Biomechanics*, 37(1):81–88, 2004.
- [31] PU Saunders, DB Pyne, RD Telford, and JA Hawley. Reliability and variability of running economy in elite distance runners. *Medicine and Science in Sports and Exercise*, 36(11):1972–1976, 2004.
- [32] T Oberg, A Karsznia, and K Oberg. Joint angle parameters in gait: reference data for normal subjects, 10-79 years of age. *Journal of Rehabilitation Research and Development*, 31(3):199–213, 1994.
- [33] JR Gage, PA DeLuca, and TS Renshaw. Gait analysis: principle and applications with

emphasis on its use in cerebral palsy. *Instructional Course Lectures, The American Academy of Orthopaedic Surgeons*, 77(10):1607–1623, 1995.

- [34] TD Royer and CA Wasilewski. Hip and knee frontal plane moments in persons with unilateral, trans-tibial amputation. *Gait & Posture*, 23(3):303–306, 2006.
- [35] BJ Fregly, TF Besier, DG Lloyd, SL Delp, SA Banks, MG Pandy, and DD D’lima. Grand challenge competition to predict in vivo knee loads. *Journal of Orthopaedic Research*, 30(4):503–513, 2012.
- [36] RH Miller, AY Esterson, and JK Shim. Joint contact forces when minimizing the external knee adduction moment by gait modification: a computer simulation study. *The Knee*, 22(6):481–489, 2015.
- [37] DA Winter. *Biomechanics and motor control of human movement*. John Wiley & Sons, 2005.
- [38] RL Waters and S Mulroy. The energy expenditure of normal and pathologic gait. *Gait & posture*, 9(3):207–231, 1999.
- [39] NP Fey, GK Klute, and RR Neptune. Optimization of prosthetic foot stiffness to reduce metabolic cost and intact knee loading during below-knee amputee walking: a theoretical study. *Journal of Biomechanical Engineering*, 134(11):111005, 2012.
- [40] RD Snyder, CM Powers, C Fontaine, and J Perry. The effect of five prosthetic feet on the gait and loading of the sound limb in dysvascular below-knee amputees. *Journal of Rehabilitation Research and Development*, 32(4):309, 1995.
- [41] CM Powers, L Torburn, J Perry, and E Ayyappa. Influence of prosthetic foot design on sound limb loading in adults with unilateral below-knee amputations. *Archives of Physical Medicine and Rehabilitation*, 75(7):825–829, 1994.

- [42] RL Waters, J Perry, D Antonelli, and H Hislop. Energy cost of walking of amputees: the influence of level of amputation. *The Journal of Bone and Joint Surgery. American Volume*, 58(1):42–46, 1976.
- [43] SJ Mattes, PE Martin, and TD Royer. Walking symmetry and energy cost in persons with unilateral transtibial amputations: matching prosthetic and intact limb inertial properties. *Archives of Physical Medicine and Rehabilitation*, 81(5):561–568, 2000.
- [44] L Torburn, J Perry, E Ayyappa, and SL Shanfield. Below-knee amputee gait with dynamic elastic response prosthetic feet: a pilot study. *Journal of Rehabilitation Research and Development*, 27(4):369, 1990.
- [45] DH Nielsen, DG Shurr, JC Golden, and K Meier. Comparison of energy cost and gait efficiency during ambulation in below-knee amputees using different prosthetic feet: preliminary report. *JPO: Journal of Prosthetics and Orthotics*, 1(1):24–31, 1988.
- [46] AK Silverman, NP Fey, A Portillo, JG Walden, G Bosker, and RR Neptune. Compensatory mechanisms in below-knee amputee gait in response to increasing steady-state walking speeds. *Gait & Posture*, 28(4):602–609, 2008.
- [47] C Grumillier, N Martinet, J Paysant, J-M André, and C Beyaert. Compensatory mechanism involving the hip joint of the intact limb during gait in unilateral trans-tibial amputees. *Journal of Biomechanics*, 41(14):2926–2931, 2008.

CHAPTER V

COMPARING METABOLIC ENERGY MODELS USING EXPERIMENTAL DATA AND PREDICTIVE SIMULATIONS

Whether humans minimize metabolic energy cost in gait is debated. The goal of this work is to solve a predictive simulation of gait minimizing metabolic cost from a random initial guess and compare this to a predictive simulation minimizing effort. First, predictions of metabolic energy expenditure of seven metabolic energy expenditure models were compared to select the model that correlates best with experimental data. Ground reaction forces, marker data, and pulmonary gas exchange data were recorded for six walking trials at combinations of two speeds, 0.8 m/s and 1.3 m/s, and three inclines, -8% (downhill), level, and 8% (uphill). The metabolic cost, calculated with the metabolic energy models was compared to the metabolic cost from the pulmonary gas exchange rates. A repeated measures correlation showed that the model by Bhargava et al. [1] and the model by Lichtenwark and Wilson [2] correlated best with the experimental data, while the metabolic energy expenditure model by Margaria [3] had the lowest model error between the calculated and measured energy cost across the six walking trials. Four models were chosen as an objective for the predictive simulation. These models were adapted to be twice differentiable, so that a gradient based optimization method can be used. It was shown that these models correlate well with the original. Predictive simulations of a reaching task and gait were solved using this continuous model and by minimizing effort. The reaching task simulation showed that energy minimization predicts unrealistic movements when compared to effort

minimization. The predictive gait simulations showed that a realistic gait cycle cannot be created using just an objective of energy or effort minimization.

Statement of Contribution

This chapter contributes in terms of scientific results and methods. This is the first comparison of metabolic energy models for conditions other than level walking, which provides future researchers information to decide which metabolic energy model to use for their study. Additionally, it is the first to solve a periodic predictive simulation of gait successfully while minimizing metabolic energy without using any data. In terms of methods, the metabolic energy models were adapted to have a continuous first derivative, so that they can be used as objective in a gradient-based optimization algorithm.

Publications:

- Koelewijn, A. D., Heinrich, D. and Van den Bogert, A. J. (2018). Metabolic Cost Calculations of Gait using Musculoskeletal Energy Models, a Comparison Study. *Journal of Biomechanics*, in review.
- Koelewijn, A. D., Dorschky, E. and Van den Bogert, A. J. (2017). A comparison of metabolic energy and effort as objectives of gait using predictive simulations. *Computer Methods in Biomechanics and Biomedical Engineering*, in press.

5.1 Introduction

Predictive gait simulations can provide theoretical explanations for features of human gait [4] and can be useful to predict the effect of an altered mechanical environment on human gait. Recently, these simulations have been used to analyze ‘what-if scenarios’ such as the effect of an intervention like a prosthesis [5], an exoskeleton [6], an ankle-foot orthosis [7], or an additional weight [8] on gait, as well as the effect of loaded and inclined walking [9] or changing the gait pattern to one that minimizes knee reaction force [10] on gait.

Predictive simulations solved using direct collocation are found quickly, allow for complex control inputs, and periodicity can be enforced easily [4, 11]. Currently, an objective based on effort, or muscle activation, is often used with direct collocation [4, 5, 8]. Previous work showed that this objective can only predict the main features of gait without using any data [4]. Therefore, it is our goal to investigate if a more realistic gait cycle can be achieved when instead of effort, energy expenditure is minimized.

People prefer to walk in energetically optimal ways. Walking speed [12], the ratio between step length and step frequency [13], step width [14] and vertical movement of the center of mass [15, 16] are chosen such that energy expenditure is minimized. Whole-body energy expenditure can be measured using direct calorimetry, by measuring the heat production in the body, or indirect calorimetry, using pulmonary gas exchange measurements [17]. Muscular effort cannot be measured, so it is unknown if minimal muscular effort coincides with minimal energy expenditure. Therefore, it is unsure if minimization of muscular effort or metabolic energy is the true objective of human gait.

If minimal metabolic energy is the true objective of human gait, predictive simulations that minimize metabolic energy should be more realistic than predictive simulations that minimize muscular effort. However, measurements of energy expenditure are not available for predictive simulations. Several models exist that describe metabolic energy expenditure as a function of muscle activation, length and velocity [1, 2, 18, 19]. Using such model

as objective, it is possible to compare a predictive gait simulation minimizing metabolic energy expenditure to a predictive gait simulation minimizing effort and find if either objective results in a more realistic simulation.

Previously, Anderson and Pandy [20], Sellers et al. [21], Miller et al. [22], and Miller [23] created simulations of walking by minimizing metabolic energy. These optimizations required gradient-free optimization algorithms [21–23] or shooting [20]. Gradient-free optimization algorithms are known to be slow [21]. Shooting requires a forward simulation for each optimization variable to determine the gradient with respect to that optimization variable, and so is slow as well. Therefore, their simulations required thousands of CPU hours [20, 23], sometimes to find only simple control profiles [23]. The solutions were not periodic gait cycles [20, 23], and often data was used to create an initial guess [22, 23], which might influence the final solution. If direct collocation could be combined with an objective of minimization of metabolic energy, the advantages of the method and the objective could be employed to find a gait cycle that minimizes metabolic energy, and is periodic, has a large number of control variables, while it solves relatively fast.

In literature several energy models were suggested. The Huxley crossbridge model [24] finds the muscle force and the energy expenditure of a muscle [1], but requires up to 18 states [25]. Instead, Hill-type muscle models [26] are typically used to simulate muscles, but these do not output metabolic energy expenditure. Therefore, several metabolic energy models have been proposed that calculate the energy expenditure during walking based on Hill-type muscles [1–3, 18, 19, 27], or joint angles and moments [28].

There is an additional advantage of metabolic energy models over experimental data of energy expenditure. These models can also provide more information than measurements of energy-expenditure, which can only measure the energy expenditure of the full body. With metabolic energy expenditure models, the energy expenditure of single muscles [29], or joints [23] can be calculated separately. Therefore, these models can be used for detailed studies into energy expenditure of different body parts.

Our aim is to use one of these models to investigate if it is possible to create a realistic predictive simulation of a gait cycle by minimizing metabolic energy, without using any data. Therefore, this study has two parts. In the first part, a metabolic energy model will be selected for which the metabolic cost correlates best with metabolic cost from measurements of pulmonary gas exchange. In the second part, this metabolic energy model is used to solve a predictive gait simulation, which is compared to a predictive gait simulation found by minimizing muscular effort.

An experiment will be performed to compare the metabolic energy models. So far, these models have only been compared and used on level walking studies and self-selected speed (e.g. [1, 18, 23]). However, it is important to know how well these models can represent changes in energy cost due to altered control or environment. Specifically it is known that in downhill walking, knee extensor activity increases [30, 31] while metabolic cost decreases [3], that in uphill walking metabolic cost increases [3], and that between 2 and 5 km/h, metabolic cost is independent of speed [32]. However, it is unknown if the metabolic energy expenditure models could predict these observations and which model coincides best with energy expenditure measurements. Consequently, we aimed to compare metabolic cost calculated with the different models to metabolic cost measured with indirect calorimetry on walking trials with different speeds and slopes.

After the comparison of the metabolic energy expenditure models, our second goal is to investigate if it is possible to create a realistic gait cycle by minimizing metabolic energy. For this, it is necessary to adapt the metabolic energy model such that the first derivative is continuous. We show that the continuous version of the metabolic energy models correlates well with the original model over a range of walking and running speeds. We create predictive simulations of a single joint reaching task to highlight the differences between metabolic rate and effort minimizations. Finally, we present a predictive gait simulations that minimizes metabolic rate from a random initial guess, and compare to a predictive gait simulation that minimizes effort.

5.2 Comparison of Metabolic Energy Expenditure Models

Predictions of metabolic energy expenditure of seven metabolic energy expenditure models were compared to select the model that correlates best with experimental data. Ground reaction forces, marker data, and pulmonary gas exchange data were recorded for six walking trials at combinations of two speeds, 0.8 m/s and 1.3 m/s, and three inclines, -8% (downhill), level, and 8% (uphill). The metabolic cost, calculated with the metabolic energy models was compared to the metabolic cost from the pulmonary gas exchange data. A repeated measures correlation showed that the model by Bhargava et al. [1] and the model by Lichtwark and Wilson [2] correlated best with the experimental data, while the metabolic energy expenditure model by Margaria [3] had the lowest model error between the calculated and measured energy cost across the six walking trials.

5.2.1 Methods

Subjects and experiment

Twelve healthy participants (6 female, 6 male, mean \pm SD age 24 ± 5 years, weight 67 ± 11 kg, and height 173 ± 8 cm) provided informed consent and performed the experiment. The experimental protocol was approved by the institutional review board of Cleveland State University (IRB-FY2017-286). First, the subjects stood on the treadmill for three minutes to determine their resting metabolic rate. They performed six walking trials in random order, three at 0.8 m/s and three at 1.3 m/s. For each speed, there were three different inclines: level walking, downhill walking with a negative incline of 8%, and uphill walking with a positive incline of 8%. Pulmonary gas exchange rates were measured with the COSMED K4b2 system (COSMED, Italy). An instrumented treadmill with two six degree of freedom force plates (R-Mill, Forcelink, Culemborg, the Netherlands) was used to measure the ground reaction forces. A motion capture system with 10 Osprey cameras and Cortex software (Motion Analysis, Santa Rosa, CA) was used to record 27 markers,

given the markerset in appendix 7.2.

Metabolic energy models

Seven metabolic energy models were selected for this study: models Bhargava [1], Houdijk [19], Umberger [18], Lichtwark [2], Minetti [27], Margaria [3], and Kim [28]. Six models use muscle states (contractile element length, activation, stimulation) to determine the energy rate of the individual muscles. Model Kim calculates the energy rate for each joint instead of each muscle, using the angular velocity and joint moment.

The calculated metabolic cost of walking, C_{calc} , is determined in J/kg/m as follows:

$$C_{calc} = \frac{1}{Tmv} \int_{t=0}^T \sum_{i=1}^{N_{mus}} \dot{E}_i(t) m_{mus(i)} dt \quad (5.1)$$

where T denotes the motion duration, m the participant's mass, v the speed, N_{mus} the number of muscles, and \dot{E}_i the energy rate of muscle i normalized to muscle mass m_{mus} .

Models Bhargava, Houdijk, Umberger, and Lichtwark calculate the energy rate as a function of work rate, \dot{w} , and heat rates, due to activation, \dot{h}_a , maintenance of contraction, and \dot{h}_m , and muscle shortening and lengthening, \dot{h}_{sl} [1, 2, 18, 19]:

$$\dot{E} = \dot{w} + \dot{h}_a + \dot{h}_m + \dot{h}_{sl} \quad (5.2)$$

Model Minetti determines the energy rate for each muscle incorporating an empirical function of the ratio between the contractile element velocity, v_{CE} and the maximum contractile element velocity, $v_{CE(max)}$ [27]:

$$\dot{E} = a F_{max} v_{CE(max)} \phi \quad (5.3)$$

$$\text{where } \phi = \frac{0.054 + 0.506 \bar{v}_{CE} + 2/46 \bar{v}_{CE}^2}{1 - 1.13 \bar{v}_{CE} + 12.8 \bar{v}_{CE}^2 - 1.64 \bar{v}_{CE}^3} \quad (5.4)$$

where a is the muscle activation, F_{max} the maximum isometric force, and \bar{v}_{CE} is the ratio

of the contractile element velocity to the maximum contractile element velocity.

Model Margaria is based on the observation that muscles are 25% efficient when shortening, and 120% efficient when lengthening [3]:

$$\dot{E} = \begin{cases} \frac{w}{0.25} & \text{if: } v_{CE} < 0 \\ -\frac{w}{1.2} & \text{if: } v_{CE} \geq 0 \end{cases} \quad (5.5)$$

Model Kim calculates the energy rate using the work rate and heat dissipation at each joint:

$$\dot{E} = \dot{h}_{am}\dot{\theta}_{max}|M| + \dot{h}_{sl}|M\dot{\theta}| + \dot{Q}_{cc}P_{max} + M\dot{\theta} \quad (5.6)$$

where $\dot{\theta}$ denotes the angular velocity of the joint, M the joint moments, and $P = \dot{\theta}M$ the power. The subscript *max* indicates the maximum over the gait cycle. $h_{am} = 0.054$ is the heat rate for activation and maintenance, $h_{sl} = 0.283$ is the shortening-lengthening heat rate for positive power, and $h_{sl} = 1.423$ is the shortening-lengthening heat rate for negative power, and $\dot{Q}_{cc} = 0.004$ is the co-contraction heat rate [28]. Note that for model Kim, the summation in equation 5.2 is performed over the number of joints, instead of the number of muscles, and the energy rate is not normalized to muscle mass. The implementation of all models is detailed in appendix 7.2.

Kinetic and Kinematic Data Processing

A two step approach was used to calculate the joint angles, moments, and muscle states and inputs necessary to determine the metabolic cost of walking level, uphill and downhill using the metabolic energy models.

In the first step, the joint angles and moments were determined from marker and ground reaction force data. The data was filtered backwards and forwards with a second order Butterworth filter with a cut-off frequency of 6 Hz. Angles, angular velocities and accelerations, and segment accelerations were calculated from marker positions, velocities, and

accelerations [33]. The data was split into gait cycles and resampled to 100 data points per gait cycle.

The joint angles were determined using the orientation from the proximal to the distal marker on the body segment. For example, for the tibia these were the knee and ankle markers. The joint moments were determined from the marker data and the ground reaction forces using Winter's method [34]. The joint angles, moments, and ground reaction forces were averaged over all left and right gait cycles to find one average gait cycle.

In the second step, the muscle states (activation and contractile element length) and stimulations were determined from an optimization problem using the sagittal plane musculoskeletal model with nine degrees of freedom and 16 muscles that was described in section 2.6 (see also [8]). The model's height and mass was the same as the subject's height and mass. Segment mass distribution was based on [34]. The stimulations $u(t)$, activations $a(t)$, and contractile element lengths $l_{CE}(t)$ were found by solving the following optimal control problem [35]:

$$\underset{l_{CE}(t), a(t), u(t)}{\text{minimize}} \quad \int_{t=0}^T \sum_{i=1}^{N_{mus}} a_i(t)^2 dt \quad (5.7)$$

$$\begin{aligned} \text{Subject to: } & F_{SEE}(\theta(t)) - F_{CE}(a(t), l_{CE}(t), v_{CE}(t)) \\ & -F_{PEE}(\theta(t)) = 0 \quad 0 \leq t \leq T \end{aligned} \quad (5.8)$$

$$\dot{a} - (u(t) - a(t)) \left(\frac{u(t)}{T_{act}} + \frac{1-u(t)}{T_{deact}} \right) = 0 \quad 0 \leq t \leq T \quad (5.9)$$

$$DF_{SEE} - M_{winter} = 0 \quad 0 \leq t \leq T \quad (5.10)$$

where F_{SEE} , F_{PEE} and F_{CE} denote the series elastic, parallel elastic and contractile element force, θ the joint angles, v_{CE} the contractile element velocity, the first derivative of the contractile element length. T_{act} is the activation time constant, T_{deact} is the deactivation time constant, D denotes a matrix of muscle moment arms, and M_{winter} the moments that were calculated previously. Periodic boundary conditions were used: $u(T) = u(0)$, $a(T) = a(0)$, and $l_{CE}(T) = l_{CE}(0)$.

This optimization problem was solved using direct collocation, with 100 collocation points per gait cycle and a backward Euler formulation. IPOPT 3.11.0 was used to solve the optimization problem [36]. Finally, the muscle state trajectories, or the joint angular velocities and moments were inserted in the seven metabolic energy models to find the calculated metabolic cost.

Pulmonary Data Processing

The measured metabolic cost was derived from the pulmonary gas exchange data using indirect calorimetry. The first 30 seconds of the resting trial, and the first three minutes of each walking trial were disregarded. The rate of oxygen consumption, $\dot{V}O_2$ in mL/min/kg, and respiratory quotient, R were averaged over time. The metabolic rate in W/kg was determined as follows for the resting and walking trials [37]:

$$W = \frac{4.184}{60} (3.941 + 1.106R) \dot{V}O_2 \quad (5.11)$$

The resting trial was subtracted from each walking trial. The metabolic rate was divided by walking speed to find the measured metabolic cost in J/kg/m:

$$C_{meas} = \frac{(W_{meas} - W_{rest})}{v} \quad (5.12)$$

5.2.2 Analysis

The implementation of the metabolic energy models was verified first. Similar to [23], the metabolic rate was determined for three speeds (shortening, isometric and lengthening), and five activation levels (0.05, 0.25, 0.5, 0.75 and 1), and compared to [23].

The calculated metabolic cost was reported for all joints individually and the total (equation 5.1) was compared to measured metabolic cost (equation 5.12). Each model was assessed using the error between the calculated and measured metabolic cost, and a repeated measures correlation [38].

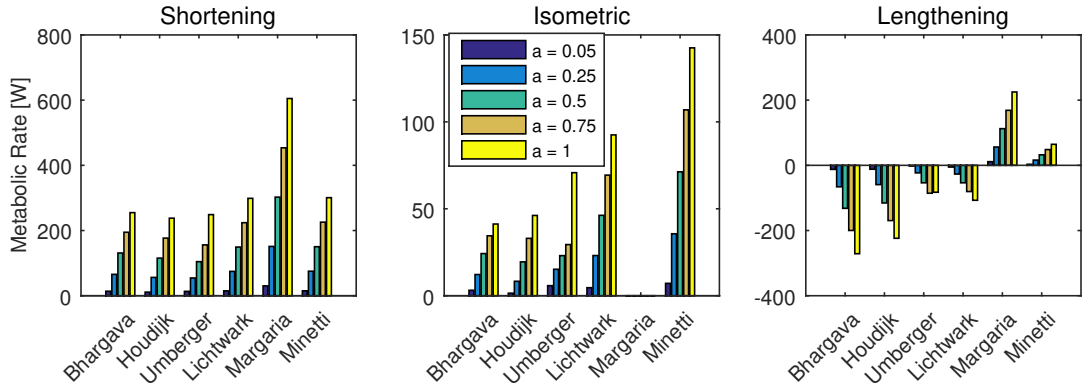


Figure 26: Metabolic rate of the soleus muscle at four activation levels, for an isometric condition, and a shortening and lengthening velocity of one optimal fiber length per second.

5.2.3 Results

Verification of Metabolic Energy Models

Figure 26 shows the metabolic power of the Soleus for several activation levels and a shortening and lengthening velocity of $1 \text{ } l_{CE(OPT)}/\text{s}$, where $l_{CE(OPT)}$ is the optimal contractile element length, and an isometric condition. The metabolic rate for shortening is more than twice as high from model Margaria than for all other models. In the isometric condition model Minetti has the largest metabolic rate, while model Margaria has zero metabolic rate, since no work is done at zero speed. The metabolic rate is most different between the models during lengthening, where only models Margaria and Minetti had a positive metabolic rate.

Joint Kinetics and Kinematics

Figure 27 shows the ground reaction forces, joint angles, joint moments, and muscle forces for all trials at 1.3 m/s. The downhill trial has a larger peak vertical ground reaction force and braking horizontal ground reaction force than the level trial. The peak hip flexion angle is smaller than the level trial, while the peak hip and knee extension angle are larger. The ankle angles are similar to the level trial. The stance hip moment, and peak ankle plantarflexion moment are smaller, while the peak knee extension moment is larger.

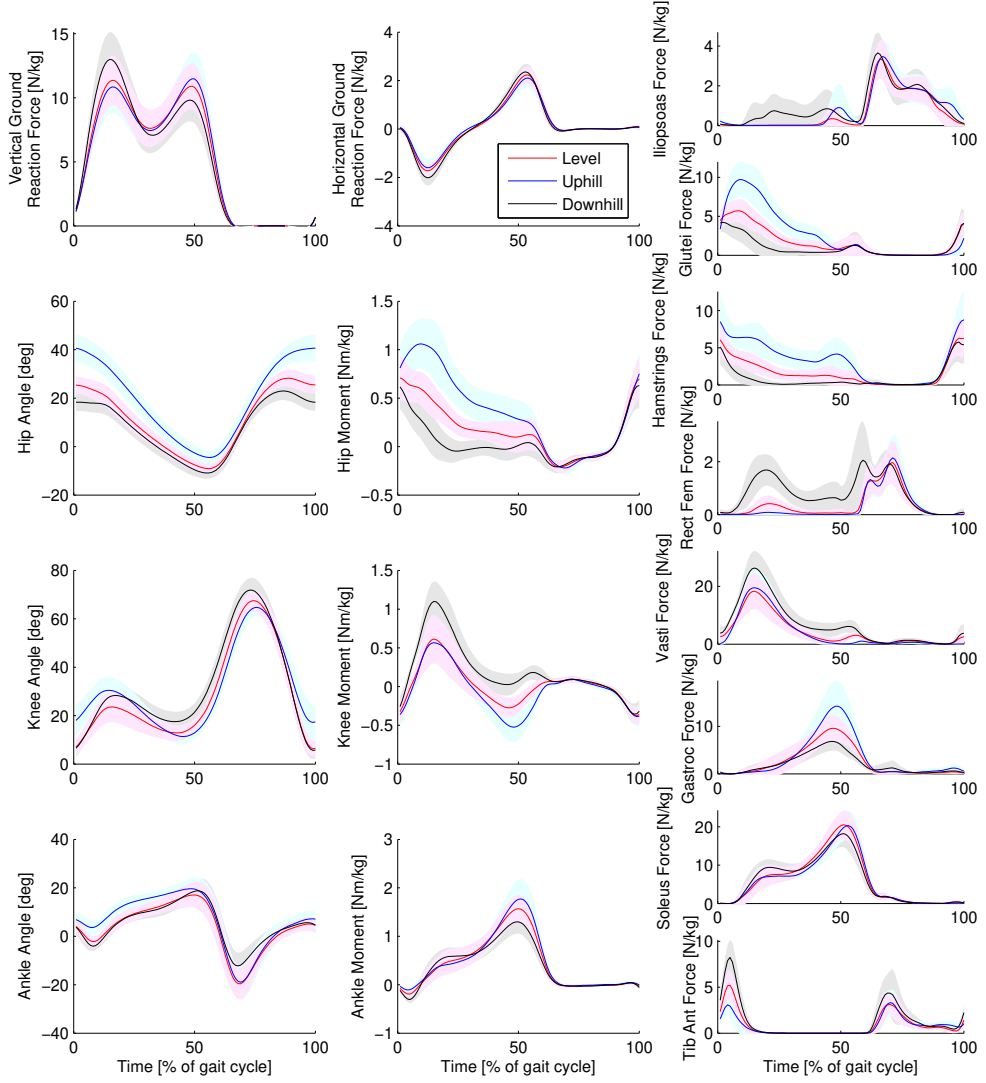


Figure 27: Average ground reaction forces, joint angles, joint moments, and muscle forces for all trials at the normal speed. The shaded area denotes one standard deviation. The figures use Winter's sign convention, where flexion angles and extension moments are positive for hip and knee. Dorsiflexion angle and plantarflexion moment are positive for the ankle.

In the uphill trial, the ground reaction force is similar to the level trial, while the hip angle is shifted towards higher flexion. The knee angle is similar to the level trial, while the ankle has more dorsiflexion in the first half of the gait cycle. The stance hip moment, peak knee flexion moment, and peak ankle plantarflexion moment are larger than the level trial.

The Iliopsoas and Rectus Femoris are only active during stance in the downhill trial, while the force during swing is similar between trials. In the Gluteus, Hamstrings, and Gastrocnemius the peak force is highest for the uphill trial, and lowest for the downhill trial. The Vasti has the largest peak force in the downhill trial, and similar force in the other trials. The Tibialis Anterior has the highest peak force in the downhill trial, and the lowest in the uphill trial. The Soleus has similar force in all trials.

Figure 28 shows the ground reaction forces, joint angles, joint moments, and muscle forces for all trials at 0.8 m/s. The pattern of the downhill, level, and uphill trials are very similar to the patterns seen for the normal speed. The muscle forces in the slow trials also show similar trends, but with lower force. One difference to normal speed is the smaller peak in the Soleus in the downhill trial.

Metabolic Energy Expenditure

Figure 29 shows the calculated metabolic cost for each model, separated for the hip, knee and ankle joints. The mean calculated metabolic cost was lowest with model Houdijk, and highest for model Minetti, ranging from 0.88 J/kg/m to 5.2 J/kg/m for the downhill trials, from 1.6 J/kg/m to 5.7 J/kg/m for the level trials and from 2.9 J/kg/m to 7.8 J/kg/m for the uphill trials. The mean measured metabolic cost ranged from 2.0 J/kg/m for the downhill trial at 1.3 m/s to 5.9 J/kg/m for the uphill trial at 1.3 m/s (see bottom right graph). One measurement was missing for the downhill trial at 1.3 m/s due to a malfunction of the metabolic cart.

Comparing the different inclines, the metabolic cost increased with incline for all mod-

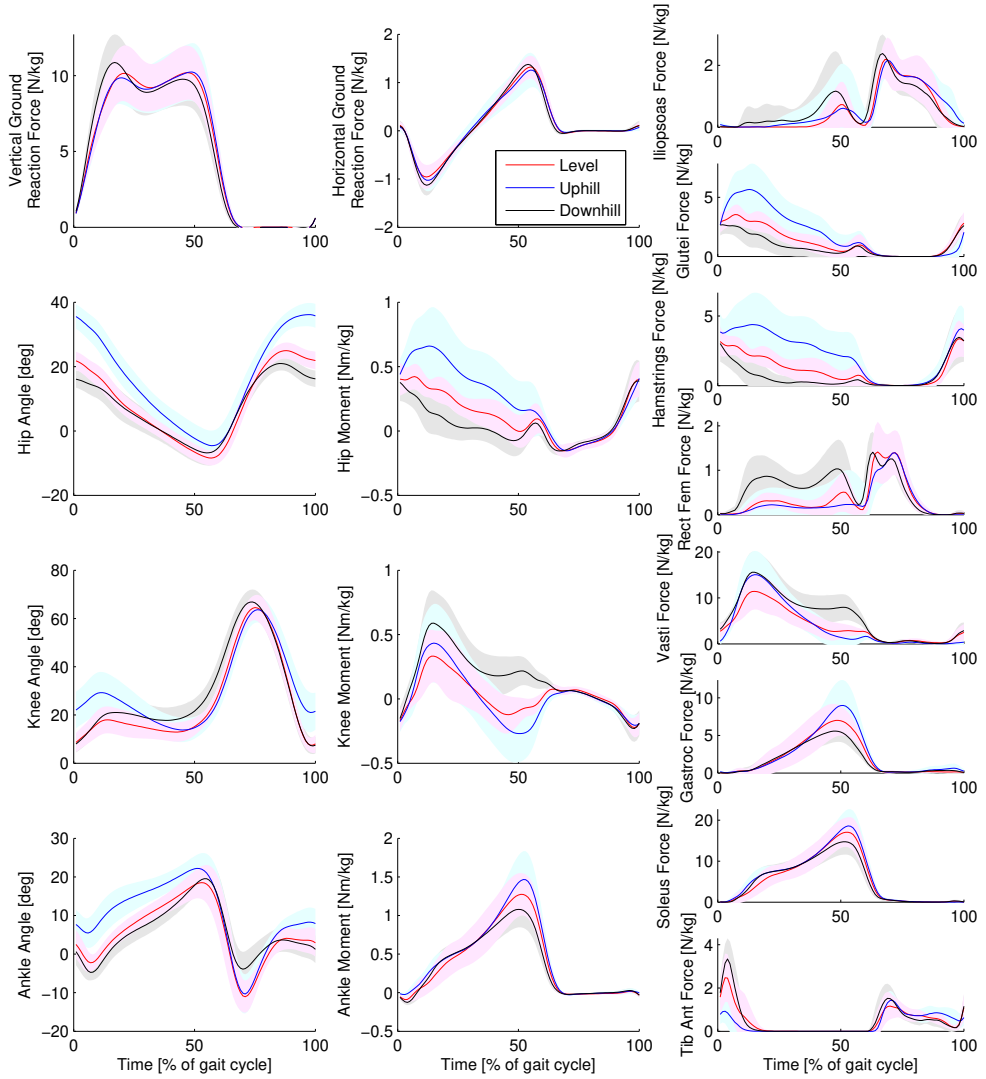


Figure 28: Average ground reaction forces, joint angles, joint moments, and muscle forces for all trials at the slow speed. The shaded area denotes on standard deviation. The figures use Winter's sign convention, where flexion angles and extension moments are positive for hip and knee. Dorsiflexion angle and plantarflexion moment are positive for the ankle.

els except model Kim, where the metabolic cost of the downhill trials was larger than in the level trials. Every model calculated more energy expenditure at the hips with an increasing slope. In all models except model Kim, the energy expenditure at the knee and ankle remained similar, while for model Kim the metabolic cost in the knee decreased from downhill to level.

The effect of speed differed among the models. The metabolic cost at the ankle at larger speed was larger for model Houdijk, while the metabolic cost was slightly lower at the knee. For models Bhargava, Umberger, Lichtwark, and Minetti the metabolic cost decreased with speed in the hip and knee, while the metabolic cost in the ankle increased, and the overall metabolic cost decreased. The metabolic cost increased with speed for model Margaria, with all joints expending more energy. The metabolic cost calculated with model Kim also increased with speed, but the metabolic cost in the ankle decreased, while the metabolic cost in the knee and hip increased.

Figure 30 shows the difference between the metabolic cost measured during the experiment and calculated by the metabolic models. Model Margaria predicted three trials reasonably (the 95% confidence interval crosses zero), the uphill trials and the level trial at 0.8 m/s. Model Kim (level trials) and model Lichtwark (uphill trials) predicted two trials reasonably. Model Bhargava (downhill at 0.8 m/s) and model Umberger (level at 1.3 m/s) predicted one trial reasonably. Model Houdijk underestimated the metabolic cost of all trials with about 2 J/kg/m for the uphill trials and 1 J/kg/m for the other trials. Model Minetti overestimated all trials, with the largest overestimation at the downhill trials and the smallest at the uphill trials.

Figure 31 shows the linear regression model that was fitted during the correlation analysis for each metabolic energy model. Table V shows the correlation coefficients of all models. The highest correlation coefficient was 0.96 for model Bhargava and model Lichtwark, followed by model Houdijk with a coefficient of 0.94. The correlation coefficient of model Kim was lowest, with 0.49. The slope of the regression model for model Margaria

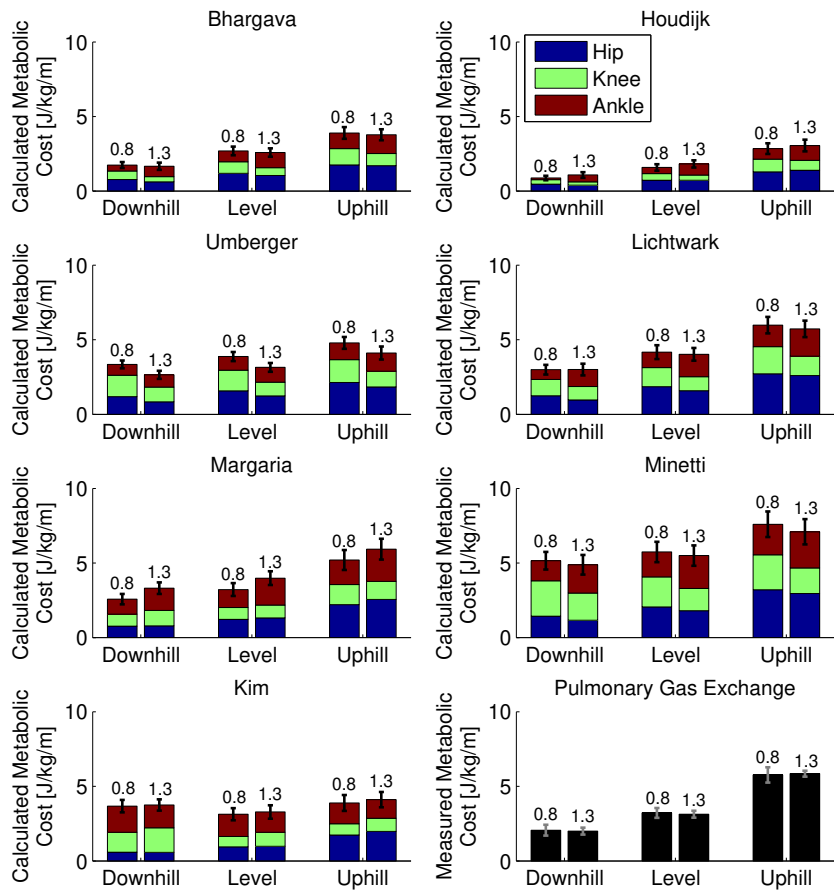


Figure 29: Calculated metabolic cost for all speeds and inclines, for each model, separately for the joints. The number above the bar indicates the speed of the trial. Biarticular muscles were added by ratio of the moment arm, similar to [23]

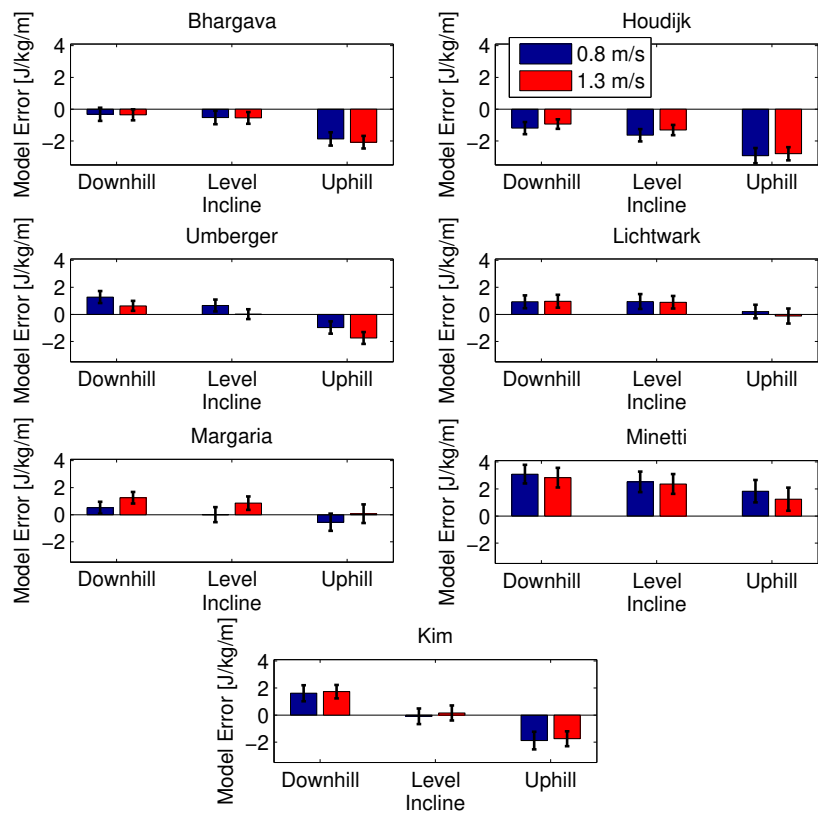


Figure 30: Average difference between measured and calculated metabolic cost with 95% confidence interval for all models and all trials.

Table V: Correlation coefficient r with 95% confidence interval (CI) of the repeated measures correlation analysis, and slope of the fitted repeated measured correlation model.

Model	r	(95 % CI)	Slope
Bhargava	0.96	(0.93 - 0.97)	1.75
Houdijk	0.94	(0.90 - 0.97)	1.81
Umberger	0.83	(0.72 - 0.89)	1.87
Lichtwark	0.96	(0.93 - 0.97)	1.28
Margaria	0.90	(0.83 - 0.94)	1.18
Minetti	0.91	(0.86 - 0.95)	1.39
Kim	0.49	(0.26 - 0.66)	1.98

(1.18) was closest to unity, while the slope for model Kim (1.98) was farthest from unity.

5.2.4 Discussion

The goal of this work was to compare metabolic cost calculated with seven metabolic models to metabolic cost measured with indirect calorimetry on walking trials with different speeds and slopes, and to determine which model correlated best with the data and which one showed the most similar trend. Comparing the calculated metabolic cost to the measured metabolic cost, model Margaria predicted three trials reasonably, model Lichtwark predicted two trials reasonably, and model Bhargava and model Umberger predicted one trial reasonably (figure 30). Model Kim, which was fitted to pulmonary measurements of level walking, predicted both level trials reasonably. Model Houdijk underestimated the metabolic cost of all trials and model Minetti overestimated all trials. Model Bhargava and model Lichtwark correlated best with the experimental data, while model Houdijk correlated slightly worse. The regression model of model Margaria had a slope closest to unity. All models except model Kim predicted a lower metabolic cost in the downhill trials than in the level trials, despite a larger force in the knee extensors (Rectus Femoris throughout stance and Vasti during late stance), similar to observed in previous studies [3, 30, 31]. Models Bhargava, Lichtwark, Minetti, and Kim predicted similar cost between the two speeds [32].

The calculated metabolic cost in this study is slightly lower than calculated by Miller

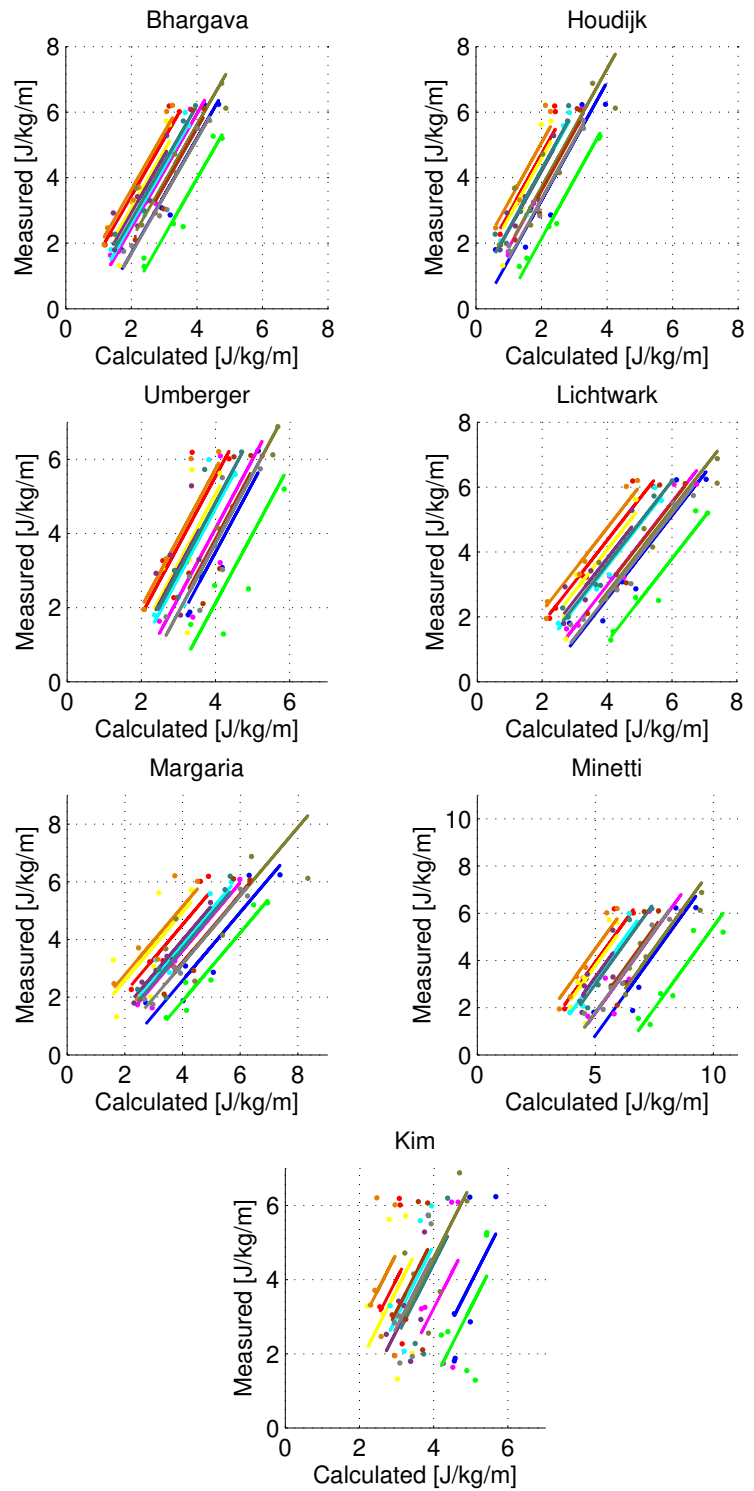


Figure 31: Correlation graphs between calculated and measured metabolic costs for each model. The lines show the regression model that was fitted by the repeated measured correlation.

[23] and Bhargava et al. [1], who included resting metabolic rate, and higher than Umberger et al. [18] at 1.2 m/s: (3.2 J/kg/m versus 2.7 J/kg/m). A 10% increase compared to Umberger et al. [18] and Bhargava et al. [1] is expected since arm swing was not accounted for in this work [39]. The other studies use a three-dimensional model [1, 18, 23], while this work used a sagittal plane model with eight muscles. Hicks et al. [40] mention that this should be sufficiently accurate for walking, since this motion is almost entirely in the sagittal plane. Model Umberger underestimated the increase in metabolic cost from level to uphill, and the decrease in metabolic cost from level to downhill. Dembia et al. [6] found a similar result using this model to predict the increase in metabolic cost from unloaded walking to loaded walking with 38 kg on the torso.

The kinematic and kinetic data are similar to previous studies of sloped walking [31, 41]. The trend of the muscle forces with the slope was similar to Alexander and Schwameder [42] for the Gluteals, Hamstrings, Rectus Femoris and Gastrocnemius. This study used a model with 18 muscles in each leg, compared to eight in this work, which could explain the higher forces in the Iliopsoas, Hamstrings, Vasti and Soleus than in Alexander and Schwameder [42], while the force in the Gluteals was lower, and the force in the Rectus Femoris, Gastrocnemius and Tibialis Anterior was similar to Alexander and Schwameder [42].

The handling of muscular energy expenditure during lengthening is still debated [23]. During lengthening, the energy rate can be negative, which is physically impossible. However, the negative work should be subtracted from the metabolic cost in models Bhargava, Houdijk, Umberger, and Lichtwark [1, 2, 18, 19]. We aimed to see if predictions improved without this subtraction, which is physically more sensible. When negative work was not subtracted, the calculated metabolic cost increased. Model Bhargava predicted the metabolic cost of the level trials correctly, model Houdijk predicted the downhill trials correctly, model Umberger the level trial at 1.3 m/s and model Lichtwark the uphill trial at 1.3 m/s. The correlation coefficient decreased by 0.01 for two models (Bhargava and Licht-

wark), 0.02 for model Houdijk, and 0.06 for model Umberger. The lengthening heat rate coefficient was updated in model Umberger according to Umberger [43], so it is interesting that the difference was largest for this model.

Figure 26 showed that the models were correctly implemented. The results for models Minetti, Bhargava, Houdijk, Lichtwark, and Umberger were very similar to fig. 2 in [23]. Note that model Umberger in Miller [23] does not allow negative work, so the result differs for lengthening.

Correlation coefficients were high for all subjects individually, except for one (purple line in figure 31). This subject had an outlier of the uphill trial at slow speed. The intercept of the correlation lines in figure 31 was related to the weight of the participant for all models. A higher weight yielded a smaller intercept and a smaller weight yielded a higher intercept, so a systematic bias existed in the calculated metabolic cost. This might explain that most models correlated well with the experimental data, despite not all of them predicting the metabolic cost of all trials well.

Commonly, muscle activations are found in gait analysis by static optimization [44] or computed muscle control (CMC) [45]. Static optimization only finds muscle activations, whereas model Bhargava and model Umberger require activation and stimulation. All models, except model Kim, require the contractile element length and velocity. CMC requires a full-body model and markerset to solve for these variables. The approach in this work required only a lower-extremity model and six markers. A larger markerset was used to aid data processing in Cortex. Similar to static optimization [44], solutions were robust to changes in the objective function (equation 5.7). An optimization with an objective of cubed activations, with and without muscle volume weighting, yielded similar muscle forces.

In summary, we have compared seven metabolic energy models to experimental data and found that two models (Bhargava and Lichtwark) correlated best with the measured metabolic cost, and that model Margaria had the lowest model error. All models except

model Kim predicted a lower metabolic cost in the downhill trials than in the level trials. Models Bhargava, Lichtwark, Minetti, and Kim predicted similar cost between the two speeds. We conclude that different models are most suited for different situations. For example, when one aims to find the relative increase of metabolic cost between two trials, model Bhargava or Lichtwark is most suited. When one aims to calculate the minimum metabolic cost over a range of conditions, model Margaria will be more suitable.

5.2.5 Model Selection for Predictive Simulations

Correlation is the most important selection criteria when choosing an objective for predictive gait simulations, since it is most important that the solution that is found is at the actual minimum metabolic cost. The value is of lesser importance. Therefore, the metabolic energy models with the highest correlation, model Bhargava and model Lichtwark were selected. Model Houdijk was selected as well, since this model had a correlation almost as high as the other two models, within the 95% confidence interval of the correlation of model Bhargava and model Lichtwark.

Additionally, model Umberger was selected. This model is implemented in OpenSim [45], and has been used to determine metabolic cost in many other studies [6, 21, 22, 46–50]. Therefore, it was decided that the quality of this model should be assessed as well.

5.3 Predictive Simulation of Gait Minimizing Metabolic Cost Compared to Minimizing Effort

Predictive simulations were solved using the selected models. These models were adapted to be twice differentiable, so that a gradient based optimization method can be used. It was shown that these models correlate well with the original. Predictive simulations of a reaching task and gait were solved using this continuous model and by minimizing effort. The reaching task simulation showed that energy minimization predicts unrealistic movements when compared to effort minimization. The predictive gait simula-

tions showed that a realistic gait cycle cannot be created using just an objective of energy or effort minimization.

5.3.1 Adaptations to Models Necessary for Gradient-Based Optimization

Any objective function should have a smooth first derivative when using a gradient-based optimization algorithm such as IPOPT [36]. Therefore, several adaptations were made to the metabolic energy models. This section explains the adaptations necessary to create a continuous version of the models, and shows that this continuous version correlates well with the original version. A problem with a simple pendulum is solved to highlight the differences between minimizing metabolic energy and effort.

Model Adaptations

Model Bhargava, model Houdijk, model Lichtwark and model Umberger all used different equations for heat generation during shortening and lengthening, which creates a discontinuity in the derivatives. This was solved by using a separate shortening velocity, $\tilde{v}_{CE(S)}$, and lengthening velocity, $\tilde{v}_{CE(L)}$. These were determined as follows:

$$\tilde{v}_{CE(S)} = \frac{1}{2} \left(\tilde{v}_{CE} - \sqrt{\tilde{v}_{CE}^2 + \varepsilon^2} \right) \quad (5.13)$$

$$\tilde{v}_{CE(L)} = \frac{1}{2} \left(\tilde{v}_{CE} + \sqrt{\tilde{v}_{CE}^2 + \varepsilon^2} \right) \quad (5.14)$$

where ε is a small number. The superscript \sim denotes a normalization to optimal fiber length. Equation 5.13 ensured that the shortening velocity is zero when the muscle is lengthening, and nonzero when the muscle is shortening. Equation 5.14 worked similarly for lengthening.

Another discontinuity was present since work was not allowed to be negative. This is different from section 5.3, because early tests found that the optimization process would take advantage of the negative work to find gait cycles that had a negative energy rate,

which is physically impossible. Section 5.3 also shows that the models still correlate well with the measured metabolic cost if negative work was not allowed. Therefore, work w_{CE1} was calculated as follows from nominal work w_{CE} :

$$w_{CE1} = \frac{1}{2} \left(w_{CE} + \sqrt{w_{CE}^2 + \varepsilon^2} \right) \quad (5.15)$$

Model Umberger has two additional discontinuities in the first derivative, caused by the dependency of the shortening-lengthening heat rate changes on activation and stimulation (see [18]). The heat rate is dependent on $A(t)$, which is equal to stimulation, $u(t)$, if the stimulation is larger than the activation, $a(t)$, and dependent on the average between the activation and stimulation if the stimulation is smaller than the activation, which can be described as follows:

$$A(t) = \begin{cases} u(t) & \text{if } u(t) > a(t) \\ \frac{a(t)+u(t)}{2} & \text{if } u(t) < a(t) \end{cases} \quad (5.16)$$

This equation was rewritten to the following continuous version:

$$A(t) = u(t) + \frac{1}{2} \left(\frac{a(t) - u(t)}{2} + \sqrt{\left(\frac{a(t) - u(t)}{2} \right)^2 + \varepsilon^2} \right) \quad (5.17)$$

where ε is the same in equation 5.17 and equations 5.13 and 5.14 for simplicity.

The final discontinuity is the relationship between $A(t)$ and the shortening-lengthening heat rate. This relationship is quadratic for shortening [51–53], but no information was available for lengthening [18]. Umberger et al. [18] used a linear relationship. There is no evidence for a linear or a nonlinear relationship, though Umberger et al. claimed that this relationship is likely nonlinear as well [18]. Therefore, a quadratic relationship is used for lengthening to make the relationship continuous, since this is the simplest nonlinear relationship. Appendix 7.2 describes the full continuous version of model Umberger.

Model Lichtwark and model Bhargava have an additional discontinuity due to their

use of the stimulation time of the muscle. This value does not have an analytical gradient when direct collocation is used. Therefore, in model Lichtwark, $\gamma = 1.5$ is used in equation 5.18 [54]. In model Bhargava, $\phi = 0.2$ is used in equation 17, based on the average time the muscles are active during gait.

Finally, model Lichtwark has a discontinuity in the calculation of the maintenance heat rate, \dot{h}_m (see appendix A):

$$\dot{h}_{m(s)} = \gamma \frac{\tilde{v}_{ce(max)}}{G^2} \quad (5.18)$$

$$\dot{h}_{m(l)} = 0.3 \left(\gamma \frac{\tilde{v}_{ce(max)}}{G^2} \right) + 0.7 \left(\gamma \frac{\tilde{v}_{ce(max)}}{G^2} \right) e^{-7\tilde{v}_{ce(max)}(g(v_{CE})-1)} \quad (5.19)$$

where $\dot{h}_{m(s)}$ is the maintenance heat rate during shortening, and $\dot{h}_{m(l)}$ is the maintenance heat rate during lengthening. $\tilde{v}_{ce(max)}$ is the maximum normalized shortening velocity (positive in model Lichtwark), G is the curvature of the force-velocity curve, and $g(v_{CE})$ the force-velocity relationship.

This function was made continuous using a cosine function between $-\pi/2 \leq v_{CE} \leq 0$, where this function has a derivative of zero at $-\pi/2$ and 0:

$$\dot{h}_m = \begin{cases} \dot{h}_{m(s)} & v_{CE} > 0 \\ \left(\frac{1}{2}(\dot{h}_{m(s)} + \dot{h}_{m(l)}) - \frac{(\dot{h}_{m(l)} - \dot{h}_{m(s)})}{2} \cos(1000v_{CE}) \right) & -\pi/2 \leq v_{CE} \leq 0 \\ \dot{h}_{m(l)} & v_{CE} < -\pi/2 \end{cases} \quad (5.20)$$

Model Verification using Simulated Gait

A correlation analysis between the original and continuous version of the models was performed using the metabolic cost of walking and running simulations. These simulations were found using an objective of muscular effort and tracking of gait data, using a procedure identical to the one used by Van den Bogert et al. [8] and in chapter III.

Simulations were used from 20 virtual subjects, randomly sampled with mean (\pm SD)

height of 176 ± 5.3 cm and weight of 73.5 ± 6.2 kg. Dimensions and inertial properties were taken from Winter [34]. All muscle parameters were varied around their original value with a standard deviation of 5% of the original value. For each virtual subject, gait simulations were generated at four different speeds, walking at 1.3 m/s and 1.8 m/s, and running at 3.6 m/s and 4.3 m/s.

The metabolic cost of the simulations was calculated with the original and continuous version of each model. These were compared using repeated measures correlation [38], since four data points were available for each subject. The correlation coefficient and its confidence interval were used to evaluate how well the continuous model agreed with the original model. This statistical analysis was performed in R.

Results

Figure 32 shows the metabolic cost in the continuous version of the models versus the metabolic cost in the original version. The models correlate very well with the original versions, which is also supported by the correlation coefficients, and root mean square (RMS) errors given in table VI. This table also shows the slope of the relationship between the original and continuous models and the RMS error. The RMS error is small for all models compared, less than 5% of the metabolic cost. All models overestimate metabolic cost at higher speeds, so the slopes of the relationship between the original and continuous models are lower than one.

Discussion

The original and continuous versions of all models correlated very well ($R > 0.99$). The slopes were smaller than one, since the continuous version overestimate the metabolic cost compared to the original versions. This is due to the fact that negative muscle work was not

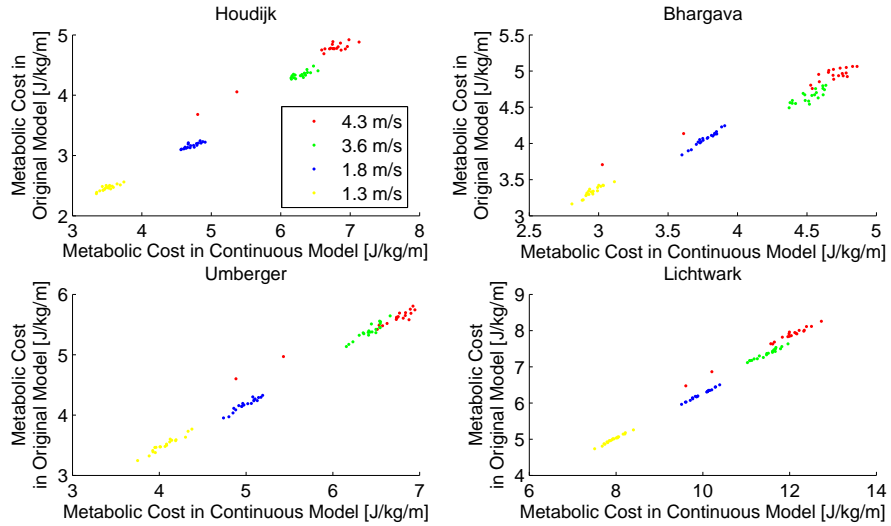


Figure 32: Correlation between the continuous and original metabolic energy model for twenty virtual subjects for two walking speeds and two running speeds.

Table VI: Correlation coefficients between the continuous and original versions of models Houdijk, Bhargava, Umberger, and Lichtwark.

Model	Correlation coefficient	RMS error	Slope
Houdijk	0.996	0.0838 J/kg/m	0.71
Bhargava	0.993	0.0708 J/kg/m	0.88
Umberger	0.997	0.0624 J/kg/m	0.80
Lichtwark	0.996	0.0963 J/kg/m	0.70

taken into account in the continuous versions. The high correlation coefficient indicated that the continuous model matched the original model very well. Therefore, the changes in the continuous model only had a small effect on the metabolic energy expenditure calculation and the models are suitable to solve a predictive gait simulation.

Predictive Simulation of a Single Joint Reaching Task

Next, predictive gait simulations minimizing metabolic rate were compared to a predictive simulation minimizing muscular effort. This comparison was performed on a simple problem to highlight the different trajectories found with these objectives. The differences in the optimal trajectory, metabolic rate, and muscle activation were studied.

An arm, rotating around a single joint, controlled by two muscles, performed a reaching

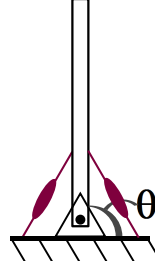


Figure 33: Sketch of the arm, operated by muscles.

Table VII: Overview of muscle parameters used.

Activation Time	T_{act}	0.012 s
Deactivation Time	T_{deact}	0.0476 s
Maximum Force	F_{max}	1100 N
Optimal Fiber Length	$l_{CE(OPT)}$	7 cm
SEE slack length	$l_{SEE(slack)}$	5 cm
PEE slack length	$l_{PEE(slack)}$	8.4 cm
SEE stiffness	K_{SEE}	$1.76 \cdot 10^8$ N/m ²
PEE stiffness	K_{PEE}	77 N/m ²
Muscle length	l_0	12 cm
Moment Arm	D	2 cm
% Fast Twitch Fibers	FT	45 %

task in the horizontal plane. The task was to move 90 degrees and back in five seconds.

Figure 33 shows the arm at $\theta = 90$ degrees. The two muscles were Hill-type muscles, with a contractile element with activation and contraction dynamics, a series elastic element, and a parallel elastic element, both modeled as nonlinear springs. Their properties were similar to muscle properties of a Brachialis [55] (see table VII).

The dynamics were formulated implicitly using state $x = [\theta \ \omega \ a_1 \ a_2 \ \tilde{l}_{CE(1)} \ \tilde{l}_{CE(2)}]^T$, and control input $u = [u_1 \ u_2]^T$ with angular velocity ω , activation a_j , stimulation u_j , and normalized fiber length $\tilde{l}_{CE(j)}$ for muscle j :

$$f(x(t), \dot{x}(t), u(t)) = 0 \quad (5.21)$$

where:

$$f(x(t), \dot{x}(t), u(t)) = \begin{bmatrix} \dot{\theta}(t) - \omega(t) \\ \frac{M(t)}{J} - \dot{\omega}(t) \\ \dot{a}_1(t) - (u_1(t) - a_1(t))(\frac{1}{T_{act}}(u_1(t) + 1) - \frac{1}{T_{deact}}) \\ \dot{a}_2(t) - (u_2(t) - a_2(t))(\frac{1}{T_{act}}(u_2(t) + 1) - \frac{1}{T_{deact}}) \\ F_{SEE(1)}(t) - F_{PEE(1)}(t) - F_{CE(1)}(t) + bv_{CE(1)}(t)F_{max} \\ F_{SEE(2)}(t) - F_{PEE(2)}(t) - F_{CE(2)}(t) + bv_{CE(2)}(t)F_{max} \end{bmatrix}, \quad (5.22)$$

$$\text{and: } F_{CE(j)}(t) = a_j(t)F_{max}f(l_{CE(j)}(t))g(v_{CE(j)}(t)) \quad (5.23)$$

where the torque is equal to the product of the force in the series elastic element and the moment arms, $M = DF_{SEE}$. T_{act} and T_{deact} are the activation and deactivation time constants of the muscle, $F_{PEE(j)}$ is the force in the parallel elastic element (PEE), $g(v_{CE(j)})$ the force-velocity relationship and b is a small damping term used to aid the optimization, equal to 0.001 s/m^2 . The SEE and the PEE are modeled as quadratic springs. The slack lengths and stiffnesses were given in table VII.

The following optimization problem was solved to find the optimal state and control trajectories, $x(t)$ and $u(t)$, to perform the reaching task over time T :

$$\underset{u(t)}{\text{minimize}} \quad J = \int_{t=0}^T c(x(t), u(t))dt \quad 0 \leq t \leq T \quad (5.24a)$$

$$\text{subject to: } f(x(t), \dot{x}(t), u(t)) = 0 \quad 0 \leq t \leq T \quad (5.24b)$$

$$\theta(0) = 0 \quad (5.24c)$$

$$\theta(T/2) = \frac{\pi}{2} \quad (5.24d)$$

$$\omega(0) = \omega(T/2) = 0 \quad (5.24e)$$

$$x(T) - x(0) = 0 \quad (5.24f)$$

The objective to minimize metabolic rate is as follows:

$$J(x(t), u(t)) = \frac{1}{Tm_{pend}} \sum_{j=1}^2 \int_{t=0}^T \dot{E}_j(t) m_{mus(j)} dt \quad (5.25)$$

where m_{pend} is the total mass of the pendulum, and $\dot{E}_j(t)$ is different for each model that was used.

The objective to minimize muscular effort is as follows:

$$J(x(t), u(t)) = \frac{1}{T} \int_{t=0}^T \sum_{j=1}^2 a_j(t)^2 dt \quad (5.26)$$

These optimal control problems were solved using direct collocation, with 200 collocation points and a backward Euler formulation. The average between the upper and lower bounds was used as initial guess for the states, while a very small stimulation, 10^{-4} was used as initial guess for the controls. The bounds for the angle were $\theta_{min} = -5\pi$, and $\theta_{max} = 6\pi$, for the angular velocity $\dot{\theta}_{min} = -1000$ rad/s, $\dot{\theta}_{max} = 1000$ rad/s was used. The bounds of the activation were 0 and 1, and the bounds of the normalized fiber length were 0 and 4. The problem minimizing metabolic rate was first solved using $\varepsilon = 10^{-2}$, and this solution was used as an initial guess for $\varepsilon = 10^{-3}$. IPOPT 3.11.0 [36] was used to solve the optimization problem.

Results

Figure 34 shows the reaching task that minimizes metabolic rate with model Umberger. The angle (top left figure) increases almost linearly from 0 degrees to 90 degrees, so the velocity is constant during most of the movement. This is due to the muscle stimulation (middle left figure), which is zero, except for a short burst around $t = 0$ s, $t = 2.5$ s and $t = 5$ s which were the motion changes direction. The metabolic rate was 0.38 W/kg with the continuous model, and 0.26 W/kg using the original metabolic model. The results

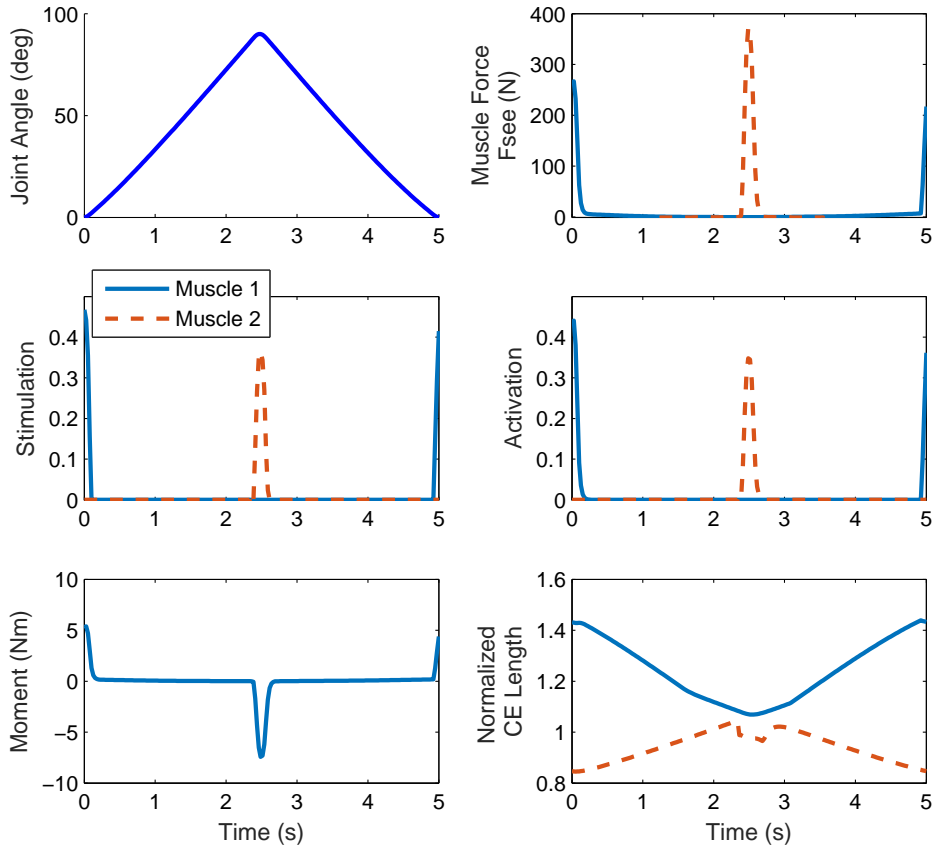


Figure 34: Optimal trajectory for the single arm reaching task, minimizing metabolic energy using model Umberger.

with model Bhargava, model Houdijk, and model Lichtwark were similar and are shown in appendix 7.2.

Figure 35 shows the optimal solution that was found when minimizing effort. In this solution, the trajectory of the angle (top left figure) is smoother because the muscles are active during the full task, though the peak activation was lower (see middle left figure). The metabolic rate in this movement was 0.74 W/kg using the original metabolic model.

Discussion

Trajectory optimization problems were solved successfully on a musculoskeletal dynamic

system with muscles. The metabolic energy solutions were highlighted by high muscle activations for shorter periods of time. This approach corresponds with the result of FitzHugh, who describes that when minimizing metabolic energy, the motor signal consists of three phases: maximal stimulation to accelerate the mass to the optimal velocity, an intermediate level to maintain the velocity and zero stimulation to have the mass slow down [56]. The reaching task yielded the same result, except that the intermediate level is equal to 0 due to the absence of friction and gravity, while activation of the other muscle is required to slow the arm down. Accelerating and decelerating the mass happen as fast as possible. This was verified by repeating the optimization using Umberger's model with 50 and 100 collocation points, since the acceleration is limited by the number of collocation points. With a smaller number of collocation points, the peak acceleration was reduced, which indicates an impulsive control strategy.

When minimizing effort, or the squared muscle activation, the highest activation was much lower, while the muscles were activated longer compared to a solution that minimizes metabolic rate. When the square of the muscle activation is minimized, larger activation levels are penalized more heavily and smaller activation levels over a longer time are favored. However, this increases the required metabolic energy.

For the predictive simulations, the difference between the metabolic cost reported by the original model and the continuous model was larger than in the regression comparison in section 5.3.1. There was a 30% difference for the reaching task. The fiber velocity was small in the simulations that minimize metabolic rate, since this minimizes muscle work and shortening-lengthening heat rate. Therefore, when the muscle is lengthening, the shortening velocity $\tilde{v}_{CE(S)}$ will make a significant contribution to the shortening-lengthening heat and vice versa (equations 5.13 and 5.14). Additionally, the muscle work w_{CE} is smaller due to the smaller velocities, meaning that the shortening-lengthening heat rate also has a larger contribution to the total energy rate. The effect was greater with a larger ε .

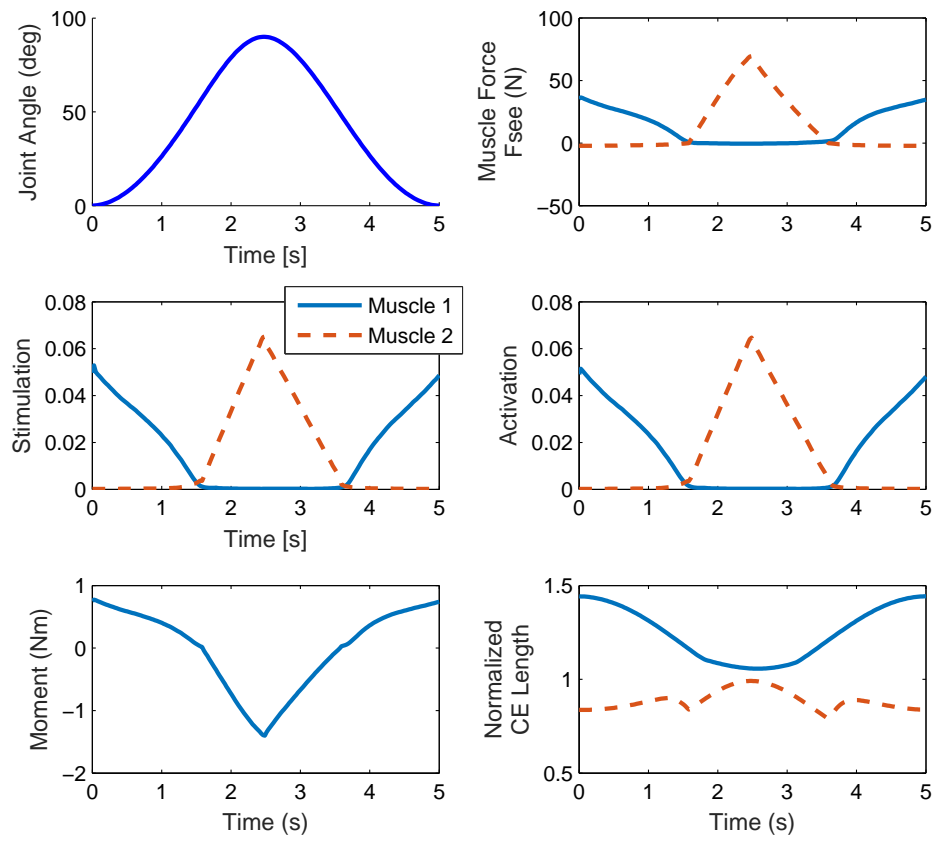


Figure 35: Optimal trajectory for the single arm reaching task, minimizing effort.

5.3.2 Predictive Simulation of Gait

Predictive gait simulations were solved from a random initial guess. The objective of minimizing metabolic energy was compared to the objective of minimizing effort. These simulations were performed using a sagittal plane musculoskeletal model with nine degrees of freedom: the position and orientation of the trunk, two hip angles, two knee angles, and two ankle angles. The multibody dynamics, muscle model, and ground contact model are described by Koelewijn and Van den Bogert [5] and chapter II.

Methods

The following optimal control problem was defined for a gait cycle of time T with speed $v = 1.325$ m/s:

$$\underset{u(t)}{\text{minimize}} \quad J = \frac{1}{TM} \sum_{j=1}^{16} \int_{t=0}^T \dot{E}_j(t) m_{mus(j)} dt \quad 0 \leq t \leq T, \quad (5.27a)$$

$$\text{subject to:} \quad f(x(t), \dot{x}(t), u(t)) = 0 \quad 0 \leq t \leq T, \quad (5.27b)$$

$$x_{sym}\left(\frac{T}{2}\right) - x(0) - \frac{1}{2}vTe_1 = 0, \quad (5.27c)$$

where equation 5.27c describes the periodicity constraint, and e_1 denotes a unit vector that describes which states should be displaced, such as the horizontal component of the trunk. Left/right symmetry was assumed, meaning that the states and controls of the left leg at time $T/2$ should be the same as the states and controls of the right side at time 0 and vice versa.

Three optimal control problems were solved for each metabolic energy model to find the solution from a random initial guess. First, a problem was solved with $\varepsilon = 10^{-2}$ and first-order regularization ($W_{reg} = 0.012$, see section 2.5.1). This problem was less nonlinear and therefore easier to solve from the random initial guess. The solution of this problem was used as an initial guess for a second problem, with less regularization ($W_{reg} = 1.2 \cdot 10^{-4}$). The solution of this problem was used as initial guess for the final optimal

control problem, with no regularization and $\varepsilon = 10^{-3}$. This process was repeated with twenty-five random initial guesses. The solution with the lowest objective was presented.

This solution is compared to a predictive simulation found with minimizing muscular effort, using the cost function described in equation 5.26. The same approach was used with the same two intermediate solutions with a regularization term, and twenty-five random initial guesses. Again, the solution with the lowest objective was used.

Direct collocation with 30 collocation points per half gait cycle was used to solve these problems, using IPOPT 3.11.0 [36]. More details on the solution method can be found in [4] and [8] and appendix 7.2.

Results

Twenty-five optimal control problems for gait were solved from random initial guesses when minimizing metabolic rate for each metabolic energy mode, and when minimizing muscular effort. The optimization minimizing metabolic rate took about 40 minutes for model Houdijk, 45 minutes for model Bhargava, and 90 minutes for model Lichtwark and model Umberger, while the optimization minimizing effort took about 10 minutes computer with an Intel Core i5-3210M CPU at 2.5 GHz clock speed.

Table VIII shows termination message of IPOPT, and the number of time this message was returned. 22 problems were solved with model Houdijk and model Bhargava. Both also had an infeasible problem once, and in model Houdijk an invalid number was detected twice, while in model Bhargava the restoration phase failed twice. Model Lichtwark solved all problems. Model Umberger solved three times, and the restoration phase failed for all other initial guesses. 24 of the problem solved successfully when minimizing effort, while an infeasible problem was detected once.

Table IX shows the metabolic rate of each optimal solution, minimizing metabolic cost or effort, calculated with the original version of all models. The solution with the second-lowest objective was reported for models Lichtwark, Bhargava, and Houdijk, since

Table VIII: Overview of termination messages by IPOPT

Objective	Optimal solution found	Infeasible problem	Restoration phase failed	Invalid number detected
Model Houdijk	22	1	0	2
Model Bhargava	22	1	2	0
Model Lichtwark	25	0	0	0
Model Umberger	3	0	22	0
Effort	24	1	0	0

Table IX: Metabolic rate in W/kg calculated by each model for the solutions with the lowest objectives. The bold number indicates the lowest metabolic rate for each row. The first row indicates that using (the original version of) model Houdijk, the predictive simulation found using model Lichtwark had a lower metabolic rate than the predictive simulation found with model Houdijk. It was expected that the lowest metabolic rate is found when the objective is the same as the model that was used.

Objective	Metabolic Rate Houdijk	Metabolic Rate Bhargava	Metabolic Rate Umberger	Metabolic Rate Lichtwark
Model Houdijk	1.24	1.60	1.60	2.33
Model Bhargava	1.30	1.59	1.68	2.46
Model Umberger	1.27	1.68	1.38	2.52
Model Lichtwark	1.20	1.63	1.57	1.91
Effort	1.83	2.49	2.44	3.54

inspection of the results showed that the solutions with the lowest objectives should be rejected. In this solution, the knee and ankle accelerated very quickly, which makes the solution inaccurate with the number of collocation points that was used. Therefore, the solutions with second-lowest objective were analyzed instead.

Table IX shows the metabolic rate calculated with the original version of each model, for each of the objective. The metabolic rate is lowest for the solution that was optimized with the continuous version of the same model, except for model Houdijk. The metabolic rate of model Lichtwark's solution was lower than model Houdijk's solution. For all solutions, the original version of model Lichtwark calculated a higher metabolic rate than the three other models. For example, the metabolic rate model Houdijk's solution is 1.24 W/kg with model Houdijk, but 2.33 W/kg with model Lichtwark, which is almost twice as high. Also, the objective of effort yielded the highest metabolic rate for all models, at least 1

W/kg higher.

Figure 36 shows joint angles, moments and muscle forces of the optimal solutions. The stance phase is highlighted on the horizontal axis. The shaded area shows normal walking data from Winter [57]. All solutions had a larger than normal first peak in the vertical ground reaction force, and the solution minimizing model Lichtwark and effort had a larger than normal peak negative horizontal ground reaction force as well. The hip angle was comparable to Winter's data for all solutions, the effort solution had a larger peak flexion angle, and model Lichtwark's solution a larger peak extension angle. All solutions found knee flexion during stance, thought it was higher than normal for the effort solution. Model Houdijk's solution did not reach a peak extension angle in late stance, and had a smaller peak flexion angle during swing. The effort solution does as well. Model Bhargava's and model Lichtwark's solution had a normal ankle angle, while the other solutions had a smaller than normal dorsiflexion angle in late stance, and the effort solution also had a larger than normal plantarflexion angle at push-off.

The hip moment of the simulations minimizing metabolic rate showed brief bursts, separated by periods where there was no moment at all. The values are within normal range. The result for the knee moment varies amongst solutions. The effort solution follows the normal data well. Model Lichtwark's and model Bhargava's solution had a larger and earlier peak extension moment during stance and a larger and earlier flexion moment during late stance, Model Umberger's solution also had a larger and earlier flexion moment during late stance, and had no peak extension moment during stance. Similarly, model Houdijk's solution did not have a peak knee extension moment during stance, and only a small knee extension moment during swing. The ankle moment was most similar to normal for model Lichtwark's solution, followed by model Bhargava's solution. All other solutions had an extra early plantarflexion peak in the stance phase. All solutions had a similar plantarflexion moment peak during push-off.

The muscle forces on the right side of figure 36 show that not all muscles are used in the

solutions that minimize metabolic rate. Model Houdijk's solution did not activate the Hamstrings, Vasti, and Gastrocnemius, while model Bhargava's and model Lichtwark's solution did not activate the Gluteals. Model Lichtwark's solution also only has a small activation in the Rectus Femoris muscle. Model Umberger's solution did not use the Hamstrings and Vasti. The Soleus is activated in the solutions of model Houdijk, model Umberger, and the effort solution to generate the extra peak plantarflexion moment in the ankle.

Discussion

The goal of this work was to compare a predictive simulation minimizing metabolic rate, solved from a random initial guess, to a predictive simulation minimizing effort. Predictive simulations were solved successfully using four different metabolic energy expenditure models and by minimizing squared activation, which represents effort. The solutions minimizing metabolic rate had more realistic joint angles and did not use all muscles, while the solution minimizing effort had more realistic joint moments, especially in the knee and hip, and used all muscles. The metabolic rate was lower than expected for all solution, but more realistic when effort was minimized compared instead of metabolic rate, which is similar to Miller et al. [22]. Cost due to arm swing and resting metabolic rate was disregarded, so the cost is expected to be somewhat lower than normal (4.0-4.3 W/kg, see [18]). Possibly, the metabolic rate is lower than in experiments due to the idealized dynamics and control, as well as the fact that a sagittal plane model with only eight muscles was used.

The joint moments in the solutions that minimize metabolic rate solution were characterized by periods of muscle activation, and thus joint moments, and passive periods where there is no joint moments. This approach corresponds with the result of FitzHugh [56] and the results in section 5.3.1. This human model was more complex than the simple model used by FitzHugh, but a similar pattern is seen in the hip, where there is a moment only when an acceleration is required to change the direction of the velocity.

The smaller range of motion in the ankle seen in this work was also reported by Miller

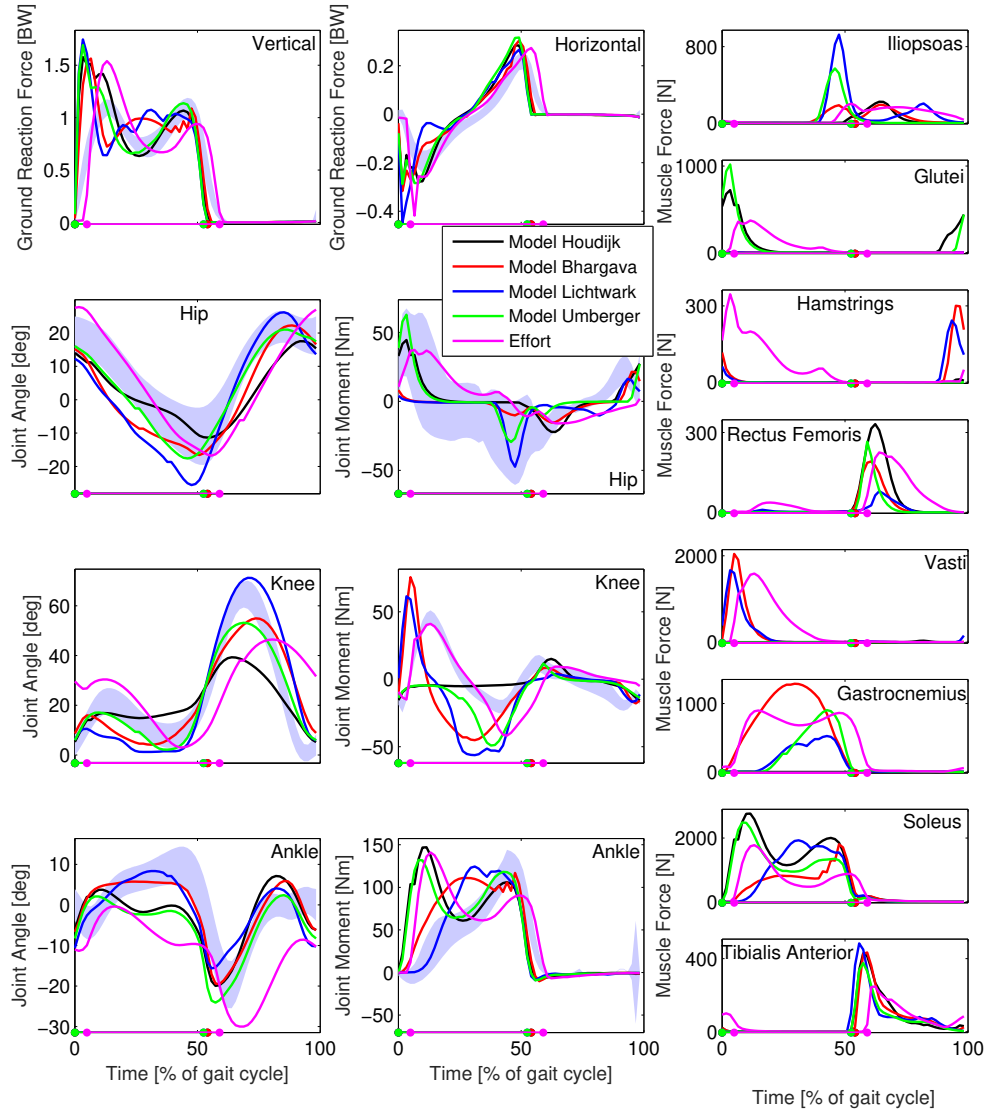


Figure 36: Joint angles (flexion/dorsiflexion positive), joint moments (extension/plantarflexion positive), and muscle forces for predictive gait simulations that minimize metabolic energy expenditure (red, dash) and effort (black, solid). The shaded area shows data from Winter [57]. The stance phase of both solutions is highlighted on the horizontal axis (crosses for minimum-energy solution and dots for minimum-effort solution).

[23], who minimized metabolic energy using a tracking solution as initial guess. Contrary to Miller's study, in this work the model was able to predict knee flexion in early stance [23].

Another reason for the joint moment and muscle force pattern, as well as the smaller ankle range of motion could be the lack of uncertainty in this model, similar to the reaching task. A walking motion with zero joint moments is unstable and hard to control in practice, and therefore will not be optimal when uncertainty is taken into account. However, a zero moment is optimal if stability is not an issue, since this requires no muscle activation. The lack of uncertainty also explains the smaller ankle range of motion. The smaller ankle range of motion was due to the model standing on the toe early in stance, which is unstable as well.

Several muscles (Hamstrings, Vasti and Gastrocnemius) were not used in the solutions that minimize metabolic rate. A reason for this is that the metabolic energy models are normalized to muscle mass. Therefore, the objective of the optimization is proportional to the weight of the muscles, which means that it is optimal to avoid a muscle with a high mass. The unrealistic joint force patterns might also be improved by taking into account uncertainty in the environment, since this would yield more realistic joint moments and thus more work from the muscles.

The solution that minimized effort found large knee flexion in the stance phase, similar to Ackermann and Van den Bogert [4]. A possible reason is that activation is minimized. To reduce the required activation, the largest muscle, the quadriceps, is recruited, and used at optimal fiber length, which is achieved at larger knee flexion. This is also shown in figure 36, where the force in the Vasti is largest for the minimal effort solution.

Table IX showed that the metabolic rate of model Lichtwark's solution was lower than the metabolic rate of model Houdijk's solution, when using model Houdijk to calculate the metabolic rate. However, the metabolic rate was calculated with the original versions of the models. When calculating the metabolic rate with the continuous model that was used as

an objective, the metabolic rate of model Houdijk's solution was lower than the metabolic rate of model Lichtwark's solution.

This study was performed by modeling one representative subject. It is not expected that the use of a model with a different weight and height will change the results, since the results were not realistic enough that it would be possible to differentiate between different walking patterns. If a more realistic walking solution is found, future studies could aim to identify differences in walking style based on a person's body type, or due to age-related changes, for example.

Five solutions with the lowest objectives were analyzed for each objective, and are presented in appendix 7.2. Note that only three are plotted for model Umberger, since only three problems were solved successfully. The gaits found by minimizing metabolic rate were consistent, except for the discarded solutions of model Bhargava, model Houdijk, and model Lichtwark. This implies that the reported result is similar to the global minimum of the problem. When minimizing effort, the five gaits with the lowest objective were dissimilar, which means that the global minimum is hard to find, and might not be found yet.

After comparing the solutions minimizing metabolic rate to the solution minimizing effort, it cannot yet be concluded that either effort or metabolic rate is the objective that humans use to choose their gait. It is likely that other variables play an important role that are currently not accounted for, such as uncertainty in the environment. Also, none of the models that were used to determine metabolic rate performed better than the other models. Model Lichtwark found the most realistic ankle moment, while model Umberger found the most realistic knee motion, but often did not solve successfully, model Bhargava found the most realistic ankle motion, and model Houdijk was the fastest.

5.4 Conclusion

The aims of this chapter were to find which metabolic energy model was best able to predict metabolic cost of walking, to use this model to solve a predictive gait simulation from a random initial guess, and to compare this solution to a predictive simulation that minimized effort. It was found that model Bhargava and model Lichtwark correlated best with the experimental metabolic cost data, while model Houdijk correlates only slightly worse. These models, as well as model Umberger were then used to solve a predictive gait simulation minimizing metabolic rate. Compared to minimizing effort, minimizing metabolic rate yielded more realistic joint angles, but less realistic joint moments and muscle forces, since several muscles were not used at all. In future work, other objectives, such as stability, should be taken into account to make simulations more realistic.

5.5 References

- [1] LJ Bhargava, MG Pandy, and FC Anderson. A phenomenological model for estimating metabolic energy consumption in muscle contraction. *Journal of Biomechanics*, 37(1):81–88, 2004.
- [2] GA Lichtwark and AM Wilson. A modified Hill muscle model that predicts muscle power output and efficiency during sinusoidal length changes. *Journal of Experimental Biology*, 208(15):2831–2843, 2005.
- [3] R Margaria. Positive and negative work performances and their efficiencies in human locomotion. *Internationale Zeitschrift für angewandte Physiologie einschließlich Arbeitsphysiologie*, 25(4):339–351, 1968.
- [4] M Ackermann and AJ van den Bogert. Optimality principles for model-based prediction of human gait. *Journal of Biomechanics*, 43(6):1055–1060, 2010.
- [5] AD Koelewijn and AJ van den Bogert. Joint contact forces can be reduced by improv-

- ing joint moment symmetry in below-knee amputee gait simulations. *Gait & Posture*, 49:219–225, 2016.
- [6] CL Dembia, A Silder, TK Uchida, JL Hicks, and SL Delp. Simulating ideal assistive devices to reduce the metabolic cost of walking with heavy loads. *PloS one*, 12(7): e0180320, 2017.
- [7] DJJ Bregman, MM Van der Krog, V De Groot, J Harlaar, M Wisse, and SH Collins. The effect of ankle foot orthosis stiffness on the energy cost of walking: a simulation study. *Clinical Biomechanics*, 26(9):955–961, 2011.
- [8] AJ van den Bogert, M Hupperets, H Schlarb, and B Krabbe. Predictive musculoskeletal simulation using optimal control: effects of added limb mass on energy cost and kinematics of walking and running. *Proceedings of the Institution of Mechanical Engineers, Part P: Journal of Sports Engineering and Technology*, pages 1–11, 2012.
- [9] TW Dorn, JM Wang, JL Hicks, and SL Delp. Predictive simulation generates human adaptations during loaded and inclined walking. *PloS one*, 10(4):e0121407, 2015.
- [10] RH Miller, SCE Brandon, and KJ Deluzio. Predicting sagittal plane biomechanics that minimize the axial knee joint contact force during walking. *Journal of Biomechanical Engineering*, 135(1):011007, 2013.
- [11] Y-C Lin and MG Pandy. Three-dimensional data-tracking dynamic optimization simulations of human locomotion generated by direct collocation. *Journal of Biomechanics*, 59:1–8, 2017.
- [12] HJ Ralston. Energy-speed relation and optimal speed during level walking. *Internationale Zeitschrift für Angewandte Physiologie Einschliesslich Arbeitsphysiologie*, 17(4):277–283, 1958.

- [13] MY Zarrugh, FN Todd, and HJ Ralston. Optimization of energy expenditure during level walking. *European Journal of Applied Physiology and Occupational Physiology*, 33(4):293–306, 1974.
- [14] JM Donelan, R Kram, and AD Kuo. Mechanical and metabolic determinants of the preferred step width in human walking. *Proceedings of the Royal Society of London B: Biological Sciences*, 268(1480):1985–1992, 2001.
- [15] JD Ortega and CT Farley. Minimizing center of mass vertical movement increases metabolic cost in walking. *Journal of Applied Physiology*, 99(6):2099–2107, 2005.
- [16] KE Gordon, DP Ferris, and AD Kuo. Metabolic and mechanical energy costs of reducing vertical center of mass movement during gait. *Archives of Physical Medicine and Rehabilitation*, 90(1):136–144, 2009.
- [17] GP Kenny, SR Notley, and D Gagnon. Direct calorimetry: a brief historical review of its use in the study of human metabolism and thermoregulation. *European Journal of Applied Physiology*, 117(9):1765–1785, 2017.
- [18] BR Umberger, KGM Gerritsen, and PE Martin. A model of human muscle energy expenditure. *Computer Methods in Biomechanics and Biomedical Engineering*, 6(2):99–111, 2003.
- [19] H Houdijk, MF Bobbert, and A De Haan. Evaluation of a Hill based muscle model for the energy cost and efficiency of muscular contraction. *Journal of Biomechanics*, 39(3):536–543, 2006.
- [20] FC Anderson and MG Pandy. Dynamic optimization of human walking. *Journal of Biomechanical Engineering*, 123(5):381–390, 2001.
- [21] WI Sellers, GM Cain, W Wang, and RH Crompton. Stride lengths, speed and energy costs in walking of australopithecus afarensis: using evolutionary robotics to predict

- locomotion of early human ancestors. *Journal of the Royal Society Interface*, 2(5):431–441, 2005.
- [22] RH Miller, BR Umberger, J Hamill, and GE Caldwell. Evaluation of the minimum energy hypothesis and other potential optimality criteria for human running. *Proceedings of the Royal Society of London B: Biological Sciences*, pages 1498–1505, 2011.
- [23] RH Miller. A comparison of muscle energy models for simulating human walking in three dimensions. *Journal of Biomechanics*, 47(6):1373–1381, 2014.
- [24] HE Huxley. The double array of filaments in cross-striated muscle. *The Journal of Biophysical and Biochemical Cytology*, 3(5):631–648, 1957.
- [25] MB Propp. A model of muscle contraction based upon component studies. *Lectures on Mathematics in the Life Sciences*, 16:61–119, 1986.
- [26] JM Winters. Hill-based muscle models: a systems engineering perspective. In *Multiple Muscle Systems*, pages 69–93. Springer, 1990.
- [27] AE Minetti and RMcN Alexander. A theory of metabolic costs for bipedal gaits. *Journal of Theoretical Biology*, 186(4):467–476, 1997.
- [28] JH Kim and D Roberts. A joint-space numerical model of metabolic energy expenditure for human multibody dynamic system. *International Journal for Numerical Methods in Biomedical Engineering*, 31(9), 2015.
- [29] TK Uchida, JL Hicks, CL Dembia, and SL Delp. Stretching your energetic budget: how tendon compliance affects the metabolic cost of running. *PloS one*, 11(3):e0150378, 2016.
- [30] AN Lay, CJ Hass, TR Nichols, and RJ Gregor. The effects of sloped surfaces on

- locomotion: an electromyographic analysis. *Journal of Biomechanics*, 40(6):1276–1285, 2007.
- [31] NT Pickle, AM Grabowski, AG Auyang, and AK Silverman. The functional roles of muscles during sloped walking. *Journal of Biomechanics*, 49(14):3244–3251, 2016.
- [32] R Margaria. *Biomechanics and Energetics of muscular exercise*. Oxford University Press, USA, 1976.
- [33] AJ van den Bogert and JJ De Koning. On optimal filtering for inverse dynamics analysis. In *Proceedings of the IXth biennial conference of the Canadian society for Biomechanics*, pages 214–215. Simon Fraser University Vancouver, 1996.
- [34] DA Winter. *Biomechanics and motor control of human movement*. John Wiley & Sons, 2005.
- [35] F de Groote, AL Kinney, AV Rao, and BJ Fregly. Evaluation of direct collocation optimal control problem formulations for solving the muscle redundancy problem. *Annals of Biomedical Engineering*, 44(10):2922–2936, 2016.
- [36] A Wächter and LT Biegler. On the implementation of an interior-point filter line-search algorithm for large-scale nonlinear programming. *Mathematical Programming*, 106(1):25–57, 2006.
- [37] JB de V Weir. New methods for calculating metabolic rate with special reference to protein metabolism. *The Journal of Physiology*, 109(1-2):1–9, 1949.
- [38] JZ Bakdash and LR Marusich. Repeated measures correlation. *Frontiers in Psychology*, 8, 2017.
- [39] BR Umberger. Effects of suppressing arm swing on kinematics, kinetics, and energetics of human walking. *Journal of Biomechanics*, 41(11):2575–2580, 2008.

- [40] JL Hicks, TK Uchida, A Seth, A Rajagopal, and SL Delp. Is my model good enough? best practices for verification and validation of musculoskeletal models and simulations of movement. *Journal of Biomechanical Engineering*, 137(2):020905, 2015.
- [41] S Kimel-Naor, A Gottlieb, and M Plotnik. The effect of uphill and downhill walking on gait parameters: A self-paced treadmill study. *Journal of Biomechanics*, 60:142–149, 2017.
- [42] N Alexander and H Schwameder. Effect of sloped walking on lower limb muscle forces. *Gait & Posture*, 47:62–67, 2016.
- [43] BR Umberger. Stance and swing phase costs in human walking. *Journal of the Royal Society Interface*, 7(50):1329–1340, 2010.
- [44] RD Crowninshield and RA Brand. A physiologically based criterion of muscle force prediction in locomotion. *Journal of Biomechanics*, 14(11):793–801, 1981.
- [45] SL Delp, FC Anderson, AS Arnold, P Loan, A Habib, CT John, E Guendelman, and DG Thelen. OpenSim: open-source software to create and analyze dynamic simulations of movement. *IEEE Transactions on Biomedical Engineering*, 54(11):1940–1950, 2007.
- [46] A Nagano, BR Umberger, MW Marzke, and KGM Gerritsen. Neuromusculoskeletal computer modeling and simulation of upright, straight-legged, bipedal locomotion of Australopithecus afarensis (al 288-1). *American Journal of Physical Anthropology*, 126(1):2–13, 2005.
- [47] BR Umberger, KGM Gerritsen, and PE Martin. Muscle fiber type effects on energetically optimal cadences in cycling. *Journal of Biomechanics*, 39(8):1472–1479, 2006.

- [48] M Ackermann and W Schiehlen. Dynamic analysis of human gait disorder and metabolical cost estimation. *Archive of Applied Mechanics*, 75(10-12):569–594, 2006.
- [49] NP Fey, GK Klute, and RR Neptune. Optimization of prosthetic foot stiffness to reduce metabolic cost and intact knee loading during below-knee amputee walking: a theoretical study. *Journal of Biomechanical Engineering*, 134(11):111005, 2012.
- [50] MS Shourijeh and J McPhee. Forward dynamic optimization of human gait simulations: a global parameterization approach. *Journal of Computational and Nonlinear Dynamics*, 9(3):031018, 2014.
- [51] HPJ Buschman, G Elzinga, and RC Woledge. Energetics of shortening depend on stimulation frequency in single muscle fibres from *xenopus laevis* at 20C. *Pflügers Archiv*, 430(2):160–167, 1995.
- [52] HPJ Buschman, G Elzinga, and RC Woledge. The effects of the level of activation and shortening velocity on energy output in type 3 muscle fibres from *xenopus laevis*. *Pflügers Archiv*, 433(1-2):153–159, 1996.
- [53] HPJ Buschman, M Linari, G Elzinga, and RC Woledge. Mechanical and energy characteristics during shortening in isolated type-1 muscle fibres from *xenopus laevis* studied at maximal and submaximal activation. *Pflügers Archiv*, 435(1):145–150, 1997.
- [54] GA Lichtwark and AM Wilson. Is achilles tendon compliance optimised for maximum muscle efficiency during locomotion? *Journal of Biomechanics*, 40(8):1768–1775, 2007.
- [55] MDK Breteler, CW Spoor, and FCT Van der Helm. Measuring muscle and joint geometry parameters of a shoulder for modeling purposes. *Journal of Biomechanics*, 32(11):1191–1197, 1999.

- [56] R FitzHugh. A model of optimal voluntary muscular control. *Journal of Mathematical Biology*, 4(3):203–236, 1977.
- [57] DA Winter. *Biomechanics and motor control of human gait: normal, elderly and pathological*. University of Waterloo Press, 2 edition, 1991.

CHAPTER VI

PREDICTIVE SIMULATIONS IN A STOCHASTIC ENVIRONMENT

The aim of this chapter was to take into account uncertainty in the dynamics to further investigate co-contraction of muscles. An approach to solving predictive simulations in a stochastic environment was proposed and used to solve trajectory optimization problems. This method optimized several episodes of the same task in a stochastic environment, instead of the standard approach in trajectory optimization, which is to optimize a single episode in a deterministic environment. The optimization found feedforward and feedback control simultaneously. This method was verified on a classic pendulum swing-up problem, where it was shown that a different trajectory is optimal in a stochastic environment than in a deterministic environment. It was also shown that for certain tasks, co-contraction in addition to feedback control was more energy efficient than using only feedback control. Then, it was shown that non-zero foot clearance is optimal in a stochastic environment, and that the amount of foot clearance increases with the noise amplitude. Finally, the method was applied to gait of persons with a transtibial amputation. The results indicated that co-contraction of the thigh muscles minimizes muscular effort in a stochastic environment on the prosthesis side in gait of persons with a transtibial amputation, but this result might be affected by the controller design.

Statement of Contribution

This is the first work that incorporated environmental uncertainty in predictive gait simulations. A method is proposed to solve predictive gait simulations in a stochastic environment and applied to several problems. In certain tasks, co-contraction is optimal in terms of effort in a stochastic environment, despite literature often describing co-contraction as inefficient with respect to energy [1, 2]. It was also shown on a human model with torque control that non-zero foot clearance minimizes effort in a stochastic environment. Finally, the method was attempted to see if persons with a transtibial amputation have larger muscle activation on the prosthesis side in the thigh due to uncertainty in the environment..

Publications:

Koelewijn, A., Richter, H. and Van den Bogert, A. J. (2018). A Novel Approach to Find Predictive Gait Simulations in a Stochastic Environment. In preparation.

Conference Presentations:

- Koelewijn, A. and Van den Bogert, A. J. (2017). Predictive simulations of gait predict larger foot clearance in a stochastic environment. Proceedings of the ASME 2017 IDETC & CIE Conference, Cleveland (OH).
- Koelewijn, A., and Van den Bogert, A. J. (2017). Better safe than sorry: stochastic optimal-control of gait predicts larger foot clearance. Dynamic Walking, Mariehamn (Finland)
- Koelewijn, A., and Van den Bogert, A. J. (2016). A Novel Approach to Solve Predictive Simulations in a Stochastic Environment. BANCOM, Mt Sterling (OH).
- Koelewijn, A., Richter, H., and Van den Bogert, A. J. (2016). Trajectory Optimization in Stochastic Multibody Systems using Direct Collocation. Fourth International Conference on Multibody System Dynamics, Montreal (QC).

6.1 Introduction

Predictive simulations have been used to show the effect of interventions on gait [3–8]. However, they fail to predict several key patterns of human gait [9], and data tracking is often used to improve predictions (e.g. [6]). Examples of key patterns that were not predicted are found in this dissertation. Most importantly, in chapter III the simulations failed to predict increased activation of the muscles of the thigh, which is observed in studies of TTA gait [10, 11]. Also, the predictions in chapter III predict zero ground clearance in the swing phase of the gait cycle, while humans typically have a ground clearance of 1.29 cm [12]. Predictive simulations using the three-dimensional model did not predict activation of the plantarflexors and thus zero moment during early stance and midstance (see chapter IV). Finally, in chapter V, the predictive simulations that minimize only metabolic cost found a gait cycle with zero joint moments in the stance phase.

These observations may be connected to environmental uncertainty. All previous predictive simulations were found without accounting for the uncertainty in the environment. However, a gait cycle with zero joint moments will be hard to control in a stochastic environment. Similarly, zero ground clearance of the feet is not optimal because the feet will scuff and the person might trip when the ground is uneven. The increased activation in the thigh muscles is suspected to be related to the loss of control and sensory feedback in the prosthetic leg and the imperfect connection between the prosthesis and the residual leg. Therefore, predictive simulations might be improved if the uncertainty could be taken into account.

Generally, it is assumed that humans optimize a certain cost function, for example to minimize energy cost, when they choose their gait. However, predictive simulations do not take into account uncertainty in the environment, while several studies have shown that uncertainty is important when choosing movement patterns [13–15]. It seems that predictive simulations could be improved if an objective of energy minimization was used while uncertainty was taken into account.

An example of the importance of uncertainty is work by Hiley and Yeadon in gymnastics [13]. They aimed to predict the upstart motion, a specific move in gymnastics. Early attempts aimed to minimize joint torque, but this criteria could not explain the motion that was performed by the gymnasts [16, 17]. However, Hiley and Yeadon optimized the rate of success for an upstart assuming some random variability in the neural control. This approach yielded a technique close to the gymnast's technique, much closer than other objectives that did not account for variability [13].

Kim and Collins [14] also show that external variability is taken into account when choosing a gait strategy. They found that metabolic cost and step width variability decreased using a prosthesis with a stabilizing controller compared to a neutral controller and a destabilizing controller. This means that if stability is increased, it is possible to choose a strategy that is less safe but more energy efficient. This study used healthy subjects with a simulated transtibial amputation.

Donelan et al. [15] showed the importance of variability on gait as well. They showed that healthy subjects require less metabolic energy and prefer a smaller step width when there is external lateral stabilization at the hip. The smaller step width indicates that a different gait pattern, which is harder to control, is chosen in an environment where less lateral stabilization is required. The lower metabolic energy cost indicates that this strategy is more energy efficient.

We would like to include uncertainty into predictive simulations, specifically to improve predictions of TTA gait. As said, currently simulations do not predict increased activation in the thigh muscles, where co-contraction is used to stiffen the knee joint. We suspect that this is an optimal strategy, since it is more energy efficient to anticipate any perturbations by increasing the stiffness of the knee than to react to them.

6.1.1 Co-contraction of muscles

Co-contraction is an important concept when talking about movement under variability. It is a feedforward approach to human movement control and is often described as inefficient [1, 2], because it does not produce any useful work while it requires energy [18]. This section will introduce the concept of co-contraction and highlight research that was done into this concept.

Muscles can only pull in one direction. Therefore, multiple muscles are required to control a joint. For example, at least two muscles are required in case of a revolute joint: one to flex the joint and one to extend it. In practice, all joints have more muscles than required to operate them. Therefore, it is impossible to know how much force is in a muscle based solely based on the joint moment that is exerted, because different muscles can be used to generate the same torque.

When a moment is acting on a joint, the muscles can be split up into two categories. The agonist muscles are the muscles that work in the direction of the moment, while the antagonist muscles work in the opposite direction. Co-contraction is the simultaneous activation of different muscles to create the moment. This can happen between several agonist muscles, but also between an agonist and antagonist muscle.

The forces in the muscles can be found by measuring electromyography (EMG) signals, or they can be predicted by solving an optimization problem. Crowninshield and Brand [19] suggested the following objective, based on endurance of the muscle:

$$J = \sum_{i=1}^{N_{mus}} \left(\frac{F_i}{PCSA_i} \right)^n \quad (6.1)$$

where n is an integer power, and $PCSA$ is the physiological cross-sectional area of the muscle, the area perpendicular to the muscle fibers. Initially, due to limited computer power, the power was chosen equal to 1. The solution of this problem is that only the muscle with the largest $PCSA$ is used until its maximum activation, after which the muscle

with the second largest *PCSA* is used, and so on, until the required torque is generated. However, verification with EMG showed soon that this is not how muscles in the body work (e.g. [20]).

A more realistic solution is found with a higher n [19]. Starting from $n = 2$, the objective will favor agonistic co-contraction, where two muscles that operate in the direction of the moment work together to generate the required force at lower activation levels [20]. A similar objective is used to minimize effort in our predictive simulations (see chapters III and IV). At even larger powers, the objective approaches the so-called min-max approach, which means that the maximum stress in all muscles is minimized, to have an as equal as possible stress distribution between the different muscles.

However, one problem of this objective is that it will never predict co-contraction between an agonistic and an antagonistic muscle in a simple one-joint system [21]. This form of co-contraction will increase joint stiffness and stability [18]. However, when an objective of endurance is used, it is not optimal, because an even larger activation of the agonist muscle is required when the antagonist muscle is activated. However, this type of co-contraction is often observed in human movements (e.g. [19]). From now on, co-contraction will refer to this type of co-contraction, with a pair of agonistic and antagonistic muscles.

Co-contraction might be necessary when a bi-articular muscle is activated, a muscle that spans multiple joints, since a torque is required around one joint, but not around the other. Then, an opposite activation is required around the second joint to keep the complete system stable. Also, since the muscles operate a multibody system, a muscle can affect a joint it does not span. Therefore, it was thought that co-contraction around one joint might have a favorable effect on another joint [22].

However, this assumption could not explain all co-contraction that is observed in EMG measurements. Hogan [18] showed that humans can use co-contraction to control the stiffness of the joint, and thus the stability. To show this, he solved an optimization problem

where the goal was to minimize energy while remaining in the desired position in a stochastic environment. The problem was solved without noise first, after which the stochastic problem was solved by linearizing around the solution in the deterministic environment. He proposed that co-contraction is required because the time-delay in the nervous system does not allow a human to rely solely on feedback control, and therefore a combination of feedback, which is energy efficient, and co-contraction is required [18].

Other studies also showed that co-contraction increased stability of the joint [23, 24], and reduced the effect of internal noise and increased movement accuracy [25]. Then, several studies attempted to improve the objective that was proposed by Crowninshield and Brand to be able to predict co-contraction. Raikova proposed to use negative coefficients, instead of $PCSA_i$ in the objective function. However, that violates the underlying assumption that endurance is minimized with this objective. Several other studies added a second objective to represent stability, which could be just a parameter [26], or an equation based on entropy, interpreted as similarity of forces between the muscles [24], or using the second derivative of the potential energy [27]. The weighting between the two objectives was determined based on the load magnitude, the joint angle, skill level, and muscle states, for example [24].

As said before, stability is not accounted for in predictive simulations. Adding an objective related to stability as was done in previous work creates a conflict with the objective of minimizing endurance or energy expenditure. We suspect that co-contraction is already optimal with respect to energy expenditure alone, and that stability emerges from minimizing effort only and does not need to be specified. Therefore, we would like to find an approach that can account for environmental uncertainty in the predictive simulation without changing the objective, to show that co-contraction is the most efficient control strategy for the human under uncertain conditions.

6.1.2 Trajectory Optimization in a Stochastic Environment

Optimal feedback control has been found in stochastic systems using linear quadratic Gaussian (LQG) control. This approach requires a linear system, with a performance criteria that is globally quadratic, and additive noise [28]. However, human walking is nonlinear, and its performance criteria is not necessarily globally quadratic (see chapter V), and noise may be signal dependent [28]. Therefore, a different approach is required.

Trajectory optimization problems in a stochastic environment require solving of stochastic differential equations, or the stochastic Hamilton-Jacobi-Bellmann equation, which are difficult to solve and become intractable for high dimensions [29]. Solution methods exist for problems where the control input is linear and additive to the dynamics [29, 30]. However, for human gait with a musculoskeletal model, the control input is not linear and additive to the dynamics. Additionally, due to the high the number of states in a human model, it is computationally expensive to solve the problem in a stochastic environment. Therefore, stochasticity in the system is usually ignored and the problem is solved in a deterministic environment [30].

Several methods were proposed to estimate the solution of trajectory optimization problem in stochastic environments. The most commonly used approach is the Monte Carlo method [31–33]. In this method, a large number of forward simulations are performed, where the uncertain variables are sampled from their distribution. Using the solution of each of the forward simulations, a distribution of the outcome variables is provided. This method is rather costly, since it requires a large number of simulations to obtain an accurate solution [32].

Another approach is based on the theory of generalized polynomial chaos (gPC), which was introduced by Wiener [34]. gPC states that a second order stochastic process can be approximated by a combination of stochastic basis functions, which are different based on the type of noise that is used. These approximations can be used to solve the problem with the stochastic Galerkin method or with stochastic collocation [31, 32] and is much faster than

the Monte Carlo approach [35]. Similar to the Monte Carlo approach, stochastic collocation takes advantage of sampling and solves the problem for different noise samples [31]. The approach combining gPC with stochastic collocation has been used to optimize collision-free plane trajectories under uncertain wind conditions [33], and to solve a design problem of a vehicle suspension system [36].

6.1.3 Goal of this Work

This chapter proposes an approach to solving predictive simulations of gait in a stochastic environment and show that optimal trajectories of human movements are affected by the stochastic environment. The method that is proposed in this chapter can be seen as using a Monte Carlo approach within direct collocation, or gPC with basis functions of the first order, solved using stochastic collocation.

This method is applied first to a classic one degree of freedom pendulum swing-up problem to show that this method can successfully predict the effect of a stochastic environment. Then, it is applied to a pendulum operated by muscles to show that for certain tasks in a stochastic environment co-contraction minimizes effort in a stochastic environment. Next, it will be applied to a torque-driven able-bodied model to show that non-zero foot clearance is optimal in a stochastic environment. Finally, the method will be applied to TTA gait using a musculoskeletal model, to investigate if co-contraction of the thigh muscles is optimal in terms of energy in a stochastic environment.

6.2 Proposed Method for Predictive Simulations in a Stochastic Environment

Conventional predictive simulation methods find a set of open-loop control inputs that optimize a single episode of the trajectory. Chapter II describes the set up of such a problem. In a stochastic environment, the dynamics are also dependent on noise, ε :

$$\dot{x}(t) = f(x(t), u(t), \varepsilon(t)) \quad (6.2)$$

where $x(t)$ is the state of the system and $u(t)$ the input.

The path will deviate from the desired path due to noise, so the trajectory will be different for each noise sample if the same open-loop control is used. This will also cause the objective of the trajectory to be different each noise sample, meaning that the optimal solution for one episode might not be the optimal solution for another episode with a different noise sample.

Theoretically, an optimal trajectory in the stochastic environment can be found using an infinite number of episodes, since then it is possible to account for all possible noise samples. However, this would be computationally intractable. Therefore, we propose to solve the trajectory optimization problem in a stochastic environment by optimizing over a finite number of episodes of the trajectory. The number of episodes should be large enough to correctly approximate the theoretical optimal objective. Each episode should have the same open-loop inputs and the same closed-loop control parameters, while the closed-loop control can vary with the state. The expected value of the objective is approximated using the average over the episodes.

The trajectory optimization problem is solved using a collocation method (see chapter II). Therefore, the optimization is performed over the states over all collocation points and episodes, and controls of all collocation points: $X = [x_1(1) \dots x_1(N) \dots x_{N_s}(1) \dots x_{N_s}(N) u_0(1) \dots u_0(N) K]^T$, where $[u_0(1) \dots u_0(N)]^T$ are the open-loop inputs and K represents the parameters of the closed-loop control. N is the number of collocation points, and N_s

the number of episodes. This yields the following problem formulation:

$$\underset{X}{\text{minimize}} \quad \frac{1}{N_s} \sum_{j=1}^{N_s} J([x_j(1) \dots x_j(N), u_0(1) \dots u_0(N), K]) \quad (6.3)$$

$$\text{subject to:} \quad \dot{x}_j(n) = f(x_j(n), u_j(n), \varepsilon_j(n)) \quad \begin{matrix} \forall n \in 1 \dots N, \\ j \in 1 \dots N_s \end{matrix} \quad (6.4)$$

$$g_h(x_j(k), u_j(k)) = 0 \quad \forall h \in 1 \dots N_g \quad (6.5)$$

$$\text{with} \quad u_j(n) = u_0(n) + Kx_j(n) \quad (6.6)$$

$$\varepsilon_j(n) \sim N(0, \sigma^2) \quad (6.7)$$

where n denotes the collocation point, j denotes the episode, h indicates the task constraint and N_g the number of task constraints. The objective of the problem is described in equation 6.3, which is averaged over all episodes. Equation 6.4 represents the dynamics constraints, which should be met for all collocation point and all episodes. Noise will be added at each collocation point. Equation 6.5 represents the task constraints, which are applied at collocation point k , usually at the initial and final state. Equation 6.6 denotes the feedback law, with a proportional and a derivative feedback gain.

Note that the control law is written differently from normal. Usually $u(t) = u_{ff}(t) + K(x(t) - x_{des}(t))$ is used, where u_{ff} is the feedforward control and x_{des} the desired state. Instead, u_0 is used, which is equal to $u_0(t) = u_{ff}(t) - Kx_{des}(t)$. The feedforward control and the desired state are both dependent on time only. They are combined into u_0 , since the problem would not have a unique solution if these were separated.

6.3 Pendulum Swing-Up

In this section, the classical problem of a pendulum swing-up from a downward to an upward position minimizing the squared torque is solved in a deterministic and a stochastic environment. This problem is nonlinear and the upward position is an unstable equilibrium. This would not affect the solution in a deterministic environment, but in the stochastic

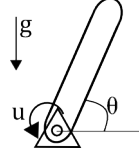


Figure 37: Pendulum used for the swing-up problem. The goal was to move this pendulum from the downward to the upward position in ten seconds, while minimizing the squared torque.

environment control is required to remain in this position. Therefore, a different trajectory will be optimal in a deterministic environment than in a stochastic environment.

6.3.1 Methods

Figure 37 shows the pendulum that was used in the swing-up problem. The task was to swing up from the downward position, $\theta(0) = -\pi/2$, to the upward position, $\theta(T) = \pi/2$, in $T = 10$ seconds while minimizing the square torque. Given state $x(t) = [\theta(t) \quad \omega(t)]^T$, the pendulum dynamics $\dot{x}(t) = f(x(t), u(t), \varepsilon(t))$ were as follows:

$$\dot{x}(t) = \begin{bmatrix} \omega(t) \\ -\frac{g}{l} \cos(\theta(t)) + \frac{u(t)}{ml^2} + \varepsilon(t) \end{bmatrix} \quad (6.8)$$

$$\text{with:} \quad \varepsilon(t) \sim N(0, \sigma^2) \quad (6.9)$$

where g denotes gravity, the length of the pendulum was $l = 0.6$ m and its mass was $m = 2$ kg. The input to the system was the torque u at the base of the pendulum. In the deterministic case, the input was only feedforward, $u(t) = u_0(t)$, while in the stochastic case, there was a feedforward and feedback control on the position and velocity, $u(t) = u_0(t) + Kx(t)$. Normally distributed noise, $\varepsilon(t)$, was added to the angular acceleration with a standard deviation σ .

In the deterministic environment, the trajectory optimization problem was described as

follows:

$$\underset{X}{\text{minimize}} \quad \frac{1}{2} \int_{t=0}^T u(t)^2 \quad (6.10)$$

$$\text{subject to: } \dot{x}(t) = f(x(t), u(t)) \quad 0 \leq t \leq T \quad (6.11)$$

$$x(0) + \begin{bmatrix} \frac{\pi}{2} \\ 0 \end{bmatrix} = 0 \quad (6.12)$$

$$x(T) - \begin{bmatrix} \frac{\pi}{2} \\ 0 \end{bmatrix} = 0 \quad (6.13)$$

where $X = u(t)$, $0 \leq t \leq T$ are the optimization variables, equation 6.10 is the objective, equation 6.11 represents the dynamics constraints and equations 6.12 and 6.13 indicate the task constraints of starting in the downward position and finishing in the upward position, respectively.

In the stochastic environment, the optimization was performed over N_s episodes. The objective was to minimize the average square torque over the episodes. The dynamics constraints were the same, as was the constraint on the initial position (equation 6.12). The endpoint constraint (equation 6.13) was placed on the average end position over all episodes, since in the stochastic environment the end position of an individual trajectory

cannot be constrained separately. This yielded the following problem description:

$$\underset{X}{\text{minimize}} \quad \frac{1}{2N_s} \sum_{j=1}^{N_s} \sum_{n=1}^N u_j(n)^2 \quad (6.14)$$

$$\text{subject to: } \dot{x}_j(n) = f(x_j(n), u_j(n), \varepsilon_j(n)) \quad n = 1 \dots N \quad \forall j \in 1 \dots N_s \quad (6.15)$$

$$x_j(1) + \begin{bmatrix} \frac{\pi}{2} \\ 0 \end{bmatrix} = 0 \quad \forall j \in 1 \dots N_s \quad (6.16)$$

$$\frac{1}{N_s} \sum_{j=1}^{N_s} x_j(N) - \begin{bmatrix} \frac{\pi}{2} \\ 0 \end{bmatrix} = 0 \quad \forall j \in 1 \dots N_s \quad (6.17)$$

$$\text{with: } u_j(n) = u_0(n) + Kx_j(n) \quad (6.18)$$

$$\varepsilon_j(n) \sim N(0, \sigma^2) \quad (6.19)$$

where the optimization variables were $X = [u_0(t) \ K]^T$, $0 \leq t_j \leq T$ for all j episodes. $u_0(t_j)$ denotes the open loop control and $Kx_j(t_j)$ denotes the proportional-derivative feedback controller. The noise was randomly sampled at the collocation points, meaning that the sampling rate was 0.16 s.

The deterministic solution was solved starting from a random initial guess. This solution was then used as the initial guess to find a trajectory in a stochastic environment with a small standard deviation of 0.001 rad/s². This process was repeated for increasing standard deviations: 0.01, 0.05, 0.1, 0.5 and 1 rad/s² to be able to compare between noise amplitudes. The deterministic solution was compared against the stochastic solutions with a standard deviation of 0.05 rad/s² or larger. This process was repeated using only open-loop control to show the effect of the feedback control.

A convergence analysis was performed to find the minimum number of swing-ups required to approach the theoretical optimal solution. Since this solution was unavailable, it was assumed that the theoretical optimal solution was approached once a change in the number of samples did not yield a change in value of the objective function. The number of samples N_s was varied between one and 100 trajectories. Each problem was solved ten

times to account for variability in the results due to the simulated noise.

The trajectory optimization problems were solved using direct collocation, with $N = 60$ collocation points for each episode and a midpoint Euler formulation:

$$\dot{x}(n) = \frac{x(n+1) - x(n)}{h} = f\left(\frac{x(n+1) - x(n)}{2}, \frac{u(n+1) - u(n)}{2}\right) \quad (6.20)$$

In the deterministic environment, the optimization variables were the states and inputs at each collocation point, $X = [x(1) \ u(1) \ \dots \ x(N) \ u(N)]^T$. The number of optimization variables was equal to $3N$, since there were two states and one input at each collocation point. There were $2N$ equality constraints. In the stochastic environment, the optimization variables were the states at each collocation point for each episode, the open loop inputs for collocation point and the feedback position and derivative gain, $X = [x_1(1) \dots \ x_1(N) \ x_2(1) \dots \ x_{N_s}(N) \ u_0(1) \dots \ u_0(N) \ K_P \ K_D]^T$. The total number of optimization variables was equal to $2NN_s + N + 2$. The number of constraints was equal to $2NN_s$.

The objective and the dynamics and task constraints, as well as their derivatives with respect to x , \dot{x} and u were coded in MATLAB (Mathworks, Natick, MA, USA). The resulting constrained optimization problem was solved using IPOPT 3.11.0 [37].

6.3.2 Results

The goal of this work was to show that the proposed method was able to find a different optimal trajectory in a stochastic environment than in a deterministic environment. The upper graph in figure 38 shows the mean trajectory of 30 episodes of the optimal solution for different noise amplitudes. The average trajectory over 10 optimizations is plotted to account for variation due to the noise samples. In the stochastic environments, a different trajectory was optimal than in the deterministic environment, since the timing of the swing up changes such that the final swing-up (between 8 and 10 seconds) occurred later for a larger noise amplitude.

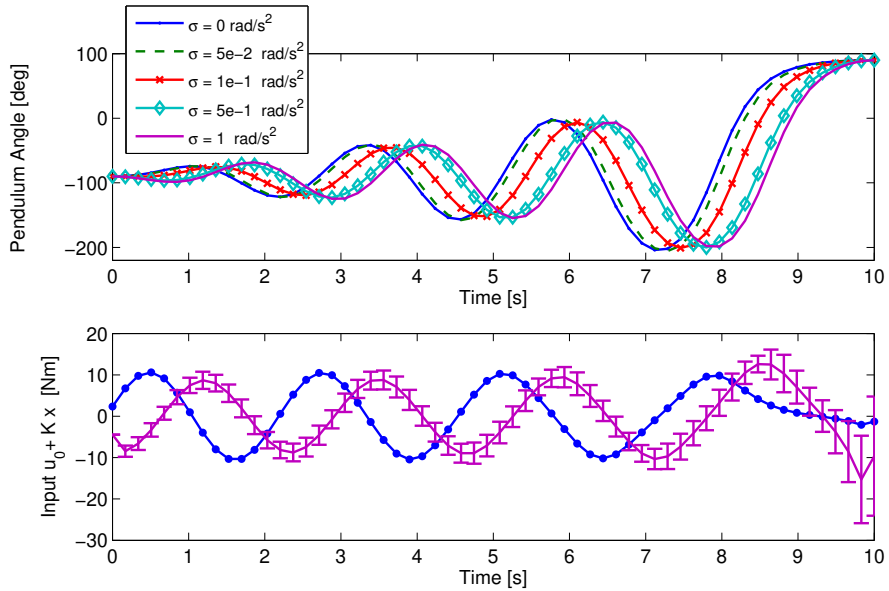


Figure 38: Optimal pendulum swing-up trajectories (upper graph) and control torque (lower graph) with different levels of noise. 30 episodes were used for this results, and it was repeated ten times to account for variability due to the noise. The error bars in the lower graph shows the standard deviation of the input over the 30 episodes, averaged over the ten repetitions. With a larger standard deviation, the swing up of the pendulum occurred later to limit the time spent in the unstable, upright equilibrium. The timing of the input changed with the change in timing in the swing up trajectory. The variation of the input was largest near the end of the trajectory.

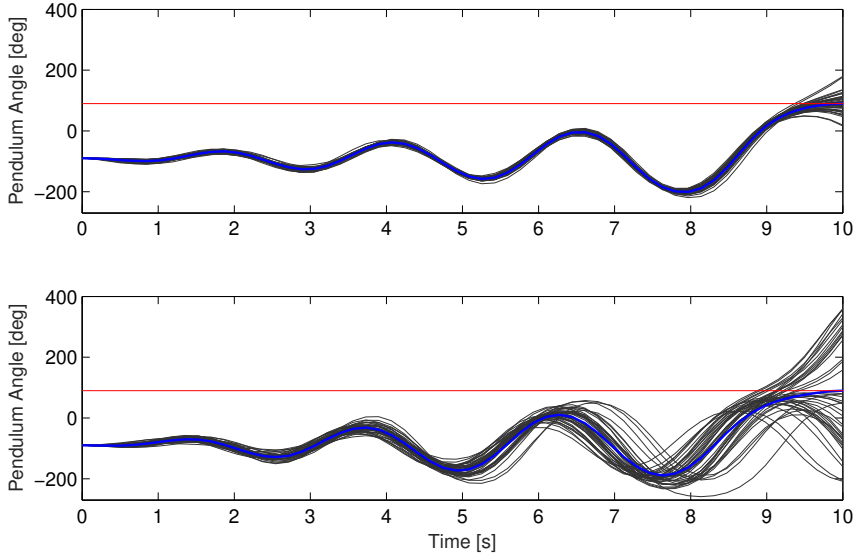


Figure 39: Comparison of the trajectories found with feedback control (top figure) and without feedback control (bottom figure) for a standard deviation of 1 rad/s^2 . The blue line shows the average trajectory, while the (40) black lines show each individual trajectory and the red line shows the 90 degrees.

The lower graph in figure 38 shows the average control input over 10 optimization runs as a function of time in the deterministic environment and the stochastic environment with $\sigma = 1 \text{ rad/s}^2$. The vertical bars show the standard deviation of the control torque over the 30 episodes due to the feedback control. Similar to the optimal trajectory, a phase-shift was present between the input in the deterministic solution and the stochastic solution. Compared to the deterministic environment, the average peak inputs were lower in the beginning of the trajectory, and higher in the second part of the trajectory in the stochastic environment. The variation of the control was largest near the end of the trajectory.

Figure 39 shows the trajectories that were found using open-loop and closed-loop control (upper) and with open-loop control only. One can see that the variation was much higher using only open-loop control, such that certain episodes did not swing-up, while others overshot and ended up in the downward position.

Figure 40 was used for the convergence analysis. It shows the objective of the optimal solution as a function of the number of episodes. When more than 20 trajectories were

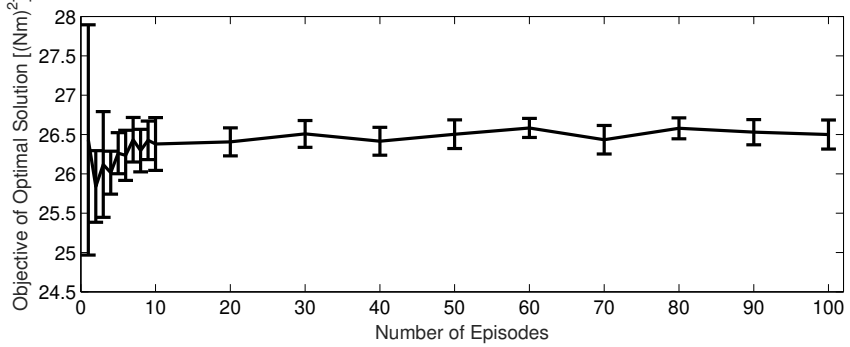


Figure 40: Convergence analysis of the objective of the optimal solution. Convergence occurred after 20 samples to a value of 26.5 (Nm)^2 .

used, the objective converged to a value of 26.5 (Nm)^2 and did not change more than 1% compared to the objective found with 100 episodes, the largest number of episodes used. Also, the variation of the objective remained lower than 0.2 Nm using 20 or more episodes.

6.3.3 Discussion

In figure 38, the optimal trajectory of the pendulum swing-up changed with the noise amplitude. This can be explained in two ways. Firstly, when the environment was deterministic ($\sigma = 0 \text{ rad/s}^2$) the swing-up was mostly passive when close to the goal and the inertia of the pendulum and gravity was used to brake the pendulum and stop in the upright position. However, this was not optimal in a stochastic environment, because the noise caused the pendulum to undershoot or overshoot the upright position. Therefore, an active swing-up, using a strategy with larger control input to swing-up and brake, yielded less variation between the samples. This approach also explains the larger variation in control near the end of the trajectory.

Secondly, less time was spent in the upright position because this equilibrium is unstable. The smallest deviation would cause the pendulum to swing back to the downward position, the stable equilibrium. Therefore, it would be more costly to remain in the upright position in a stochastic environment and less time is spent in the upright position in the stochastic environment to reduce the required control input. However, a larger con-

trol input at the end of the trajectory was necessary because the final swing-up was faster. Todorov [30] also found that in a stochastic environment, the least possible time was spent in the upright position due to the high energy cost of the control.

The combination of closed-loop and open-loop control decreased the variability of the results, as can be seen in figure 39. However, the conclusion was the same, since the average trajectory without feedback control also swung up later in the stochastic environment than in the deterministic environment. The stability of the system with these feedback gains in the upright position was checked by linearizing the system around the upright position and checking if the real part of the eigenvalues were negative. Stable feedback gains were found for all problems with more than 10 episodes for all standard deviations, while solutions with fewer episodes were stable or marginally stable. This suggests that this method could also be used in robotics, to simultaneously find an optimal trajectory and a controller in one optimization procedure. With a conventional approach in a deterministic environment, only an optimal trajectory is found. The controller is found separately, for example by linearizing around the trajectory.

The convergence analysis showed that the objective did not change more than 1% when at least 20 episodes were used. Also, the standard deviation over 10 solutions remained 0.2 Nm. Figure 40 shows that already with seven samples, a good estimate of the optimal objective in the stochastic environment was found. With five or more episodes, the trend is visible that was shown in figure 38, that the swing-up occurred increasingly late with a larger standard deviation.

6.4 Pendulum with Muscular Control

The same pendulum, controlled with muscles, was used to see if co-contraction is optimal in certain tasks. The goal was to keep the pendulum in the upright equilibrium. This does not require any effort in a deterministic environment, but in a stochastic environment, some control is required to keep the pendulum from falling. We investigated if a combina-

tion of co-contraction input and activation of the agonist muscle was more energy efficient than only activating the agonist muscle.

6.4.1 Methods

Figure 41 shows the pendulum with muscles. The muscles were modeled as Hill-type muscles with a series elastic element, a parallel elastic element and a contractile element with activation dynamics, a force-length relationship and a force-velocity relationship (see section 2.6.1) with parameters as given in table VII.

The input to the system was a muscle stimulation signal, u_k for muscle k . This system had six states, because four muscle states were added. So, the state was $x = [\theta(t) \omega(t) a_1(t) a_2(t) l_{CE(1)}(t) l_{CE(2)}(t)]^T$, where a_k was the activation and $l_{CE(k)}$ the contractile element length of muscle k . The dynamics were described implicitly to avoid singularities:

$$f(x(t), \dot{x}(t), u(t)) = \quad (6.21)$$

$$\begin{bmatrix} \omega(t) - \dot{\theta}(t) \\ -\frac{g}{l} \cos(\theta(t)) + \frac{\tau}{ml^2} + \varepsilon(t) - \dot{\omega}(t) \\ \dot{a}_1(t) - (u_1(t) - a_1(t))(\frac{1}{T_{act}}(u_1(t) + 1) - \frac{1}{T_{deact}}) \\ \dot{a}_2(t) - (u_2(t) - a_2(t))(\frac{1}{T_{act}}(u_2(t) + 1) - \frac{1}{T_{deact}}) \\ F_{SEE(1)}(\theta, l_{CE}, t) - F_{PEE(1)}(\theta, l_{CE}, t) - F_{CE(1)}(t) + bv_{CE(1)}(t)F_{max} \\ F_{SEE(2)}(\theta, l_{CE}, t) - F_{PEE(2)}(\theta, l_{CE}, t) - F_{CE(2)}(t) + bv_{CE(2)}(t)F_{max} \end{bmatrix}$$

$$\text{with: } F_{CE(k)}(t) = a_k(t)F_{max}f(l_{CE(k)}(t))g(v_{CE(k)}(t)) \quad (6.22)$$

$$\text{and: } \varepsilon(t) \sim N(0, \sigma^2) \quad (6.23)$$

where $\tau = (F_{SEE(1)} - F_{SEE(2)})D$, was the moment resulting from force in the series elastic element, F_{SEE} , multiplied with the muscle moment arm D , T_{act} and T_{deact} were the activation and deactivation time of the muscles, respectively, F_{PEE} was the force in

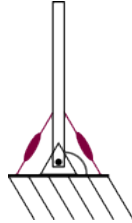


Figure 41: Pendulum operated with muscles that is used to show that co-contraction is optimal in certain tasks in a stochastic environment.

the parallel elastic element, F_{max} was the maximum isometric force, $f(l_{CE(k)})$ was the force-length relationship, $g(v_{CE(k)})$ was the force-velocity relationship, and b was a small damping term to aid convergence of IPOPT.

The optimal control problem was to remain in the upright position with minimal effort. Also, a periodicity constraint was used, such that theoretically the pendulum was kept upright indefinitely. This yielded the following problem:

$$\underset{x}{\text{minimize}} \quad \int_{t=0}^T \left(W \left(\theta(t) - \frac{\pi}{2} \right)^2 + \sum_{k=1}^2 u_k(t)^2 \right) dt \quad (6.24)$$

$$\text{subject to} \quad f(x(t), \dot{x}(t), u(t)) = 0 \quad 0 \leq t \leq T \quad (6.25)$$

$$x(T) - x(0) = 0 \quad (6.26)$$

$$\text{with:} \quad u_k(t) = u_{k(0)} + Kx(t) \quad (6.27)$$

where $X = [u_{k(0)} \quad K]^T$ were the optimization variables, W was a weighting factor that determines how much the deviation from the upright position is penalized compared to minimizing effort. The duration T was 10 seconds. The open-loop control input, $u_{k(0)}$, was bounded to be larger than zero.

The control law had only one open-loop control signal, $u_{k(0)}$ for each muscle because the aim of this problem was not to find a trajectory, but a fixed position, so the open-loop control input was independent of time. Therefore, each collocation point was regarded as an episode in the stochastic environment. The sign of the feedback gains K was opposite in each muscle, but the value could be different. Also, the open-loop control signal and the

muscle activation were bound to be nonnegative. If the input u_0 in the optimal solution is nonzero in both muscles, it means that the combination of co-contraction and activation of the agonist muscle yields a lower objective than only using the agonist muscle.

The optimal control problems were solved using direct collocation, with 600 collocation points and a backward Euler formulation. The number of collocation points was high to fully capture the activation dynamics. The dynamics equations, as well as their derivatives with respect to x , \dot{x} and u were coded in MATLAB (Mathworks, Natick, MA, USA). The resulting constrained optimization problem was solved using IPOPT 3.11.0 [37].

Co-contraction was dependent on the noise amplitude and on the relative importance of the deviation from the upright position. Therefore, the standard deviation of the noise in equation 6.4.1 was varied between 0 and 1 and the weighting factor W was varied between 10 and 50000. Noise was added at each collocation point. Its value was divided by the square of the time step length to have a dimensionless standard deviation. Similar to the pendulum swing-up problem, solutions in the stochastic environment were found using a solution with a lower standard deviation as initial guess, starting from the deterministic environment. The open-loop input was compared between the different problems to see if co-contraction was optimal. Each problem was solved 5 times to account for variability due to the simulated noise.

6.4.2 Results

Figure 42 shows the open-loop input, u_0 , as a function of the noise amplitude and the weight W in equation 6.24. The open-loop input increased with both the noise amplitude and the weight. Without any noise, there was no open-loop input, and thus no co-contraction, because the pendulum remained in the upright position without effort. When noise was present, a combination of co-contraction and closed loop control was optimal. The open-loop input was low for a small weight, because staying upright was not emphasized and the pendulum would sway with the noise, which required less effort. The

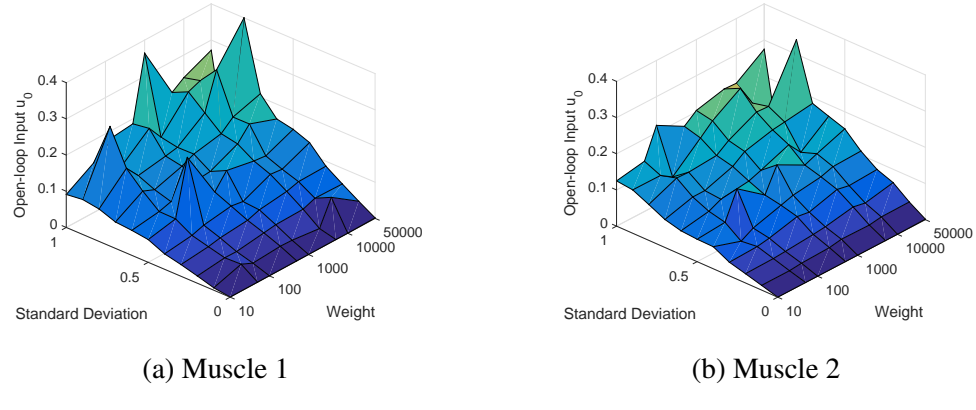


Figure 42: Optimal open-loop control input for different weights W and noise amplitudes for both muscles. Co-contraction occurs because the open-loop control input is nonzero for both for larger weights and noise amplitudes. The open-loop input, u_0 , increases with weight as well as with the noise amplitude.

co-contraction input increased when staying upright was emphasized in the stochastic environment.

Figure 43 compares the trajectory that was found in the deterministic environment ($\sigma = 0$) with a trajectory that was found in a stochastic environment ($\sigma = 1$ and $W = 50000$). In the deterministic environment, the pendulum angle was exactly 90 degrees during the complete trajectory. No force was produced, and the contractile element length was optimal throughout the trajectory. In the stochastic environment, there was a variation of about 0.2 degrees in the pendulum angle in both directions. The bottom left graph shows the input, which went up to 1 and down to -0.5 .

The graphs in the top right corner of figure 43 show the force in the series elastic element, the activation state and contractile element length. All graphs indicate co-contraction of the muscles. Both muscles produce a force that fluctuates around 400 N, while both muscles are activated throughout the trajectory, fluctuating around 0.4. The bottom graph also shows that the muscle is shortened slightly, to 98% of the optimal length. The lower right graph shows the torque, which fluctuates around zero.

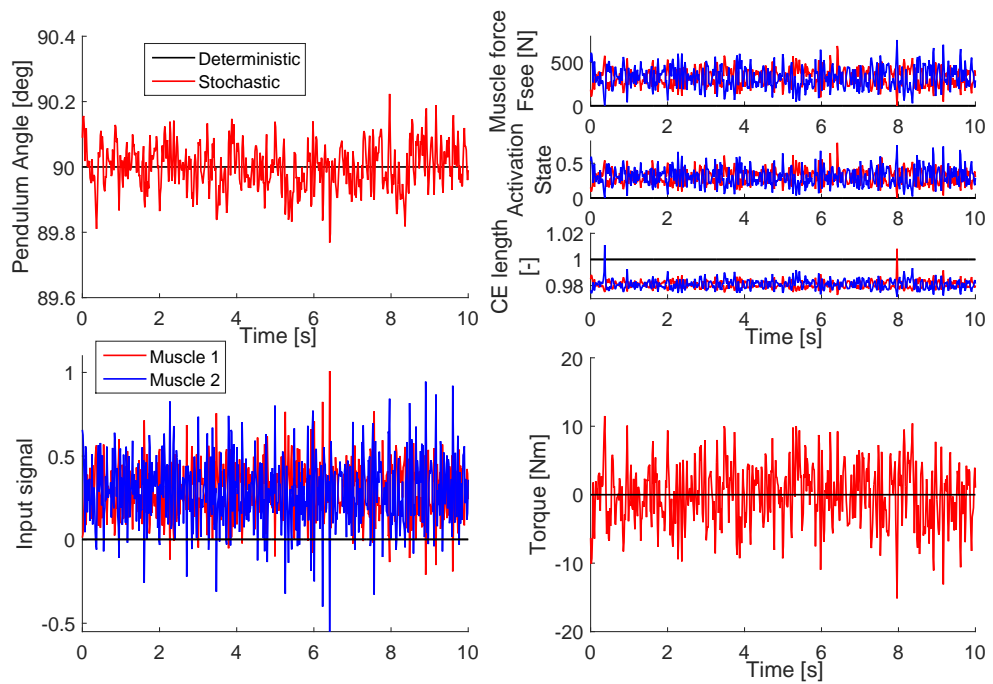


Figure 43: Comparison of the optimal trajectory for $\sigma = 0$ (deterministic environment) and $\sigma = 1$ and $W = 50000$. All black lines show the solution for the deterministic environment. The top left shows that the pendulum remained in the upright position in the deterministic solution, while the noise caused some motion in the stochastic environment. The bottom left figure showed that co-contraction occurred when $\sigma=1$, since the input was nonzero in both muscles.

6.4.3 Discussion

Figure 42 shows that co-contraction was optimal in certain tasks in a stochastic environment. When little emphasis was placed on staying in the upright position, so for low weights W , the open-loop input was very small. More co-contraction was required when more emphasis was placed on staying in the upright position. This means that it is more energy efficient to stiffen the joint using antagonistic co-contraction than to avoid co-contraction and only activate the agonist muscle to withstand environmental uncertainty.

Note that figure 43 showed that the input value ranged between -0.5 and 1 , while a value between zero and one is expected in a human muscle. It was decided to not place bounds on the inputs, because the goal of this problem was to show that co-contraction could be optimal and bounds might have influenced the results. Therefore, only the co-contraction input was not allowed to be smaller than zero. Also, despite these high input values, the activation state remained between 0 and 1 , which is as expected.

Literature often describes co-contraction as inefficient [1, 2], because it does not produce any useful work while it requires energy [18], contradicting studies showing that humans choose their movements to minimize energy. This work showed that for some tasks co-contraction is energy efficient, because our trajectory optimization methods finds a combination of co-contraction and activation of the agonist muscle as optimal solution when only energy is stability, and not some form of stability. This supports a previous study that co-contraction reduces the effect of internal noise and increases movement accuracy [25].

Our results show that co-contraction is optimal in tasks where it is important not to deviate far from the trajectory. One such task is walking, where deviations from the trajectory can result in a fall easily. For example, a passive dynamic walker only has a very small region of attraction that yields a stable gait [38]. In TTA gait, muscle co-contraction is observed in the thigh on the prosthesis side [10, 11], which could be related to the loss of control and senses in the lower leg, and the imperfect connection between the prosthesis and the residual leg. When the proposed method is applied to TTA gait, it can be

investigated if this co-contraction is energy efficient in a stochastic environment.

The trajectory optimization problems were hard to solve by IPOPT, since the optimization would often find a local minimum, or not find a solution within 1000 iterations. Therefore, the graphs in figure 42 have outliers. To reduce the chance of finding a local minimum, the open-loop control input was bound between 0 and 0.4. This ensured that no local minimum was found in the deterministic environment. Previous simulations with larger bounds showed that this range was large enough for the weights and standard deviations that were used. Additionally, the optimizations were repeated five times, and the average was used only of those solutions that were optimal and within 10% of the lowest objective that was found. Some variation in the optimal solution was expected due to the stochasticity of the environment, but a large difference indicated that a local optimum was found.

6.5 Torque-driven Able-bodied Gait

We have shown that the proposed method can predict the optimal trajectory in a stochastic environment, and that co-contraction of muscles is optimal for certain tasks. Next, we aim to use the method on a gait problem with a torque-driven human model to eliminate the muscle states and thus lower the number of optimization variables. This makes the problem more tractable. The goal was to show that in a stochastic environment, a larger foot clearance is optimal when energy is minimized than in a deterministic environment. Noise was introduced in the joint torques, to simulate noisy control.

6.5.1 Methods

Model

The human model shown in figure 5 will be used in this work but it will be operated using joint torques, instead of muscle stimulations. Further description of the multibody dynamics and ground contact model can be found in section 2.6. The dynamics were

described as follows (see equation 2.18):

$$M(q(t))\dot{v}(t) + C(q(t), v(t))v(t) + G(q(t)) = \tau(t) + J_c(t)^T F_c(t) + T_{pas}(t) \quad (6.28)$$

where $M(q)$ was the mass matrix, $C(q, v)$ contained the Coriolis forces, $G(q)$ the gravity forces, $J_c^T F_c$ the ground reaction forces, T_{pas} the passive joint torques, and τ was a vector of generalized forces. The first three elements of the generalized force vector, τ , were zero since these degrees of freedom were unactuated. The six joint moments $\tau_4(t)$ to $\tau_9(t)$ were the torque inputs, $u_1(t)$ to $u_6(t)$, which were determined as follows:

$$u_j(t) = u_{0(j)}(t) + K_P \theta_j(t) + K_D \omega_j(t) \quad (6.29)$$

In the stochastic environment, uniform noise was added at each collocation point to the torque inputs u_i to simulate noisy neural control. The noise was sampled with a sampling rate of 0.037 s. Similar to the methods used for the pendulum swing-up (see section 6.3), the problem was solved for noise with an increasing amplitude. The amplitude was varied between 0 Nm in the deterministic environment and 100 Nm.

Optimal Control Problem

The objective comprised of two parts. One part minimized the square torque to minimize the energy used. The second part penalized a tracking error between the simulation and data of normal walking [39] of the joint angles in the hip, knee and ankle, the ground reaction force and the duration of the gait cycle. This objective was necessary in the torque-controlled model to create a realistic gait cycle. The speed of the gait cycle was fixed, while the duration was tracked. A similar objective, minimizing square muscle activation, was

shown to predict human gait well [3, 6], see chapter III. This yields the following objective:

$$\begin{aligned} J(x, u) = & \frac{1}{N_{\text{track}} + 1} \left(\frac{1}{T_{\text{tot}}} \sum_{k=1}^{N_{\text{track}}} \int_0^{T_{\text{tot}}} \left(\frac{s_k(x(t)) - x_{m_k}(t)}{\sigma_k} \right)^2 dt \right. \\ & \left. + \left(\frac{T_{\text{tot}} - N_s T_m}{\sigma_T} \right)^2 \right) + \frac{W_{\text{torque}}}{6T} \sum_{j=1}^6 \int_0^{T_{\text{tot}}} u_j(t)^2 dt \end{aligned} \quad (6.30)$$

where N_{track} was the number of tracked state variables, next to the duration, $s_k(x(t))$ denotes the data of the joint angles and ground reaction forces that were tracked, with standard deviation σ_k , T_{tot} the sum of the duration of all gait cycles, and T_m the tracked duration with standard deviation σ_T , which is multiplied by the number of gait cycles, N_s . The combined closed-loop and open-loop input, $u_j(t)$, were given in equation 6.18. $W_{\text{torque}} = 0.001$ was used to create a realistic gait cycle. Note that this number is much lower compared to effort minimization in chapter III because the values for torque are higher than muscle stimulations.

It was assumed that the gait cycles had left-right symmetry, therefore only half a gait cycle was simulated. The following periodicity constraint was used on the horizontal position, x_t when one gait cycle was simulated:

$$x_t \left(\frac{T}{2} \right) = x_t(0_{\text{sym}}) + v \frac{T}{2} \quad (6.31)$$

where T was the duration of the full gait cycle, the subscript sym denoted the mirror of the state, meaning that the joint angles and angular velocities were switched between the left and right leg, and v is the speed.

In the stochastic environment, a predictive simulation was solved over N_s gait cycles. A periodicity constraint was placed only between the first and last gait cycle:

$$x_t \left(\frac{T_{\text{tot}}}{2} \right) = x_t(0_{\text{sym}}) + \frac{1}{2} \sum_{i=1}^{N_s} v T(i) \quad (6.32)$$

where T_{tot} denoted the total duration of all gait cycles, $T(i)$ denoted the duration of gait cycle i . Dynamics constraints were used between the other gait cycles, such that a series of steps was found.

The optimal control problem was solved through direct collocation, with 30 collocation points per half-gait cycle and a backward Euler formulation. One collocation node was added to ensure periodicity. Since the dynamics were similar to the dynamics described in section 2.6, the same MEX-function was used as in chapter III. The maximum isometric muscle forces was set to zero and torques were added to the dynamics as external torques. Details of the solution method can be found in chapter II and chapter III. The resulting constrained optimization problem was solved using IPOPT 3.11.0 [37].

First, a gait cycle was found in a deterministic environment. This gait cycle was used as an initial guess to solve the problem in a stochastic environment with a noise amplitude of 0.1 Nm. Then, this solution was used as an intial guess for an environment with an amplitude of 0.5 Nm, followed by 1 Nm, 5 Nm and 10 Nm. This process was repeated to obtain solutions with a noise amplitude of up to 100 Nm. The foot clearance of these solutions were compared. 10 gait cycles created an optimization problem with 7000 optimization variables.

A convergence analysis was performed to find the required number of gait cycles to solve the stochastic optimization problem. An optimization will be performed for five different noise samples, and the solution with the lowest objective will be analyzed. To limit the required computation time, the noise amplitude used in the convergence analysis was 10 Nm. The simulations for the convergence analysis were created on the OSC supercomputer [40].

6.5.2 Results

Figure 44 shows the average foot clearance at the heel and toe for noise amplitudes from 0 Nm to 100 Nm. During the stance phase, the clearance is negative, due to the

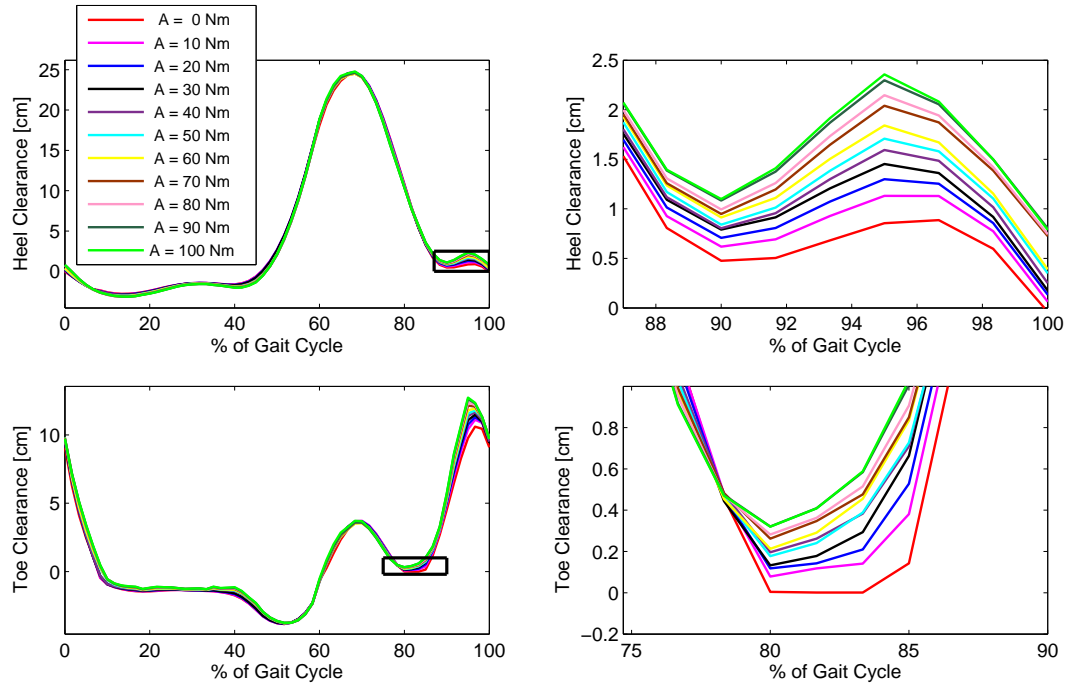


Figure 44: Average heel (top figures) and toe clearance over 10 gait cycles for solutions with different noise amplitudes. One can see that with an increasing noise amplitude, the clearance of the heel and toe increases.

ground penetrating contact model that was used (see section 2.6). The heel penetrated throughout the stance phase, while the toe penetrated only in late stance to generate the required push-off force. The graphs on the right show the part of the swing phase where the foot almost hits the ground. In this phase, the foot clearance was exactly zero in an environment without noise, but the foot clearance increased with the noise amplitude.

Figure 45 shows the result of the convergence analysis. The top graph shows the minimum objective value over five different noise samples. The bottom graph shows the accompanying minimum foot clearance. The graphs seem to converge very fast, and with just five gait cycles the objective and foot clearance were already very similar to the objective and foot clearance found with 40 gait cycles. However, at 30, 45, and 50 gait cycles, the objective and minimum foot clearance were much higher, therefore it seemed as if the graph diverges after 40 gait cycles.

Figure 46 shows the average foot clearance over 50 gait cycles. Similar to figure 44,

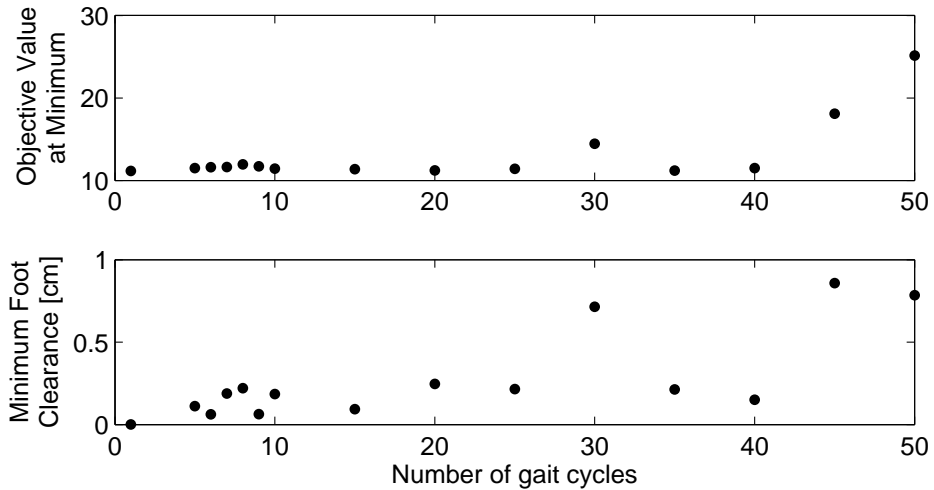


Figure 45: Convergence analysis of the required number of gait cycles. The top graph shows the minimum objective of the five solutions that were found. The bottom graph shows the average minimum foot clearance of the solution with the lowest objective.

the clearance increased with the noise amplitude. However, throughout the gait cycle, the foot did not move smoothly, which indicates that the solution that was found was not the global optimum.

6.5.3 Discussion

The goal was to show that while zero foot clearance is optimal in a deterministic environment, nonzero foot clearance is optimal in a stochastic environment when energy is minimized. A secondary goal was to see how many gait cycles were required to correctly estimate the problem in a stochastic environment using a convergence analysis. Figure 44 shows that the optimal foot clearance increases with the noise amplitude in the uncertain environment. The convergence analysis showed that a realistic solution was found with five gait cycles.

The foot clearance over the full 10 gait cycles was inspected as well. It was found that the foot clearance at one instance in time was equal to exactly zero. This means that the average ground clearance was just high enough to prevent scuffing. This is similar to normal walking, since people also choose their foot clearance just high enough to prevent

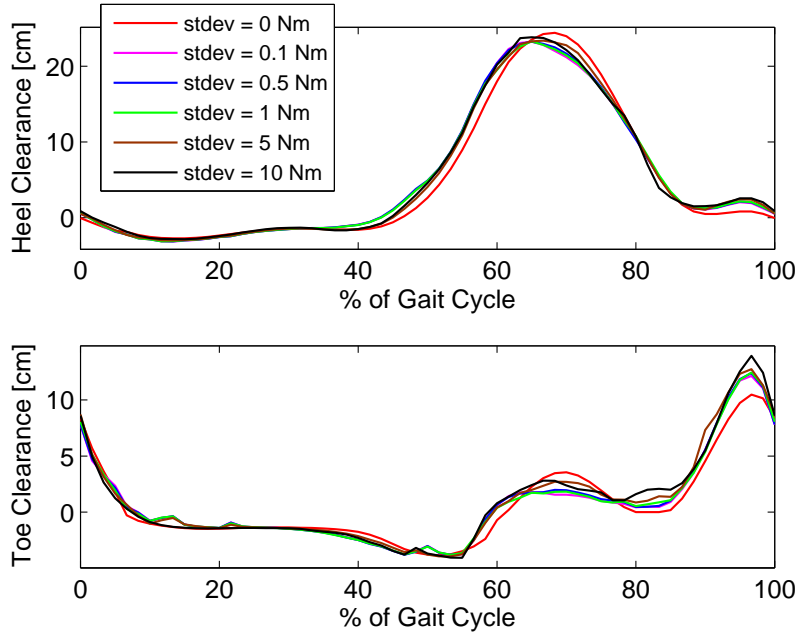


Figure 46: Average heel (top figures) and toe clearance over 50 gait cycles for solutions with different noise amplitudes. One can see that the result is not smooth, which indicates that this solution is not the global optimum.

scuffing, but as low as possible to minimize metabolic energy cost [41].

A simple controller was used, with only two variables besides the open-loop control inputs. This was done to limit the search space of the problem. It is likely that a controller with more free variables will yield a solution with a lower objective. However, this would also require a larger number of gait cycles to correctly estimate the theoretical optimal solution in the stochastic environment. 10 gait cycles required approximately four hours on a standard laptop, so it was decided not to increase the number of controller parameters. Also, it is not expected that a more complex controller would significantly alter the conclusion that larger foot clearance is optimal in a stochastic environment, compared to a deterministic environment.

The convergence analysis converged after five gait cycles, but diverged again when 30, 45 or 50 gait cycles were used. It is likely that for these large numbers of gait cycles, IPOPT had difficulty finding a good optimal solution. This is illustrated in figure 46, which shows the average foot clearance for 50 gait cycles. This result was much less smooth than

the results for 10 gait cycles shown in figure 44. The variance in the objective value over the five optimal solutions was much larger for a larger number of gait cycles, which also suggests that the problem became numerically more difficult with a larger number of gait cycles. If more than different initial guesses were attempted, it would probably be possible to find a lower objective.

Uniform noise was added in this problem instead of Gaussian noise, since it was found that for the convergence analysis IPOPT had trouble solving the trajectory optimization problems successfully when Gaussian noise was used. Gaussian noise can have extremely large outliers, whereas uniform noise is bounded. Therefore it is possible that with Gaussian noise, a problem was created that was impossible to solve. Uniform noise was used to avoid this. Figure 44 was also created with Gaussian noise, and a similar effect was seen, with the foot clearance increasing with the standard deviation of the noise.

6.6 Predictive Gait Simulation with a Lower Leg Prosthesis in a Stochastic Environment

Finally, the proposed method is applied to the problem that motivated this research originally: is co-contraction in the thigh on the residual side in TTA gait energy efficient? A musculoskeletal model of the human is used. Due to the large number of states and optimization variables, this problem could be too large for IPOPT to solve. Therefore, this work should be seen as an initial attempt to this problem, and recommendations for future improvements will be made.

6.6.1 Methods

The model, with nine degrees of freedom and eight muscles in each leg, was described in chapter II. The Gastrocnemius, Soleus and Tibialis Anterior in the right leg were removed and replaced by a passive spring with a stiffness of 600 Nm/rad and damping of 15 Nm/s/rad [42] to simulate TTA gait (see chapter III and chapter IV). The mass and inertial

properties were not altered. Muscle stimulations were generated with the control law given in equation 6.29, using feedforward control and feedback from the joint angles and velocities. The position and derivative gain were the same for each muscle, meaning that two parameters were added to the optimization problem.

The objective was to minimize effort (see equation 3.2):

$$J(x, u) = \frac{W_{\text{effort}}}{16T} \sum_{j=1}^{16} \int_0^T u_j(t)^2 dt \quad (6.33)$$

Noise was added to the torque at the knees and hips. The noise was drawn from a uniform distribution, with an amplitude to 10 Nm. It was added to the collocation points, yielding a sampling rate of 0.037 s. The optimal control problems was solved using direct collocation, with 10 gait cycles and 60 collocation points per gait cycle and a backward Euler formulation.

The MEX-function described in chapter III was used. Regularization with weight $W_{\text{reg}} = 1$ was added to aid the optimization. Details of the solution method can be found in chapter II and chapter III. The resulting optimization problem will be solved using IPOPT 3.11.0 [37]. The TTA solutions were found using the OSC supercomputer [40].

First, an able-bodied gait cycle was found in a deterministic environment. This solution was used as an initial guess to find an able-bodied simulation in a stochastic environment, and a TTA gait simulation in the deterministic environment. A series of problems with noise amplitudes of 0.1 Nm, 1 Nm and 10 Nm was solved to find the gait cycles in the stochastic environment, both for able-bodied gait and TTA gait. The initial guess for the smallest amplitude was the gait cycle in the deterministic environment, and then the previous solution was used as initial guess. The process was repeated for TTA gait to ensure that the result was not due to the effect of the noise sample.

The joint angles and joint moments of the TTA gait solution in the stochastic environment with a noise amplitude of 10 Nm were compared to the joint angles and joint

moments of the able bodied gait solution and to normal data [2]. The co-contraction index was compared against the able-bodied solution, the TTA gait solution in the deterministic environment, and the TTA gait solution without joint moment symmetry found in chapter III. The index was calculated for the first 40% of the gait cycle, which is where Powers et al. [11] report increased activation of the Vastus Lateralis and Semimembranosus, which is part of the Hamstrings. The co-contraction index of the Vasti and Hamstrings was determined using Method 1 in [43]:

$$CI = \frac{2 \left(\int_{t_1}^{t_2} u_{HAM}(t) dt + \int_{t_2}^{t_3} u_{VAS}(t) dt \right)}{\int_{t_1}^{t_3} u_{HAM}(t) + u_{VAS}(t) dt} \quad (6.34)$$

where $[t_1, t_2]$ denotes the time period where the stimulation in the Hamstrings is lower than in the Vasti, and $[t_2, t_3]$ denotes the time period where the stimulation in the Vasti is lower than in the Hamstrings.

6.6.2 Results

Figure 47 show the joint angles and moments of the simulation in the stochastic environment in the able-bodied and TTA solution. The grey fill shows normal joint angles and moments from [2]. For the able-bodied solution, the hip had similar range of motion to normal, while the motion in the knee was smaller, especially during swing, and the motion in the ankle was larger, especially the plantarflexion angle at push-off. The hip flexion moment during late stance was absent, as well as the knee extension moment in early and midstance. The ankle moment was larger than normal during midstance, and smaller than normal during push-off.

In the TTA solution, the hip range of motion was normal on the prosthesis side, but larger on the intact side. On the prosthesis side, the knee flexion angle during stance was absent, while on the intact side it was larger than normal. The ankle range of motion was small on the prosthesis side, and larger than normal on the intact side. The peak hip

moment extension moment on the prosthesis side was larger than normal and the able-bodied solution. The peak knee extension moment was absent on the prosthesis side, but similar to normal on the intact side. The ankle moment was slightly lower than normal on the prosthesis side, while on the intact side there was a peak in early stance which is absent in normal gait.

Figure 48 shows the muscle stimulations of the Vasti and Hamstrings for the prosthesis side of the TTA solution, and the corresponding leg in the able-bodied solution. The Hamstrings and Vasti were both active longer during early and mid stance, and the Hamstrings activity also increased. The co-contraction index for the first 40% of the gait cycle was equal to 33% for the able-bodied solution, and 63% for the TTA solution, which indicates more co-contraction in the TTA configuration. The second solution of the TTA gait found 69% co-contraction. The solution in chapter III with no joint moment symmetry objective had a co-contraction index of 42%.

Figure 49 shows the muscle stimulations of the Vasti and Hamstrings for the prosthesis side of the TTA solution in the deterministic environment and in the stochastic environment. The activation of the Hamstrings was higher in the stochastic environment, compared to the deterministic environment. Both the Hamstrings and the Vasti were also active longer, the Vasti for 40% of the gait cycle, instead of 25%, and the Hamstrings were active until 65% of the gait cycle, compared to 45% in the deterministic environment. The co-contraction index was 67% for TTA gait in the deterministic environment.

6.6.3 Discussion

The goal of this work was to see if in a stochastic environment, co-contraction of the thigh muscles on the prosthesis side is optimal with respect to minimizing muscular effort. By optimizing for muscular effort only in a stochastic environment, it was shown that the co-contraction index in the first 40% of the gait cycle was higher in a simulation of TTA gait than in a simulation of able-bodied gait. This result is similar to Powers et al., who

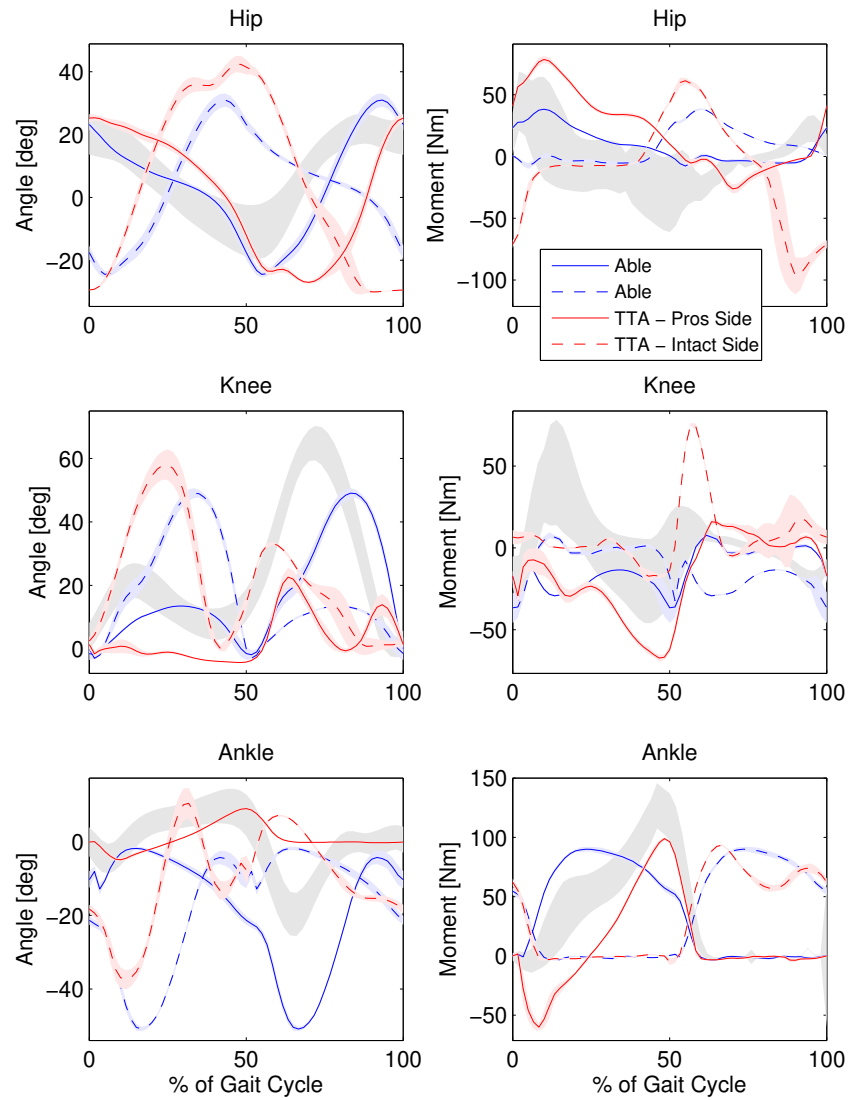


Figure 47: Average joint angles (left) and moments (right) for a gait cycle for the able bodied solution (blue) and TTA solution (red). Dashed line shows the intact side, solid line the prosthesis side. The colored fill around the lines shows the standard deviation over 10 gait cycles, while the grey fill shows normal walking data [2].

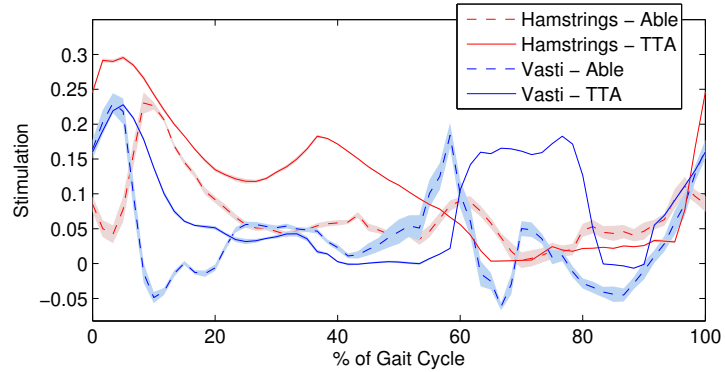


Figure 48: Average muscle stimulation of the Vasti (blue) and Hamstrings (red) for the prosthesis side of the TTA simulation (solid line) and the corresponding leg in the able-bodied solution (dashed line). The fill indicates the standard deviation over 10 gait cycles.

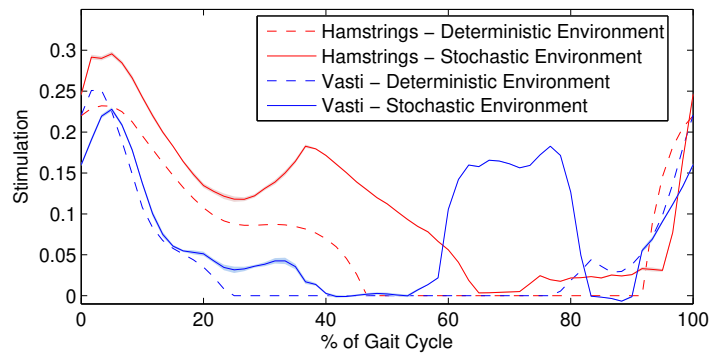


Figure 49: Average muscle stimulation of the Vasti (blue) and Hamstrings (red) for the prosthesis side of the TTA simulation in the stochastic environment (solid line) and in the deterministic environment (dashed line). The fill indicates the standard deviation over 10 gait cycles.

also showed that the hamstrings in TTA gait were stimulated more, while both the Vasti and Hamstrings were active longer during initial and mid-stance [11]. The simulation in the stochastic environment was solved twice with similar result, which showed that the solution was likely not a local optimum.

The co-contraction index in TTA gait was also higher in a simulation in a stochastic environment than in a simulation of TTA gait in a deterministic environment with an objective of muscular effort and tracking. The co-contraction index was similar for TTA gait in a deterministic environment. However, figure 49 indicated higher and longer activation in the stochastic environment, which was the expected result that was also seen by Powers et al. [11]. The co-contraction index was high for this solution because the activation levels were more similar, but this did not take into account the higher activation levels.

With no tracking in the objective function, the resulting gait cycle was not as realistic as when tracking is used (see chapter III). It was decided to not use tracking to rule out that the amount of co-contraction increased because the simulation attempted to walk normally, instead of minimizing effort. Possibly, a more realistic gait cycle could be found when minimizing for metabolic cost instead of effort. Also, other objectives could be considered, such as minimization of head motion.

The chosen controller could also have influenced the results. The feedback gains were the same in each muscle and were of the order 10^{-2} in the optimal solution. This could be because the noise amplitude was small (10 Nm, while previously 100 Nm was used). It was found in section 6.5 that the feedback gain increased with the amplitude of the noise. The smaller order of magnitude of the feedback gains could also be explained by the design of the control law, with only two free variables. This might have limited the optimization. Both the low noise amplitude and the control law where chosen to limit the computation time. The low noise amplitude reduced the number of problems that should be solved, while the control law limited the number of gait cycles. It is possible that this control law was too limiting for the problem. The effect of the controller on the gait cycle should be

further explored, since more control freedom might yield a different optimal solution.

The gait cycles in this section were found using a gait cycle in a deterministic environment that minimized effort as initial guess. Depending on the initial guess and the addition of regularization, different solutions to this problem were found. However, it was found that the able-bodied solution in the stochastic environment was similar when different solutions found in the deterministic environment were used as initial guess.

This work did not take into account the instability of the connection between the prosthesis and the residual leg. Instead, noise was added to the joint moments. This simulated noisy neural control. It is expected that the effect of an unstable connection between the prosthesis and residual leg has a similar effect on the knee on the prosthesis side. However, the instability of this connection, and the lack of sensory feedback, are likely important causes of gait adaptations. The effect of these should be accounted for in future work.

Noise was not added to the ankle joints. It would be unrealistic to add to the prosthesis, because there is no neuromuscular control. It was decided to also not add it to the ankle joint on the intact side, because it was found in the section 6.5 that noise at the ankle would create unrealistic motion of the foot.

6.7 Conclusion

This chapter introduced a method to solve trajectory optimization problems in a stochastic environment. It was shown that optimal trajectories of human movements are affected by the stochastic environment. Therefore, this method can be used to explain certain human motor control behavior, which could not be explained by trajectory optimizations in a deterministic environment. Specifically, the method was used to show that for certain tasks, co-contraction of muscles to stiffen a joint minimizes muscular effort in a stochastic environment. We also showed that nonzero foot clearance is optimal in gait in a stochastic environment. Finally, it was applied to TTA gait to analyze co-contraction of the thigh muscles on the prosthesis side. The results indicated that uncertainty in the environment

could explain this co-contraction, however the methods should be further improved before this conclusion can be made.

6.8 References

- [1] K Falconer and DA Winter. Quantitative assessment of co-contraction at the ankle joint in walking. *Electromyography and Clinical Neurophysiology*, 25(2-3):135, 1985.
- [2] DA Winter. *Biomechanics and motor control of human movement*. John Wiley & Sons, 2005.
- [3] AD Koelewijn and AJ van den Bogert. Joint contact forces can be reduced by improving joint moment symmetry in below-knee amputee gait simulations. *Gait & Posture*, 49:219–225, 2016.
- [4] CL Dembia, A Silder, TK Uchida, JL Hicks, and SL Delp. Simulating ideal assistive devices to reduce the metabolic cost of walking with heavy loads. *PloS one*, 12(7):e0180320, 2017.
- [5] DJJ Bregman, MM Van der Krog, V De Groot, J Harlaar, M Wisse, and SH Collins. The effect of ankle foot orthosis stiffness on the energy cost of walking: a simulation study. *Clinical Biomechanics*, 26(9):955–961, 2011.
- [6] AJ van den Bogert, M Hupperets, H Schlarb, and B Krabbe. Predictive musculoskeletal simulation using optimal control: effects of added limb mass on energy cost and kinematics of walking and running. *Proceedings of the Institution of Mechanical Engineers, Part P: Journal of Sports Engineering and Technology*, pages 1–11, 2012.
- [7] TW Dorn, JM Wang, JL Hicks, and SL Delp. Predictive simulation generates human adaptations during loaded and inclined walking. *PloS one*, 10(4):e0121407, 2015.

- [8] RH Miller, SCE Brandon, and KJ Deluzio. Predicting sagittal plane biomechanics that minimize the axial knee joint contact force during walking. *Journal of Biomechanical Engineering*, 135(1):011007, 2013.
- [9] M Ackermann and AJ van den Bogert. Optimality principles for model-based prediction of human gait. *Journal of Biomechanics*, 43(6):1055–1060, 2010.
- [10] E Isakov, O Keren, and N Benjuya. Trans-tibial amputee gait: Time-distance parameters and EMG activity. *Prosthetics and Orthotics International*, 24(3):216–220, 2000.
- [11] CM Powers, S Rao, and J Perry. Knee kinetics in trans-tibial amputee gait. *Gait & Posture*, 8(1):1–7, 1998.
- [12] DA Winter. Foot trajectory in human gait: a precise and multifactorial motor control task. *Physical Therapy*, 72(1):45–53, 1992.
- [13] MJ Hiley and MR Yeadon. Investigating optimal technique in a noisy environment: application to the upstart on uneven bars. *Human Movement Science*, 32(1):181–191, 2013.
- [14] M Kim and SH Collins. Once-per-step control of ankle-foot prosthesis push-off work reduces effort associated with balance during walking. *Journal of Neuroengineering and Rehabilitation*, 12(1):1, 2015.
- [15] JM Donelan, DW Shipman, R Kram, and AD Kuo. Mechanical and metabolic requirements for active lateral stabilization in human walking. *Journal of Biomechanics*, 37 (6):827–835, 2004.
- [16] J Davis. Undersomersaults on parallel bars. *Gym Craft*, 14:6–7, 2005.
- [17] T Yamasaki, K Gotoh, and X Xin. Optimality of a kip performance on the high

- bar: An example of skilled goal-directed whole-body movement. *Human Movement Science*, 29(3):464–482, 2010.
- [18] N Hogan. Impedance control: An approach to manipulation: Part IIimplementation. *Journal of Dynamic Systems, Measurement, and Control*, 107(1):8–16, 1985.
- [19] RD Crowninshield and RA Brand. A physiologically based criterion of muscle force prediction in locomotion. *Journal of Biomechanics*, 14(11):793–801, 1981.
- [20] W Herzog and P Binding. Predictions of antagonistic muscular activity using nonlinear optimization. *Mathematical Biosciences*, 111(2):217–229, 1992.
- [21] RE Hughes and DB Chaffin. Conditions under which optimization models will not predict coactivation of antagonist muscles. *Journal of Biomechanics*, 21(10):862, 1988.
- [22] W Herzog and P Binding. Cocontraction of pairs of antagonistic muscles: analytical solution for planar static nonlinear optimization approaches. *Mathematical Biosciences*, 118(1):83–95, 1993.
- [23] S Hirokawa, M Solomonow, Z Luo, Y Lu, and R D’ambrosia. Muscular co-contraction and control of knee stability. *Journal of Electromyography and Kinesiology*, 1(3):199–208, 1991.
- [24] Z Jiang and GA Mirka. Application of an entropy-assisted optimization model in prediction of agonist and antagonist muscle forces. In *Proceedings of the Human Factors and Ergonomics Society Annual Meeting*, volume 51, pages 923–927. SAGE Publications Sage CA: Los Angeles, CA, 2007.
- [25] LPJ Selen, PJ Beek, and JH van Dieën. Can co-activation reduce kinematic variability? a simulation study. *Biological Cybernetics*, 93(5):373–381, 2005.

- [26] E Forster, U Simon, P Augat, and L Claes. Extension of a state-of-the-art optimization criterion to predict co-contraction. *Journal of Biomechanics*, 37(4):577–581, 2004.
- [27] Stephen HM Brown and Jim R Potvin. Constraining spine stability levels in an optimization model leads to the prediction of trunk muscle cocontraction and improved spine compression force estimates. *Journal of Biomechanics*, 38(4):745–754, 2005.
- [28] Emanuel Todorov. Stochastic optimal control and estimation methods adapted to the noise characteristics of the sensorimotor system. *Neural computation*, 17(5):1084–1108, 2005.
- [29] HJ Kappen. Linear theory for control of nonlinear stochastic systems. *Physical Review Letters*, 95(20):200201–1–200201–4, 2005.
- [30] E Todorov. Finding the most likely trajectories of optimally-controlled stochastic systems. In *World Congress of the International Federation of Automatic Control (IFAC)*, pages 4728–4734, 2011.
- [31] H Tiesler, RM Kirby, D Xiu, and T Preusser. Stochastic collocation for optimal control problems with stochastic pde constraints. *SIAM Journal on Control and Optimization*, 50(5):2659–2682, 2012.
- [32] A Sandu, C Sandu, and M Ahmadian. Modeling multibody systems with uncertainties. part I: Theoretical and computational aspects. *Multibody System Dynamics*, 15(4):369–391, 2006.
- [33] Y Matsuno, T Tsuchiya, J Wei, I Hwang, and N Matayoshi. Stochastic optimal control for aircraft conflict resolution under wind uncertainty. *Aerospace Science and Technology*, 43:77–88, 2015.
- [34] N Wiener. The homogeneous chaos. *American Journal of Mathematics*, 60(4):897–936, 1938.

- [35] C Sandu, A Sandu, and M Ahmadian. Modeling multibody systems with uncertainties. part II: Numerical applications. *Multibody System Dynamics*, 15(3):241–262, 2006.
- [36] J Hays, A Sandu, C Sandu, and D Hong. Parametric design optimization of uncertain ordinary differential equation systems. *Journal of Mechanical Design*, 134(8):081003, 2012.
- [37] A Wächter and LT Biegler. On the implementation of an interior-point filter line-search algorithm for large-scale nonlinear programming. *Mathematical Programming*, 106(1):25–57, 2006.
- [38] AL Schwab and M Wisse. Basin of attraction of the simplest walking model. In *Proceedings of the ASME Design Engineering Technical Conference*, volume 6, pages 531–539, 2001.
- [39] DA Winter. *Biomechanics and motor control of human gait: normal, elderly and pathological*. University of Waterloo Press, 2 edition, 1991.
- [40] Ohio Supercomputer Center. Ohio supercomputer center. <http://osc.edu/ark:/19495/f5s1ph73>, 1987.
- [41] AR Wu and AD Kuo. Determinants of preferred ground clearance during swing phase of human walking. *Journal of Experimental Biology*, 219(19):3106–3113, 2016.
- [42] RJ Zmitrewicz, RR Neptune, and K Sasaki. Mechanical energetic contributions from individual muscles and elastic prosthetic feet during symmetric unilateral transtibial amputee walking: a theoretical study. *Journal of Biomechanics*, 40(8):1824–1831, 2007.
- [43] E Kellis, F Arabatzi, and C Papadopoulos. Muscle co-activation around the knee

in drop jumping using the co-contraction index. *Journal of Electromyography and Kinesiology*, 13(3):229–238, 2003.

CHAPTER VII

CONCLUSION

Predictive simulations have the potential to improve design of prostheses, since they can be used to analyze the effect of the prosthesis on gait in simulation. Therefore, this dissertation applied predictive simulations to increase understanding of gait of persons with a transtibial amputation (TTA gait) and improved the quality of predictive simulation. Four aims were defined:

- **Aim 1: Application** - Explain joint moment asymmetry in the knee and hip in TTA gait using predictive simulations
- **Aim 2: Application** - Compare the effect of different prosthesis alignments on TTA gait
- **Aim 3: Improvement** - Compare the gait objective of metabolic energy minimization to muscular effort minimization
- **Aim 4: Improvement** - Propose an approach to solve predictive simulations in a stochastic environment and implement it to explain certain behaviors that are seen in human movement

In chapter III, it was shown that joint moment asymmetry in gait of persons with a transtibial amputation could be explained by the human intention to walking energy efficiently. In chapter IV, predictive simulations were solved for different prosthesis alignments. It was shown that a flexion alignment change reduced metabolic cost and joint

reaction loads, and that a lateral translation or an external rotation reduced the knee adduction reaction moment without affecting other gait parameters, which could alleviate skin problems due to a reduction in skin stresses. Since subject studies on prosthesis alignment are very limited, this comprehensive study could be seen as a starting point for future experimental studies. In chapter V, it was found that the metabolic energy expenditure models by Lichtwark and Wilson [1] and Bhargava et al. [2] correlate best with metabolic cost from pulmonary gas exchange measurements, while the model by Houdijk et al. [3] correlated only slightly worse. When a predictive simulation is solved with metabolic cost as objective, the joint angles become more realistic compared to a predictive simulation minimizing muscular effort, but the joint moments and joint forces are more realistic when effort is minimized. Finally, in chapter VI, a method was introduced to solve predictive simulations of gait in a stochastic environment. It was shown that for certain tasks, co-contraction is optimal in a stochastic environment, and that foot clearance is larger in a stochastic environment than in a deterministic environment. Finally, it was applied to TTA gait. The result indicates that in a stochastic environment co-contraction in the upper leg on the prosthesis side in TTA gait is optimal with respect to muscular effort, but these results might be affected by the chosen controller.

7.1 Future Perspective

Predictive simulations could become an integral part of design of assistive devices as computer power increases, and musculoskeletal models will become increasingly realistic. Before this will happen, there should be a track record of scientific questions that were answered correctly using predictive simulation to show that the method works. This dissertation is part of this effort.

In order to produce realistic predictions, predictive simulations currently require tracking of normal gait data as a secondary objective, next to minimization of effort. This dissertation aimed to remove the necessity of tracking gait data by using metabolic energy

minimization as objective, and by accounting for uncertainty in the environment. However, these methods did not improve the accuracy of the simulations as much as desired. Therefore, at this point data tracking is still required. However, it would be worthwhile to attempt to improve predictive simulations by improving the ground-contact model. Also, the stochastic optimization approach should be explored further.

When tracking data, it is possible that the result is influenced by the data that is used, which is why it is desired to not use data. However, if tracking data is required, further work should aim to reduce the influence of the data as much as possible. One option would be to identify and track parameters that describe a more general walking motion, instead of data taken from a specific person. For example, principal component analysis could be employed to extract the so-called principal components, and these could be tracked instead of tracking joint angles, ground reaction forces, and gait cycle duration to create a more general solution.

Further studies in different directions should be performed before predictive simulation will be integrated in design of interventions. One of these directions is the optimization of a device for a specific patient, for example the stiffness of a prosthesis. Together with a technique like 3D printing, a personalized prosthesis can be created for every patient in a cost-effective way. Another direction is personalization of the models, since the importance of this is unclear. It should be investigated if changing the weight and height of the model, or certain muscle parameters, improves the quality of the predictions. This will likely also be dependent on the application of the prediction.

A commercial application of predictive simulations could be in shoe design, starting with optimization of shoes of elite athletes. Currently, efforts are underway by several research groups to enable a runner to run a marathon in under two hours. That requires a personalized shoe that is as energy efficient as possible. A model personalized to the runner can predict the shoe parameters that lead to optimal performance. Similarly, predictive simulations can also be used in a store to help amateur runners decide on what shoe best

fits their needs. In the longer run, a three-dimensional model could also be used to define shoe parameters for other sports where ankle support during sideways motions can improve the participants' agility.

7.2 References

- [1] GA Lichtwark and AM Wilson. Is achilles tendon compliance optimised for maximum muscle efficiency during locomotion? *Journal of Biomechanics*, 40(8):1768–1775, 2007.
- [2] LJ Bhargava, MG Pandy, and FC Anderson. A phenomenological model for estimating metabolic energy consumption in muscle contraction. *Journal of Biomechanics*, 37(1):81–88, 2004.
- [3] H Houdijk, MF Bobbert, and A De Haan. Evaluation of a Hill based muscle model for the energy cost and efficiency of muscular contraction. *Journal of Biomechanics*, 39(3):536–543, 2006.

APPENDIX A. Metabolic Models

This appendix describes the metabolic energy models that were used in chapter V. Note that some mention basal metabolic rate as part of the model. However, the models will be implemented without the basal metabolic rate, to have a fair comparison. Also, some models are normalized to mass, while others are not. In this dissertation, the nonnormalized energy rate is used.

All models use the following equation to calculate the metabolic rate for a motion:

$$J = \frac{1}{Tm} \int_{t=0}^T \sum_{i=1}^{N_{mus}} \dot{E}_i(t) dt \quad (1)$$

where T is the duration of the gait cycle, m the full mass, and \dot{E}_i the energy rate of the muscle i , or in case of the model by Kim and Roberts, the energy rate of joint i . The following sections describe how each model calculates the energy rate.

Metabolic Energy Model by Umberger et al.

Model Umberger determines the metabolic rate per muscle in W as follows:

if $l_{CE} \leq l_{CE(OPT)}$

$$\dot{E} = m_{mus}(\dot{h}_{AM}A_{AM}S + \dot{h}_{SL}S) - w \quad (2)$$

if $l_{CE} > l_{CE(OPT)}$

$$\dot{E} = m_{mus}((0.4\dot{h}_{AM} + 0.6\dot{h}_{AM}f(l_{CE}))A_{AM}S + \dot{h}_{SL}Sf(l_{CE})) - w$$

where \dot{h}_{AM} is the activation-maintenance heat rate, $A_{AM} = A^{0.6}$, and S is a scaling factor, equal to 1.5 in aerobic conditions. When the fiber length is longer than optimal, \dot{h}_{AM} is split up into two parts, 40% represents the activation heat rate, while 60% represents the activation heat rate, which is dependent on the location on the force-length relationship [1].

The following equation is used to find the activation-maintenance heat rate [1]:

$$h_{AM} = \begin{cases} 25 & a \leq f_{ST} \\ 128f_{FT} + 25 & a > f_{ST} \end{cases} \quad (3)$$

The shortening-lengthening heat rate, \dot{h}_{SL} is different for shortening and lengthening velocity and is determined as follows:

$$\dot{h}_{SL} = \begin{cases} (-\alpha_{S(ST)}\tilde{v}_{CE}(1 - f_{FT}) - \alpha_{S(FT)}\tilde{v}_{CE}f_{FT}) A^2 & \text{if } \tilde{v}_{CE} \leq 0 \\ \alpha_L \tilde{v}_{CE} A & \text{if } \tilde{v}_{CE} > 0 \end{cases} \quad (4)$$

where the first term, $\alpha_{S(ST)}\tilde{v}_{CE}(1 - f_{FT})$, cannot exceed 100 W/kg [1].

$\tilde{v}_{CE} = v_{CE}/l_{CE(OPT)}$ is the muscle fiber velocity in s^{-1} normalized to the optimal fiber length, $l_{CE(OPT)}$. $\alpha_{S(ST)} = 100/\tilde{v}_{CE(MAX-ST)}$ and $\alpha_{S(FT)} = 153/\tilde{v}_{CE(MAX-FT)}$ are the shortening heat coefficients for slow twitch (ST) and fast twitch (FT) fibers, respectively, in J/kg. They are dependent on the maximum fiber velocity of ST and FT fibers. $\alpha_L = 4\alpha_{S(ST)}$ is the lengthening heat coefficient, which is based on experimental data [1].

A is a scaling factors that depend on the stimulation and activation:

$$A = \begin{cases} u & \text{when } u > a \\ \frac{u+a}{2} & \text{when } u \leq a \end{cases} \quad (5)$$

Finally, the work is determined as follows [1]:

$$w = -F_{ce}v_{ce} \quad (6)$$

Metabolic Energy Model by Lichtwark and Wilson

Shortening velocity is positive in model Lichtwark [2]. This model calculates the metabolic rate as a sum of the heat rate, \dot{h} , and the work:

$$\dot{E} = \dot{h} + w \quad (7)$$

The heat rate is a sum of the shortening-lengthening heat rate and the maintenance heat rate:

$$\dot{h} = (0.3a\dot{h}_M + 0.7af(l_{CE})\dot{h}_M + af(l_{CE})\dot{h}_{SL}) \quad (8)$$

where 30% of the maintenance heat rate represents activation, which is only scaled by the activation [2].

The maintenance heat rate is determined as follows:

$$\dot{h}_M = \begin{cases} \gamma \frac{\tilde{v}_{CE(max)}}{G^2} & \text{if } v_{CE}(t) > 0 \\ 0.3\gamma \frac{\tilde{v}_{CE(max)}}{G^2} + 0.7\gamma \frac{\tilde{v}_{CE(max)}}{G^2} \exp(-7\tilde{v}_{CE(max)}(g(v_{CE}(t)) - 1)) & \text{if } v_{CE}(t) \leq 0 \end{cases} \quad (9)$$

where γ is a heat rate value that decays with the stimulation time, $G = 4$ is the curvature of the force-velocity curve, and $g(v_{CE})$ is the location on the force-velocity relationship [2].

γ is determined as follows [2]:

$$\gamma = 0.8 \exp(-0.72t_{stim}) + 0.175 \exp(-0.022t_{stim}) \quad (10)$$

The shortening-lengthening heat rate is determined as follows [2]:

$$\dot{h}_{SL} = \begin{cases} \frac{\tilde{v}_{CE}}{G} & \text{if } v_{CE} > 0 \\ -0.5g(v_{CE})v_{CE} & \text{if } v_{CE} \leq 0 \end{cases} \quad (11)$$

Finally, the work is determined as follows [2]:

$$w = F_{ce}v_{ce} \quad (12)$$

Metabolic Energy Model by Bhargava et al.

Bhargava et al. describe a model that calculates the muscular energy consumption as a sum of the activation heat rate, the maintenance heat rate, the shortening heat rate, and the work rate [3]:

$$\dot{E} = \dot{h}_a + \dot{h}_m + \dot{h}_s + w_{ce} \quad (13)$$

The activation heat rate is calculated as the sum as the portion due to FT and ST fibers [3]:

$$\dot{h}_a = \phi m \left(f_{FT} \dot{A}_{FT} u_{FT} + f_{ST} \dot{A}_{ST} u_{ST} \right) \quad (14)$$

where ϕ is a decay function, m is the muscle mass, $f_{FT/ST}$ is the mass fraction of FT and ST fibers, $\dot{A}_{FT} = 133$ W/kg and $\dot{A}_{ST} = 40$ W/kg are the activation heat rate constants for FT and ST fibers, and $u_{FT/ST}(t)$ are the stimulation levels of the FT and ST fibers. These levels are based on the stimulation of the full muscle as follows: [3]:

$$u_{FT}(t) = 1 - \cos \left(\frac{\pi}{2} u \right) \quad (15)$$

$$u_{ST}(t) = \sin \left(\frac{\pi}{2} u \right) \quad (16)$$

The decay function, ϕ , models the behavior that more heat is produced early during activation [4] and is determined as follows:

$$\phi = 0.06 + e^{-t_{stim} \frac{u}{\tau_\phi}} \quad (17)$$

where τ_ϕ is the decay time constant, 45 ms and t_{stim} is the time that the muscle was stimu-

lated over 10% [3].

The maintenance heat rate is also determined separately for FT and ST fibers as follows:

$$\dot{h}_m = L(\tilde{l}^M)m \left(f_{FT}\dot{M}_{FT}u_{FT} + f_{ST}\dot{M}_{ST}u_{ST} \right) \quad (18)$$

where $L(\tilde{l}^M)$ models the dependence of the maintenance heat rate on muscle length [5] (see Fig. 2 in [3]), and $\dot{M}_{FT} = 111 \text{ W/kg}$ and $\dot{M}_{ST} = 74 \text{ W/kg}$ are the maintenance heat rate constants for FT and ST fibers [3].

The shortening heat rate is proportional to the shortening velocity [6] as follows:

$$\dot{h}_s = -\alpha v_{ce} \quad (19)$$

where α is a constant. For shortening, the constant is dependent on the isometric force at the current length and activation level, $a_f(l_{ce})F_{iso}$ and the actual force, F_{ce} , [3], while for lengthening, it is only dependent on the actual force [7]:

$$\alpha = 0.16a_f(l_{ce})F_{ISO} + 0.18F_{ce} \quad v_{ce} \leq 0 \quad (20)$$

$$\alpha = 0.157F_{ce} \quad v_{ce} > 0 \quad (21)$$

Finally, the work is determined as follows [3]:

$$w_{ce} = -F_{ce}v_{ce} \quad (22)$$

Metabolic Energy Model by Houdijk et al.

Model Houdijk [8] calculates the metabolic rate in W as a sum of the activation heat rate, h_A , the maintenance heat rate, h_M , the shortening/lengthening heat rate, h_{SL} , and the

work, w .

$$\dot{E} = \dot{h}_A + \dot{h}_M + \dot{h}_{SL} + w \quad (23)$$

The activation heat rate is determined as follows:

$$\dot{h}_A = m_{mus} \bar{h}_A \nu \frac{1 - \exp(-0.25 - \frac{18.2}{\nu \nu_{max}})}{1 - \exp(-0.25 - \frac{18.2}{\nu_{max}})} \quad (24)$$

where \bar{h}_A is the activation heat rate constant, $\nu = a(t)^2$ is the relative stimulation frequency, and $\nu_{max} = k_1 + k_2 a$ is the maximum stimulation frequency. These constants are defined for ST and FT fibers and calculated for each muscles by taking the product of the constant for ST fibers and the percentage of ST fibers, and adding to this the product of the constant for FT fibers and the percentage of FT fibers. These values are given in table X [8].

The maintenance heat rate is determined as follows:

$$\dot{h}_M = m_{mus} (\bar{h}_A + \bar{h}_M) a \left(f(l_{CE}) - \frac{\bar{h}_A}{\bar{h}_A + \bar{h}_M} \right) \quad (25)$$

where \bar{h}_M is the maintenance heat rate constant, different for ST and FT fibers, as given in table X [8].

The shortening-lengthening heat rate is calculated as follows:

$$\dot{h}_{SL} = \bar{h}_{SL} a f(l_{CE}) - v_{CE} \quad \text{where: } v_{CE} < 0 \quad (26)$$

where \bar{h}_{SL} is given in table X for ST and FT fibers [8].

Finally, the work is determined as follows [3]:

$$w = -F_{ce} v_{ce} \quad (27)$$

Table X: Constants for slow twitch and fast twitch fibers.

Variable	Fast twitch	slow twitch
h_A	52.5 W/kg	10.98 W/kg
\bar{h}_M	97.5 W/kg	13.42 W/kg
k_1	12	6
k_2	14	8
\bar{h}_{SL}	$0.28 F_{max}$	$0.16 F_{max}$

Metabolic Energy Model by Kim and Roberts

Model Kim does not use muscle states, but calculates the metabolic rate based on joint moments and angular velocities. The metabolic rate is still the sum of the heat rate and the work [9]:

$$\dot{E} = h + p \quad (28)$$

where the power, p , is the product of the joint moment and angular velocity [9]:

$$p_i = M_i \dot{q}_i \quad (29)$$

where M is the joint moment at joint i and the heat rate is determined as follows [9]:

$$h_i = h_M \dot{q}_{i(max)} |M_i| + h_{SL} |M_i \dot{q}_i| + \dot{q}_{cc} (M_i \dot{q}_i)_{max} \quad (30)$$

where $h_M = 0.054$ is the heat rate for activation and maintenance, $h_{SL} = 0.283$ is the shortening-lengthening heat rate for positive power, and $h_{SL} = 1.423$ is the shortening-lengthening heat rate for negative power, and \dot{q}_{cc} is the co-contraction heat rate [9]. The maximum power and angular velocity during the gait cycle were used as maximum.

Metabolic Energy Model by Minetti and Alexander

Minetti and Alexander predict metabolic energy of walking as a function of muscle fiber velocity and activation. The metabolic energy is determined as follows [10]:

$$\dot{E} = a F_{ISO} v_{CE(max)} \phi \quad (31)$$

$$\text{where } \phi = \frac{0.054 + 0.506 \bar{v}_{CE} + 2.46 \bar{v}_{CE}^2}{1 - 1.13 \bar{v}_{CE} + 12.8 \bar{v}_{CE}^2 - 1.64 \bar{v}_{CE}^3} \quad (32)$$

where \bar{v}_{CE} is the ratio of the contractile element velocity to the maximum contractile element velocity [10].

Metabolic Energy Model by Margaria

This is a very simple observation that when walking uphill, muscles have an efficiency of 25 %, while muscles have an efficiency of 120 % when walking downhill. This can be related to muscle shortening and lengthening, creating the following metabolic energy model [11]:

$$\dot{E} = \begin{cases} -\frac{w}{0.25} & \text{if: } v_{CE} < 0 \\ \frac{w}{1.2} & \text{if: } v_{CE} \geq 0 \end{cases} \quad (33)$$

References

- [1] BR Umberger, KGM Gerritsen, and PE Martin. A model of human muscle energy expenditure. *Computer Methods in Biomechanics and Biomedical Engineering*, 6(2): 99–111, 2003.
- [2] GA Lichtwark and AM Wilson. A modified Hill muscle model that predicts muscle power output and efficiency during sinusoidal length changes. *Journal of Experimental Biology*, 208(15):2831–2843, 2005.
- [3] LJ Bhargava, MG Pandy, and FC Anderson. A phenomenological model for estimat-

- ing metabolic energy consumption in muscle contraction. *Journal of Biomechanics*, 37(1):81–88, 2004.
- [4] E Homsher, WFHM Mommaerts, NV Ricchiuti, and A Wallner. Activation heat, activation metabolism and tension-related heat in frog semitendinosus muscles. *The Journal of Physiology*, 220(3):601, 1972.
- [5] WF Mommaerts. Energetics of muscular contraction. *Physiological Reviews*, 49(3):427–508, 1969.
- [6] AV Hill. The effect of load on the heat of shortening of muscle. *Proceedings of the Royal Society of London B: Biological Sciences*, 159(975):297–318, 1964.
- [7] BC Abbott and XM Aubert. Changes of energy in a muscle during very slow stretches. *Proceedings of the Royal Society of London B: Biological Sciences*, 139(894):104–117, 1951.
- [8] H Houdijk, MF Bobbert, and A De Haan. Evaluation of a Hill based muscle model for the energy cost and efficiency of muscular contraction. *Journal of Biomechanics*, 39(3):536–543, 2006.
- [9] JH Kim and D Roberts. A joint-space numerical model of metabolic energy expenditure for human multibody dynamic system. *International Journal for Numerical Methods in Biomedical Engineering*, 31(9), 2015.
- [10] AE Minetti and RMcN Alexander. A theory of metabolic costs for bipedal gaits. *Journal of Theoretical Biology*, 186(4):467–476, 1997.
- [11] R Margaria. Positive and negative work performances and their efficiencies in human locomotion. *Internationale Zeitschrift für angewandte Physiologie einschließlich Arbeitsphysiologie*, 25(4):339–351, 1968.

APPENDIX B. Results of Single Joint Reaching Task with Model Bhargava, Model Houdijk, and Model Lichtwark

This appendix shows the results of the pendulum problem that was solved in section 5.3.1 for the other three models: model Bhargava (figure 50), model Houdijk (figure 51), and model Lichtwark (figure 52).

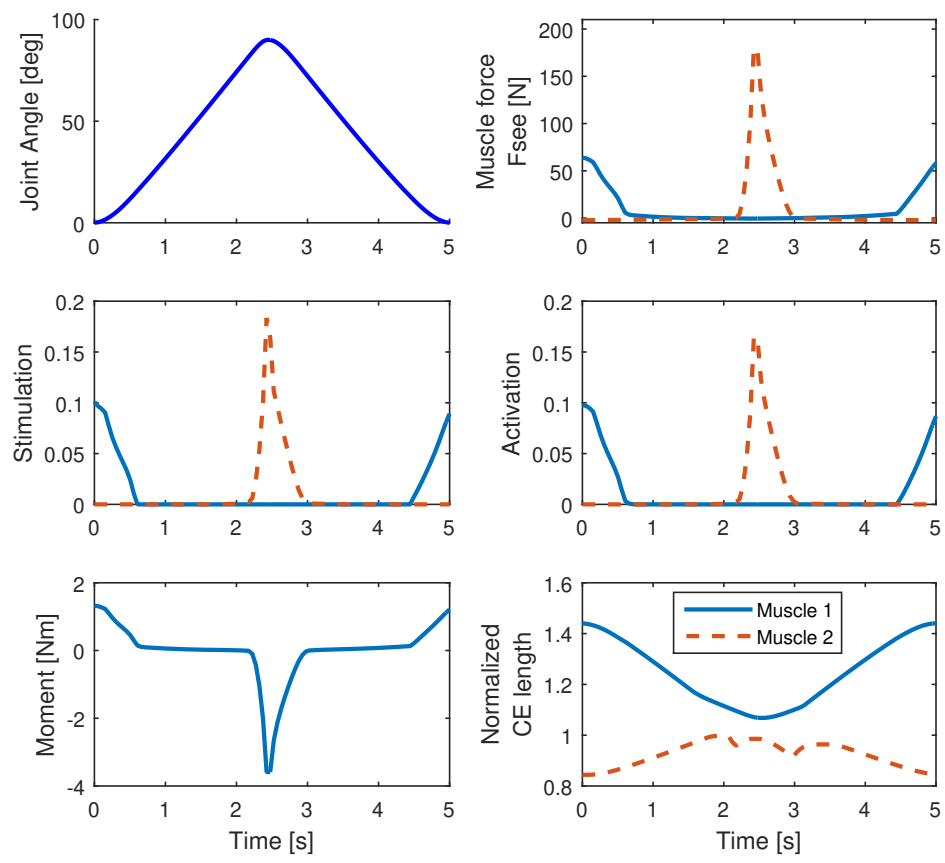


Figure 50: Optimal trajectory for the single arm reaching task, minimizing metabolic energy using model Bhargava.

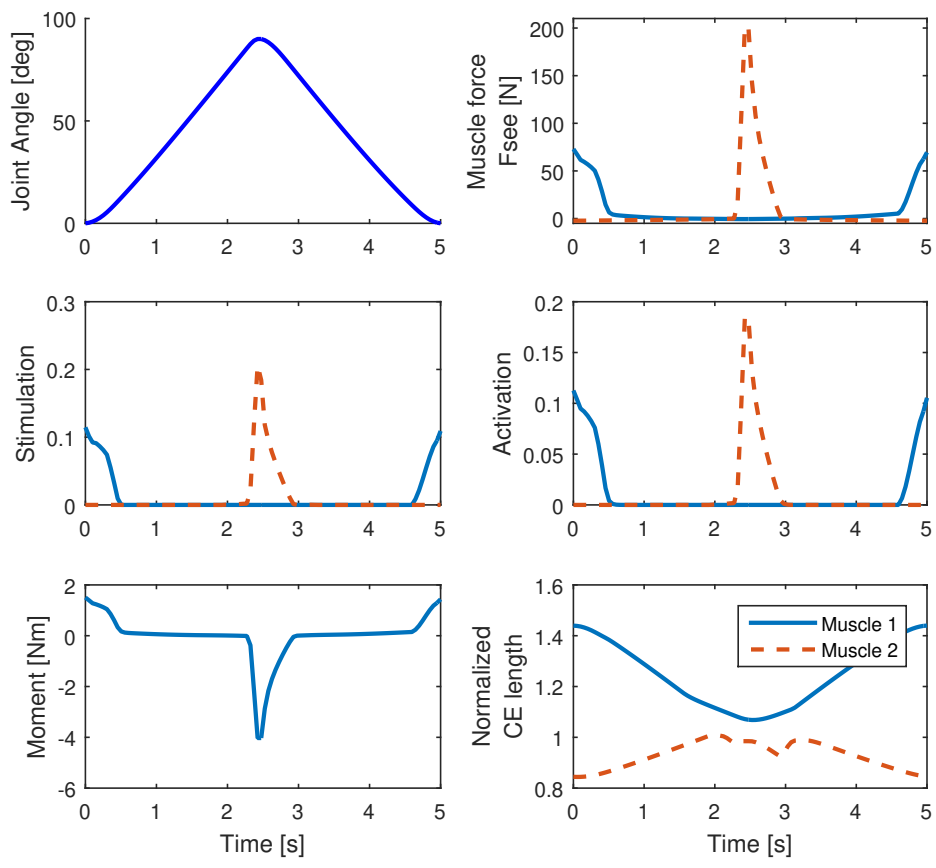


Figure 51: Optimal trajectory for the single arm reaching task, minimizing metabolic energy using model Houdijk.

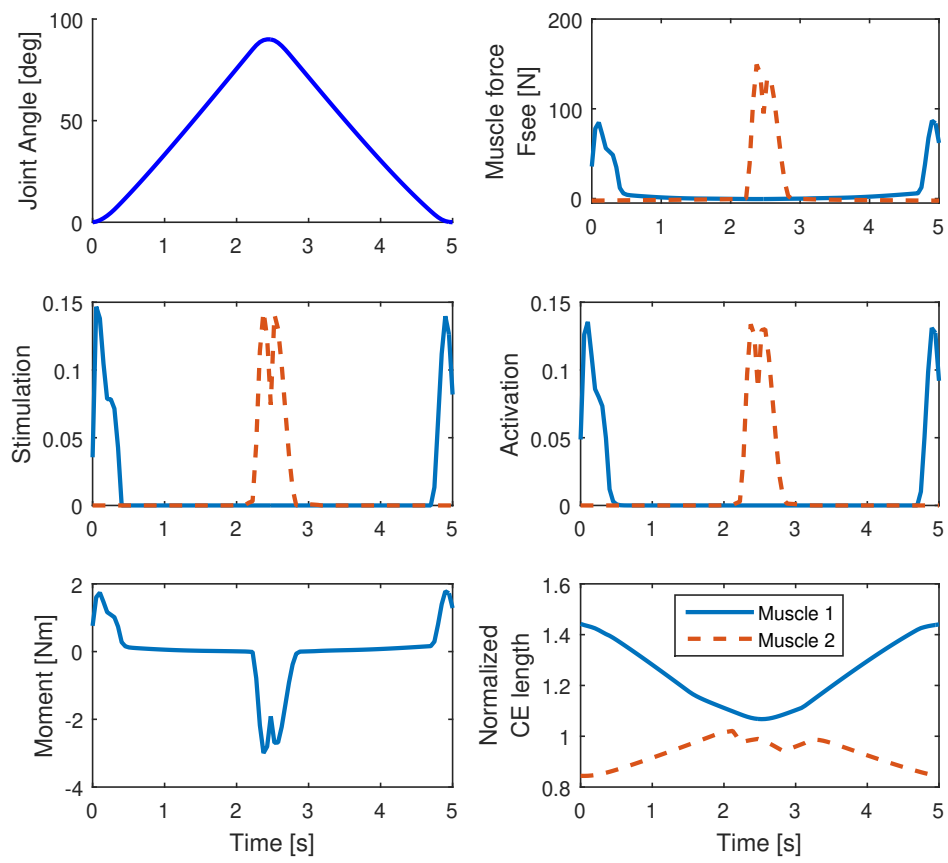


Figure 52: Optimal trajectory for the single arm reaching task, minimizing metabolic energy using model Lichtwark.

APPENDIX C. Continuous Version of Model Umberger

The model by Umberger et al. [1, 2] calculates the energy as a function of the heat rate from the activation of muscles and its maintenance, \dot{h}_{AM} , the heat rate due to shortening and lengthing of muscles, \dot{h}_{SL} , and the mechanical work rate, w_{CE} :

$$\dot{E}(t) = \dot{h}_{AM} + \dot{h}_{SL} + w_{CE} \quad (34)$$

The following equation is used to find the activation/maintenance heat rate \dot{h}_{AM} :

$$\dot{h}_{AM} = (0.4 + 0.6f(l_{CE}))\dot{\bar{h}}_{AM}A_{AM}S \quad (35)$$

where S is a factor equal to 1.5 for aerobic conditions [3], $A_{AM} = A^{0.6}$ is related to the activation and stimulation as described in equation 6 of the paper (see below), and $f(l_{CE})$ and $\dot{\bar{h}}_{AM}$ are determined as follows:

$$f(l_{CE}) = \begin{cases} 1 & l_{CE} \leq l_{CE(OPT)} \\ f(l_{CE}) & l_{CE} > l_{CE(OPT)} \end{cases} \quad (36)$$

$$\dot{\bar{h}}_{AM} = \begin{cases} 25 & a \leq ST \\ 128FT + 25 & a > ST \end{cases} \quad (37)$$

Equation 5.17 in chapter V:

$$A(t) = u(t) + \frac{1}{2} \left(\frac{a(t) - u(t)}{2} + \sqrt{\left(\frac{a(t) - u(t)}{2} \right)^2 + \varepsilon^2} \right), \quad (38)$$

where 128 W/kg and 25 W/kg are constants found using regression, $f(l_{CE})$ is the location on the force-length relationship of the muscle, and FT and ST are the ratios of fast-twitch and slow-twitch fibers in the muscle, respectively, $l_{CE(OPT)}$ is the optimal fiber length, and

$l_C E$ is the current fiber length.

When the fiber length is longer than optimal, \dot{h}_{AM} is split up into two parts, where 40% represents the activation heat rate and 60% the activation heat rate, which is dependent on the location on the force-length relationship [4]. This does not create a discontinuity in the equation, since the derivative of $f(l_{CE})$ is zero when the fiber length is optimal. Also, equation 37 is continuous since $\dot{\bar{h}}_{AM}$ is a constant.

The shortening-lengthening heat rate is calculated as follows:

$$\dot{h}_{SL} = A_{SL} \dot{\bar{h}}_{SL} f(l_{CE}) S \quad (39)$$

where A_{SL} is equal to A^2 , and $\dot{\bar{h}}_{SL}$ is determined as follows:

$$\dot{\bar{h}}_{SL} = \alpha_L \tilde{v}_{CE(l)} - \alpha_{FT} \tilde{v}_{CE(s)} FT + \begin{cases} 100 & \alpha_{ST} \tilde{v}_{CE(max)_{ST}} < -\alpha_{ST} \tilde{v}_{CE(S)} ST \\ -\alpha_{ST} \tilde{v}_{CE(S)} ST & \alpha_{ST} \tilde{v}_{CE(max)_{ST}} > -\alpha_{ST} \tilde{v}_{CE(S)} ST \end{cases} \quad (40)$$

where $\tilde{v}_{CE(l)}$ and $\tilde{v}_{CE(s)}$ are the shortening and lengthening velocities normalized to optimal fiber length, respectively. $\tilde{v}_{CE(max)_{ST}}$ is the normalized maximum shortening velocity for slow-twitch fibers, 4.8 fiber lengths per second. α_{ST} , α_{FT} and α_L are the shortening heat coefficients for slow-twitch and fast-twitch fibers in J/kg, and the lengthening heat coefficient, respectively:

$$\alpha_{ST} = \frac{100}{\tilde{v}_{CE(max)_{ST}}}, \quad \alpha_{FT} = \frac{153}{\tilde{v}_{CE(max)_{FT}}}, \quad \alpha_L = 0.3\alpha_{ST} \quad (41)$$

where $\tilde{v}_{CE(max)_{FT}}$ is the maximum shortening velocity for fast-twitch fibers, assumed to be 12 fiber lengths per second.

The shortening and lengthening velocities are determined as described in the paper:

$$\tilde{v}_{CE(l)} = \frac{1}{2} \left(\tilde{v}_{CE} + \sqrt{\tilde{v}_{CE}^2 + \varepsilon^2} \right) \quad (42)$$

$$\tilde{v}_{CE(l)} = \frac{1}{2} \left(\tilde{v}_{CE} - \sqrt{\tilde{v}_{CE}^2 + \varepsilon^2} \right) \quad (43)$$

Note that the term $\alpha_{ST}\tilde{v}_{CE(S)}ST$ for $\dot{\bar{h}}_{SL}$ cannot exceed 100 W/kg. However, this level is not reached during gait.

The work rate is determined as follows to ensure that it is never negative:

$$w_{CE} = \frac{1}{2} \left(w_{CE(or)} - \sqrt{w_{CE(or)}^2 + \varepsilon^2} \right) \quad (44)$$

where

$$w_{CE(or)} = -(F_{CE}v_{CE})/m_{mus} \quad (45)$$

where m_{mus} is the muscle mass, F_{CE} is the force in the contractile element, and v_{CE} is the fiber velocity, negative when shortening. ε is a small number, used to decrease the nonlinearity of the problem. For simplicity, the same value for ε is used for the shortening/lengthening velocity and the work rate.

The muscle mass is determined as follows:

$$m_{mus} = \frac{F_{max}\rho}{\sigma l_{CE(OPT)}} \quad (46)$$

where F_{max} is the maximum isometric force, σ is the maximum muscle stress, 250 kPa, ρ is the muscle density, 1059.7 kg/m³, and $l_{CE(OPT)}$ is the optimal fiber length.

References

- [1] BR Umberger, KGM Gerritsen, and PE Martin. A model of human muscle energy expenditure. *Computer Methods in Biomechanics and Biomedical Engineering*, 6(2):

99–111, 2003.

- [2] BR Umberger. Stance and swing phase costs in human walking. *Journal of the Royal Society Interface*, 7(50):1329–1340, 2010.
- [3] J González-Alonso, B Quistorff, P Krustrup, J Bangsbo, and B Saltin. Heat production in human skeletal muscle at the onset of intense dynamic exercise. *The Journal of Physiology*, 524(2):603–615, 2000.
- [4] E Homsher and CJ Kean. Skeletal muscle energetics and metabolism. *Annual Review of Physiology*, 40(1):93–131, 1978.

APPENDIX D. Five Best Solutions of Optimization Problems in Chapter V

The figures below show the five best solutions found from a random initial guess.

Model Umberger solved only three times, so this figure only shows three solutions.

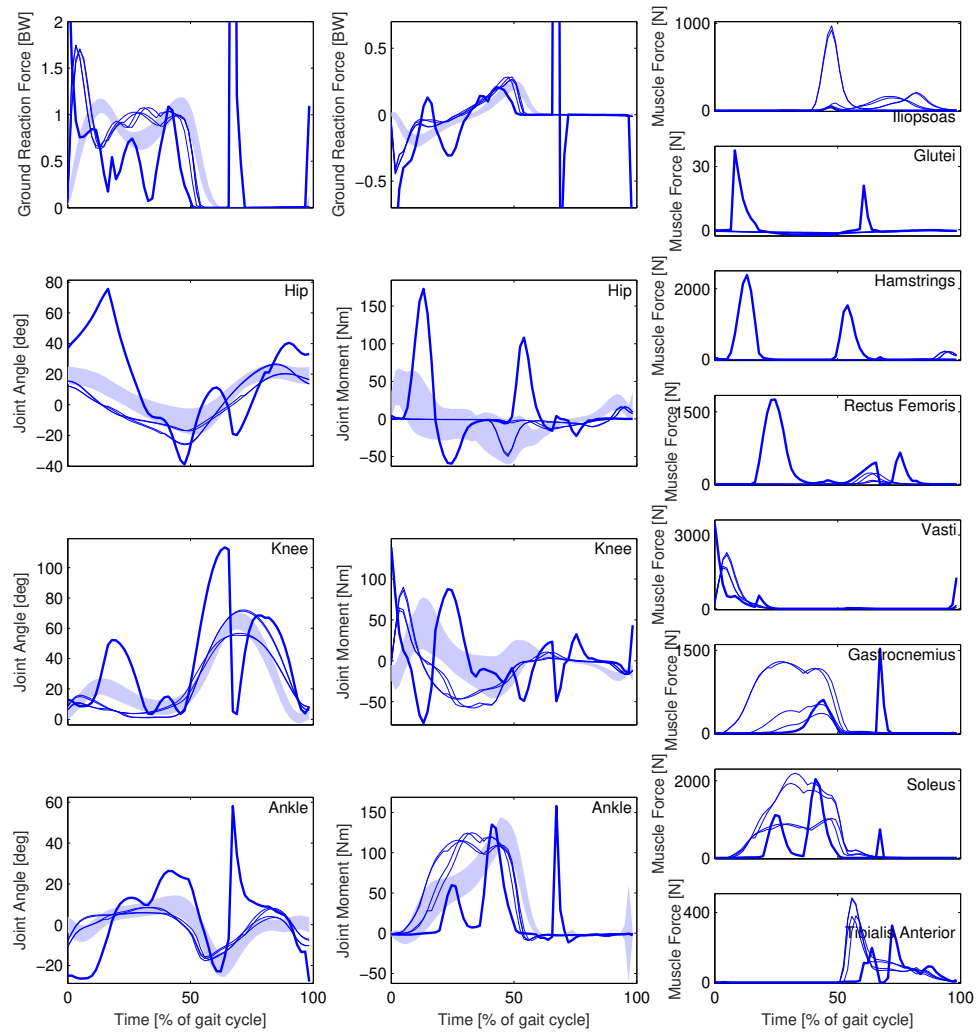


Figure 53: Ground reaction force, joint angles, moments, and muscle forces of the five solutions with the lowest objective found using model Lichtwerk. The fill shows normal data from Winter [1]

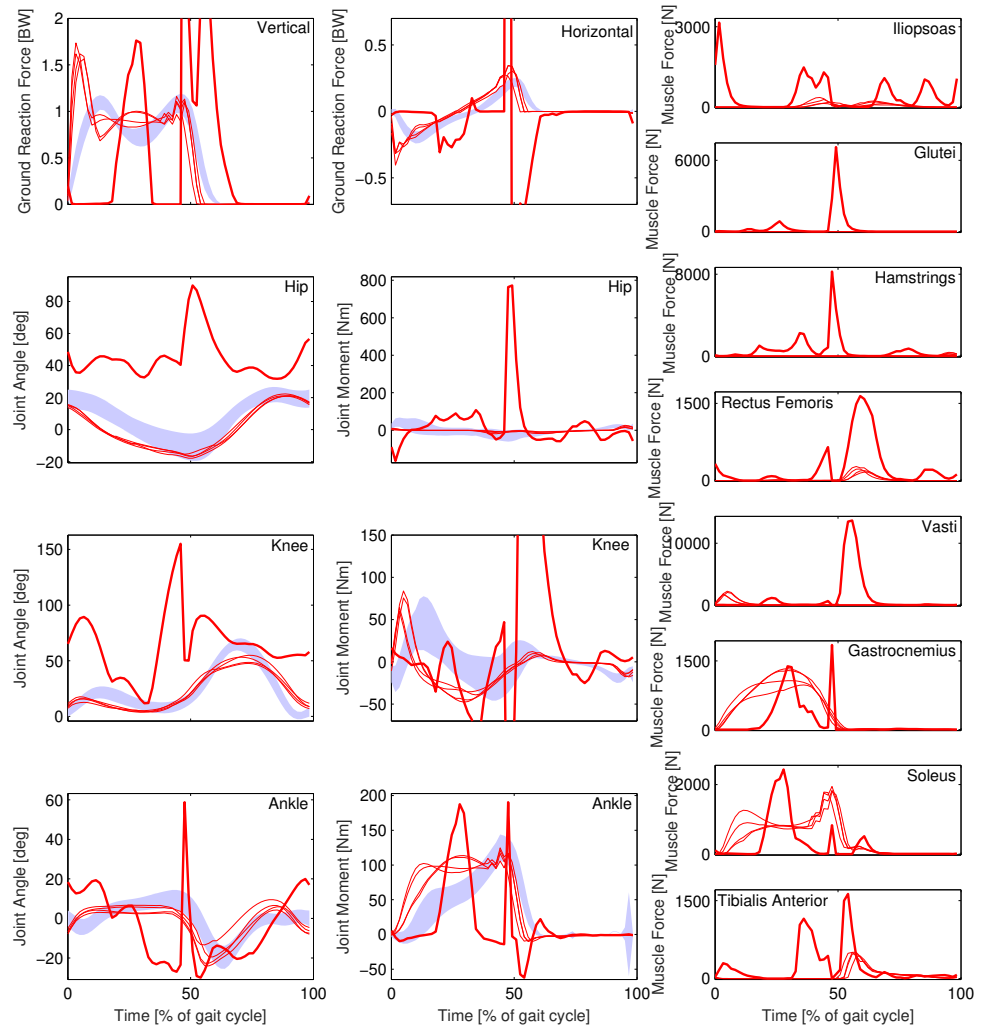


Figure 54: Ground reaction force, joint angles, moments, and muscle forces of the five solutions with the lowest objective found using model Bhargava. The fill shows normal data from Winter [1]

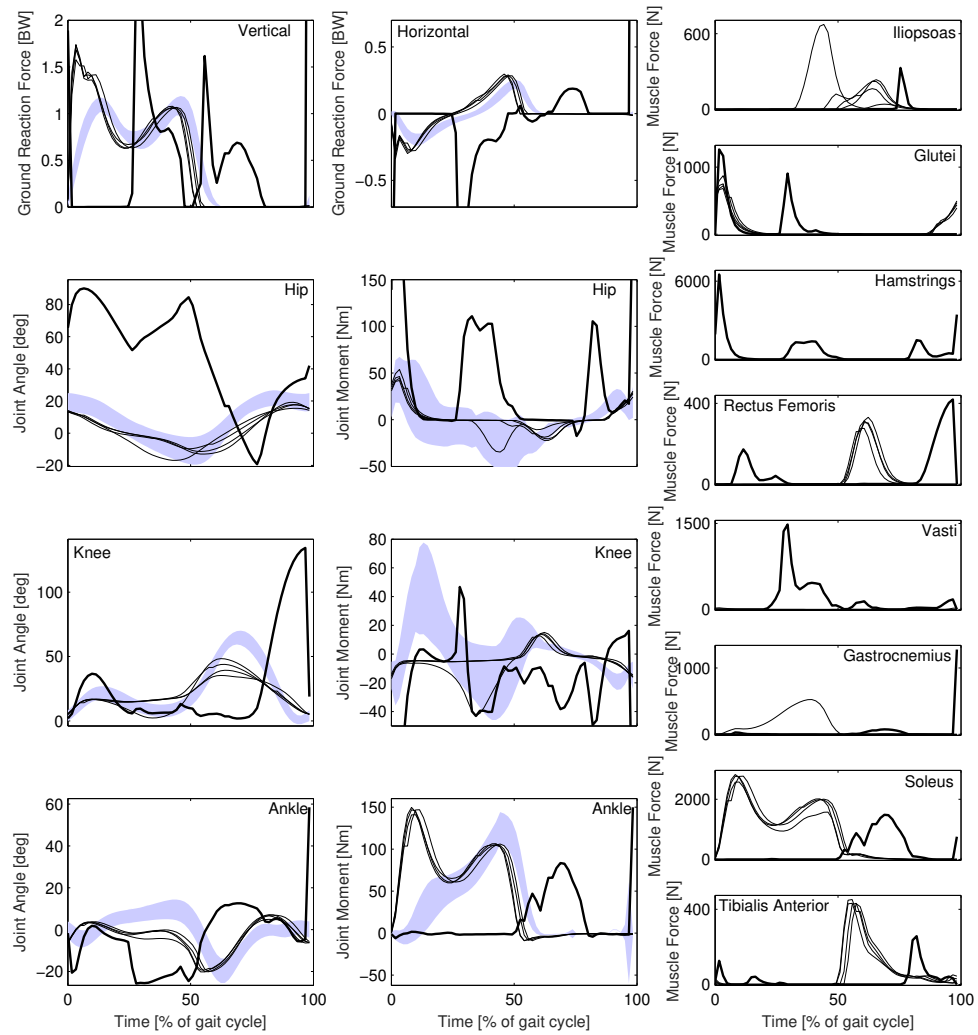


Figure 55: Ground reaction force, joint angles, moments, and muscle forces of the five solutions with the lowest objective found using model Houdijk. The fill shows normal data from Winter [1]

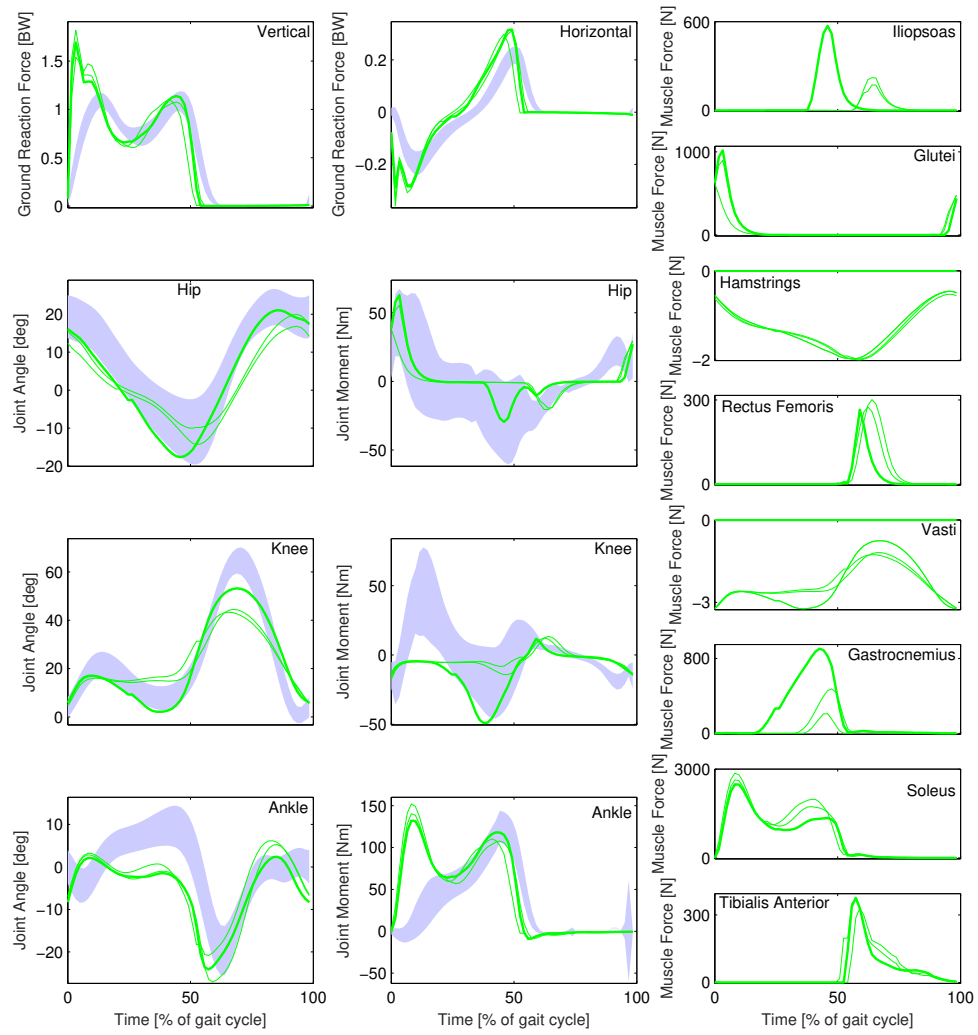


Figure 56: Ground reaction force, joint angles, moments, and muscle forces of the three solutions with the lowest objective found using model Umberger. The fill shows normal data from Winter [1]

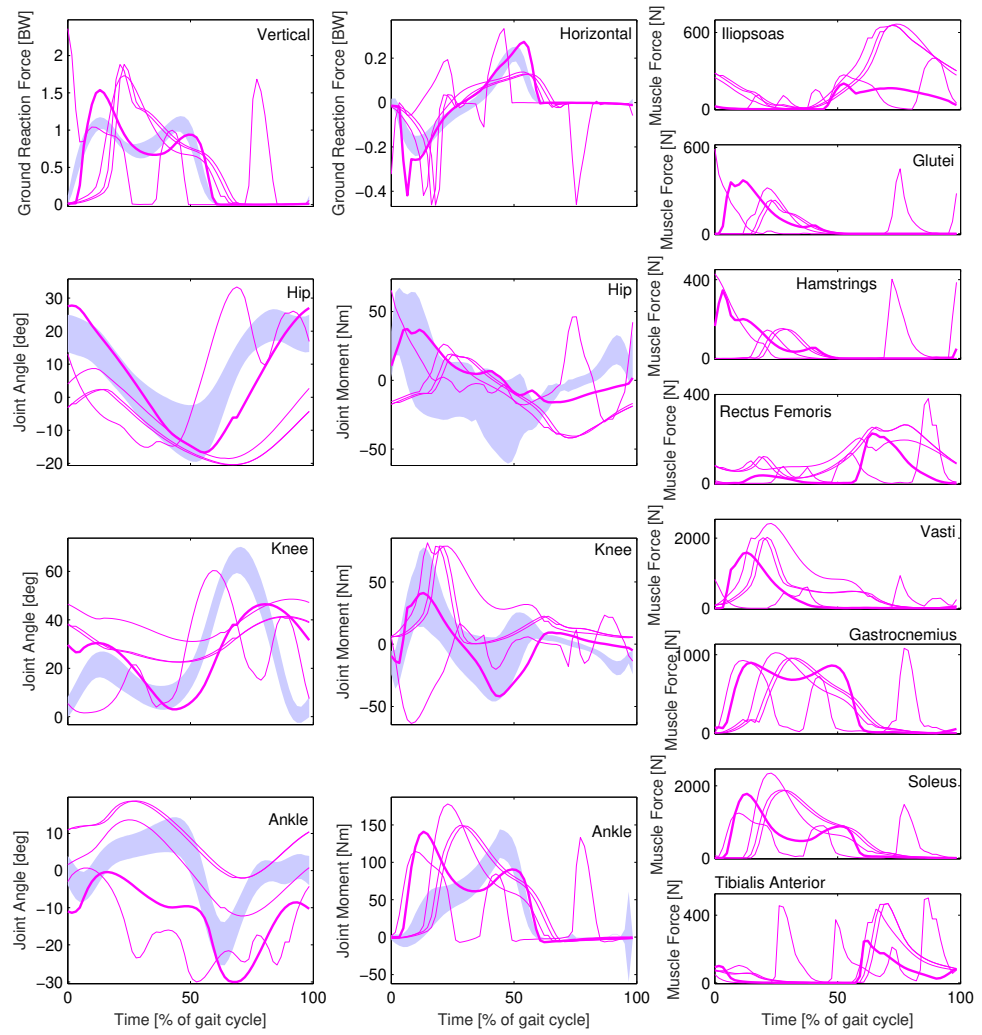


Figure 57: Ground reaction force, joint angles, moments, and muscle forces of the five solutions with the lowest objective found using effort minimization. The fill shows normal data from Winter [1]

References

- [1] DA Winter. *Biomechanics and motor control of human movement*. John Wiley & Sons, 2005.

APPENDIX E. Marker Placement

This appendix describes the marker placement for the experiment described in chapter V. These markers are used to obtain the joint angles and moments. Table XI describes the location of each marker on the body. Figure 58 shows the location of the markers on a human skeleton.

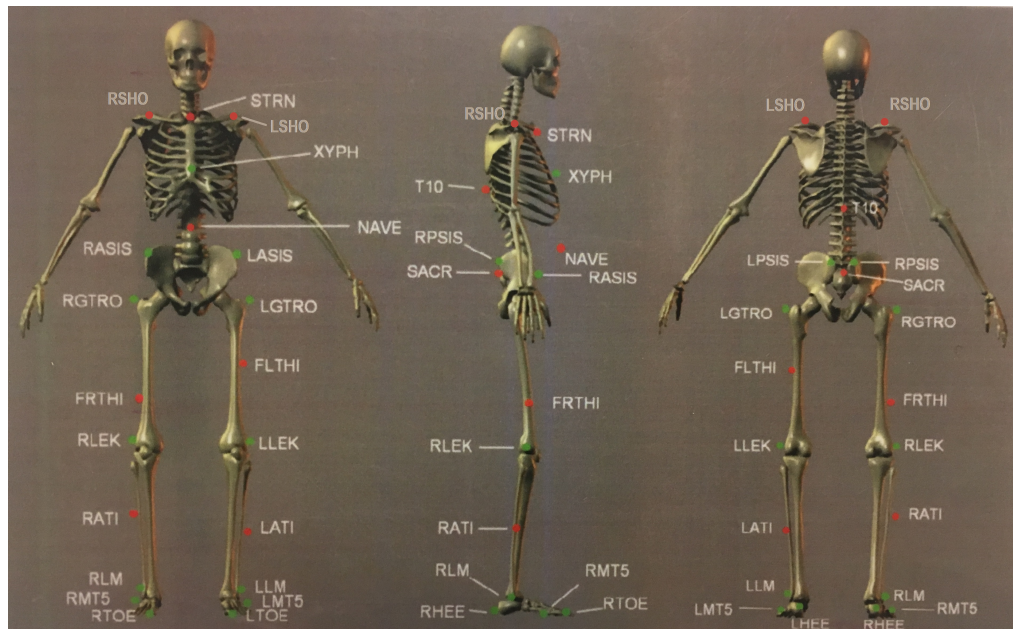


Figure 58: Placement of markers on the body.

Table XI: Marker placement.

No.	Name	Position
1	T10	10th thoracic vertebrae
2	SACR	Sacrum bone
3	NAVE	Navel
4	XYPH	Xiphoid process
5	STRN	Sternum
6	LASIS	Pelvic bone left front
7	RASIS	Pelvic bone right front
8	LPSIS	Pelvic bone left back
9	RPSIS	Pelvic bone right back
10	LGTRO	Left greater trochanter of femur
11	FLTHI	Left thigh
12	LLEK	Left lateral epicondyle of the knee
13	LATI	Left anterior of the tibia
14	LLM	Left lateral malleolus of the ankle
15	LHEE	Left heel
16	LTOE	Left toe
17	LMT5	Left 5th metatarsal
18	RGTRO	Right trochanter major of the femur
19	FRTHI	Right thigh
20	RLEK	Right lateral epicondyle of the knee
21	RATI	Right anterior of the tibia
22	RLM	Right lateral malleolus of the ankle
23	RHEE	Right heel
24	RTOE	Right toe
25	RMT5	Right 5th metatarsal
26	RSHO	Right Shoulder
27	LSHO	Left Shoulder

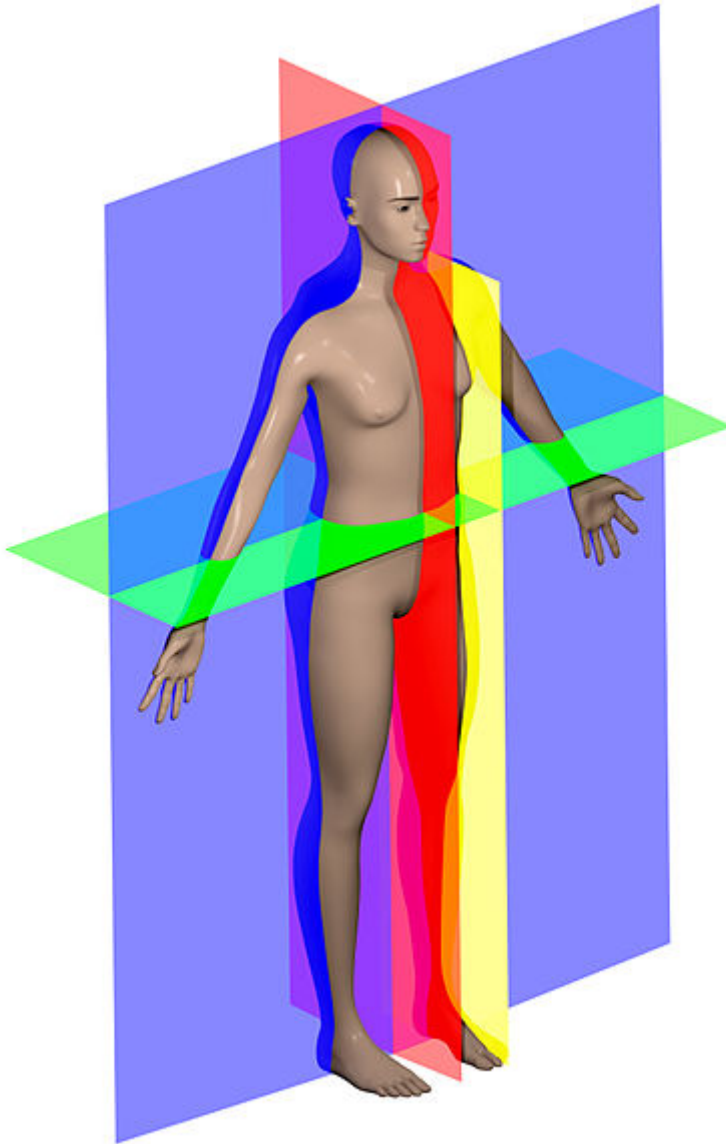
APPENDIX F. Copyright Letters



File:Human anatomy planes.jpg

[all sizes](#)

From Wikimedia Commons, the free media repository

[Use this file
on the web](#)[Use this file
on a wiki](#)[Email a link
to this file](#)[Information
about reusing](#)

Size of this preview: 410 × 600 pixels.

[Original file](#) (2,526 × 3,696 pixels, file size: 454 KB, MIME type: image/jpeg)
; ZoomViewer: [flash/no flash](#)

[Open in Media Viewer](#)

Summary

Description	English: Anatomical planes, including median (red), parasagittal (yellow), frontal or coronal plane (blue) and transverse or axial plane (green).
Date	25 October 2014

Source	Own work
Author	David Richfield (User:Slashme) When using this image in external works, it may be cited as follows: ■ Richfield, David (2014). "Medical gallery of David Richfield (https://en.wikiversity.org/wiki/Medical_gallery_of_David_Richfield_2014)". <i>WikiJournal of Medicine</i> 1 (2). DOI:10.15347/wjm/2014.009 (https://doi.org/10.15347/wjm/2014.009). ISSN 2002-4436 (https://www.worldcat.org/issn/2002-4436).
Other versions	Human anatomy planes.svg

Made with the default [MakeHuman](#) model (intermediate gender proportions) with breast size reduced to be more androgynous, posed in standard anatomical position. [Blender](#) source available on [GitHub](#) (<https://github.com/slashme/AnatomicPlanes>).

Licensing

I, the copyright holder of this work, hereby publish it under the following licenses:



Permission is granted to copy, distribute and/or modify this document under the terms of the [GNU Free Documentation License](#), Version 1.2 or any later version published by the [Free Software Foundation](#); with no Invariant Sections, no Front-Cover Texts, and no Back-Cover Texts. A copy of the license is included in the section entitled [GNU Free Documentation License](#).

This file is licensed under the [Creative Commons Attribution-Share Alike 4.0 International](#) (<https://creativecommons.org/licenses/by-sa/4.0/>), [3.0 Unported](#) (<https://creativecommons.org/licenses/by-sa/3.0/deed.en>), [2.5 Generic](#) (<https://creativecommons.org/licenses/by-sa/2.5/deed.en>), [2.0 Generic](#) (<https://creativecommons.org/licenses/by-sa/2.0/deed.en>) and [1.0 Generic](#) (<https://creativecommons.org/licenses/by-sa/1.0/deed.en>) license.



You are free:

- **to share** – to copy, distribute and transmit the work
- **to remix** – to adapt the work

Under the following conditions:

- **attribution** – You must attribute the work in the manner specified by the author or licensor (but not in any way that suggests that they endorse you or your use of the work).
- **share alike** – If you alter, transform, or build upon this work, you may distribute the resulting work only under the same or similar license to this one.

You may select the license of your choice.

**WOLTERS KLUWER HEALTH, INC. LICENSE
TERMS AND CONDITIONS**

Feb 27, 2018

This Agreement between Anne D Koelewijn ("You") and Wolters Kluwer Health, Inc. ("Wolters Kluwer Health, Inc.") consists of your license details and the terms and conditions provided by Wolters Kluwer Health, Inc. and Copyright Clearance Center.

License Number	4297171047150
License date	Feb 27, 2018
Licensed Content Publisher	Wolters Kluwer Health, Inc.
Licensed Content Publication	Journal of Bone & Joint Surgery
Licensed Content Title	Gait Analysis: Principles and Applications. Emphasis on Its Use in Cerebral Palsy * **
Licensed Content Author	James R. GAGE, Peter A. Deluca, and Thomas S. Renshaw
Licensed Content Date	Oct 1, 1995
Licensed Content Volume	77
Licensed Content Issue	10
Type of Use	Dissertation/Thesis
Requestor type	Individual
Portion	Figures/table/illustration
Number of figures/tables/illustrations	2
Figures/tables/illustrations used	Figures 1 and 2
Author of this Wolters Kluwer article	No
Title of your thesis / dissertation	Predictive Simulations of Gait and their Application in Prostheses Design
Expected completion date	Jun 2018
Estimated size(pages)	110
Requestor Location	Anne D Koelewijn 1960 E 24th St FH269 CLEVELAND, OH 44113 United States Attn: Anne D Koelewijn
Publisher Tax ID	13-2932696
Billing Type	Invoice
Billing Address	Anne D Koelewijn 1960 E 24th St FH269 CLEVELAND, OH 44113 United States Attn: Anne D Koelewijn
Total	0.00 USD

[Terms and Conditions](#)**Wolters Kluwer Terms and Conditions**

1. **Transfer of License:** Wolters Kluwer hereby grants you a non-exclusive license to reproduce this material for this purpose, and for no other use, subject to the conditions herein.
2. **Credit Line:** will be prominently placed and include: For books – the author(s), title of book, editor, copyright holder, year of publication; For journals – the author(s), title of article, title of journal, volume number, issue number, inclusive pages and website URL to the journal page.
3. **Warranties:** The requestor warrants that the material shall not be used in any manner which may be considered derogatory to the title, content, or authors of the material, or to Wolters Kluwer.
4. **Indemnity:** You hereby indemnify and hold harmless Wolters Kluwer and their respective officers, directors, employees and agents, from and against any and all claims, costs, proceeding or demands arising out of your unauthorized use of the Licensed Material.
5. **Geographical Scope:** Permission granted is non-exclusive, and is valid throughout the world in the English language and the languages specified in your original request.
6. Wolters Kluwer cannot supply the requestor with the original artwork, electronic files or a "clean copy."
7. Permission is valid if the borrowed material is original to a Wolters Kluwer imprint (Lippincott-Raven Publishers, Williams & Wilkins, Lea & Febiger, Harwal, Rapid Science, Little Brown & Company, Harper & Row Medical, American Journal of Nursing Co, and Urban & Schwarzenberg - English Language, Raven Press, Paul Hoeber, Springhouse, Ovid).
8. **Termination of contract:** If you opt not to use the material requested above please notify RightsLink or Wolters Kluwer within 90 days of the original invoice date.
9. This permission does not apply to images that are credited to publications other than Wolters Kluwer books/journals or its Societies. For images credited to non-Wolters Kluwer books or journals, you will need to obtain permission from the source referenced in the figure or table legend or credit line before making any use of the image(s) or table(s).
10. **Modifications:** With the exception of text size or color, no Wolters Kluwer material is permitted to be modified or adapted without publisher approval.
11. **Third party material:** Adaptations are protected by copyright, so if you would like to reuse material that we have adapted from another source, you will need not only our permission, but the permission of the rights holder of the original material. Similarly, if you want to reuse an adaptation of original LWW content that appears in another publishers work, you will need our permission and that of the next publisher. The adaptation should be credited as follows: Adapted with permission from Wolters Kluwer: Book author, title, year of publication or Journal name, article author, title, reference citation, year of publication. Modifications are permitted on an occasional basis only and permission must be sought by Wolters Kluwer.
12. **Duration of the license:** Permission is granted for a one-time use only within 12 months from the date of this invoice. Rights herein do not apply to future reproductions, editors, revisions, or other derivative works. Once the 12 - month term has expired, permission to renew must be submitted in writing.
 - i. For content reused in another journal or book, in print or electronic format, the license is one-time use and lasts for the 1st edition of a book or for the life of the edition in case of journals.
 - ii. If your Permission Request is for use on a website (which is not a journal or a book), internet, intranet, or any publicly accessible site, you agree to remove the material from such site after 12 months or else renew your permission request.
13. **Contingent on payment:** While you may exercise the rights licensed immediately upon issuance of the license at the end of the licensing process for the transaction, provided that you have disclosed complete and accurate details of your proposed use, no license is finally effective unless and until full payment is received from you (either by publisher or by CCC) as provided in CCC's Billing and Payment terms and conditions. If full payment is not received on a timely basis, then any license preliminarily granted shall be deemed automatically revoked and shall be void as if never granted. Further, in the event that you breach any of these terms and conditions or any of CCC's Billing and Payment terms and conditions, the license is automatically revoked and shall be void as if never granted. Use of materials as described in a revoked license, as well as any use of the materials beyond the scope of an unrevoked license, may constitute copyright infringement and publisher

- reserves the right to take any and all action to protect its copyright in the materials.
14. **Waived permission fee:** If the permission fee for the requested use of our material has been waived in this instance, please be advised that your future requests for Wolters Kluwer materials may incur a fee.
 15. **Service Description for Content Services:** Subject to these terms of use, any terms set forth on the particular order, and payment of the applicable fee, you may make the following uses of the ordered materials:
 - i. **Content Rental:** You may access and view a single electronic copy of the materials ordered for the time period designated at the time the order is placed. Access to the materials will be provided through a dedicated content viewer or other portal, and access will be discontinued upon expiration of the designated time period. An order for Content Rental does not include any rights to print, download, save, create additional copies, to distribute or to reuse in any way the full text or parts of the materials.
 - ii. **Content Purchase:** You may access and download a single electronic copy of the materials ordered. Copies will be provided by email or by such other means as publisher may make available from time to time. An order for Content Purchase does not include any rights to create additional copies or to distribute copies of the materials.

For Journals Only:

1. Please note that articles in the **ahead-of-print stage** of publication can be cited and the content may be re-used by including the date of access and the unique DOI number. Any final changes in manuscripts will be made at the time of print publication and will be reflected in the final electronic version of the issue. Disclaimer: Articles appearing in the Published Ahead-of-Print section have been peer-reviewed and accepted for publication in the relevant journal and posted online before print publication. Articles appearing as publish ahead-of-print may contain statements, opinions, and information that have errors in facts, figures, or interpretation. Accordingly, Wolters Kluwer, the editors and authors and their respective employees are not responsible or liable for the use of any such inaccurate or misleading data, opinion or information contained in the articles in this section.
2. Where a journal is being published by a learned society, the details of that society must be included in the credit line.
 - i. **For Open Access journals:** The following statement needs to be added when reprinting the material in Open Access journals only: "promotional and commercial use of the material in print, digital or mobile device format is prohibited without the permission from the publisher Wolters Kluwer. Please contact permissions@lww.com for further information."
 - ii. **Exceptions:** In case of reuse from **Diseases of the Colon & Rectum, Plastic Reconstructive Surgery, The Green Journal, Critical Care Medicine, Pediatric Critical Care Medicine, the American Heart Association Publications and the American Academy of Neurology** the following guideline applies: no drug/ trade name or logo can be included in the same page as the material re-used.
3. **Translations:** If granted permissions to republish a full text article in another language, Wolters Kluwer should be sent a copy of the translated PDF. Please include disclaimer below on all translated copies:
 - i. ***Wolters Kluwer and its Societies take no responsibility for the accuracy of the translation from the published English original and are not liable for any errors which may occur.***
4. **Full Text Articles:** Reuse of full text articles in English is prohibited.

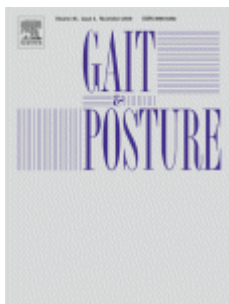
STM Signatories Only:

1. Any permission granted for a particular edition will apply also to subsequent editions and for editions in other languages, provided such editions are for the work as a whole in situ and does not involve the separate exploitation of the permitted illustrations or excerpts. Please click [here](#) to view the STM guidelines.

Other Terms and Conditions:

v1.17

**Questions? customercare@copyright.com or +1-855-239-3415 (toll free in the US) or
+1-978-646-2777.**



Title: Joint contact forces can be reduced by improving joint moment symmetry in below-knee amputee gait simulations
Author: Anne D. Koelewijn, Antonie J. van den Bogert
Publication: Gait & Posture
Publisher: Elsevier
Date: September 2016

© 2016 Elsevier B.V. All rights reserved.

LOGIN

If you're a [copyright.com user](#), you can login to RightsLink using your copyright.com credentials. Already a [RightsLink user](#) or want to [learn more?](#)

[BACK](#)[CLOSE WINDOW](#)

Copyright © 2018 [Copyright Clearance Center, Inc.](#). All Rights Reserved. [Privacy statement](#). [Terms and Conditions](#).
Comments? We would like to hear from you. E-mail us at customercare@copyright.com